UNIVERSITÀ DEGLI STUDI FIRENZE

UNIVERSITÀ DI PISA

GHENT UNIVERSITY

International Doctorate in Civil and Environmental Engineering

CICLE XXX

COORDINATOR Prof. Fabio Castelli

N_2O emissions and aeration efficiency in wastewater treatment: improved monitoring, mechanistic modelling and data mining

Scientific Disciplinary Sector ICAR/03

Candidate
Dr. Bellandi Giacomo

Tutor
Prof. Gori Riccardo

Tutor
Prof. Nopens Ingmar

_____ _____ _____

Coordinator

Prof. Castelli Fabio

_____

Anni 2014-2017

Examination committee:
Prof. Dr. Eng. Giampaolo Manfrida (Chair, Florence University)
Prof. Dr. ir. Stijn Van Hulle (Ghent University)
Prof. Dr. David Gabriel (Autonomous University of Barcelona)
Dr. Eng. Giulio Munz (Florence University)
Prof. Dr. Ramon Ganigué (Ghent University)

Promotors:
Prof. Dr. Eng. Riccardo Gori *
Prof. Dr. ir. Ingmar Nopens **

* Department of Civil and Environmental Engineering DICEA
School of Engineering
Florence University

** Department of Mathematical Modelling, Statistics and Bioinformatics
BIOMATH research group: Model-based analysis and optimization of bioprocesses
Faculty of Bioscience Engineering
Ghent University

Dean:
Prof. dr. ir. Marc Van Meirvenne (Ghent University)
Prof. Dr. Eng. Fabio Castelli (Florence University)

Rector:
Prof. Dr. ir. Rik Van de Walle (Ghent University)
Prof. Dr. Luigi Dei (Florence University)

Please refer to this work as follows:

Giacomo Bellandi (2018). N_2O emissions and aeration efficiency in wastewater treatment: improved monitoring, mechanistic modelling and data mining. PhD Thesis, Ghent University, Belgium.

ISBN 9789463570954

Giacomo Bellandi

N_2O emissions and aeration efficiency in wastewater treatment: improved monitoring, mechanistic modelling and data mining

The thesis is submitted for the fulfilment of the requirement for the degree of Doctor (PhD) in Applied Biological Sciences

Per Ivaldo,

Acknowledgements *o ringraziamenti*

This journey has been, as all wonderful journeys are, a combination of exciting moments, difficulties to overcome, deadlines to beat, happiness, desperation, laughing, and sharing. The learning curve has been steep and dense, but getting here was worth every effort. Also, you can't make such an escalate to the PhD mountain without the support of people, it just wouldn't work. The wonderful network of people that take either a small or big part in your journey, make the difficulties enjoyably challenging. Now, finally getting to the PhD finish line, I look behind and see that whole beautiful crowd, feeling that each person helped me in a singular way to get here. I feel like I own to each one of you a personal thank, but I'm also aware of my worldwide-known memory limits ☺, and I'll try my best to acknowledge you all in this page.

First of all I would like to thank my promoters, Riccardo and Ingmar, the two people that have been actively supporting me at the forefront of this work. You both taught me a lot, science and life-wise. With your kindness and propositive attitude you are an example for your teams. I want to thank Riccardo for welcoming me in his group and involving me in this PhD program, giving me the chance to come back to Italy and start a brand new collaborative framework with my previous working environment. Thanks for the wonderful discussions, for being always open for collaborations, for welcoming new ideas, and for sharing your vision and passion with the kindness that makes you a great tutor and mentor.

Ingmar, I'll never thank you enough for giving me trust and support, ever since we first met (and with this I still thank Prof. Stefano Marsili Libelli for triggering this whole in the first instance almost 10 years ago). Thanks Ingmar for taking part in this joint program with your usual enthusiasm and dedication, supporting my will to live in Italy and sharing my view on this as an opportunity to enlarge boundaries and networks, rather than a mere goodbye. Thanks for your precious and inspiring support and mentoring. You have always been my source of inspiration on how to approach science and business, motivate people and successfully balance a gigantic workload with quality free-time. For me, you are the perfect example of how a mentor should be (a scientific dad or big brother!), and I'm proud I can say I've been part of your team.

The working environment is made of people, colleague, friends, and they are a key part of the quality of our life and research. I want to thank all colleagues from both the Italian and Belgian side, for their open mind, willingness to share, and availability whenever help is needed. Laura, Iacopo and Francesco you are wonderful persons and uniquely dedicated and passionate researchers, let me thank you all three together because you are for me "a team in the team", you have been a source of strength and great fun. Giuseppe and Cecilia, thanks for trying to teach me the art of organization and for always supporting with joy in the tedious jungle of the Italian bureaucracy which for me was very meaningful. Tommaso, you are the example that, in my very modest part, I meant to make when I decided to come back to Florence, please keep up the good work and keep on inspiring students as you do with your contagious positive attitude. This is the way to go. Sara, thank you, it was a pleasure tutoring a student with you and I really enjoyed your innovative thinking going well along with your vintage touch. Alberto, you have been a good friend to me since the beginning of the university, thanks for all the interesting chats, smoking or not, to me you're like a brother. Thank you Giulio, for your inspirational dedication to research and for your kind attitude, although mostly hidden behind a tough and

impenetrable questioning look, but often revealed through a hint of a warm smile meaning more than many others.

Thanks to the BIOMATH team (or family I should rather say), a group of people with which I shared 8 years of my life and to which I owe a great part of my scientific and human background. Thanks Tinne for all your help, you're the backbone of this group, your aggressive but kind attitude is an enjoyable characteristic that I love and that shines when is about getting something done, she nails it! Thanks Youri for having a supportive and propositive word in every moment and for being a real good friend. Thanks Raul for being a great party organizer, fine beer estimator, and kind person, although I still don't get what you're working on. Thanks David, for all the interesting chats and for being so passionate in your research. Thanks Jose for sweetening the working hours with tasty dates (and great tips about Mexico that made me really fall in love with it, will go back for sure). Thank you Andreia, for being so active and positive, contributing to a great environment where fun and work go very well along with each other. Thanks to the whole simulation lab. Thanks Timpe for your great support on both the football and the bureaucratic side, and all the great chats about music! Thanks Sophie, for all the nice time and parties. Thanks Mitralliette Michael, for the great football and smoking time. Thanks to Chaïm for the great and efficient collaboration and for the amazing free-time together. Thanks also to all the beautiful people filling the offices in that marvelous corridor! Aisling, you're the party animal of this corridor and its social glue, thanks for this! Ivaylo, Dorien, Bram, Niels, Jenna, Christina, Peter, Wouter, Séverine, Daan, Chamberlain, there should be an entire thesis to thank you all!

Thanks Jose (Porro) for your precious suggestions and contribution in our research, always present and enjoyably kind. Thanks to Stijn, former BIOMATH, for the support on the realization of a crucial part of this PhD. And thanks to Katrijn, also former BIOMATH, for being so patient to let him work even on strange hours when we had to hit a deadline. But also thanks to old times friends/colleagues Thomas, Ashish, Timothy, Mehul, and to those that I (surely) forgot.

A special thanks to all those, Italian and Belgians, that have literally been in the shit with me, cleaning up after numerous measurement campaigns. Hope to have more of those moments together, well ok, it might not be that great getting dirty in a WWTP, but you'd all agree with me on the great feeling when in the end, with clean hands, we high-five and cheer to the great job done. Thanks for this.

I want to thank the friends I made in Belgium outside the department and with which we keep on seeing each other and this is great! Giacomo (ibbarni un po' outlier), Vincenzo, Veronica, Stephen, Nina, Anna, Ivan, Iva, Ester, Ludovico, Eligio, thanks for the relaxing time after work, for the inspiring chats, loughs, and BBQs!

Thanks to all the operators, lab technicians, and plant managers of Publiacqua, De Dommel, and ACEA for always being available and supportive in our, often difficult, requests. Without your help nothing would really advance.

Thanks to the WEST Systems guys, Simone, Luca, Davide, Paolo, Giorgio, for always being supportive and available with the ultimate findings and solutions to our problems and weird ideas.

Thanks to Bartolini Tendaggi, Tiziana, Ale, Quintilio, for the commitment and the passionate support in designing and building our hood even though it was completely out of your sunny domain.

Voglio ringraziare i miei amici per essere sempre lì, ogni momento, non solo in questi ultimi anni, ma sempre, da quando eravamo bimbetti. Siete per me parte della famiglia, ed io vi sento forte come fratelli. A parte il Simo che è la mia seconda moglie e Leo che è nostro figlio, chiaramente un adulterio, ma pazienza, non porto rancore. Grazie per ogni volta (innumerevoli) che siete venuti a salutarmi per una partenza ed ad accogliermi ad un ritorno, sempre con lo stesso calore e voglia di stare insieme. Grazie per tutti i momenti a ritrovarsi per due chiacchiere davanti al fuoco con i piedi gelati, piuttosto che a sudare facendo la birra, o a lamentarsi del caldo sulla panchina del bar. Questo, per me è sempre stato e sempre sarà ossigeno, linfa vitale. Grazie per ogni canzone suonata insieme e per ogni discorso andato in fumo. Grazie delle mangiate e delle bevute. Grazie Tizy per tutti i dolci e la dolcezza, grazie Max, Masseeyy, Tozzeeyy, Glosseeyy, Skyy, Herrereeyy, siete bellissimi (in senso lato). E stasera Tozzey offre da be'!

Grazie alla mia famiglia. A Gianluca, Elena e Annalisa che sono la forza che mi serve ogni giorno, il pensiero dolce, la risata, l'affetto, la sicurezza. Quando ci sono momenti difficili io penso a voi, che siete una parte di me (a Gianluca sul divano, a Elena sui libri e a Annalisa in laboratorio), e divento forte come una roccia. In quel momento, con voi che mi proteggete, sono il più forte di tutti e non mi spaventa più nulla. Ma anche quando ci sono momenti belli penso a voi! Insomma, io vi penso sempre, perché senza di voi non avrei mai avuto la forza di far niente. E quindi ringrazio anche mamma e babbo che vi hanno fatto! Grazie a mamma e babbo che ci sostenete senza mai cedere, con una potenza d'animo unica, che solo il bene del genitore può concepire. Grazie per aver avuto tutta la forza e la pazienza infinita per darmi fiducia, anche quando uno normale non ne avrebbe avuta più. Grazie per farci studiare e crescere ammodo, ricoperti di amore e affetto, ma anche affettato e belle mangiate. Grazie alla zia Urbana e alla nonna, per gli abbracci da lotta libera, le parole dolci, i consigli preziosi, i calzini ricuciti, e ancora, le mangiate. Grazie a tutta la famiglia, zio Urbano, zia Maria, zio Roberto, zia Roberta, zio Mario, zia Adriana, Erika, Angelica, Luca, Silvia, Lucia, Francesca, Lorenzo, Ernesto, Giorgia, e annessi, e anche chi arrivera' dopo. Vi amo con tutto me.

Linda è la persona che questa tesi l'ha vissuta più da vicino, e senza la quale non ci sarebbe stata mai alcuna tesi, né dottorato, ma probabilmente nemmeno una laurea! Io ti ringrazio per ogni giorno che passiamo insieme, perché sei bella, brava, intelligente, solare, simpatica, modesta, gentile, intraprendente e coraggiosa, e non c'è motivo perché tu debba stare con me se non per un inspiegabile amore che ci tiene uniti e forti da diversi bellissimi anni. Grazie per l'amore che mi dai e per fare risplendere ogni giorno insieme. Con te accanto potrei scrivere altre mille tesi e milioni di trattati. Non lo farò, ma teoricamente potrei.

Senza tutto questo non c'è dottorato! Ora potete anche saltare il resto del libro.
(Without all this, there's no PhD! Now you can even skip the rest of the book. ☺)

Giacomo

Outline

Summary

Due to the growing awareness of climate change, there is a need to quantify GHGs from different sources. The water industry, which provides the water supply, wastewater collection, and treatment and discharge, contributes significantly to total energy consumption and consequently to GHG emissions in developed countries. In WRRFs, large amounts of organic and inorganic matter are transformed and transferred from the water phase to the atmosphere, lithosphere, and/or biosphere through emissions from process tanks, and treated effluents and biosolids that are disposed in the environment. All three main GHGs (i.e. CO_2, CH_4, and N_2O) are emitted from WRRFs. N_2O is currently the GHG of major concern with regards to direct emissions from WRRFs. N_2O has a GWP 265–298 times that of CO_2 for a 100-year timescale which makes this the single most important ozone depleting compound of our century. Anthropogenic activity is responsible for about 40% of the global N_2O production and a 15% concentration increase has been observed since 1750. To date 3% of the anthropogenic N_2O production is recognized to be generated by wastewater treatment. WRRFs designed for nutrients removal have been observed to emit up to 7% of the influent nitrogen load as gaseous N_2O.

In a WRRFs the bioreactor is currently recognized as the most emitting treatment step in these terms. In addition to this, the aerated compartment of bioreactors is generally recognized to cause between 45 to 75 % of the plant's energy expenditure. Considering both the contribution of N_2O emissions and energy expenditure, the biological step of a WRRF represents the large majority of the CFP of a WRRF.

Measuring and accounting for N_2O emissions and aeration efficiency requires standard methods allowing to obtain comparable measurements among different WRRFs and reproducible within the same facility in order to derive solid classifications. However, especially for N_2O, there is the need of a unified protocol with general standardized guidelines for a sound assessment at different WRRFs. Both N_2O and aeration efficiency measurements protocols present major lacks and assumptions. This thesis puts in evidence major weaknesses of protocols for N_2O emission and aeration efficiency measurements proposing possible improvements in terms of sampling strategy, calculation methods and equipment.

As measurements of N_2O emissions and aeration efficiency are used to understand process dynamics and design new CFP minimization scenarios, also modelling WRRFs is very important in this view, given the system complexity. Modelling tools allow to design new plant operation and control strategies (aimed at minimizing these emissions) and evaluate their long term effect on the WRRF limiting trials (and risks). Current N_2O kinetic models are highly developed in describing the biochemical processes, however, as they are developed in lab-controlled conditions, they are yet troublesome when it comes to full-scale applications. This is most probably due to a poor representation of local concentrations by the plant's model layout and often to an over-parametrization of the biokinetic model. The modelled description of the plant's layout is nowadays often erroneously underestimated, but its design should be one of

the most important steps in the definition of a plant's model as it has important effects on the calculation effort, the calibration of the kinetic model, and nonetheless, on its predictive power. This thesis considers one of the most advanced kinetic models available in the literature and shows how, using a better representation of hydrodynamics, this can improve its performances.

As effective applications, and applicability, of kinetic models for N_2O prediction in full scale are still limited, possible modelling alternatives are evaluated in this work. The application of a qualitative, knowledge-based risk assessment model (N_2O risk model) to a full-scale datasets is provided to prove the concept of its use. The N_2O risk model shows to be effective in helping to unravel the dynamics behind N_2O production and to be able to give valuable insight in the mechanisms of N_2O production.

In addition to this, seen the crescent quantity of data that current WRRFs have available, and the fact that the amount of information is too often unused wasting part of the value of sensors and SCADA systems. A data mining approach is also presented. In this regard, this thesis gives a practical application of a data mining technique to derive potential relations with respect to N_2O emission among variables that are routinely measured at WRRFs. The testing of different clustering algorithms and their critical evaluation is shown in view of an online application. This is furnishing a possible new root to the use of SCADA data for understanding and mitigating N_2O emissions by translating hidden information into clear operational instructions.

In summary, this thesis raises the main concerns about N_2O and aeration efficiency assessment analyzing major weaknesses and suggesting possible solutions for developing more robust standardized methods. It further provides an overview of different N_2O modelling approaches proposing possible developments to enhance capabilities to recognize sources of emission and provide clues for developing CFP reduction strategies.

Samenvatting

Wegens de toenemende bewustwording van de klimaatverandering is er een nood om broeikasgassen van verschillende bronnen te kwantificeren. De waterindustrie, die instaat voor waterbevoorrading, afvalwatercollectie en – behandeling, draagt significant bij tot energieverbruik en als dusdanig tot broeikasgasemissies in ontwikkelde landen. In water- en grondstofwinnings faciliteiten (WGWF) worden grote hoeveelheden organische en anorganische stoffen omgevormd en getransfereerd van de waterige fase naar de atmosfeer, litosfeer en/of biosfeer door emissies van procesreactoren en behandelde effluenten en vaste stoffen die worden geloosd in het milieu. De drie voornaamste broeikasgassen, zijnde CO_2, CH_4, en N_2O, worden door WGWF's uitgestoten. N_2O is momenteel het meest verontrustende broeikasgas met betrekking tot directe uitstoot vanuit WGWF's. N_2O heeft een GWP van 265–298 dan dat van CO_2 over een 100 jaar tijdshorizon, wat het tot meest ozon vernietigende gas maakt van deze eeuw. Antropogene activiteit is verantwoordelijk voor ca. 40% van de globale N_2O productie en een concentraitetoename van 15% sinds 1750 werd waargenomen. Bij sommige WGWF's ontworpen voor nutriëntenverwijdering werd een N_2O emissie van zoveel als 7% van de influent stikstofbelasting waargenomen.

In een WGWF wordt de bioreactor tot op heden aanzien als de grootste emissiebron. Bovendien is het beluchte deel daarvan ook nog eens verantwoordelijk voor 45 tot 75% van het energieverbruik. Dit in acht nemende, is de biologische trap van een WGWF verantwoordelijk voor het leeuwendeel van de koolstofvoetafdruk van een WGWF.

Het meten en in rekening brengen van N_2O emissies en beluchtingsefficiëntie heeft nood aan standaardmethodes die toelaten om vergelijkbare metingen tussen verschillende WGWF's te bekomen, die bovendien herhaalbaar moeten zijn tussen verschillende installaties om een solide klassificatie toe te laten. Zeker voor N_2O is er nood aan een eenduidig protocol met algemene gestandardiseerde regels voor een betrouwbare inschatting in een WGWF. Zowel de huidige meetprotocols voor N_2O en beluchtingsefficiëntie meetprotocols vertonen tekortkomingen en veronderstellingen. Dit werk illustreert deze tekortkomingen en stelt verbeteringen voor met betrekking tot staalnameprocedure, berekeningsmethoden en meettoestellen.

Aangezien metingen van N_2O emissies en beluchtingsefficiëntie worden gebruikt om procesdynamica beter te begrijpen en scenario's voor te stellen voor koolstofvoetafdrukreductie, is ook wiskundige modellering van WGWF's zeer belangrijk gezien de systeemcomplexiteit. Modellering laat toe om betere bedrijfsvoering en controlestrategiëen te ontwerpen met als doel emissies te minimaliseren, alsook de lange termijn effecten en risico's te evalueren. De huidige kinetische modellen voor N_2O zijn sterk ontwikkeld met betrekking tot de biochemische processen. Deze werden echter ontwikkeld in een labo omgeving en blijken nog problematisch voor toepassing op volle schaal. Dit is wellicht te wijten aan een ondermaatse predictie van lokale concentraties en een overparameterisatie van het

biokinetische model. De modellering van de spatiale component gebeurt meestal zeer summier, in tegenstelling tot het belang ervan voor berekening en calibratie van het kinetische model en aldus de predictieve kracht van het model. Dit werk illustreert hoe een betere spatiale representatie in combinatie met de meest geavanceerde kinetische modellen in de literatuur, de modelperformantie kan verbeteren.

Gezien de effectieve toepassing van kinetische modellen voor N_2O predicites nog op zich laat wachten werden ook alternatieven voor modellering geëvalueerd. De toepassing van kwalitatieve kennis-gebaseerde risico inschattingsmodellen (N_2O risico model) op volle schaal data werd geïllustreerd. Het N_2O risico model bleek in staat om mede de dynamica van N_2O productie te ontrafelen en de productiemechanismen beter te doorgronden.

Dit soort technieken zijn interessant gezien de steeds toenemende kwantiteit aan data beschikbaar in WGWF's en het feit dat deze informatie vaak ondergebruikt wordt, wat de echte kracht van sensoren en SCADA ondermijnt. Mede hiervoor werd een datamining techniek toegepast in dit werk om verder de potentiële verbanden tussen N_2O emissies en regulier gemeten grootheden in een WGWF bloot te leggen. Verschillende clusteralgoritmen werden getest en hun prestatie kritisch geëvalueerd met het oog op online toepassing. Dit is een mogelijke nieuwe route voor gebruik van SCADA data voor het begrijpen en reduceren van N_2O emissies door de verborgen informatie om te zetten in duidelijke operationele instructies.

Samengevat droeg dit werk bij tot het in de verf zetten van het belang van analyse van N_2O emissies en beluchtingsefficiëntie en de tekortkomingen ervan, alsook voorstellen voor betere oplossingen en robustere standaarmethodes. Verder geeft het werk een overzicht van verschillende modelleringsmethoden voor N_2O waarbij uitbreidingen en nieuwe methoden worden voorgesteld om de koolstofvoetafdruk te reduceren.

Abbreviations and acronyms

α – correction factor to process conditions for oxygen transfer measurements

$\alpha SOTE$ – Standard Oxygen Transfer Efficiency in process conditions

β – correction factor to process conditions for DO at saturation

θ – geometric temperature correction coefficient

a – available area for exchange of oxygen

$AMRE$ – Absolute Mean Relative Error

ASM – Activate Sludge Model

$ASMG1$ – Activated Sludge Model for GHG n.1

$ASMG2d$ – Activated Sludge Model for GHG n.2d

AFR – Air Flow Rate

AS – Activated Sludge

AD – Anaerobic Digestion

a_{spec} – specific area of diffusers

$bio - P$ – biologically related phosphorous removal

BOD – Biochemical Oxygen Demand

CAS – Conventional Activated Sludge

CF – Carbon Footprint

CH_4 – Methane

CM – Compartmental Model

CO_2 – Carbon Dioxide

COD – Chemical Oxygen Demand

COD/N – ratio of COD to N

$CSTR$ – Completely Stirred Tank Reactor

ECT – Equivalent Contact Time

D – diffusion coefficient for oxygen

DO – Dissolved Oxygen

$DO^*_{S_{20}}$ - saturation of oxygen in clean water at 20°C

$DO^*_{S_T}$ - saturation of oxygen in clean water at temperature T

DO_i – instant concentration of oxygen in the liquid

EF - emission factor

FNA – Free Nitrous Acid

FA – Free Ammonia

GC – Gas Chromatography

GHG – Greenhouse Gas

$GWRC$ – Global Water Research Coalition

IWA – International Water Association

k_L - oxygen mass transfer coefficient

KMO – Kayser Meyer-Olkin

LH – Latin Hypercube

$MARE$ – Mean Absolute Relative Error

MEA – Mean Absolute Error

$MEAPE$ – Median of Absolute Prediction Error

$MPCA$ - Multi-way PCA

$MR_{o/i}$ - molar ratio of oxygen to inerts in ambient air (inlet gas)

$MR_{og/i}$ - molar ratio of oxygen to inerts in the off-gas

MSE – Mean Squared Error

$MSLE$ – Mean Squared Logarithmic Error

$MSRE$ – Mean Squared Relative Error

NH_4^+ - ammonia

NO – nitric oxide

NO_2^- - nitrite

NO_3^- - nitrate

N_2O - nitrous oxide

NOH – nitrosyl radical

NH_2OH – hydroxylamine

N_d – number of diffusers

OAT - One sample At Time

OD - Oxidation Ditch

OHO - Ordinary Heterotrophic Organisms

OTE – Oxygen Transfer Efficiency

PAO – Phosphorous Accumulating Organisms

PCA – Principal Components Analysis

PC – Principal Component

Q_{air} – air flow

RCV – Relative Cumulative Variance

$RMSE$ – Root Mean Squared Error

$RRMSE$ – Relative Root Mean Squared Error

RV – Relative Variance

RVE – Relative Volume Error

$SARE$ – Sum of Absolute Relative Error

SBR - sequencing batch reactor

$SCADA$ – Supervisory Control and Data Acquisition

SRT - Sludge Retention Time

SSE – Sum of Squared Errors

$UASB$ – Upflow Anaerobic Sludge Blanket Reactors

t_e – bubble residence time in the liquid

$WRRF$ – Water Resource Recovery Facility

Y_r - mole fractions of water vapor in ambient air (inlet gas)

Y_{og} - mole fractions of water vapor in the off-gas

Y_{CO_2r} - mole fractions of CO_2 in ambient air (inlet gas)

Y_{CO_2og} - mole fractions of CO_2 in the off-gas

Z – diffusers submergence

Chapter 1

1. Introduction

1.1. Problem statement

1.1.1. A global view

It took just 100 years during the 20th century for the world population to increase from 1.6 to 6.1 billion people (UN Population Fund). There are more than 7.5 billion people on the planet at this moment and, with a growth rate of 1.2 %, this is expected to reach 10 billion by 2050 (Figure 1.1) (http://www.worldometers.info). All these people need and deserve proper sanitation services and access to safe drinking water while maintaining a sustainable water withdrawal (Figure 1.2). Currently, only 27% of the global population (1.9 billion people) use private sanitation facilities connected to sewers from which wastewater is treated (http://www.who.int). With the expected population growth and relative urbanization, the global need for water treatment becomes a dramatic emergency becoming part of the Sustainable Development Goals of the United Nations (UN) with Goal 6 to "Ensure access to water and sanitation for all" (http://www.un.org). At a global level, this is so important to directly connect and relate to a number of other UN targets such as "Ensure healthy lives and promote well-being for all at all ages" (Goal 3) in first instance, but also "Promote inclusive and sustainable economic growth, employment and decent work for all" (Goal 8) since without proper water availability and treatment there is no sustainable development, "Take urgent action to combat climate change and its impacts" (Goal 13) given that this is a key step in the fight against climate change, "Conserve and sustainably use the oceans, seas and marine resources" (Goal 14) as a result of proper water treatment and discharge, "Sustainably manage forests, combat desertification, halt and reverse land degradation, halt biodiversity loss" (Goal 15), and finally "Promote just, peaceful and inclusive societies" (Goal 16) since water scarcity and transboundary water disputes are historically known to trigger conflicts worldwide (Kreamer, 2012).

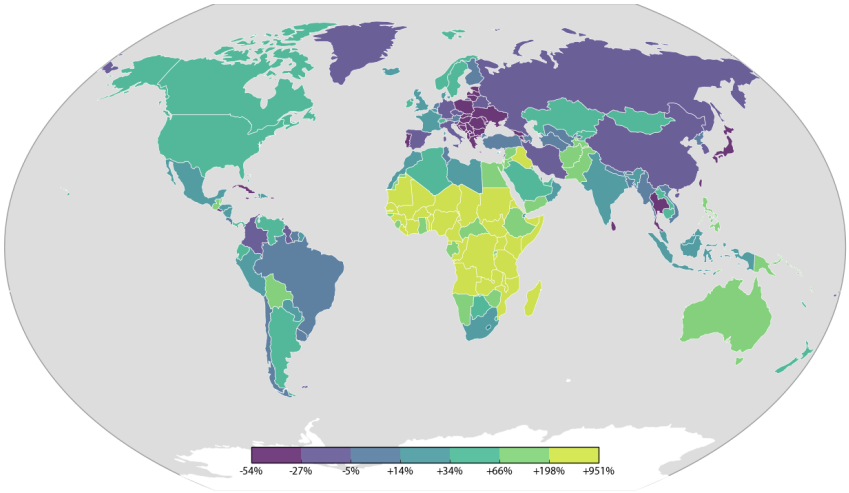

Figure 1.1 - World population growth projection to 2100 (http://geoffboeing.com/)

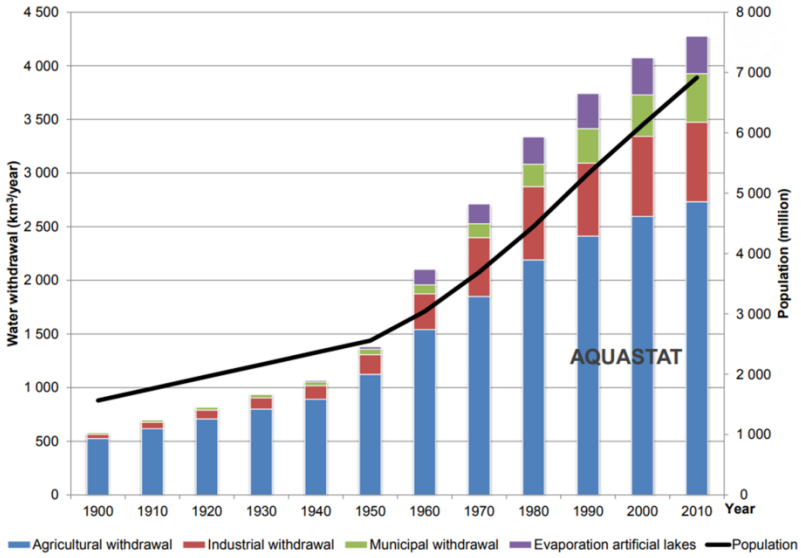

Figure 1.2 – Global population and water withdrawal over time (http://www.fao.org, AQUASTAT data)

Water scarcity is a direct consequence of the overexploitation due to population growth. Earth is estimated to contain a total 1.338 billion km^3 of water (https://water.usgs.gov) of which barely 0.007 % is freshwater available for people. This means that, ideally, each individual has about 12500 m^3 of water available on earth. This value is highly volatile depending on the continent and local conditions (Figure 1.3). Some regions are relatively rich of water while others, depending on geography, climate, availability of technology and local regulations are instead facing draught and sever pollution.

12500 m^3 per capita might at first sight seem a big number, but it must be kept in mind that this water should serve for both municipal use, agriculture and industry (Figure 1.2). Therefore, considering that the fraction remaining for urban use is in average 10% of it, this means that for the case of a country currently not experiencing particular scarcity like Italy, each inhabitant has to live the whole life with about 300 m^3, 100 m^3 for Belgium. Hence, there is a globally spread need for water reuse, adequate treatment, supply and sanitation.

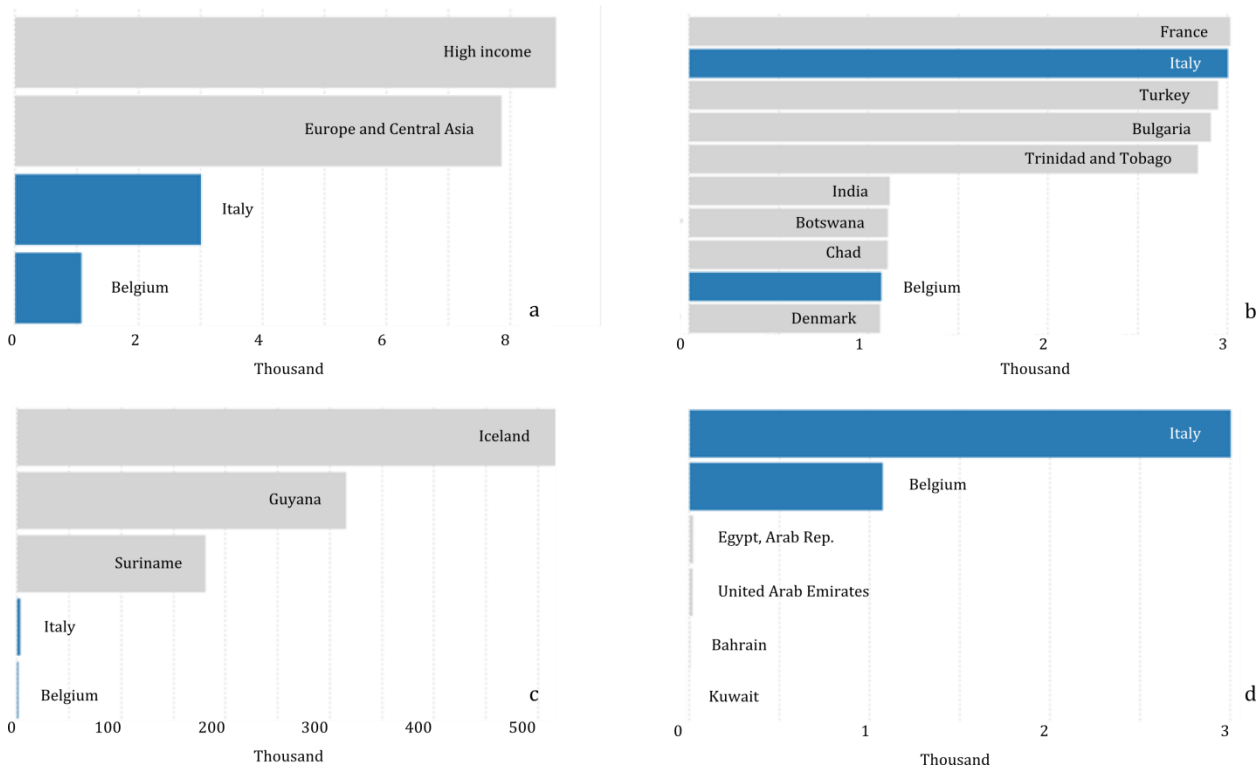

Figure 1.3 – Renewable internal freshwater resources per capita in m³ in Belgium and Italy compared with: a) averages of high income countries and Europe-Central Asia; b) nations with similar figures; c) countries with high water availability; d) countries with severe scarcity (https://data.worldbank.org).

Discharging improperly treated water creates severe environmental and health problems among which the accumulation of nutrients (nitrogen booms and hypoxia with critical consequences for both fauna and flora. Recently, nitrogen has been also observed accumulating in soils of anthropogenic landscapes (Van Meter et al., 2016). But nitrogen is relatively abundant in nature, even though the vast majority of it is strongly bound as N_2 in the atmosphere. On the other hand, phosphorous, other than representing an important source of nutrients for plants, is becoming a scarce element increasingly interesting for resource recovery for industrial applications (Neset and Cordell, 2012; Ulrich and Frossard, 2014). This is due to its (yet) non-renewable character, since the only source of phosphorous to overcome our needs is to date (increasingly expensive) mining.

In the European context, the EU Water Framework Directive (WFD – directive 2000/60/EC) has been applied to develop a common framework for waterbodies protection within the European Union. Among the primary objectives of the WFD is the protection of the environment against uncontrolled (waste)water discharge and, probably the main aim of the agreement is the achievement of a degree of "good status" for all European surface waters. The application of the directive was supposed to ensure the availability of adequate wastewater treatment, and the establishment of concentration limits for target compounds in urban and industrial discharges prior to the receiving waters. Despite the fact that the directive failed in reaching some of the key targets at the 2015 deadline, and some criticism raised on many organizational and economical

aspects of WFD that need improvement (Van Engelen et al., 2008; Voulvoulis et al., 2017), the directive significantly boosted the spreading of advanced biological treatment. Also, the application of secondary (biological) treatment for all areas was set as a mandatory requisite, thus boosting the spread out of adequate water treatment in less developed regions.

1.1.2. Water treatment

Since more than a century, the activated sludge (AS) (Ardern and Lockett, 1914) is the most widespread advanced biological treatment of wastewater (Kolarik and Priestley, 1995). The need for properly removing nitrogen from the water stream and the discovery of some heterotrophic bacteria capable of converting nitrate to nitrogen gas (McCarty, 1964) led to the nitrification-denitrification concept of the AS process. The implementation of the pre-denitrification step followed and the combination of the two processes with the introduction of the recycle flow was a successful improvement also regarding biological phosphorous removal (Barnard, 1973). The strong increase in population of the 1970s was the cause of two main issues for the sanitation field. Firstly, the necessity of city areal expansion caused the incorporation of many treatment plants, initially built outside the urban area, inside the residential space. Therefore, when the consequential need of increasing the treatment capacity of these plants became tangible, space efficient technologies such as MBRs successfully entered the market. Secondly, the energy crisis pushed the attention of the research towards the development and improvement of anaerobic processes (e.g. UASB), and towards the optimization and further understanding of the most energy demanding steps such as aeration and pumping. Wastewater treatment plants, were lately refreshed in the conceptual name with the more renewable attribute of Water Resource Recovery Facilities (WRRFs).

These technologies are nowadays complex industrial applications in need of adequate control, management and maintenance to prevent them from becoming sources of pollution themselves. A WRRF can remove important amounts of pollutants from the water and make its discharge safer, but they also require a relevant amount of energy to operate (e.g. pumps, aerators, mixers), which is yet generated burning fossil fuels in large majority. The vast majority of the energy used in a WRRF is used to provide sufficient oxygen to the microorganisms able to degrade the contaminants. The aerobic step of a WRRF can account for as much as 60 % of the total plant energy requirement (WEF, 2010). WRRFs can also become source of gaseous emissions contributing to the greenhouse effect, such as methane (CH_4), nitrous oxide (N_2O) and carbon dioxide (CO_2). These emissions represent a growing concern and a timely issue in WRRF optimization. In particular N_2O has a global warming potential of 298 times the one of CO_2 and its generation can significantly impact the carbon footprint of a WRRF becoming in some cases as important as the carbon emission due to its energy consumption (Daelman et al., 2013). In the latest years, the persistent and growing concern for climate change have placed a considerable amount of focus on measuring and modelling full-scale WRRF emissions.

1.1.3. WRRF emissions

Due to the growing awareness of climate change, there is a need to quantify GHGs from different sources. With regard to this need, some governments have started to implement regulations that force water authorities to report their GHG emissions (GWRC, 2011). Indeed, the water industry, which provides the water supply, wastewater collection, and treatment and discharge, contributes significantly to the total energy consumption and consequently to GHG emissions in developed countries, and thus it may play a dominant role in some regions (Olsson, 2011). In water resource recovery facilities WRRFs, large amounts of organic and inorganic matter are transformed and transferred from the water phase to the atmosphere, lithosphere, and/or biosphere through emissions from process tanks, and treated effluents and biosolids that are disposed in the environment. WRRFs emit all three main GHGs (i.e. CO_2, CH_4, and N_2O) and are responsible for a large portion of the GHG emissions from the water industry (Caniani et al., 2015).

Focusing on WRRFs, several pathways and processes taking place both within and outside their boundaries are responsible for GHG emissions, which can be classified as direct, indirect internal, and indirect external (WRI and WBCSD, 2004). These three sources belong to the scopes established by the World Resources Institute and the World Business Council for Sustainable Development in the GHG Protocol Standard to classify emissions (Scope I, Scope II, and Scope III, respectively).

Direct emissions (also referred to as Scope I emissions) are those produced and discharged into the atmosphere within the WRRF boundary, and one of their main contributors are biological processes and sections treating by-products of wastewater treatment (e.g. biogas produced from anaerobic sludge digestion, AD).

Indirect internal GHG emissions (also referred to as Scope II emissions) are a consequence of activities that take place within the WRRFs' boundary, but occur at sources owned or controlled by another entity. Indirect internal emissions are associated with the consumption of electrical power imported to supply electromechanical devices.

Indirect external emissions (also referred to as Scope III emissions) are those related to sources not directly controlled inside the WRRF boundary (e.g. off-site sludge disposal, production of chemicals used in the process, third party transportation, etc.) and are typically excluded from carbon accounting since they are Scope I emissions for other parties.

All major GHGs (CO_2, CH_4 and N_2O) can be produced by the biological processes used in WRRFs and contribute to its direct emissions. A schematic representation of the locations at a WRRF where GHG can be emitted is presented in Figure 1.4.

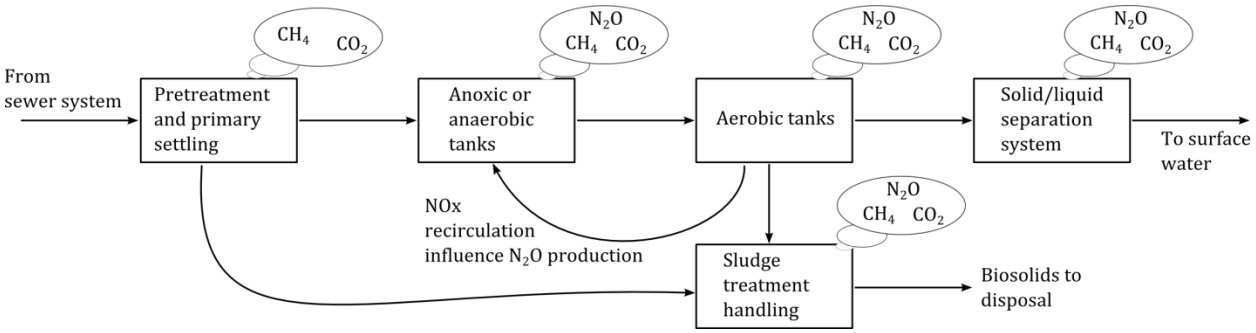

Figure 1.4 – Schematic overview of a WRRF treating urban wastewater and the locations where GHG can be emitted (direct emissions)

CO_2 is directly produced in both aerobic and anaerobic biological processes. In the former case, organic compounds are oxidized into CO_2 and other metabolites and accompanied by cell growth, while in the latter, organic matter is transformed into biogas (CO_2 and CH_4 in proportions of 30-40% and 60/70% v/v, respectively) (Tchobanoglous et al., 2014). According to the accounting protocol of the IPCC (2006), CO_2 derived from wastewater treatment is assumed to originate from short-lived biogenic material. However, fossil organic carbon was found in the incoming wastewater of WRRFs, and related direct fossil CO_2 emissions from oxidation by AS may vary with the wastewater composition and treatment configuration (Griffith et al., 2009; Law et al., 2013; Tseng et al., 2016).

In WRRFs, N_2O is produced by both heterotrophic bacteria and by ammonia oxidizing bacteria through different pathways (*inter alia:* Foley et al., 2010; Kampschreur et al., 2009). Due to the complexity of the N_2O formation process and to the influence of several operational parameters on such processes, N_2O emissions from WRRFs vary substantially among plants, ranging from negligible to substantial, depending on the different process design and operating conditions making this a troublesome emission to assess.

Table 1.1 – Examples of N_2O emissions from WRRFs reported in literature.

WRRF configuration	N_2O emission (% of influent NH_4-N)	Reference
Two-step CAS plug flow	1st step: 0.68% 2nd step: 3.5%	Pan et al. (2016)
SBR	6.8%	Rodriguez-Caballero et al. (2015)
Partial nitratation/anammox	2%	Castro-Barros et al. (2015)
CAS WRRF	0.03% 0.14%	Tumendelger et al. (2014)
nitratation/anammox	1.7% nitritation 0.6% ANAMMOX	Kampschreur et al. (2008)

In WRRFs, CH_4 is produced in anaerobic processes, but can also be generated in unwanted anaerobic zones due to e.g. bad mixing. Generally the AD process is used to generate all possible CH_4 to recover energy. However, the AD represents not only a carbon sink, but can also represent a source of GHGs under different aspects (e.g., emergency biogas emissions via the pressure relief valves due to process malfunctioning, improper biogas combustion, fugitive emissions). Also, elevated concentrations of H_2 in the biogas are known to be responsible for NO_x production during biogas combustion (Jeong et al., 2009; Porpatham et al., 2007). Methanogenic activity in aerobic tanks is deemed to be insignificant (Gray et al., 2002), but CH_4 can enter aerobic AS reactors in dissolved form from sewers (Guisasola et al., 2008) or sections of the WRRFs where anaerobic conditions occur, then being both stripped and biologically oxidized (Daelman et al., 2013).

Throughout the last decade, scientific activities aimed at monitoring and accounting for GHG emissions from WRRFs have increased considerably (*inter alia:* Ahn et al., 2010; Caivano et al., 2017; Daelman et al., 2013; Kampschreur et al., 2009; Law et al., 2012; Monteith et al., 2005), and several attempts have been made to establish protocols to quantify GHGs. Due to the relevant importance that energy consumption and N_2O emissions showed in the recent years with regards to WRRFs CFP, efforts of the present work were concentrated on N_2O emissions and energy consumption from aeration devices.

In order to understand and minimize emissions from WRRFs and optimize their treatment efficacy, research has invested a lot of efforts and resources for defining reliable protocols for assessing these emissions. Standardized measurement methods have been developed throughout the years in order to generate comparable measures of gaseous emissions by introducing the concept of an EF (Chandran, 2011) and efficiency of aerators (ASCE, 1997) that could classify WRRFs and ease the development of strategies for minimizing emissions. However, the diversity of methods available,

and some major assumptions in the assessment and reporting of EFs (Massara et al., 2017) are some of the drivers that motivated this research activity.

By nature, WRRF design and the water treated are heterogeneous, making it difficult to define a general procedural approach applicable to all cases. Hence, the need for new developments. In particular, local (e.g. tank geometry) and temporal (e.g. influent variability) differences in a biological tank are a reality that significantly affects these measurements and the relative development of emission reduction strategies.

1.1.4. Modelling WRRF

Mathematical modelling has been used to unravel several complex biological and physical mechanisms, among which also those behind both the oxygen transfer and the generation of N_2O. The activated sludge models (ASM), based on the equation developed by Monod (1950), are a representation of microorganisms growth depending on half saturation indices (K-values) and substrate availability. These models have been largely used to optimize WRRF operation by mimicking biological growth, as well as oxygen and contaminant depletion, in order to boost the development of optimal scenarios that could be applied in reality. However, growth and its related substrate consumption, largely depends on the local substrate (e.g. ammonium) and electron acceptor (e.g. generally oxygen and nitrate) concentrations (Henze et al., 2000), and the representation of these biological tanks was also observed to have a relevant importance.

Mechanistic knowledge of biological processes is nowadays very detailed and more modelling efforts have been made for unraveling complex biological functions, too often underestimating the hydrodynamic effects of the reactor design on local conditions. The application of mechanistic models for describing N_2O production has nowadays been proved at laboratory scale. However, full-scale applications are still lacking sound validation due to their troublesome nature in the calibration step (Ni et al., 2013). The incorrect representation of local conditions and relative differences in substrate concentrations are most probably the main reasons for the narrow applicability of calibration values.

The complexity of WRRFs required a crescent amount of controls and monitoring sensors all of which are often recorded in a database and un(der)used. These data represent information on the plant operation and can be used to understand and develop data powered models. Alternatives to the mechanistic approach are also available. Models based on the knowledge built on the literature (Knowledge-based) and stochastic models developed on historical data are valid examples of these alternatives. There are examples of the application of knowledge-based models for e.g. optimizing operation against bulking sludge (Comas et al., 2003) and of the development of promising data mining techniques for enhancing control based on historical data (Villez et al., 2008).

1.2. Objectives

The worldwide crescent need for treatment of both industrial and civil wastewaters significantly contributes to increasing both the global energy demand and the relative greenhouse gas (GHG) emissions. In this view, the present work puts focus on:

- Assembling an analyzer for aeration efficiency and N_2O emission measurements from biological tanks of WRRFs;
- Contributing at improving the assessment and definition of an EF for N_2O production in full scale plants. Available measurements methods and techniques are critically analyzed and improvements are proposed with testing on WRRFs;
- Refining the measurement and sampling technique for estimating aeration efficiency in biological tanks. Measurement methods and concepts of aeration efficiency indicators are critically presented proposing possible improvements;
- Demonstrating the capabilities of kinetic models for N_2O production making use of an improved representation of hydrodynamics for a real case scenario;
- Providing practical applications of knowledge based models and data mining tools to full scale data for process understanding and development of gaseous emission minimization strategies.

1.3. References

Ahn, J.H., Kim, S., Park, H., Rahm, B., Pagilla, K., Chandran, K., 2010. N2O Emissions from Activated Sludge Processes, 2008—2009: Results of a National Monitoring Survey in the United States. Environ. Sci. Technol. 44, 4505–4511.

Ardern, E., Lockett, W.T., 1914. Experiments on the oxidation of sewage without the aid of filters. J. Chem. Technol. Biotechnol. 33, 523–539.

ASCE, 1997. Standard Guidelines for In-Process Oxygen Transfer Testing (18-96). American Society of Civil Engineers, New York, NY.

Barnard, J.L., 1973. Biological nutrient removal without the addition of chemicals. Water Res. 9, 485–490.

Caivano, M., Bellandi, G., Mancini, I.M., Masi, S., Brienza, R., Panariello, S., Gori, R., Caniani, D., 2017. Monitoring the aeration efficiency and carbon footprint of a medium-sized WWTP: experimental results on oxidation tank and aerobic digester. Environ. Technol. 38, 629–638.

Caniani, D., Esposito, G., Gori, R., Mannina, G., 2015. Towards a new decision support system for design, management and operation of wastewater treatment plants for the reduction of greenhouse gases emission. Water (Switzerland) 7, 5599–5616.

Castro-Barros, C.M., Daelman, M.R.J., Mampaey, K.E., van Loosdrecht, M.C.M., Volcke, E.I.P., 2015. Effect of aeration regime on N2O emission frompartial nitritation-anammox in a full-scale granular sludge reactor. Water Res. 68, 793–803.

Chandran, K., 2011. Protocol for the Measurement of Nitrous Oxide Fluxes from Biological Wastewater Treatment Plants, in: Methods in Enzymology. Elsevier Inc., pp. 369–385.

Comas, J., Rodríguez-Roda, I., Sànchez-Marrè, M., Cortés, U., Freixó, A., Arráez, J., Poch, M., 2003. A knowledge-based approach to the deflocculation problem: Integrating on-line, off-line, and heuristic information. Water Res. 37, 2377–2387.

Daelman, M.R.J., van Voorthuizen, E.M., van Dongen, L.G.J.M., Volcke, E.I.P., van Loosdrecht, M.C.M., 2013. Methane and nitrous oxide emissions from municipal wastewater treatment – results

from a long-term study. Water Sci. Technol. 67, 2350.

Foley, J., de Haas, D., Yuan, Z., Lant, P., 2010. Nitrous oxide generation in full-scale biological nutrient removal wastewater treatment plants. Water Res. 44, 831–844.

Gray, N.D., Miskin, I.P., Korniova, O., Curtis, T.P., Head, I.M., 2002. Occurrence and activity of Archaea in aerated activated sludge wastewater treatment plants. Environ. Microbiol. 4, 158–168.

Griffith, D.R., Barnes, R.T., Raymond, P.A., 2009. Inputs of fossil carbon from wastewater treatment plants to U.S. Rivers and oceans. Environ. Sci. Technol. 43, 5647–5651.

Guisasola, A., de Haas, D., Keller, J., Yuan, Z., 2008. Methane formation in sewer systems. Water Res. 42, 1421–30.

GWRC - Global Water Research Coalition, 2011. N2O and CH4 emission from wastewater collection and treatment systems. London.

Henze, M., Gujer, W., Mino, T., van Loosdrecht, M.C.M., 2000. Activated Sludge Models ASM1, ASM2, ASM2d and ASM3. IWA Publ. 121.

IPCC, 2006. Guidelines for National Greenhouse Gas Inventories, Prepared by the National Greenhouse Gas Inventories Programme. Kanagawa.

Jeong, C., Kim, T., Lee, K., Song, S., Chun, K.M., 2009. Generating efficiency and emissions of a spark-ignition gas engine generator fuelled with biogas-hydrogen blends. Int. J. Hydrogen Energy 34, 9620–9627.

Kampschreur, M.J., Temmink, H., Kleerebezem, R., Jetten, M.S.M., van Loosdrecht, M.C.M., 2009. Nitrous oxide emission during wastewater treatment. Water Res. 43, 4093–4103.

Kampschreur, M.J., van der Star, W.R.L., Wielders, H. a., Mulder, J.W., Jetten, M.S.M., van Loosdrecht, M.C.M., 2008. Dynamics of nitric oxide and nitrous oxide emission during full-scale reject water treatment. Water Res. 42, 812–826.

Kolarik, L.O., Priestley, A.J., 1995. Modern techniques in water and wastewater treatment. CSIRO, East Melbourne, Vic., Australia.

Kreamer, D.K., 2012. The Past, Present, and Future of Water Conflict and International Security. J. Contemp. Water Res. Educ. 149, 87–95.

Law, Y., Jacobsen, G.E., Smith, A.M., Yuan, Z., Lant, P., 2013. Fossil organic carbon in wastewater and its fate in treatment plants. Water Res. 47, 5270–5281.

Law, Y., Ye, L., Pan, Y., Yuan, Z., 2012. Nitrous oxide emissions from wastewater treatment processes. Philos. Trans. R. Soc. B Biol. Sci. 367, 1265–1277.

Massara, T.M., Malamis, S., Guisasola, A., Baeza, J.A., Noutsopoulos, C., Katsou, E., 2017. A review on nitrous oxide (N2O) emissions during biological nutrient removal from municipal wastewater and sludge reject water. Sci. Total Environ. 596–597, 106–123.

McCarty, P.L., 1964. Thermodynamics of biological synthesis and growth, in: Procs. 2nd Int. Conf. on Water Pollution Control. pp. 169–199.

Monod, J., 1950. Technique for continuous culture - theory and application, Ann. Inst. Pasteur.

Monteith, H.D., Sahely, H.R., MacLean, H.L., Bagley, D.M., 2005. A rational procedure for estimation of greenhouse-gas emissions from municipal wastewater treatment plants. Water Environ. Res. a Res. Publ. Water Environ. Fed. 77, 390–403.

Neset, T.S.S., Cordell, D., 2012. Global phosphorus scarcity: Identifying synergies for a sustainable future. J. Sci. Food Agric.

Ni, B.J., Yuan, Z., Chandran, K., Vanrolleghem, P. a., Murthy, S., 2013. Evaluating four mathematical models for nitrous oxide production by autotrophic ammonia-oxidizing bacteria. Biotechnol. Bioeng. 110, 153–163.

Olsson, G., 2011. Water and Energy Nexus, in: Enciclopedia of Sustainability Science and Tehnology. Springer Verlag, Germany.

Pan, Y., van den Akker, B., Ye, L., Ni, B.J., Watts, S., Reid, K., Yuan, Z., 2016. Unravelling the spatial variation of nitrous oxide emissions from a step-feed plug-flow full scale wastewater treatment plant. Sci. Rep. 6, 20792.

Porpatham, E., Ramesh, A., Nagalingam, B., 2007. Effect of hydrogen addition on the performance of a biogas fuelled spark ignition engine. Int. J. Hydrogen Energy 32, 2057–2065.

Rodriguez-Caballero, a., Aymerich, I., Marques, R., Poch, M., Pijuan, M., 2015. Minimizing N2O emissions and carbon footprint on a full-scale activated sludge sequencing batch reactor. Water Res. 71, 1–10.

Tchobanoglous, G., Burton, F.L., H.D., S., 2014. Wastewater Engineering: Treatment and Reuse (5th ed), Metcalf and Eddy, McGraw-Hill series in civil and environmental engineering. McGraw-Hill, New York.

Tseng, L.Y., Robinson, A.K., Zhang, X., Xu, X., Southon, J., Hamilton, A.J., Sobhani, R., Stenstrom, M.K., Rosso, D., 2016. Identification of Preferential Paths of Fossil Carbon within Water Resource Recovery Facilities via Radiocarbon Analysis. Environ. Sci. Technol. acs.est.6b02731.

Tumendelger, A., Toyoda, S., Yoshida, N., 2014. Isotopic analysis of N2O produced in a conventional wastewater treatment system operated under different aeration conditions. Rapid Commun. Mass Spectrom. 28, 1883–1892.

Ulrich, A.E., Frossard, E., 2014. On the history of a reoccurring concept: Phosphorus scarcity. Sci. Total Environ.

Van Engelen, D., Seidelin, C., Van Der Veeren, R., Barton, D.N., Queb, K., 2008. Cost-effectiveness analysis for the implementation of the EU Water Framework Directive. Water Policy.

Van Meter, K.J., Basu, N.B., Veenstra, J.J., Burras, C.L., 2016. The nitrogen legacy: emerging evidence of nitrogen accumulation in anthropogenic landscapes. Environ. Res. Lett. 11, 35014.

Villez, K., Ruiz, M., Sin, G., Colomer, J., Rosén, C., Vanrolleghem, P.A., 2008. Combining multiway Principal Component Analysis (MPCA) and clustering for efficient data mining of historical data sets of SBR processes. Water Sci. Technol. 57, 1659–1666.

Voulvoulis, N., Arpon, K.D., Giakoumis, T., 2017. The EU Water Framework Directive: From great expectations to problems with implementation. Sci. Total Environ.

Water Environment Federation (WEF), 2010. Energy Conservation in Water and Wastewater Facilities - Prepared by The Energy Conservation in Water and Wastewater Treatment Facilities Task Force of the Water Environment Federation, MOP No. 32. ed. McGraw Hill, Alexandria, Virginia.

World Resources Institute (WRI), World Business Council for Sustainable Development (WBCSD), 2004. Greenhouse Gas Protocol: A Corporate Accounting and Reporting Standard. USA.

1.4. Web references

http://www.worldometers.info consulted on October 13th 2017

http://www.who.int consulted on October 13th 2017

http://geoffboeing.com consulted on October 13th 2017

http://www.fao.org consulted on October 13th 2017

https://water.usgs.gov consulted on October 13th 2017

https://data.worldbank.org/indicator/ER.H2O.INTR.PC consulted on October 13th 2017

http://www.un.org/sustainabledevelopment/sustainable-development-goals/ consulted on 15th November 2017

Chapter 2

2. Literature review

Abstract

Wastewater treatment consists in a sequence of combined treatment steps, that can include physical, chemical and biological processes and operations, aimed at removing suspended and dissolved contaminants from a water stream before discharge into the environment or direct reuse.

Among these steps aeration is needed for supplying the necessary O_2 to be reduced for the oxidation of dissolved organic and inorganic contaminants by means of the microbial community composing the AS. O_2 must be dissolved from the gas phase to the liquid, but its low solubility in water (only about 10 mg O_2 /L can be dissolved at atmospheric pressure and ambient temperature) makes this one of the most expensive processes in a WRRF (cfr. § 1.1.2).

Biological activity in AS tanks, and in every step of a WRRF making use of AS technology, is deemed to be responsible for most of the N_2O direct emissions of the plant. On their turn these emissions can represent a large fraction of the CFP of a WRRF, even surpassing the contribution of energy usage (cfr. § 1.1.3). The weight of different contributors to CFP can greatly vary from one plant to another depending on several factors.

Hence, the need for reliably monitoring and deeply understanding these processes so important for the sustainability and optimization of WRRFs.

In this chapter, the processes of oxygen transfer and N_2O production are described along with available measurement protocols discussing possible ways of improvements. The state of the art on modelling approaches is also presented with particular attention to available alternatives to the case of N_2O emissions. Finally, the WRRFs objective of some of the investigations in this work of thesis are introduced and described with particular focus on the biological tank.

2.5. Aeration efficiency

2.5.1. Aeration in biological tanks

For any AS process aeration is a fundamental step since it provides the biomass with the necessary oxygen in order to oxidize dissolved contaminants. The oxygen is transferred by shearing the water surface or bubbling air through macroscopic pores or porous material, always trying to create the maximum oxygen exchange rate between the gas and liquid phase. Obviously this represents a major energy demanding process for a WRRF and was estimated to range between 45 to 75 % of the plant's energy expenditure (Reardon, 1995). The increasing cost of energy since 1970 awoke the interest of researchers towards a more in depth understanding of aeration design, specification and operation. In order to reduce operating costs and CO_2 emissions in WRRFs, energy saving is generally recognized as one of the most effective methods (Libra et al., 2002).

At present, fine bubble diffuser is the most widespread technology in European and North American WRRFs. Fine bubble diffusers are known to offer numerous advantages as compared to coarse bubble aeration including energy savings which commonly fall within the range 30-40% (USEPA 1999; Cantwell et al., 2009). However, due to the chemical nature and morphology of the materials making up the membrane, they are subject to fouling and scaling, which can affect their operation and reduce the benefits of their utilization in the long term (Rosso and Stenstrom, 2006a).

2.5.2. Available protocols and instruments

The energy consumption of the aeration system depends on the efficiency of its components (e.g. diffusers and blowers), the tank geometry and the wastewater composition. Therefore, it is difficult to make a prediction on the behavior of an aeration system under process conditions as well as of the effects of process modifications (e.g. installation of a new aeration controller). In order to assess the aeration system performances in process conditions several methods have been developed over the years (ASCE, 1997, 1983; Boyle et al., 1989; Stenstrom et al., 2006). However, official standard guidelines are missing since 1997, given that the latest release from ASCE's literature on aeration efficiency testing only concerns measurements in clean water (ASCE, 2007).

The off-gas analysis method (Redmon et al., 1983) was developed for monitoring the aeration performance of submerged devices based on a simple mass balance between the inflated and off-gas oxygen contents.

When the humidity and CO_2 content of the gas stream are removed, assuming all other components of the air inflated by the aeration system are not changing their partial pressure during the passage into the biological tank volume, it is possible to calculate the actual mass fractions of oxygen to inerts (Redmon et al., 1983):

$$MR_{o/i} = \frac{Y_r}{1-Y_r-Y_{CO_2r}} \quad (2.1)$$

$$MR_{og/i} = \frac{Y_{og}}{1-Y_{og}-Y_{CO_2og}} \quad (2.2)$$

where $MR_{o/i}$ and $MR_{og/i}$ represent the molar ratio of oxygen to inerts in the inlet and off-gas respectively. Y_r and Y_{og} are the mole fractions of oxygen in the inlet and off-gas, while Y_{CO_2r} and Y_{CO_2og} are the mole fractions of CO_2. In the case of an air sample where moisture and CO_2, are wither scrubbed or measured, OTE can be calculated with Equation 2.3.

$$OTE = \frac{MR_{o/i}-MR_{og/i}}{MR_{o/i}} \quad (2.3)$$

Most of the research and application of the off-gas method remained within the USA until the beginning of the 90s. Seen the increasing interest in this measurement technique, the first developers were called by the American Society of Civil Engineer (ASCE) to define the first standard guidelines (ASCE, 1983). These standard guidelines presented different methods for aeration systems testing, among which the off-gas method appeared as a successful and user-friendly method for submerged aeration systems operating at process conditions but, at this stage, still in need for further testing. In this early version the guidelines brought up for the first time the concern of its application to low efficiency aeration systems. In these systems obtaining the needed accuracy might be difficult since the measurement error gains of importance. Since then, significant advances have been made in the development of new measuring devices for oxygen in the gas phase and this aspect has been mostly ignored in the following updates. Although the first concerns about the duration of the test (suggested >3 times HRT), the variability of some aeration parameters with the wastewater quality, the influence of mixing properties and of the tank geometry were raised, we need to wait for later updates of these guidelines for more precise indications on how to perform these tests on different basins (ASCE, 1997; Stenstrom et al., 2006).

The updated guidelines divide the off-gas method in two principal applications: i) the stationary 24h testing, with which a single point of the tank is monitored for 24h measuring the effect of influent and aeration fluctuation on oxygen transfer; ii) the point(s) test, where the entire area of the tank should be covered in space for assessing the quality of the aeration over the whole tank. The 24h minimum time has been set in order to cover the daily influent variability normally observable in a municipal WRRF. The suggested minimum area to be covered in the points test should reach at least 2% of the tank surface. The use of hoods covering 1.2-3 m^2 has been suggested.

The standardization of the OTE readings opened to new potentials for the applicability of the off-gas analysis. Typically, for clean water applications, results are reported as standard oxygen transfer efficiency (SOTE, %), referring to zero DO, zero salinity, 20°C as water temperature and 1 atm.

The results of about three years of testing in process conditions led to the selection of the most influencing parameters affecting oxygen transfer and therefore aeration systems performance, combined in the α (-), β (-) and θ (-) factors (Stenstrom and Gilbert, 1981).

The α factor, is defined as the ratio between the overall oxygen transfer coefficient in wastewater (k_La) and the one in clean water (k_La^*) (Equation 2.4). This difference between the two k_La is influenced by the presence of surface active agents (surfactants) and others contaminants affecting the shape of the bubbles and the turbulence at the interface which affects the overall mass transfer rate between gas- and liquid- phase (Hebrard et al., 2000; Rosso and Stenstrom, 2006a; Stenstrom and Gilbert, 1981). Ultimately, also the physical properties of the liquid together with its flowing regime have been observed to influence the k_La as coalescence or breakage can vary the bubble sizes and thus the available area for gas transfer (*a* coefficient). Viscosity in particular was observed to affect the shape of a bubble plume and thus increasing the chances that a bubble has to collide with a neighboring one (Fabiyi and Novak, 2008; Ratkovich et al., 2013).

The factor β, is defined as the ratio between the saturation DO concentration in wastewater (DO_s) and the saturation concentration in clean water (DO_s^*) (Equation 2.5). β is affected by several environmental and process conditions having an effect on the maximum saturation level of DO, among which salinity, temperature, pressure, suspended solids and dissolved matter (Stenstrom and Gilbert, 1981; Vogelaar et al., 2000).

The θ factor, also known as geometric temperature correction coefficient, is used to relate mass transfer coefficients to a standard temperature. Generally a value of 1.024 is suggested to be used, unless differently specified and strongly supported, but keeping temperature differences below 10°C for appropriate correction (Redmon et al., 1983).

For process conditions, efficiency results are normally shown as αSOTE (Equation 2.6).

$$\alpha = \frac{k_L a}{k_L a^*} \tag{2.4}$$

$$\beta = \frac{DO_S}{DO_S^*} \tag{2.5}$$

$$\alpha SOTE = OTE \cdot \frac{DO^*_{S_{20}}}{(\beta \cdot DO^*_{S_T} - C_i)} \cdot \theta^{(20-T)} \tag{2.6}$$

Applications of the off-gas method can serve to a wide spectrum of purposes (Gori et al., 2014) in systems using submerged aeration:

- increase knowledge of the air distribution system by measuring local air flow around the tank;
- support the design phase of new air distribution systems and new diffusers;
- monitor the loss of efficiency in process conditions of the aerators;
- measure the fouling state of diffusers;
- plan aerators cleaning;
- evaluate the efficacy of cleaning interventions and measure the recovery of the aeration capacity;
- compare different aerators cleaning methods for minimizing operational costs;

- evaluate the aeration control strategy and compare different solutions to minimize energy expenditures;
- evaluate the influence of different operational conditions (e.g. changing the biomass concentration in the biological reactor);
- calibrate the response of an aeration control in order to optimize energy requirements during low and high load periods.

At present, to the author best knowledge, the only commercially available product of the off-gas analysis is the ALPHAMETER® (INVENT, Germany) which is claimed to be able to be directly implemented in the real time control of the aeration system. This instrument is equipped with a DO and temperature sensor along with a gas analyzer for measuring the oxygen content in the off-gas. However, given the relatively small size of the hood (apparently ranging on about 1-2 m^2) and the fact that it is installed on a fixed position, its applicability might arise some concern.

2.5.3. Pro and cons of current approach

The off-gas method has been proven to be so far the most straightforward and less intrusive method for in-process testing of oxygen transfer efficiency. In fact, the off-gas analysis is an effective technique that offers numerous advantages for testing submerged air diffusion systems (*inter alia* Capela et al., 2004; Iranpour et al., 2000; Redmon et al., 1983). It enabled the comparison of different types of diffusers (Libra et al., 2002) and their operation in different conditions (Libra et al., 2005). It has even been applied for predicting nitrification performances (Leu et al., 2010), to evaluate the design of aeration systems (Rosso et al., 2012), and to derive important relations between influent dynamics, aeration regimes and aeration efficiency (Rosso et al., 2005).

The current approach to the off-gas analysis has gained popularity for some main reasons:

- Flexibility and ease of application
- Fast results output
- Relative low cost of basic equipment
- User friendly character of the application
- Allows for the comparison of different aeration systems in process condition
- Does not require process interruptions for the execution of the measurements

On the other hand the main general limitation of the off-gas method can be summarized as:

- Not applicable for surface aeration systems;
- Not all tanks have sufficient accessibility by the personnel to easily and safely deploy instrumentation;
- Scum formation can deviate the gas exit from the surface and bias measurements;
- Turbulences can create problems in correctly placing the floating hood;
- It is necessary to entirely remove CO_2 and humidity from both the ambient air (for reference measurements) and the off-gas.

In addition to this, main limitations to the current ASCE protocol are represented by the variability of the influent relatively to the dimensions of the tank. In fact, fluctuation of influent flow and

composition are occurring every day in almost all WRRFs and these fluctuations can influence the efficiency measures in each point. Regarding the dimensions of the tank, the ASCE standard suggests to cover at least 2% of the tank which has been observed to be not sufficient to reach a sufficient level of detail when e.g. nature and location of a damage has to be detected (Iranpour et al., 2000).

Finally, the accuracy of the sensors (i.e. DO and temperature) might have an effect on the calculation of the αSOTE. It is true that the technology advances have resulted in very precise and reliable instruments, however, in order to be able to fairly compare aeration devices at low efficiencies, this error might be considered at least by defining its magnitude and perform an error propagation analysis.

2.5.4. Modelling oxygen transfer

In 1923 the two-film theory has been firstly proposed starting the process of replacing the sharp demarcation of boundary layers that was so far assumed (Whitman, 1962, 1923). Nowadays the two-film theory is the most widely used model for representing the passage of a compound from one phase to another. It is based on the assumption that two stagnant layers, one at each side, exist when gas and liquid phases come to contact. This assumption is valid at steady state, however, in reality these layers are renewed by the movement of the bulk liquid, hence the surface renewal theory (Higbie, 1935). This resulted in one of the solutions to calculate the oxygen mass transfer coefficient k_L (m/s) (Equation 2.7)

$$k_L = 2 \cdot \sqrt{\frac{D}{\pi \cdot t_e}} \tag{2.7}$$

The oxygen mass transfer coefficient is function of the diffusion coefficient D (m^2/s) and the mean bubble residence time t_e (s). Having a certain surface of the gas-liquid interface A (m^2) available for exchange in a defined liquid volume V (m^3), an overall oxygen transfer coefficient can be defined as k_La (h^{-1}).

$$k_L a = k_L \frac{A}{V} \tag{2.8}$$

Therefore, for a gas bubble immersed into a liquid, the exchange of oxygen per unit of time between the gas phase and the liquid phase can be described by Equation 2.9.

$$\frac{dC_i}{dt} = k_L a(DO_s^* - DO_i) \tag{2.9}$$

Where DO_s^* (mg/L) is the DO in clean water at saturation and DO_i (mg/L) the DO concentration in the bulk liquid at time t.

The speed with which the oxygen is dissolved in water is function of the difference between the actual concentration and the saturation concentration, but is also strongly dependent of the physical and geometrical properties of the control volume.

Influences on k_La and generally applied aeration modelling

The various testing and developments of the off-gas method led also to the definition of relations for important parameters in aeration efficiency, e.g. the use of the temperature correction factor for the mass transfer coefficient (Equation 2.10).

$$k_L a\,(T) = k_L a\,(20°) \cdot \theta^{T-20} \qquad (2.10)$$

The general agreement in the variable nature of the alpha factor pushed towards the use of the off-gas measurement for understanding its variability. The accumulation on the gas-liquid interface of surfactants has been observed to induce two major problems: the increase in rigidity of the interface and a decrease in the internal gas circulation of the bubble which have a direct effect on the diffusion coefficient and therefore on the k_La (Ferri and Stebe, 2000; Rosso and Stenstrom, 2006b)

Figure 2.1 shows values of α factors measured for different aeration devices with regard to the respective interfacial flow regimes (expressed by means of the Reynolds (Re) number). In the region of fine bubble aerators operation, diffusional transport is the driving force for mass exchange and the gas transfer is controlled by surfactant interfacial migration. In this range of flow an increase in Re leads to increased surfactants transport to the interface which decreases the α factor. With regard to coarse bubble diffusers and high shear aerators (surface aerators and turbines), operating in the turbulent flow domain, an increase in Re results in an enhanced surface renewal rate and therefore in higher α values (Garner and Hammerton, 1954; Rosso and Stenstrom, 2006b). However, it must be pointed out that the variability in α factor for a given Re value is considerably high, meaning that more mechanisms are in play.

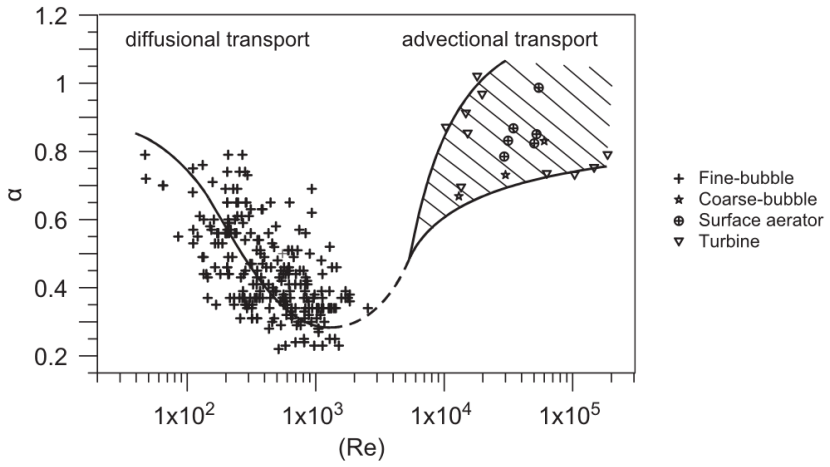

Figure 2.1 - α factors at different flow regimes (defined by the Reynolds (Re) number) for different aerator types. Adapted from (Rosso and Stenstrom, 2006a).

The mean cell retention time, or SRT, has been observed to be related to the evolution of the α value. In fact, SRT comprehends in some way the degree of degradation of contaminants in the wastewater, and therefore also of surfactants. The increase of α observed with increasing SRT have suggested that, a higher contaminants degradation ameliorated the oxygen transfer. However, some

discrepancies have been observed between the two parameters for plants working with comparable SRTs (Groves et al., 1992; Rieth et al., 1995; Rosso et al., 2005; Wagner, 1999). The parameter χ (s^2) and the regression coefficients for the α factor and aeration efficiency prediction (Equation 2.11, 2.13 and 2.14) have been defined after regression analyses of a large dataset of aeration efficiency collected in full-scale with the off-gas technique over a period of fifteen years (Rosso et al., 2005).

$$\chi = \frac{SRT}{Q_{air}} \tag{2.11}$$

$$Q_{air} = \frac{AFR}{a_{spec} \cdot N_d \cdot Z} \tag{2.12}$$

$$\alpha = 0.172 \cdot log\chi - 0.131 \tag{2.13}$$

$$\alpha SOTE = 5.717 \cdot log\chi - 6.815 \tag{2.14}$$

where AFR (m^3/s) is the air flow rate, a_{spec} (m^2) is the diffuser specific area, N_d is the total number of diffusers, Z (m) is the diffusers submergence and Q_{air} (s^{-1}) is the resulting normalized air flux. Figure 2.2 shows the efficiency parameters α and αSOTE (reported per meter of tank depth) in function of Q_{air} and SRT (reported as MCRT) for different aerator types, a subset of data used in the design of the aeration model just described (Equation 2.11-2.14).

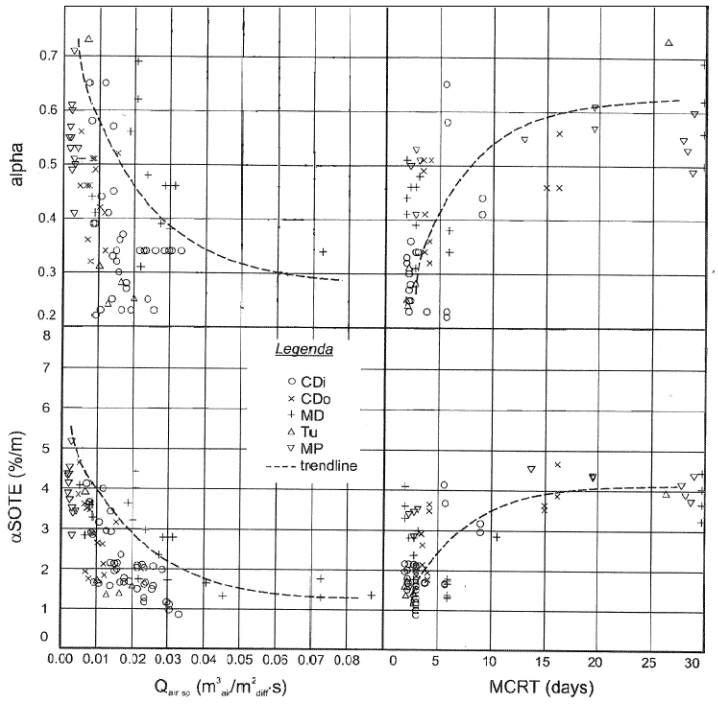

Figure 2.2 - Efficiency parameters in function of the normalized air flow rate and mean cell retention time (MCRT or SRT). CDi: ceramic discs; CDo: ceramic domes; CP: ceramic plates; MD: membrane discs; Tu: ceramic, plastic and membrane tubes; MP: membrane panels (Rosso et al., 2005).

Apparently, up to 30 % of the variability in the α value cannot be explained due to the several interactions taking place in the mass transfer process and to the lack of knowledge regarding the effect of aerator submergence (Gillot and Héduit, 2008). In order to take into account the effect of diffuser submergence the ECT, the residence time of a bubble in the liquid, was included in the prediction of α along with SRT and airflow rate (Gillot and Héduit, 2008). Although ECT seems to combine most of the generally known factors having an effect on mass transfer, for this method a calculation or estimation of the $k_La^*(20°)$ is necessary a priori complicating the application in predictive aeration models for WRRFs. However, this is one of the most accurate models available in literature, and one important advancement in the description of the oxygen transfer in WRRF modelling.

The lack of understanding on the variability of the α factor hampers significantly the applicability of aeration models. The assumptions and simplifications that characterize these models, affect the calibration of the biokinetic model. The use of in-process measured efficiencies (in different parts of the aeration system) as inputs to the WRRF model, has shown to improve the level of detail in the different sub-models so that the calibration step might be negligible (Amerlinck et al., 2016). In this view, the aid of detailed hydrodynamic studies with Computational Fluid Dynamics in improving the design of model layouts of current WRRF model configuration, may profoundly change the landscape of process modelling. The increase of detail that can be acquainted for by a better description of the hydrodynamic behavior of the tank might be very helpful in increasing the needed level of detail (Rehman, 2016).

The large uncertainties in the prediction of oxygen transfer have led to discuss the description of the aeration with a more holistic approach. A selection of the most promising techniques for aeration systems modelling has been proposed with the aim of increasing the level of detail describing the whole aeration systems (Amaral et al., 2017). Modelling the whole aeration system from the generation (i.e. blowers and distribution net), to the point of release of the bubbles (the aerator), and finally in the evolution of the bubbles size through the bulk liquid, can represent one of the new frontiers in increasing descriptive power of oxygen transfer.

2.6. N_2O production and monitoring

N_2O, at ambient temperature and pressure is a non-flammable gas, colorless, with a slight sugary smell, also known as “laughing gas” due to its euphoric effects has analgesic and anesthetic applications. Nonetheless, N_2O has a GWP 265–298 times that of CO_2 for a 100-year timescale (IPCC, 2013) which makes this the single most important ozone depleting compound of our century (Ravishankara et al., 2009). Anthropogenic activity is responsible for about 40% of the global N_2O production and a 15% concentration increase has been observed since 1750 (IPCC, 2013). N_2O emitted today remains in the atmosphere for more than 100 years, on average (http://EPA.gov). This makes N_2O a concern also in WRRFs.

2.6.1. N_2O production in WRRFs

Production of N_2O in activated sludge is caused by both heterotrophic (OHO) and autotrophic bacteria (AOB and NOB). It is influenced by several operational parameters and local conditions:

e.g., DO, NO_2^- concentrations, NH_4^+ loading rate, pH level and salinity in case of AOB; DO, NO_2^- concentration, and COD/N ratio in case of OHO (Kampschreur et al., 2009).

During nitrification, AOB (predominantly) convert NH_4^+ to NO_2^-, and NOB convert NO_2^- to NO_3^-. Although N_2O is not an intermediate in this process, AOB can produce N_2O during this step via three pathways (Law et al., 2012):

1) *NH_2OH oxidation:* NO reduction produced in NH_2OH oxidation during the conversion of NH_4^+ to NO_2^- (Law et al., 2012; Stein, 2011);
2) *NOH Chemical decomposition:* the unstable NOH is chemically decomposed during NH_2OH oxidation in the conversion of NH_4^+ to NO_2^- (Chandran et al., 2011; Law et al., 2012);
3) *AOB denitrification:* NO reduction from NO_2^- (Bock et al., 1995; Chandran et al., 2011; Kampschreur et al., 2009).

Production during nitrification

Accumulation of NO_2^- during the nitrification process can enable N_2O production through AOB denitrification when DO is limiting, as AOB can utilize NO_2^- as the electron acceptor rather than oxygen (Bock et al., 1995; Kampschreur et al., 2009). In addition to this, lower DO concentrations can also lead to higher NO_2^- concentrations due to the difference in oxygen half-saturation constants between AOB and NOB (Hanaki et al., 1990; Mota et al., 2005).

A series of batch experiments conducted by Tallec et al. (2008) on AS at different DO levels, 0.0, 0.4, 0.7, and 1.1 mg O_2/L, allowed to track N_2O production by both heterotrophic denitrification and AOB denitrification by use of inhibitors. At zero oxygen, N_2O production was 100% by heterotrophic denitrification, and quickly shifted towards mainly AOB denitrification once oxygen was introduced into the experiments.

N_2O production in presence of high DO levels, has been linked to higher NH_4^+ oxidation rates (AOR) and higher N_2O production by AOB via NH_2OH oxidation (Law et al., 2012) due to the chemical decomposition of NOH. These two pathways can be fueled in full-scale WRRFs by the action of NH_4^+ controls, which increases DO as NH_4^+ increases. This can result in conditions of non-limiting DO and non-limiting NH_4^+, which can lead to higher N_2O.

Production during denitrification

Denitrification, the reduction of NO_3^-, NO_2^-, NO, and N_2O, is performed by different microorganisms coupling it with the oxidation of organic and inorganic compounds used as substrate (Kampschreur et al., 2009). Generally, heterotrophs are the primary responsible for completing this reaction, however, depending on local conditions the denitrification process can be interrupted by the intercurrence of different consortia such as AOB. For completing this reaction, N_2O should be finally reduced to nitrogen gas (N_2) unless low COD:N ratio (Ahn et al., 2010b; Foley et al., 2010; Kampschreur et al., 2009), high NO_2^- concentraties (Ahn et al., 2010; Foley et al., 2010; GWRC, 2011; Kampschreur et al., 2009), and high DO concentrations (Kampschreur et al., 2009; Von Schulthess et al., 1994) influence this last step accumulating N_2O and thus fueling its emission.

During denitrification it is known, at the biological level, that high NO_2^- concentrations can provide faster renewal for the NO_2^- reductase and reduction of NO_2^- to N_2O, while the presence of DO can

inhibit heterotrophic denitrification (Nos enzyme), also leading to N_2O production (Von Schulthess et al., 1994). FNA and FA have been observed to inhibit NOB activity already at 0.1–1.0 mg/L and 0.2– 2.8 mg/L, respectively (Anthonisen et al., 1976). Svehla, Bartacek, et al. (2014), significantly exceeding NOB-inhibiting concentrations of FA and FNA, observed adaptation in a CSTR as compared to a SBR showing NOB-inhibition. On the other hand, FNA is used for sludge treatment and has been reported that the enzymes relevant to nitrifier denitrification were inhibited, decreasing the microbial community diversity, but increasing the abundances of AOB and denitrifiers, ultimately reducing N_2O emissions (Wang et al., 2016). Finally, despite the need for an increase in external carbon source, excluding the anaerobic phase of an SBR promoted heterotrophic denitrifiers to be responsible for aerobic nitrogen removal instead of AOB, reducing N_2O production by heterotrophic denitrification (Chen et al., 2014).

Extent of emission

Due to the complexity of the N_2O formation process and to the influence of several operational parameters on such processes, N_2O emissions from WRRFs vary substantially among plants, ranging from negligible to substantial, depending on the different process design and operating conditions (Law et al., 2013). Based on field-scale measurements, continuous flow biological nitrogen removal processes could emit up to 7% of the influent nitrogen load as gaseous N_2O and NO (Guo et al., 2013; Kampschreur et al., 2009, 2008b; Law et al., 2013; Peng et al., 2014), typically peaking in the first aerated compartment of the biological process, where the N_2O produced during nitrification is emitted together with the stripping of the carryover of the N_2O produced during denitrification.

Autotrophic nitrogen removal processes from N-rich residual streams have been observed to emit up to 6% of the incoming N-load as N_2O (Desloover et al., 2012). Domingo-Félez et al. (2014) showed that single-stage nitritation/anammox reactors could generate N_2O emissions higher than 6% of incoming TN. Similarly, Li et al. (2017) addressed most of the emission to the denitrification step.

2.6.2. Measurement protocols

The first protocol for accounting for GHG emissions from WRRFs was proposed by the Intergovernmental Panel on Climate Change (IPCC, 1995). At that time, the available knowledge of GHG emissions from the processes involved in a WRRF was quite immature, and the protocol, which was later adopted by the U.S. Environmental Protection Agency (USEPA, 2001), assumed a CH_4 EF based on incoming BOD and flow.

Monteith et al. (2005) set up a rational procedure for estimating carbon-based GHG emissions from WRRFs taking into account the treatment train of plants, thus leading to a much more accurate GHG emission estimate than the IPCC protocol.

The first IPCC protocol was then updated in 2006 (IPCC, 2006), although it still neglected or underestimated some GHG contributions (e.g., CH_4 emissions due to the incomplete combustion of digester biogas, CH_4 fugitive emissions from settling, thickening or dewatering sections, N_2O emissions due to nitrification/denitrification, and CO_2 emissions from organic matter degradation).

In the same year, the California Energy Commission (CEC, 2006) proposed a more refined document with the main assumption that all the N_2O emissions originate from the discharged wastewater. Finally, the protocol adopted by the USEPA (2007), based on the procedure proposed by the IPCC, finally takes into account the N_2O emission due to the nitrogen content in biosolids. The three protocols discussed above proposed an assessment method of GHG production merely based on EFs. These EFs were estimated considering a generic WRRF without including important characteristics of the plant (e.g., hydraulic retention time or sludge retention time). Over the years, several studies have been performed in order to establish EFs based on field data. These EFs, based on global averages for consistency and for lack of better published literature, exhibit the limitations of being associated with generalizations, such as the amount of biodegradable carbon, expressed as BOD generated per capita and per year, without any consideration on the process specific information which were emerging as having crucial importance (i.e., process configuration, retention time, reactor geometry, existence of tank cover, etc.). With regard to N_2O emissions, given the high variability observed within the same WRRFs (Aboobakar et al., 2013; Daelman et al., 2015), the use of fixed EFs is strongly in contrast to current knowledge as it overlooks the variability of process conditions.

Field measurements were indicated as a key element for improved estimations based on site-specific operating parameters and processes (Chandran, 2011). In 2011, the Global Water Research Coalition published two reports (scientific and technical) on N_2O and CH_4 emissions from WRRFs as a result of an extensive monitoring study conducted on real WRRFs in Australia, France, USA, and Netherlands, where different protocols for measuring GHG emissions were adopted (GWRC, 2011). On the basis of the results obtained in the aforementioned studies, Chandran et al. (2011) proposed a protocol for assessing N_2O emissions. This protocol has the advantage of combining the information obtained from the real-time measurements of hood-headspace N_2O concentrations with those obtained from discrete measurements of N_2O concentrations in the liquid phase. Additionally, it also takes into account the direct measurement of the advective flow rate at the hood-headspace. The significant amount of data that have to be collected for employing this protocol enable an accurate quantification of N_2O emissions. However, this protocol requires a sweeping gas on site for measurements and relies on the assumption that the sweeping gas flow is small in proportion to the surface stripping or volumetric flow. This assumption can be adequate for volumetric flows, such as those in aeration tanks, but may be error prone on the surface of non-aerated tanks. The application on non-aerated tanks, in fact, is possible if the wind profiles are taken into account and local ambient air conditions are maintained as close as possible to the natural ones (Caivano et al., 2017), implying a different wind-induced surface evaporation compared to that of the confined measurement of flux chambers. In Table 2.1, a summary of the main existing protocols for GHG emissions from WRRFs is provided with the relative description.

Table 2.1 – Overview of the main protocols for assessing GHG emissions from WRRFs

Reference	Sample type	Gas flux measurement	Use Emission Factor	GHGs	Remarks
IPCC, 2006	None	No	Yes	N_2O, CH_4	GHG emissions estimated based on EFs associated with specific populations and type of WRRFs. N_2O emissions from treated wastewater discharged in receiving water body are considered as main contribution.
CEC, 2006	None	No	Yes	N_2O, CH_4	Simplified version of the IPCC protocol (IPCC, 2006). Assumes that all N_2O emissions are originated from the WRRF effluent neglecting nitrification-denitrification contributions.
USEPA, 2007	None	No	Yes	N_2O, CH_4	Based on IPCC (2006). For N_2O emissions, also nitrogen content in biosolids is considered.
GWRC, 2011	Gas, liquid	Yes	No	N_2O, CH_4	Based on full-scale data (measured in WRRFs in Australia, France Netherlands and USA) to establish new emission factors other than the IPCC ones. Gas and liquid N_2O measurements.
Chandran, 2011	Gas, liquid	Yes	No	N_2O	Combines information of: I) online measurement of headspace N_2O concentrations; II) discrete measurements of N_2O concentrations in the liquid. Considers direct measurements of the advective flow rate of headspace.

Despite the potential of the existing resources available in literature for accounting for GHG emissions from WRRFs, there are still relevant differences among protocols, toolboxes, and methods (Caniani et al., 2015). This is also visible in the heterogeneity of calculation methods for defining the EF and in the lack of indications on the spatial and temporal sampling strategy (Massara et al., 2017).

Temporal variations have been observed to significantly impact (seasonally and daily) the assessment of EFs, and online sampling has been observed as necessary in order to sufficiently capture variability (Daelman et al., 2015). However, once this variability is captured, it is not reflected in the final EF, mostly resulting in a mere average of large datasets including peaks and valleys of emission. In this view, the potential and the meaning of online measurements is in large part wasted. Extensions to the concept of the EF are needed in order to make comparable estimates among plants (Massara et al., 2017).

Spatial variations, are also important and discrepancies in recognizing the highest emitting section of a WRRF often occur (Caivano et al., 2017; Chandran, 2011; Marques et al., 2016), due to the fact that N_2O emissions are very much specific to the treatment technology used, how the process is controlled, and of the wastewater composition (Ahn et al., 2010a; Kampschreur et al., 2008a). Nonetheless, local differences in substrates concentration within the same tank can lead to important variabilities (Rehman, 2016), warranting key considerations for designing an ad-hoc sampling strategy for a correct EF assessment.

Aerated compartments are considered to be the greatest contributors to N_2O in a WRRF (Chandran, 2011); however, although more troublesome to measure, anoxic zones also represent a central source (Ahn et al., 2010b). Emissions from non-aerated tanks or tanks using surface aeration are often neglected in literature or poorly investigated due to the lack of adequate methodologies for assessing emissions from these areas. However, in some cases they have been documented as a significant source of N_2O emissions (Ahn et al., 2010b; Caivano et al., 2017). The Global Water Research Coalition (GWRC) (2011) reported 12 studies revealing an important contribution of anoxic zones to both production and emission of N_2O. At present, we can affirm that the monitoring of both aerobic and anoxic sections is often suggested (Marques et al., 2016) and these locations should not be discarded a priori.

Unless a fully-covered WRRF is available and a single sampling point can be selected for assessing an overall EF (Daelman et al., 2013; Kosonen et al., 2016), conditions are highly variable depending on process conditions and hydrodynamics (Amerlinck et al., 2016; Guo et al., 2013). The high variability of N_2O emissions has provided a fertile ground for the scientific debate on the correct definition and use of an EF (Massara et al., 2017), but no common agreement seems to be yet achieved, also due to the lack of understanding of emission variability. This is crucial in understanding which of the N_2O pathways will be dominant and in order to properly tackle its emission by developing aimed reduction strategies.

2.6.3. Instrumentation for online monitoring

Gas measurements

N_2O emissions from WRRFs are variable over time both on the short (hourly and daily) and long term (seasonal). N_2O emissions are variable within process tanks as well, due to variability of both off-gas flow rate and/or N_2O production in the liquid phase. Hence, the importance of having a user friendly, flexible and reliable instrumentation.

In order to appreciate diurnal variations, online and high-frequency devices are normally used in the literature. Continuous online monitoring of N_2O has been employed in recent years in order to quantify the emissions from WRRFs (*inter alia:* Czepiel et al., 1995; Daelman et al., 2013). Online sensors include infrared (IR) analyzer (*inter alia:* Desloover et al., 2012; Law et al., 2012b), chemiluminescence (Kampschreur et al., 2008a), and a Fourier transform IR analyzer (Joss et al., 2009). The use of the IR analyzer is the most common solution in the literature, due its measurement accuracy and the ease of operation. For example, the IR Multi-gas Monitor model 1312/5 (Innova, Italy) detects the concentration of gas mixtures with a limit of detection of 0.03

ppmv for N_2O and 0.4 ppmv CO_2 at 20°C and 1 atm with a measurement frequency up to 1/80 s. Other examples are X-STREAM (Emerson, USA) and Model 46i (ThermoFisher Scientific, USA). The robustness and user-friendly character of an IR technology is really advantageous for field applications.

A valid alternative to the IR technology is GC. Micro-GC portable analyzers for field online measurements are available on the market. The latter can be equipped with two columns, divided into two parallel channels (one using a PoraPlotQ column and the other using a Pulsed Discharge Ionization Detector), for having the best resolution over N_2O and CO_2 readings. The analytical performance is ensured by the chromatographic technology allowing for components' separation and, resolution below the ppm. Although it is not yet as popular as IR based tools, the micro-GC is characterized by a compact design that makes it as portable as other online monitoring equipment. However, the availability onsite of a cylinder having the carrier gas can be a limitation of its operation. In addition to this, operating a GC requires technically advanced skills to be properly operated and this might be limiting its applicability as compared to IR. On the other hand, the range of measurable compounds for a micro-GC is sensibly above the possibilities of the most advanced acoustic IR. It is noteworthy that the cost of a micro-GC is generally half of that of an acoustic IR.

Liquid measurements

To the best of the author's knowledge, the only online sensor for liquid measurements of N_2O is provided by Unisense (Denmark). This instrument allows for high frequency measurements adjusted for temperature and provides the possibility to integrate the system in an online control of the full-scale plant. The resolution of the sensor is 0.01 mg $N\text{-}N_2O/l$ which is perfect for WRRF applications. Major drawbacks of the instrument are that the sensing part needs to be replaced every 8 months and bi-monthly calibration is needed, representing significant operational costs.

Alternatives to this method are based on the extraction of N_2O to the gas phase and subsequently quantifying the extracted gas by means of GC (Mampaey et al., 2015; Thaler et al., 2017). These methods are obviously more troublesome to use during an online monitoring of a full-scale WRRF since a whole set of laboratory equipment is needed on site. However, they can be applied for offline measurements after stabilization of the liquid sample with H_2SO_4.

2.6.4. Modelling N_2O production

Mechanistic models

The mathematical representation of biological mechanisms has been largely used in order to increase the insight of complex biological processes and interactions. In wastewater treatment, these models are integrated in the framework of the ASM concept started in the 80's under the guidance of what currently became the IWA. To date, ASMs have been largely applied to full scale cases for a wide variety of purposes, e.g. process and design optimization, scenario analysis, etc. (Gernaey et al., 2004).

ASM1, ASM2, ASM2d and ASM3 (Henze et al., 2000) are the most known and widely applied versions of these models and represent the basis for developing new extended versions that include e.g. N_2O production. ASM1, the first version of its series, was developed primarily for municipal

activated sludge WWTPs to describe the removal of organic carbon compounds and nitrogen, with simultaneous consumption of oxygen and nitrate as electron acceptors. However, this model presented some important limitations that later versions tried to cope with. ASM2 forms a basis for modelling bio-P removal by extending ASM1. ASM2d extends ASM2 by including denitrifying activity of PAOs for a better description of phosphate and NO_3^-. ASM3 includes storage polymers in heterotrophic activated sludge conversions.

These models have been extended for N_2O production including one or more of the pathways described earlier in this chapter and a detailed review of the available models has been provided by Ni and Yuan (2015). Understanding of complex mechanisms of N_2O formation has been significantly boosted by coupling laboratory experiments with ASMs (Peng et al., 2015). On the other hand, mechanistic models have considerably increased the detail of description of these biochemical processes thanks to laboratory controlled experiments in which the single pathway of N_2O production has been isolated (Ni et al., 2014). This synergistic approach has led to an in-depth evolution of available models for N_2O production. Most advanced N_2O models have been developed in controlled situations and have been successful for lab scale studies to understand mechanisms in small scale, however, they are often not fully operational at full scale due to over-parametrization and high parameter correlation (Ni et al., 2013, 2011).

In the framework of the ASMs, general consensus is found on Hiatt and Grady's ASMN model (Hiatt and Grady, 2008) of four step heterotrophic denitrification which includes N_2O as an intermediate. More complex mechanisms, such as AOB pathways, have been also integrated to this model including N_2O and NO production due to AOB (Mampaey et al., 2013). ASMG1 is the result of the combination of heterotrophic denitrification and AOB denitrification pathways (Guo and Vanrolleghem, 2014) with an updated DO kinetic term for considering that for N_2O production by AOB denitrification, a maximum rate occurs at relatively low DO conditions (Ni et al., 2013; Yu et al., 2010). This term is represented by modified Haldane kinetics and is used in AOB denitrification of NO_2^- to NO and finally to N_2O. A further extension of the ASMG1 model is the ASMG2d, extended for COD/N/P removal. These models count 18 state variables and 15 processes, contains the subdivision of autotrophic biomass into AOB and NOB and the distinction between different nitrogen species (i.e. NO_3^-, NO_2^-, NO, N_2O and N_2). This increase of detail in the biological mechanisms resulted in a total of 62 kinetic parameters. Guo and Vanrolleghem (2014) provide a detailed matrix for all the process kinetics and relative parameters values.

Massara et al., (2017) gives a broad overview of available models and their latest findings, suggesting the use of multi-pathway N_2O production models but also rises concerns about their calibration in full scale. ASMG1 and ASMG2d represent two of the few models available that have been calibrated and validated in full-scale (Guo, 2014; Guo and Vanrolleghem, 2014). However, concerns about the high variability of some relevant parameter through the literature has been raised (Spérandio et al., 2016). This further confirms that the level of detail in the mechanistic sense has reached a very high level, but the full-scale application requires process knowledge regarding local concentration that is currently lacking (Rehman, 2016). The current Tanks In Series (TIS) configuration is yet the most commonly used layout for representing the biological volume of a WRRF. However, complete mixing is unlikely to occur in a biological tank of a WRRF and recent

research focused on including hydrodynamic information in changing a TIS with a CM configuration. A CM is a representation of a biological tank with a conceptual network of spatially localized compartments. These compartments, are connected through convective and exchange fluxes, all based on preliminary detailed hydrodynamic modelling based on Computational Fluid Dynamics (Rehman et al., 2017). The use of a CM can take into account those local conditions and recirculation patterns in the AS tank that are important with respect to the modelling objective.

Knowledge based N_2O models

Alternatives to mechanistic models have been developed in the past for process optimization, understanding and even for control of WRRFs. A knowledge-based system has been used to identify the most suitable train of treatment of a certain wastewater based on its composition (Krovvidy et al., 1991). Integrated supervisory architectures have been presented for the supervision of WRRFs to overcome control bottlenecks (Manesis et al., 1998; Sànchez-Marrè et al., 1996). One of the first implementations of a knowledge-based system to support the operation of a real WRRF have been proposed by Rodríguez-Roda et al. (2002), reporting 3 years of successful support to the operation of a WRRF and indications on transferability of the technology. Following this, a knowledge based system was applied to a full-scale WRRF to target deflocculation problems (Comas et al., 2003).

In this view, and for the crescent demand of solutions aimed at reducing N_2O emissions, a new knowledge-based application integrated with fuzzy logic has been developed (Porro et al., 2014). This model, the risk model, was proposed for making use of the available knowledge in the literature and interpolate it with plant data for extracting information on the principal pathways responsible for N_2O formation. The risk model applies fuzzy logic and knowledge-based systems to process variables (e.g. DO, NO_2^-), to mimic the human reasoning process for evaluating the risk of producing N_2O in WRRFs.

Data mining

Data mining solutions have been used in wastewater treatment in particular for process control optimization. Given the amount of data generated from today's WRRFs, the amount of hidden information can be relevant and potentially represent a valuable return of material to the capital investment of placing a SCADA system.

Literature shows that aeration system control has been aided by a data-driven approach that considered information from both the control system and water quality data (Asadi et al., 2017). However, not many practical applications of data mining on full-scale WRRFs are reported in literature other than PCA.

PCA has been often used for process understanding, monitoring (fault detection), and control of industrial processes such as wastewater treatment (Gernaey et al., 2004). The principle of PCA is to reduce the amount of information available to a smaller number of variables (PCs) capable of explaining most of the variance of the dataset. In this way, it is possible to unravel hidden dependencies among known key variables. MPCA, a variant of PCA, has been used for process monitoring, and interpretation and analysis of sequencing batch reactors process behavior (Lee and Vanrolleghem, 2003; Villez et al., 2008).

Despite today's availability of large amounts of WRRF data and of tools for data mining, to the best of the author knowledge, documented application of these techniques to WRRF is absent when N_2O-is concerned.

2.7. Description of the WRRFs objective of the study

Eindhoven

The WRRF of Eindhoven (The Netherlands) is the third largest in the country and is operated by Waterboard De Dommel. Designed to treat the wastewater of 750,000 (250k m^3/d) inhabitant equivalents (IE) with a load of 136 gCOD/d/IE, the plant is composed of three parallel treatment lines equipped with one primary settler, one bioreactor and four secondary sedimentation tanks (Figure 2.3). The treated effluent is then discharged into the relatively small river Dommel.

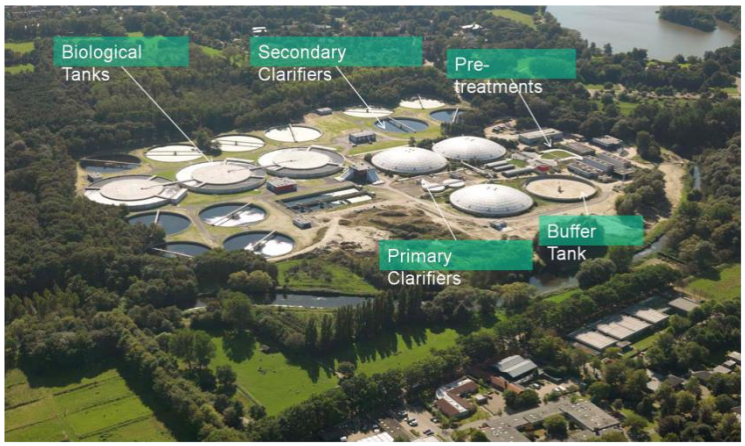

Figure 2.3 - Aerial view of the WRRF of Eindhoven and its main process units.

Each bioreactor (Figure 2.4) is designed according to the UCT layout and consists of one anaerobic tank (inner ring), one anoxic tank (middle ring) and one aerobic/anoxic tank (outer ring), all operating in plug-flow configuration. The pre-settled wastewater enters the inner (anaerobic) ring of the bioreactor and is directed around four sub-divisions ensuring its plug-flow operation. After the fourth compartment of the inner ring, the mixed liquor is directed to the middle (anoxic) ring through an opening at the bottom of the tank. At this point the AS is circulated, with a retention time of 3.5 h, by means of impellers. An overflow located at the outer wall of the middle ring is feeding the outer (aerobic/anoxic) ring of the bioreactor, while a recirculation pump returns a fraction of the mixed liquor (recycle A) to the inner ring for P removal. In the outer ring, alternated aerobic and anoxic zones are maintained. Three pairs of impellers located on three bridges around the outer ring ensure a minimum of 0.25 m/s mixed liquor flow velocity in order to prevent settling of the AS flocs (Bosma et al., 2007). The AS exits the outer ring via an underflow located at its outer wall after the summer package (cascade outflow) while a fraction of the mixed liquor is recycled back into the middle ring for denitrification.

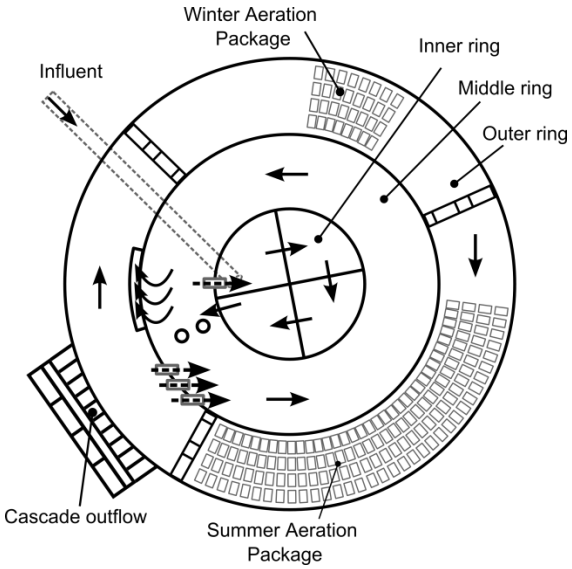

Figure 2.4 - Scheme of a bioreactor. The full black arrows show the mixed liquor direction and the dotted arrows show the recirculation flows throughout the different compartments.

Aeration to the biomass is provided in the outer ring by plate aerators divided in two sections, a continuously active summer package and a winter package. The winter package is used only occasionally to increase the aerated volume in the tank (e.g. when low temperatures decrease the bacterial activity or during rain events when the influent load increases). On the other hand, the summer package is always active and its airflow is controlled by an ammonia-DO feedback cascade control which reduces the airflow when the effluent ammonia from the bioreactor is below 1 mg/L. In addition, a feedforward control takes action when the incoming flow rate to the plant is above 11,000 m^3/h. When this happens, the DO set point is increased to 6 mg/L and both summer and winter packages are used in order to ensure nitrification.

Thanks to the very advanced Supervisory Control and Data Acquisition (SCADA) system the WRRF of Eindhoven disposes of high quality dataset of influent, effluent and process data.

Florence

The WRRF in Florence (Italy), managed by Publiacqua spa, treats urban wastewater with a capacity of 600k IE and a flowrate of approximately 200k m^3/d. It treats the wastewater coming from the entire municipality of Florence including Campi Bisenzio, Calenzano, Sesto Fiorentino, Signa, Lastra a Signa e Scandicci. It is a municipal conventional activated sludge (CAS) WRRF with a modified Ludzak-Ettinger denitrification-nitrification configuration. The plant, is composed of three parallel treatment lines equipped with one primary settler which is currently bypassed due to the diluted character of the influent, four identical bioreactors and three secondary sedimentation tanks (Figure 2.5). In principle, the influent should be equally partitioned among all bioreactors.

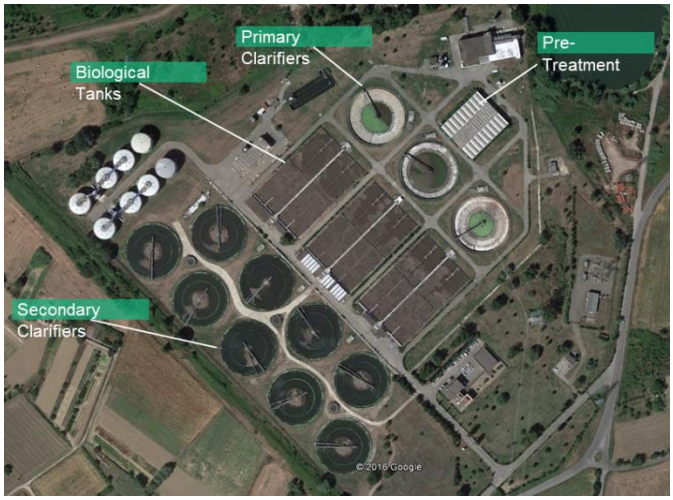

Figure 2.5 – WRRF of Florence and its main treatment units

Each bioreactor is composed of an anoxic section and an aerobic section. The anoxic section has 7 compartments divided by a concrete wall, partially submerged (.ca 10 cm) in the center and with a vertical opening at one side along the whole depth. The influent enters the biological tank at the beginning of the first anoxic compartment already mixed with the internal recirculation of the bioreactor. From the first anoxic compartment, the AS can flow over the concrete wall (center) and through the side-opening of this (Figure 2.6). The AS exiting the last anoxic compartment, enters the aerobic section.

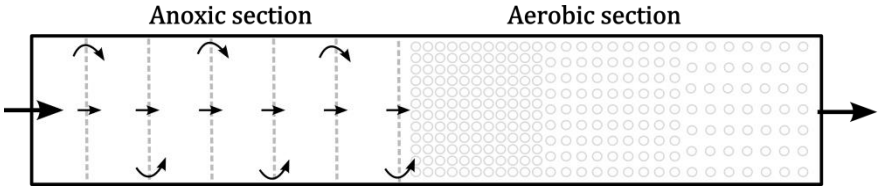

Figure 2.6 – Schematic detail of a bioreactor of the WRRF in Florence

Aeration is provided by fine-bubble diffusers (ABS, PIK300) with EPDM membranes. The plates are disposed 6.5 m deep and divided in three identical zones along the aerated area with decreasing density of aerators towards the tank outlet. The inlet of the aerobic section contains 44.0% of the aerators, while 30.5% cover the middle part of the aeration and the remaining 25.5% are present in the last third just before the outlet to the clarifiers. Aeration is balanced by an NH_4^+ - DO cascade control around a set point of 0.8 – 1.2 mg/L of DO measured at the outlet of the bioreactor.

Rome East

The WRRF of Rome East is one of the largest in Italy. It treats 900k IE (280k m^3/d) municipal wastewater for the section Rome IV and is managed by ACEA. The plant is divided in two main treatment trains. The largest train (600k IE) was in maintenance during the time that this plant was studied, therefore the smaller train was considered and only these details are reported in this work.

Similar to the WRRF in Florence, Rome East is operated bypassing the primary sedimentation due to the high amount of infiltration diluting the raw wastewater, with the purpose of maintaining

sufficient nutrition for the AS biomass. The influent, after a first coarse screening and sand trap, is directly split among the three parallel AS tanks (Figure 2.7).

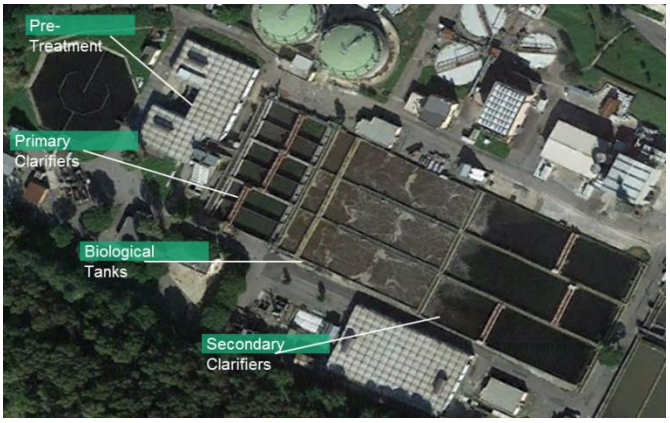

Figure 2.7 – Aerial view of the smaller treatment train of the Rome East WRRF

There is no pre-denitrification, and the influent directly enters the aerated volume after a small mixing section (Figure 2.8). The aerated tank is equipped with EPDM membrane disk diffusers (ABS, PIK 300) and installed at 5.5 m depth. The first half of the tank has 56.6% of the diffusers while the remaining 40.4% of the diffusers are placed in the second half. Aeration is run with a fixed air flow rate and adjusted once per day by the operators according to manual DO measurements and AS characteristics, i.e. mixed liquor concentration and retention time.

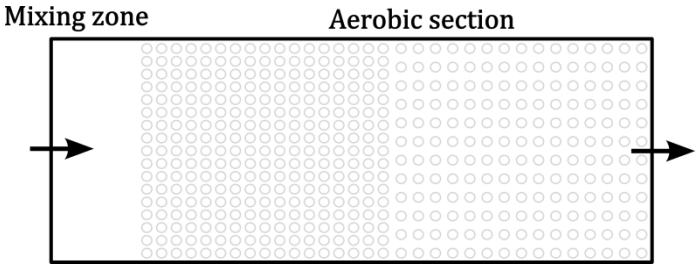

Figure 2.8 – Schematic overview of one bioreactor in Rome Est WRRF

The bioreactor is operated with the principle of a plug-flow configuration and its effluent is directed to the secondary sedimentation.

2.8. References

Aboobakar, A., Cartmell, E., Stephenson, T., Jones, M., Vale, P., Dotro, G., 2013. Nitrous oxide emissions and dissolved oxygen profiling in a full-scale nitrifying activated sludge treatment plant. Water Res. 47, 524–534.

Ahn, J.H., Kim, S., Park, H., Katehis, D., Pagilla, K., Chandran, K., 2010a. Spatial and temporal variability in atmospheric nitrous oxide generation and emission from full-scale biological nitrogen removal and non-BNR processes. Water Environ. Res. a Res. Publ. Water Environ. Fed. 82, 2362–72.

Ahn, J.H., Kim, S., Park, H., Rahm, B., Pagilla, K., Chandran, K., 2010b. N2O Emissions from Activated Sludge Processes, 2008−2009: Results of a National Monitoring Survey in the United States. Environ. Sci. Technol. 44, 4505–4511.

Amaral, A., Schraa, O., Rieger, L., Gillot, S., Fayolle, Y., Bellandi, G., Amerlinck, Y., Mortier, S.T.F.C., Gori, R., Neves, R., Nopens, I., 2017. Towards advanced aeration modelling: From blower to bubbles to bulk. Water Sci. Technol. 75.

Amerlinck, Y., Bellandi, G., Amaral, A., Weijers, S., Nopens, I., 2016. Detailed off-gas measurements for improved modelling of the aeration performance at the WWTP of Eindhoven. Water Sci. Technol. 74, 203–211.

Anthonisen, A.C., Loehr, R.C., Prakasam, T.B.S., Sri- nath, E.G., 1976. Inhibition of nitrification by ammonia and nitrous acid. J. Water Pollut. Control Fed. 48, 835–852.

Asadi, A., Verma, A., Yang, K., Mejabi, B., 2017. Wastewater treatment aeration process optimization: A data mining approach. J. Environ. Manage. 203, 630–639.

ASCE, 1983. Development of standard procedure for evaluating oxygen transfer devices. EPA, Cincinnati OH.

ASCE, 1997. Standard Guidelines for In-Process Oxygen Transfer Testing (18-96). American Society of Civil Engineers, New York, NY.

ASCE, 2007. Measurement of Oxygen Transfer in Clean Water. American Society of Civil Engineers, New York, NY.

Bock, E., Schmidt, I., Stuven, R., Zart, D., 1995. Nitrogen loss caused by denitrifying Nitrosomonas cells using ammonium or hydrogen as electron donors and nitrite as electron acceptor. Arch. Microbiol. 163, 16–20.

Bosma, A., Dalstra, G., Verhoeven, M., Reitsma, B., 2007. Meten en modelleren van het stromingsgedrag in de actief slibtanks van de rwzi Eindhoven met CFD. Afvalwaterwetenschap 6, 115–128.

Boyle, W.C., Hellstrom, B.G., Ewing, L., 1989. Oxygen transfer efficiency measurements using off-gas techniques. Water Sci. Technol. 21, 1295–1300.

Caivano, M., Bellandi, G., Mancini, I.M., Masi, S., Brienza, R., Panariello, S., Gori, R., Caniani, D., 2017. Monitoring the aeration efficiency and carbon footprint of a medium-sized WWTP: experimental results on oxidation tank and aerobic digester. Environ. Technol. 38, 629–638.

Caniani, D., Esposito, G., Gori, R., Mannina, G., 2015. Towards a new decision support system for design, management and operation of wastewater treatment plants for the reduction of greenhouse gases emission. Water (Switzerland) 7, 5599–5616.

Cantwell, J., Newton, J., Jenkins, T., Cavagnaro, P., Kalwara, C., 2009. Running an Energy-Efficient Wastewater Utility Modifications That Can Improve Your Bottom Line.

Capela, S., Heduit, A., Roustan, M., 2004. Influence of water depth on fine bubble aeration efficiency in the presence of surfactants, in: Preprints of the 3rd IWA World Water Congress.

CEC, 2006. Inventory of California Greenhouse Gas Emissions and Sinks: 1990 to 2004. Sacramento

CA.

Chandran, K., 2011. Protocol for the measurement of nitrous oxide fluxes from biological wastewater treatment plants. Methods Enzymol. 486, 369–85.

Chandran, K., Stein, L.Y., Klotz, M.G., van Loosdrecht, M.C.M., 2011. Nitrous oxide production by lithotrophic ammonia-oxidizing bacteria and implications for engineered nitrogen-removal systems. Biochem. Soc. Trans. 39, 1832–1837.

Chen, Y., Wang, D., Zheng, X., Li, X., Feng, L., Chen, H., 2014. Biological nutrient removal with low nitrous oxide generation by cancelling the anaerobic phase and extending the idle phase in a sequencing batch reactor. Chemosphere 109, 56–63.

Comas, J., Rodríguez-Roda, I., Sànchez-Marrè, M., Cortés, U., Freixó, A., Arráez, J., Poch, M., 2003. A knowledge-based approach to the deflocculation problem: Integrating on-line, off-line, and heuristic information. Water Res. 37, 2377–2387.

Czepiel, P., Crill, P., Harriss, R., 1995. Nitrous oxide emissions from municipal wastewater treatment. Environ. Sci. Technol. 29, 2352–6.

Daelman, M.R.J., van Voorthuizen, E.M., van Dongen, L.G.J.M., Volcke, E.I.P., van Loosdrecht, M.C.M., 2013. Methane and nitrous oxide emissions from municipal wastewater treatment – results from a long-term study. Water Sci. Technol. 67, 2350.

Daelman, M.R.J., van Voorthuizen, E.M., van Dongen, U.G.J.M., Volcke, E.I.P., van Loosdrecht, M.C.M., 2015. Seasonal and diurnal variability of N2O emissions from a full-scale municipal wastewater treatment plant. Sci. Total Environ. 536, 1–11.

Desloover, J., Vlaeminck, S.E., Clauwaert, P., Verstraete, W., Boon, N., 2012. Strategies to mitigate N2O emissions from biological nitrogen removal systems. Curr. Opin. Biotechnol. 23, 474–482.

Domingo-Félez, C., Mutlu, A.G., Jensen, M.M., Smets, B.F., 2014. Aeration strategies to mitigate nitrous oxide emissions from single-stage nitritation/anammox reactors. Environ. Sci. Technol. 48, 8679–8687.

Fabiyi, M.E., Novak, R., 2008. Evaluation of the factors that impact succesful membrane biological reactor operation at high solids concentration. Membr. Technol. 2008, 503–512.

Ferri, J., Stebe, K., 2000. Which surfactants reduce surface tension faster? A scaling argument for diffusion-controlled adsorption, Advances in colloid and interface science.

Foley, J., de Haas, D., Yuan, Z., Lant, P., 2010. Nitrous oxide generation in full-scale biological nutrient removal wastewater treatment plants. Water Res. 44, 831–844.

Garner, F.H., Hammerton, D., 1954. Circulation inside gas bubbles. Chem. Eng. Sci. 3, 1–11.

Gernaey, K. V., Van Loosdrecht, M.C.M., Henze, M., Lind, M., Jørgensen, S.B., 2004. Activated sludge wastewater treatment plant modelling and simulation: State of the art. Environ. Model. Softw. 19, 763–783.

Gillot, S., Héduit, A., 2008. Prediction of alpha factor values for fine pore aeration systems. Water Sci. Technol. 57, 1265–9.

Gori, R., Balducci, A., Caretti, C., Lubello, C., 2014. Monitoring the oxygen transfer efficiency of full-scale aeration systems: investigation method and experimental results. Water Sci. Technol. 70, 8–14.

Groves, K.P., Daigger, G.T., Simpkin, T.J., Redmon, D.T., Ewing, L., 1992. Evaluation of oxygen transfer efficiency and apha-factor on a variety of diffused aeration systems. Water Environ. Res. 64, 691–698.

Guo, L., 2014. Greenhouse gas emissions from and storm impacts on wastewater treatment plants: Process modelling and control. LAVAL University.

Guo, L.S., Lamaire-chad, C., Bellandi, G., Daelman, M.R.J., Maere, T., Nous, J., Flameling, T., Weijers, S., Mark, C.M., Loosdrecht, V., Volcke, E.I.P., Nopens, I., Vanrolleghem, P.A., 2013. High frequency Field Measurements of Nitrous oxyde (N2O) Gas Emissions and Influencing Factors at WWTPs under Dry and Wet Weather Conditions, in: WEF/IWA Nutrient Removal and Recovery 2013.

Guo, L.S., Vanrolleghem, P. a., 2014. Calibration and validation of an activated sludge model for greenhouse gases no. 1 (ASMG1): Prediction of temperature-dependent N2O emission dynamics. Bioprocess Biosyst. Eng. 37, 151–163.

GWRC - Global Water Research Coalition, 2011. N2O and CH4 emission from wastewater collection and treatment systems. London.

Hanaki, K., Chalermraj, W., Shinichiro, O., 1990. Nitrification at low levels of dissolved oxygen with and without organic loading in a suspended-growth reactor. Water Res. 24, 297–302.

Hebrard, G., Destrac, P., Roustan, M., Huyard, A., Audic, J.M., 2000. Determination of the water quality correction factor α using a tracer gas method. Water Res. 34, 684–689.

Henze, M., Gujer, W., Mino, T., van Loosdrecht, M., 2000. Activated sludge models ASM1, ASM2, ASM2d and ASM3. IWA Publishing.

Hiatt, W.C., Grady, C.P.L., 2008. An updated process model for carbon oxidation, nitrification, and denitrification. Water Environ. Res. 80, 2145–2156.

Higbie, R., 1935. The rate of absorption of a pure gas in a still liquid during short periods of exposure. Trans. Amer. Inst. of Chem. Engrs.

IPCC, 1995. Impacts, Adaptations and Mitigation of Climate Change: Scientific-Technical Analyses.

IPCC, 2006. Guidelines for National Greenhouse Gas Inventories, Prepared by the National Greenhouse Gas Inventories Programme. Kanagawa.

IPCC, 2013. Climate Change 2013: The Physical Science Basis. Contribution of Working Group I to the Fifth Assessment Report of the Intergovernmental Panel on Climate Change. Cambridge.

Iranpour, R., Magallanes, A., Zermen, M., Varsh, V., Abrishamchi, A., Stenstrom, M.K., 2000. Assessment of aeration basin performance efficiency: sampling methods and tank coverage. Water Res. 34, 3137–3152.

Joss, A., Salzgeber, D., Eugster, J., König, R., Rottermann, K., Burger, S., Fabijan, P., Leumann, S., Mohn, J., Siegrist, H.R., 2009. Full-scale nitrogen removal from digester liquid with partial nitritation and anammox in one SBR. Environ. Sci. Technol. 43, 5301–5306.

Kampschreur, M.J., Tan, N.C.G., Kleerebezem, R., Picioreanu, C., Jetten, M.S.M., Loosdrecht, M.C.M. van, 2008a. Effect of Dynamic Process Conditions on Nitrogen Oxides Emission from a Nitrifying Culture. Environ. Sci. Technol. 42, 429–435.

Kampschreur, M.J., Temmink, H., Kleerebezem, R., Jetten, M.S.M., van Loosdrecht, M.C.M., 2009. Nitrous oxide emission during wastewater treatment. Water Res. 43, 4093–4103.

Kampschreur, M.J., van der Star, W.R.L., Wielders, H. a., Mulder, J.W., Jetten, M.S.M., van Loosdrecht, M.C.M., 2008b. Dynamics of nitric oxide and nitrous oxide emission during full-scale reject water treatment. Water Res. 42, 812–826.

Kosonen, H., Heinonen, M., Mikola, A., Haimi, H., Mulas, M., Corona, F., Vahala, R., 2016. Nitrous Oxide Production at a Fully Covered Wastewater Treatment Plant: Results of a Long-Term Online Monitoring Campaign. Environ. Sci. Technol. 50, 5547–5554.

Krovvidy, S., William, G.W., Summers, S., Coleman, J., 1991. An AI approach for wastewater treatment systems. Appl. Intell. 1, 247–261.

Law, Y., Lant, P., Yuan, Z., 2013. The Confounding Effect of Nitrite on N 2 O Production by an Enriched Ammonia-Oxidizing Culture. Environ. Sci. Technol. 47, 130618083019001.

Law, Y., Ye, L., Pan, Y., Yuan, Z., 2012. Nitrous oxide emissions from wastewater treatment processes. Philos. Trans. R. Soc. B Biol. Sci. 367, 1265–1277.

Lee, D.S., Vanrolleghem, P.A., 2003. Monitoring of a Sequencing Batch Reactor Using Adaptive Multiblock Principal Component Analysis.

Leu, S.-Y., Libra, J. a, Stenstrom, M.K., 2010. Monitoring off-gas O2/CO2 to predict nitrification performance in activated sludge processes. Water Res. 44, 3434–44.

Li, K., Fang, F., Wang, H., Wang, C., Chen, Y., Guo, J., Wang, X., Jiang, F., 2017. Pathways of N removal and N2O emission from a one-stage autotrophic N removal process under anaerobic conditions. Sci. Rep. 7, 42072.

Libra, J. a, Sahlmann, C., Schuchardt, A., Handschag, J., Wiesmann, U., Gnirss, R., 2005. Evaluation of ceramic and membrane diffusers under operating conditions with the dynamic offgas method. Water Environ. Res. 77, 447–54.

Libra, J. a, Schuchardt, a, Sahlmann, C., Handschag, J., Wiesmann, U., Gnirss, R., 2002. Comparison of the efficiency of large-scale ceramic and membrane aeration systems with the dynamic off-gas method. Water Sci. Technol. 46, 317–24.

Mampaey, K.E., Beuckels, B., Kampschreur, M.J., Kleerebezem, R., van Loosdrecht, M.C.M., Volcke, E.I.P., 2013. Modelling nitrous and nitric oxide emissions by autotrophic ammonium oxidizing bacteria. Environ. Technol. 34, 1555–66.

Mampaey, K.E., van Dongen, U.G.J.M., van Loosdrecht, M.C.M., Volcke, E.I.P., 2015. Novel method for online monitoring of dissolved N2O concentrations through a gas stripping device. Environ. Technol. 36, 1680–90.

Manesis, S.A., Saridis, D.J., King, R.E., 1998. Intelligent Control of Wastewater Treatment Plants. Artif. Intell. Eng. 12, 275.

Marques, R., Rodriguez-Caballero, A., Oehmen, A., Pijuan, M., 2016. Assessment of online monitoring strategies for measuring N2O emissions from full-scale wastewater treatment systems. Water Res. 99, 171–179.

Massara, T.M., Malamis, S., Guisasola, A., Baeza, J.A., Noutsopoulos, C., Katsou, E., 2017. A review on nitrous oxide (N2O) emissions during biological nutrient removal from municipal wastewater and sludge reject water. Sci. Total Environ. 596–597, 106–123.

Monteith, H.D., Sahely, H.R., MacLean, H.L., Bagley, D.M., 2005. A rational procedure for estimation of greenhouse-gas emissions from municipal wastewater treatment plants. Water Environ. Res. a Res. Publ. Water Environ. Fed. 77, 390–403.

Mota, C., Head, M., Ridenoure, J., Cheng, J., de los Reyes, F., 2005. Effects of Aeration Cycles on Nitrifying Bacterial Populations and Nitrogen Removal in Intermittently Aerated Reactors. Appl. Environ. Microbiol. 71, 8565–8572.

Ni, B.J., Peng, L., Law, Y., Guo, J., Yuan, Z., 2014. Modeling of Nitrous Oxide Production by Autotrophic Ammonia-Oxidizing Bacteria with Multiple Production Pathways. Env. Sci Technol 48, 3916–3924.

Ni, B.J., Ruscalleda, M., Pellicer-Nacher, C., Smets, B.F.B.F., Pellicer, i N.C., Smets, B.F.B.F., 2011. Modelling nitrous oxide production during biological nitrogen removal via nitrification and denitrification: Extensions to the general ASM models. Env. Sci Technol 45, 7768–7776.

Ni, B.J., Yuan, Z., 2015. Recent advances in mathematical modeling of nitrous oxides emissions from wastewater treatment processes. Water Res. 87, 336–346.

Ni, B.J., Yuan, Z., Chandran, K., Vanrolleghem, P. a., Murthy, S., 2013. Evaluating four mathematical models for nitrous oxide production by autotrophic ammonia-oxidizing bacteria. Biotechnol. Bioeng. 110, 153–163.

Peng, L., Ni, B.J., Erler, D., Ye, L., Yuan, Z., 2014. The effect of dissolved oxygen on N2O production by ammonia-oxidizing bacteria in an enriched nitrifying sludge. Water Res. 66, 12–21.

Peng, L., Ni, B.J., Ye, L., Yuan, Z., 2015. Selection of mathematical models for N<inf>2</inf>O production by ammonia oxidizing bacteria under varying dissolved oxygen and nitrite concentrations. Chem. Eng. J. 281, 661–668.

Porro, J., Milleri, C., Comas, J., Rodriguez-roda, I., Pijuan, M., 2014. Risk assessment modelling of N2O production in activated sludge systems: Quality not Quantity, in: 4th IWA/WEF Wastewater Treatment Modelling Seminar (WWTmod2014). pp. 351–357.

Ratkovich, N., Horn, W., Helmus, F.P., Rosenberger, S., Naessens, W., Nopens, I., Bentzen, T.R., 2013. Activated sludge rheology: a critical review on data collection and modelling. Water Res. 47, 463–82.

Ravishankara, A.R., Daniel, J.S., Portmann, R.W., 2009. Nitrous Oxide (N2O): The Dominant Ozone-Depleting Substance Emitted in the 21st Century. Science (80-.). 326, 123–125.

Reardon, D.J., 1995. Turning down the power. Civ. Eng. 65, 54–56.

Redmon, D.T., Boyle, W.C., Ewing, L., 1983. Oxygen transfer efficiency measurements in mixed liquor using off-gas techniques. Water Pollut. Control Fed. 55, 1338–1347.

Rehman, U., 2016. Next generation bioreactor models for wastewater treatment systems by means of detailed combined modelling of mixing and biokinetics. Ghent University.

Rehman, U., Audenaert, W., Amerlinck, Y., Maere, T., Arnaldos, M., Nopens, I., 2017. How well-mixed is well mixed? Hydrodynamic-biokinetic model integration in an aerated tank of a full-scale water resource recovery facility. Water Sci. Technol. 76, 1950–1965.

Rieth, M.G., Chiesa, S.C., Polta, R.C., 1995. Effects of operational variables on the oxygen transfer performance of ceramic diffusers. Water Environ. Res. 67, 781–787.

Rodríguez-Roda, I., Comas, J., Colprim, J., Poch, M., Sànchez-Marrè, M., Cortés, U., Baesa, J., Lafuente, J., 2002. A hybrid supervisory system to support wastewater treatment plant operation: implementation and validation. Water Sci. Technol. 45, 289–297.

Rosso, D., Iranpour, R., Stenstrom, M.K., 2005. Fifteen years of off-gas tranfer efficiency measurements on fine pore aerators: key role of sludge age and normalized air flux. Water Environ. Res. 77, 266–273.

Rosso, D., Jiang, L.-M., Hayden, D.M., Pitt, P., Hocking, C.S., Murthy, S., Stenstrom, M.K., 2012. Towards more accurate design and specification of aeration systems using on-site column testing. Water Sci. Technol. 66, 627–34.

Rosso, D., Stenstrom, M.K., 2006a. Economic Implications of Fine-Pore Diffuser Aging. Water Environ. Res. 78, 810–815.

Rosso, D., Stenstrom, M.K., 2006b. Surfactant effects on alpha-factors in aeration systems. Water Res. 40, 1397–404.

Sànchez-Marrè, M., Corte´s, U., Lafuente, J., Rodriguez-Roda, I., Poch, M., 1996. DAI-DEPUR: an integrated and distributed architecture for wastewater treatment plants supervision. Artif. Intell. Eng. 10, 275–285.

Spérandio, M., Pocquet, M., Guo, L., Ni, B.J., Vanrolleghem, P.A., Yuan, Z., 2016. Evaluation of different nitrous oxide production models with four continuous long-term wastewater treatment process data series. Bioprocess Biosyst. Eng. 39, 493–510.

Stein, L.Y., 2011. Surveying N2O-Producing Pathways in Bacteria, in: Methods in Enzymology. pp. 131–152.

Stenstrom, M.K., Gilbert, R.G., 1981. Effects of alpha, beta and theta factor upon the design, specification and operation of aeration systems. Water Res. 15, 643–654.

Stenstrom, M.K., Leu, S.-Y. (Ben), Jiang, P., 2006. Theory to Practice: Oxygen Transfer and the New ASCE Standard, in: WEFTEC. pp. 4838–4852.

Svehla, P., Bartacek, J., Pacek, L., Hrncirova, H., Radechovsky, J., Hanc, A., Jenicek, P., 2014. Inhibition effect of free ammonia and free nitrous acid on nitrite-oxidising bacteria during sludge liquor treatment: influence of feeding strategy. Chem. Pap. 68, 871–878.

Tallec, G., Garnier, J., Billen, G., Gousailles, M., 2008. Nitrous oxide emissions from denitrifying activated sludge of urban wastewater treatment plants, under anoxia and low oxygenation. Bioresour. Technol. 99, 2200–2209.

Thaler, K.M., Niessner, R., Haisch, C., 2017. Laboratory and field studies on a new sensor for dissolved N2O. Anal. Bioanal. Chem. 409, 4719–4727.

USEPA, 2001. U.S. High GWP Gas Emissions 1990 – 2010: Inventories, Projections, and Opportunities.

USEPA, 2007. Inventory of U.S. Greenhouse Gas Emissions and Sinks: 1990-2005. US Environmental Protection Agency, Washington DC.

Villez, K., Ruiz, M., Sin, G., Colomer, J., Rosén, C., Vanrolleghem, P.A., 2008. Combining multiway Principal Component Analysis (MPCA) and clustering for efficient data mining of historical data sets of SBR processes. Water Sci. Technol. 57, 1659–1666.

Vogelaar, J.C.T., Klapwijk, A.M., Van Lier, J.B., Rulkens, W.H., 2000. Temperature effects on the oxygen transfer rate between 20 and 55°C. Water Res. 34, 1037–1041.

Von Schulthess, R., Wild, D., Gujer, W., 1994. Nitric and nitrous oxides from denitrifying activated sludge at low oxygen concentration. Water Sci. Technol. 30, 123–132.

Wagner, M., 1999. Factor influencing the magnitude of alpha-values of fine bubble aeration systems, in: WEFTEC.

Wang, D., Wang, Q., Laloo, A.E., Yuan, Z., 2016. Reducing N2O Emission from a Domestic-Strength Nitrifying Culture by Free Nitrous Acid-Based Sludge Treatment. Environ. Sci. Technol. 50, 7425–7433.

Whitman, W.G., 1923. The two-film theory of gas absorption. Chem. Metall. Eng. 29, 146–148.

Whitman, W.G., 1962. The Two-Film Theory of Gas Absorption. Int. J. Heat Mass Transf. 5, 429–433.

Yu, R., Kampschreur, M.J., van Loosdrecht, M.C.M., Chandran, K., 2010. Oxide and Nitric Oxide Generation during Transient Anoxia. Environ. Sci. Technol. 44, 1313–1319.

Chapter 3

3. Development of an analyzer for off-gas measurements

Abstract

Given the documented impact of both aeration efficiency and N_2O emission on the WRRF's energy requirements and CFP, in order to promote their sound assessments and replicability of their measures, there is a crescent need for reliable instrumentations and robust standardized measurement methods. Available standardized methods need to be updated and related to currently available technologies, suggesting potential configurations that can be used to generate widely comparable results or to further inspire possible improvements. In this chapter, the development of an off-gas analyzer for off-gas measurements and related extensions for N_2O emission monitoring are critically presented and evaluated.

A new instrument based on the standard guidelines and principles of the off-gas measurements was designed and developed in tight collaboration with West Systems (Pontedera, Italy) in view of including best practice principles and instrumentation for off-gas testing but also provide an improved solution with respect to the canonical method. In particular, West Systems experience in sensing software and hardware development was used to implement our knowledge in off-gas testing. We selected the most appropriate sensing devices and

The analyzer was designed and assembled with the aim of (I) limiting investment costs maintaining good data quality and quantity for wastewater application; (II) maximize instrumentation lifetime, (III) minimize maintenance and calibration needs; (IV) maximizing portability and automation; (V) emphasize the user-friendly character; (VI) increasing its applicability and replicability.

The analyzer was designed to provide all necessary features to perform aeration efficiency measurements based on the principles of the off-gas method. A dedicated transportable floating hood for capturing off-gas from aerated compartments was also developed.

In view of optimizing measurement campaign efforts including the assessment of N_2O emissions, the instrumentation was extended with in particular (I) a thermoacoustic IR N_2O analyzer for measurements of gaseous N_2O; (II) two liquid N_2O sensors; (III) a floating hood for non-aerated surfaces. To the best of the authors knowledge, this is the first time that an integrated system for aeration efficiency and N_2O emission monitoring is proposed.

The analyzer and all its components are introduced in this chapter along with laboratory and field tests.

3.1. Instrumentation, testing and field validation

An off-gas analyzer was designed for assessing the aeration efficiency of submerged aeration systems by measuring the concentrations of O_2 in the off-gas and comparing that to the ambient one. A schematic overview of the analyzer is provided in Figure 3.1.

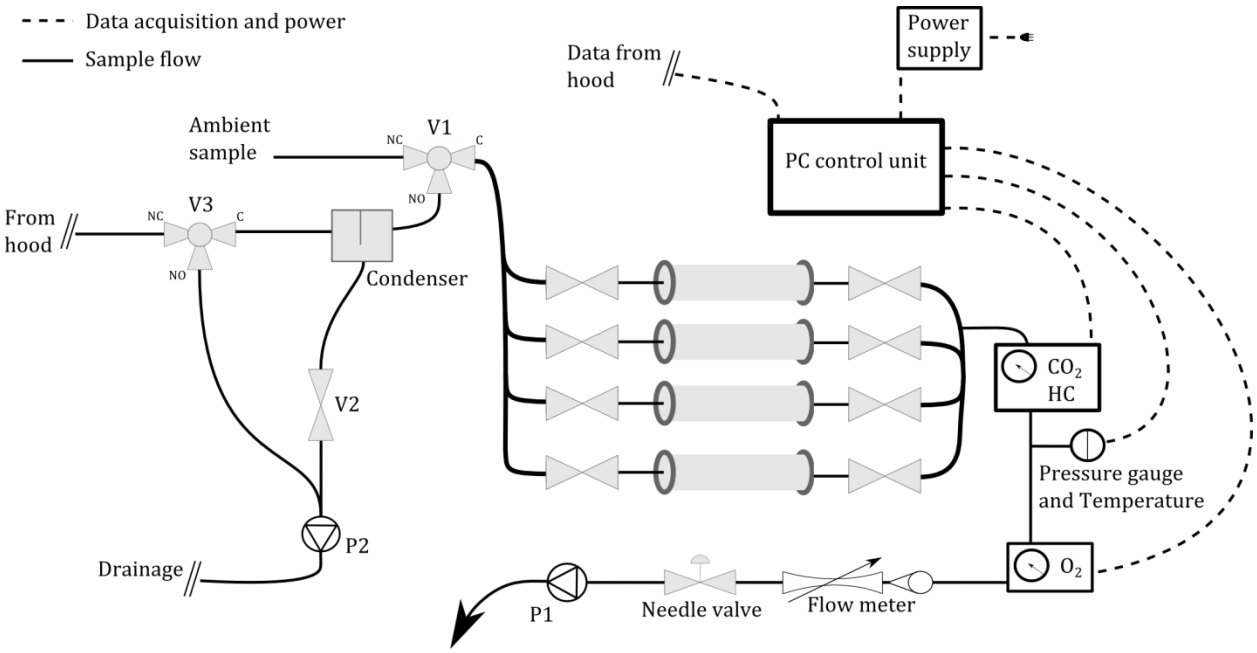

Figure 3.1 – Conceptual scheme of the off-gas analyzer sample flow and data acquisition.

The gas stream leaving the aerated tank is captured by a floating hood on which a hot wire anemometer is mounted to measure air flow rate. A small fraction (1 l/min) of the gas captured is spilled by a vacuum pump and directed to the analyzer. A desiccator unit performs the first conditioning of the gas sample in order to remove water vapor. The spilled air flow is then circulated inside a sensor cell to measure oxygen partial pressure. Ambient air can be sampled by means of a three-way valve as reference for the efficiency evaluation. DO is also measured in the mixed liquor.

3.1.1. The off-gas analyzer

The off-gas analyzer (Figure 3.2, left) was designed for use in full-scale facilities, thus considering the possibility to be left on site even under adverse weather conditions. A waterproof case was used to protect all sensitive instrumentation against rain. The case was chosen to minimize dimensions in favor of stability under strong wind. An air cooling system was mounted for ensuring safe operation during hot weather.

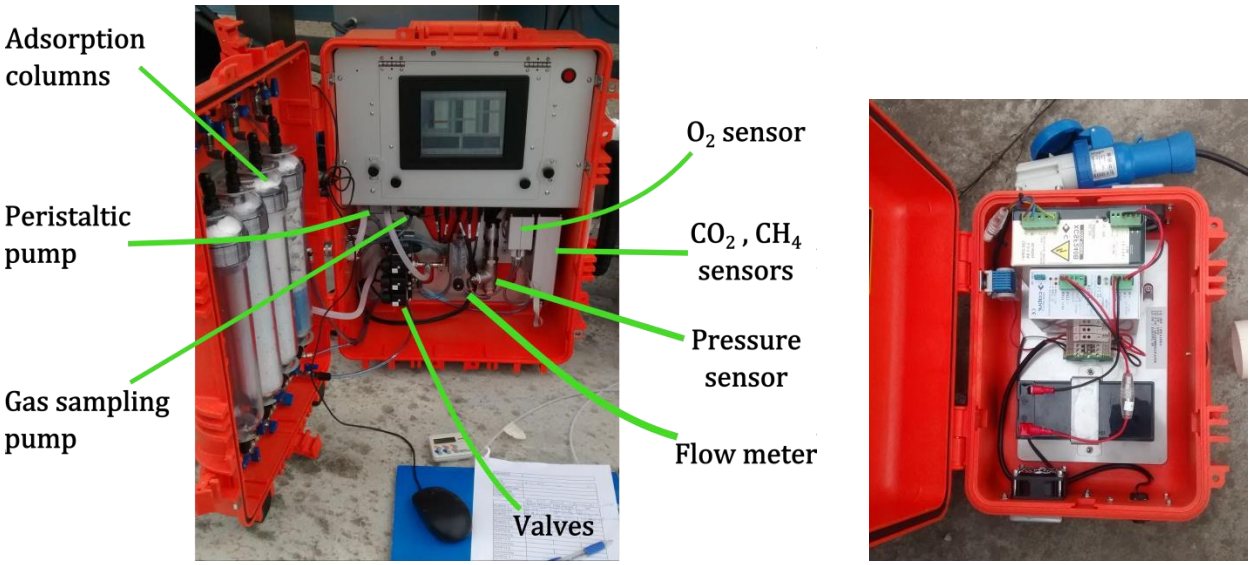

Figure 3.2 – The off-gas analyzer and its components (left), and the power supply case (right)

The power supply was included in view of providing sufficient energy to operate in case of short blackouts (about 1 hour of operation) and disconnections from the electrical net (e.g. necessity to move the instrumentation avoiding shutdown of the instrument). In order to maximize battery lifetime in case of need, the entire instrumentation is operated at the minimum voltage possible (i.e. 15 VDC), dictated by the minimum requirements of the pressure and temperature sensor. This system was embedded in a small water-proof air-cooled case which can stand diverse weather conditions similarly to the off-gas analyzer.

The analyzer is composed of the following components which will be described individually in the next sections (I) Gas sampling pump, (II) Peristaltic pump, (III) Pressure and temperature sensor, (IV) Four adsorption columns, (V) Sensor for O_2, (VI) Sensor for CO_2 and CH_4, (VII) PC, (VIII) Solenoid valves (one direct acting 2/2 -way, and two 3/2 direct acting-way), (IX) Condenser, (X) Flow meter.

Gas sampling pump (*KNF NMP 850 KNDC*)

This pump is located at the end of the internal analyzer's pipeline, in order to guide the gas sample through the internal circuit of sensors. The internal membrane can be used with slightly aggressive gases, both in vacuum (down to 230 mbar absolute pressure) and pressurized applications (up to 1.5 bar g). The vibrations induced by the pump are imperceptible by the instrumentation thanks to the needle valve positioned upstream, and can work in any position in a temperature range of 5-40°C. The gas sampling pump can reach a flow of 4.5 l/min but in this circuit is operated at 1 l/min due to design requirements of the O_2 sensor. The membrane technology allows to separate the operating mechanism from the sample side, avoiding contamination of the sample from lubricants and ambient gases.

Peristaltic pump (*ESPANGO IPS6*)

A peristaltic pump was included in the circuit in order to protect the instrumentation in case of water entering the sampling tube from the hood or rather in high presence of condensed water. The

pump has a reversible fixed flow of 6 l/min with 1 bar of pressure (10 m of water column). It is a self-priming device, being able to work with up to 2 m of water column in suction. The control action starts in presence of an under-pressure in the pipeline of the analyzer, this triggers the peristaltic pump to washout the eventual liquid present in the sampling line and causing the resistance to sampling. Normally, this problem does not occur and the pump remains mostly inactive.

***Pressure and temperature sensor (*STS ATM/T series 26)**

This pressure and temperature sensor is used to monitor the status of the gas in the sampling line inside the off-gas analyzer. The readings of temperature and pressure can be used to adjust the measurements of other sensors on the same line that do not have these corrections. In addition to this, pressure and temperature measurements are used to control the status of the sampling line and of the whole analyzer against overheating (e.g. during measurements in summer) and changes in pressure in the sampling line (e.g. clogging of the sampling line due to condensed water) that could bias the measurements or damage the instrumentation (e.g. the membrane of the O_2 sensor). The pressure sensor ranges between 70 mbar and 500 bar with a precision smaller than ± 0.5 % of full scale (4 mbar in the measuring range of ambient pressure). Over one year of operation its reading can deviate by about 4 mbar. These features make this pressure sensor highly reliable for being used in the off-gas analyzer.

Adsorption columns

Four adsorption columns (Figure 3.3) are present in the off-gas analyzer in order to provide sufficient scrubbing capacity of moisture from the off-gas sample. The removal of humidity from the gas sample is necessary prior to entering the train of sensors in order to protect delicate parts of the instrumentation (e.g. membrane of O_2 sensor). Nonetheless, moisture needs to be removed from the off-gas in order to allow a precise and comparable measurement of the volumetric content of the different components between the off-gas and ambient air. For this, the columns are filled with silica gel containing a colored humidity indicator. The volume of each column is about 1.5 L and a system of spigots allows the use of one or multiple columns in parallel or in series.

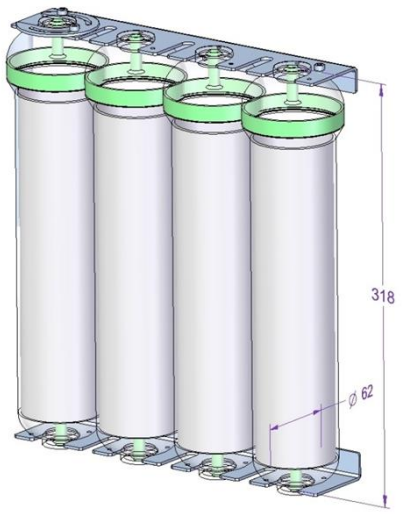

Figure 3.3 – Adsorption columns for moisture trap with silica gel. An empty column (left) and a technical drawing of the four columns fixed on their support in the analyzer (right).

In order to give an idea of the sequestration capacity of each column for humidity, it can be considered that the volume of silica contained in the single column generally allows the analyzer to sample continuously for more than a week before the last third of the silica starts to show variations in the colored indicator. Measurements with a moisture sensor during full-scale measurements demonstrated that, as far as the silica gel indicator does not change color, the sample exiting the column has an ensured dew point of -13 to -5 °C. This means that in full-scale a well dried sample can be ensured for more than a week. The time a silica gel column can last depends on ambient conditions and might slightly vary with the season, but no considerable variation from an abundant week of duration was observed.

Oxygen sensor (Alphasense O2-C2)

The O_2 sensor measures the concentration of oxygen in the gas sample and is the primary variable needed to calculate the actual efficiency of the aeration system. Therefore, this is a crucial sensor for the good performance of the analyzer.

The selected O_2 sensor operates in the range 0-30% of O_2 concentration in the gas sample, which is optimal for aeration efficiency monitoring as normally concentrations of O_2 in the off-gas of an aeration tank does not fall below 14%. The O2-C2 sensor is a galvanic sensor using an electrochemical cell in which O_2 is reduced at the anode, while at the cathode side a balancing oxidation of a metal occurs. A current proportional to the O_2 consumption is generated and used for the measurement. This sensor is preferable over the combustion chamber technology (e.g. zirconium cell) in applications where flammable gases can be present.

Combustion chamber sensors (zirconia cells) are largely used for measuring O_2 partial pressure for e.g. atmosphere control, internal combustion engines, and breathing gas of divers, thanks to their long lifetime and limited calibration needs. However, if flammable gases (e.g. CH_4) are present, they can be biased from the combustion of more compounds than solely O_2 revealing higher concentrations than in reality. As CH_4 can be generated from anaerobic activity in the sewer or

inside the WRRF and be stripped from the aeration tank, even in very small concentrations, galvanic cell technology is the most appropriate.

Electrochemical sensors have a shorter lifetime compared to the combustion chamber technology, however, since these sensing devices are claimed to be able to stand 2 years of operation before they should be replaced, their duration can be considered as adequate for aeration efficiency monitoring (i.e. a measurement campaign lasts in the order of a week/month). In addition to this, the reasonably low cost of this kind of sensors (around 20 euros) facilitates the economical aspect of its maintenance. The contained price is due to the fact that the sensor needs to be mounted by the purchaser on an acquisition board for which the manufacturer gives indications (e.g. capacitance of resistor) but not providing the hardware itself. Beside this, the relatively high maintenance required as compared to other sensors represents a bottleneck for some applications, likely not for wastewater. In fact, regarding their periodic calibration need, this does not represent an issue for aeration efficiency monitoring as the reference measurement of ambient air is always needed before the actual off-gas measurement (at least just before the start of the measurement day). The measurement of the reference (ambient) sample can be considered by itself as a calibration against a known concentration value. In the off-gas analyzer, the O_2 sensor reading is calibrated against ambient air at the beginning of each reference measurement.

The O_2 sensor operates between -30 and 55°C, and between 0.8 and 1.2 bar, which perfectly includes the vast majority of operating conditions of temperature and pressure during off-gas tests in both summer and winter. Temperature and pressure dependencies are provided by the manufacturer and were implemented in the signal processing of the analyzer. The response time is below 50s making it a fast responding device without the need of a time constant adjustment for use in aeration efficiency monitoring, where variations in the observable dynamics are far slower than the probe response time. The sensor accuracy is claimed to be $\pm$ 0.25 % of full scale (i.e. at ambient concentration of 20.9% there is an uncertainty of $\pm$0.052).

CO_2 and CH_4 measurements (Crestline instruments Model 7911)

Currently, a robust and widely accepted online measurement technology for CO_2 and CH_4 in the gas phase is Non-Dispersive Infrared (NDIR). Instruments using IR technology are normally offering a very high precision on many different compounds at a very expensive price. The advantage of NDIR is the possibility to measure different gases with a relatively simple spectroscopic sensor. In particular, this sensor represents somehow an exception on the market (i.e. 5k euros, one order of magnitude less than normal IR sensors), given its relatively low price and good performance, that fits perfectly in the aeration monitoring purpose. It is provided, similarly to the O_2 sensor discussed, without a data acquisition/power board which needs to be assembled by the customer, but which allows to sensibly decrease the price and ease its inclusion in a relatively small analyzer.

Information on CH_4 content is given as hydrocarbons concentration (HC) (0 to 4000 ppm $\pm$120ppm) and CO_2 measurements range from 350 to 160k ppm with a precision of $\pm$80 ppm.

From experience and literature studies, the CO_2 concentration in the off-gas of an aerated biological tank are known to lay in a rather large domain among different WRRFs (1 to 3%) but staying within a narrow deviation within the single facility ($\pm$400 ppm, probably due to influent dynamics), unless

critical sudden process changes occur (Bellandi et al., 2011; Caivano et al., 2017; Guo et al., 2013; Porro et al., 2014). Therefore, we can affirm that the characteristics of the selected instrument are fitting very well the purpose of the off-gas analyzer. The same can be stated for the case of the HC sensing device, for which HCs normally occur only under the form of CH_4 in wastewater systems and might follow more closely influent dynamics (Caivano et al., 2017; Daelman et al., 2013, 2012; Guo et al., 2013; Porro et al., 2014). However, it must be stated that the assessment of HCs emissions are outside the scope of this thesis and measurements are therefore not further considered.

PC controller unit (PPC-L62T)

A fanless PC contains the software and the user interface needed to control the instrumentation, acquire all signals, process data, and write text files in memory (Figure 3.4). The touchscreen allows the user to interact with the software. All monitored and controlled variables from the off-gas analyzer and from the floating hood are managed through an RS-483 port, acquired, processed in this controller unit and stored in its memory.

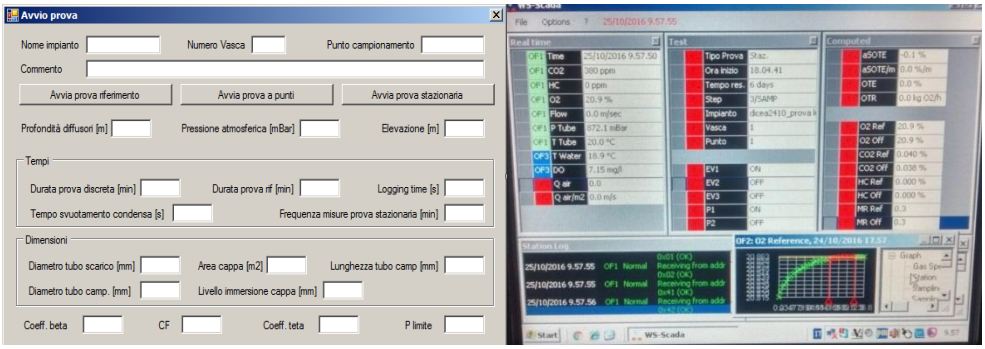

Figure 3.4 – View of the software GUI for initiating an off-gas measurement (left) and of the software interface with all measured and calculated variables during an off-gas measurement (right).

3.1.2. The floating hood

A floating hood of 2 m^2 (2x1x0.6 LxWxH) was designed and realized in collaboration with Bartolini Tendaggi (Pescia, Italy) and West Systems. The hood is composed of aluminium profiles making the skeleton of the hood light and resistant to both torsion and oxidation. The outer skeleton sustains a PVC flexible layer 2 mm thick (Figure 3.5). The profiles were designed to have a maximum length of 1 m to ease transportation.

The cover was chosen in order not to have interactions with the liquid in the biological tank and not to have interactions with the gas sample in the range of ambient temperatures to be experienced in WRRFs at European latitudes. The cover was designed with an inclined upper face in order to ease the off-gas exit towards the outlet tube, limit dead volumes, and minimize renewal time of the off-gas inside the hood (Figure 3.5).

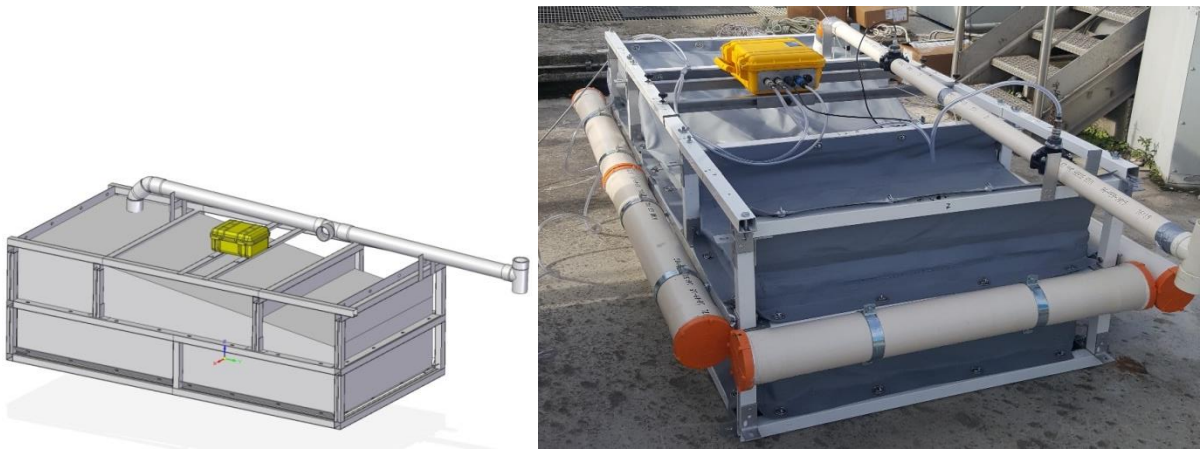

Figure 3.5 – Technical design of the hood composed of main structure, cover, off-gas discharge tube and the junction box (left). The hood assembled with floats, and the discharge hose with relative connections for anemometer and sample spill.

On the structure a waterproofed case containing a connection board was mounted (junction box, in Figure 3.6). In this junction box:

- the output signals of the anemometer and of the DO are digitalized into one single wire going to the off-gas analyzer to facilitate hood maneuvering;
- the power from the off-gas analyzer is provided to the sensors onboard;
- the sampling tube from the off-gas discharge is directed to the off-gas analyzer.

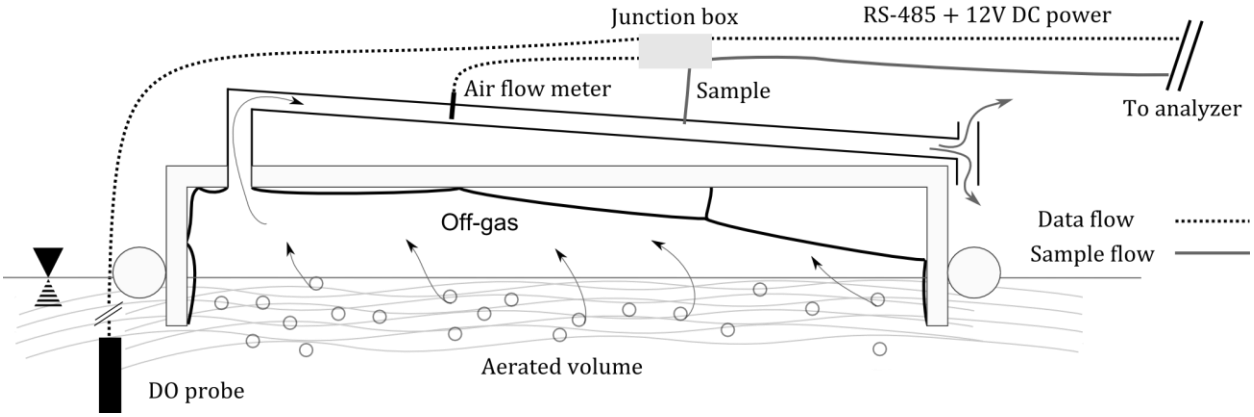

Figure 3.6 – Section of the floating hood and schematic overview of the working principle for off-gas testing, with data and sample flows towards the off-gas analyzer.

The design of this floating hood is particularly suitable for off-gas testing since it provides the user with a reasonably light, easy to clean and transportable device allowing to cover a large spot surface. As most hoods in literature covered about 1 m^2, with this hood the minimum amount of measurement points to be covered to assess the aeration efficiency (2 % of the tank surface) according to ASCE standards is thus halved. Apart from the area to be covered, also the air flow to be captured is important to supply the sensors with a sufficient amount of sample as most analyzers work at 1 L/min. Submerged fine bubble aeration systems normally supply between 0.3

to 2 L/min/m^2 of air into the liquid volume, which can be a limiting factor using a floating hood of 1 m^2 and an analyzer sampling at 1 L/min. When the airflow leaving the liquid surface approaches the sampling rate of the analyzer, the risk of biasing the off-gas sample with ambient air increases significantly. In particular, if operated in windy conditions, ambient air infiltrations are more likely.

In order to protect the exit hose of the floating hood from wind intrusion, a T shaped connection is plugged at the very end of the hose. Positioned in the vertical direction, the connection protects from wind from all directions and allows discharge of eventual moisture condensation.

Anemometer (TSI Air Velocity Transducer 8455 Series)

The anemometer is needed to measure the amount of off-gas exiting the liquid surface covered by the hood. The hot wire anemometer (Figure 3.7) is a well-established technology in this application. It is a rather robust measuring technique and requires very limited maintenance and calibration.

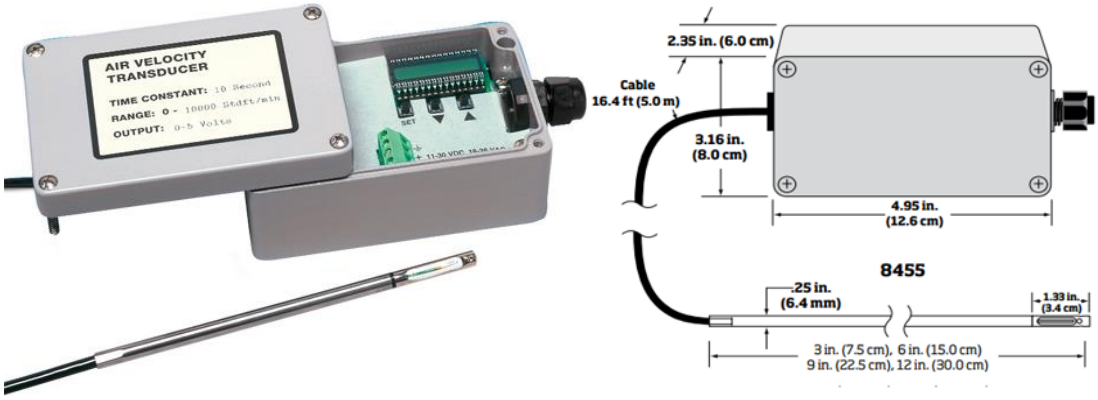

Figure 3.7 – TSI hot wire anemometer details

The instrument is delivered with built-in calibration curves according to the range of measurement in which it is expected to operate, making it a very flexible instrument. Ranges are from 0.125-1 m/s, up to 50 m/s. The anemometer main features are reported in Table 3.1.

Table 3.1 – Technical specifications of the anemometer

Measuring range selected	Response time	Accuracy	Operating temperature	Resolution	Power input	Output signal
0.125 – 10 m/s	0.2 s	±0.5 % of full scale	0-93°C (sensor)	0.07 % of full scale	11-30 VDC o 18-38 VAC, 350 mA max	0-5 V, 0-10 V, 1-5V, 2-10V, 0-20mA, 4-20mA

Considering that in wastewater treatment systems with submerged aerators the flux exiting the tank ranges between 1-3 m^3/h/m^{-2}, the range selected for outputting the instrument could ensure a resolution below 0.15 m^3/h/m^{-2}.

DO probe (Thermo Scientific AquaSensors RDO Pro-X Dissolved Oxygen Sensor)

The DO probe selected was found to be the only suitable solution among full scale sensors, using the solid optical technology, since data could be acquired without the need of purchasing a transmitter.

In fact, most full scale DO sensors require an additional device for data translation and visualization in between the probe and the actual data acquisition port. A transmitter is necessary when a sensor is embedded in the WRRF SCADA network and, in order to allow for the usual maintenance/checks onsite, a transmitter is normally needed for visualization of the probe response by the plant personnel.

For the case of the off-gas analyzer, the presence of a transmitter is considered an additional unnecessary weight, as a light, economical and robust solution is required. Therefore, this sensor was considered the most suitable solution on the market.

This luminescent DO sensor uses the phase difference between an excitation light and the return light after reflection by O_2 molecules. This technology has the main advantage of being solid and in need of minimal (or, as stated by the manufacturer, almost none) calibration, also thanks to an automated calibration reducing long-term drift. The main specification of this probe are listed in Table 3.2.

Table 3.2 – Technical specifications of the DO probe

DO range	Accuracy	Response time	Resolution
0 to 20 mg/L	±0.1 ppm up to 8 ppm ±0.2 ppm from 8 to 20 ppm	30 s	0.01 mg/L

Temperature and ambient pressure (pre-set) are used to correct the output signal already at the sensor level. As this sensor is appositely designed for wastewater applications, all specifications perfectly fit the needs.

3.1.3. Sensor testing

Preliminary tests in laboratory controlled conditions were performed for checking all sensors response over their measuring range. Given the novelty of the O2-C2 and the CO_2 sensors, their response validity needed to be tested. These devices, unlike the DO and pressure sensors which implementation and validation are rather of the plug-and-play nature, were the less known instruments of the whole analyzer and needed additional custom-made hardware to be implemented. With the exception of the measurements of HCs, not relevant for the purpose of this thesis, the response of each gas sensor was verified in the lab.

At the West Systems lab different mixture of gases of known composition were prepared in 10 L Tedlar® bags from specialized personnel for each test and the response of the sensors were monitored using the FluxRevision (West Systems) software. The sample was fed at a 1 L/min flow rate as required by the O2-C2.

CO_2 sensor comparison with LI-COR

In order to verify the reading of the CO_2 sensor, a standard gas mixture and of an additional CO_2 sensor (LI-COR, USA) were used for comparison. The LI-COR sensor uses the same NDIR measurement principle but with improvements in the application for precision and response performances which sensibly increase its value on the market.

A first sample of standard gas containing 20100 ppm of CO_2, 10200 ppm of CH_4 and N_2 for the remaining part, was fed to the sensors in three times until signal stability. Ambient air was used to clean the line in between the measurements (Figure 3.8). The results show that the CO_2 sensor detected a concentration of 18380 ppm (Figure 3.8, top). On the other hand, also the LI-COR did not detect the correct concertation deviating 658 ppm from the real value (Figure 3.8, bottom). This is due to the fact that the LI-COR was measuring at its higher limit of the measuring range showing some drift in the signal processing.

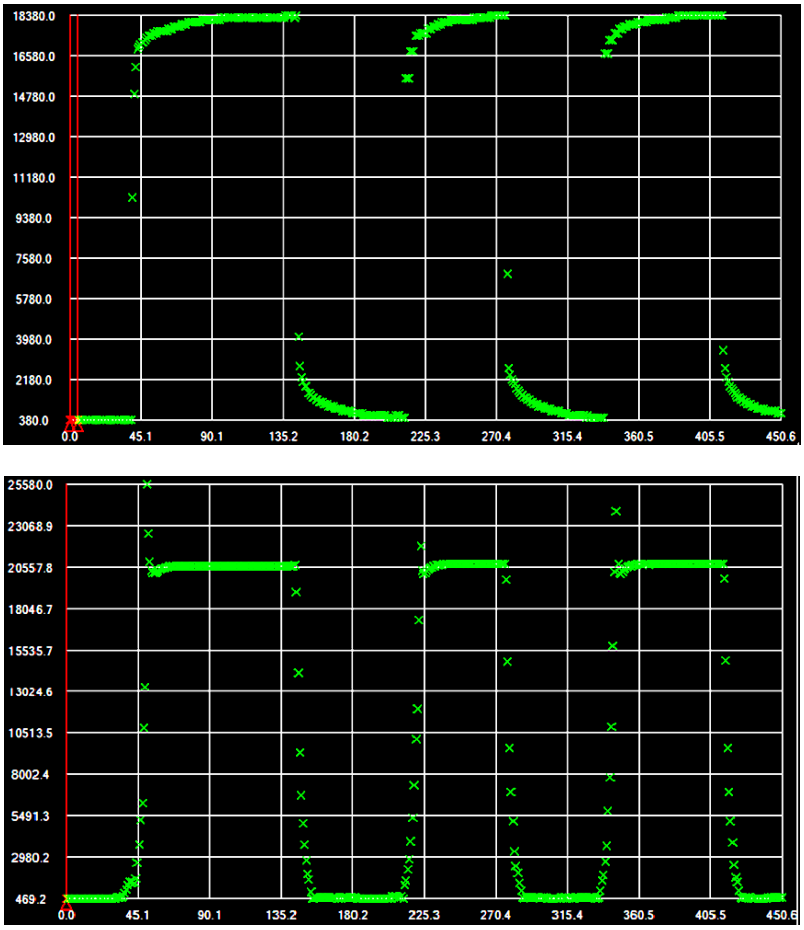

Figure 3.8 – CO_2 measurements of the CO_2 sensor (top) and of the LI-COR (bottom). Time (s) and concentration (ppm) on horizontal and vertical axis respectively (Screenshot of the FluxRevision software.).

This known standard concentration can be used to recalibrate the CO_2 sensor according to the difference between the actual and the measured concentrations (i.e. 1.094). However, a one point calibration might only be representative for the concentration of the standard gas. In order to be able to use this value for adjustment of the signal over the whole expectable range of concentrations known to occur in WRRF off-gas measurement campaigns, requires the assumption of its linearity.

To build a calibration curve and check the CO_2 sensor for its linear response, a series of known dilutions were performed on the standard gas progressively adding known amounts of N_2 (Figure

3.9). In this case the LI-COR measurements reflected very accurately the expected concentrations while the CO_2 sensor showed a need for recalibration of the signal.

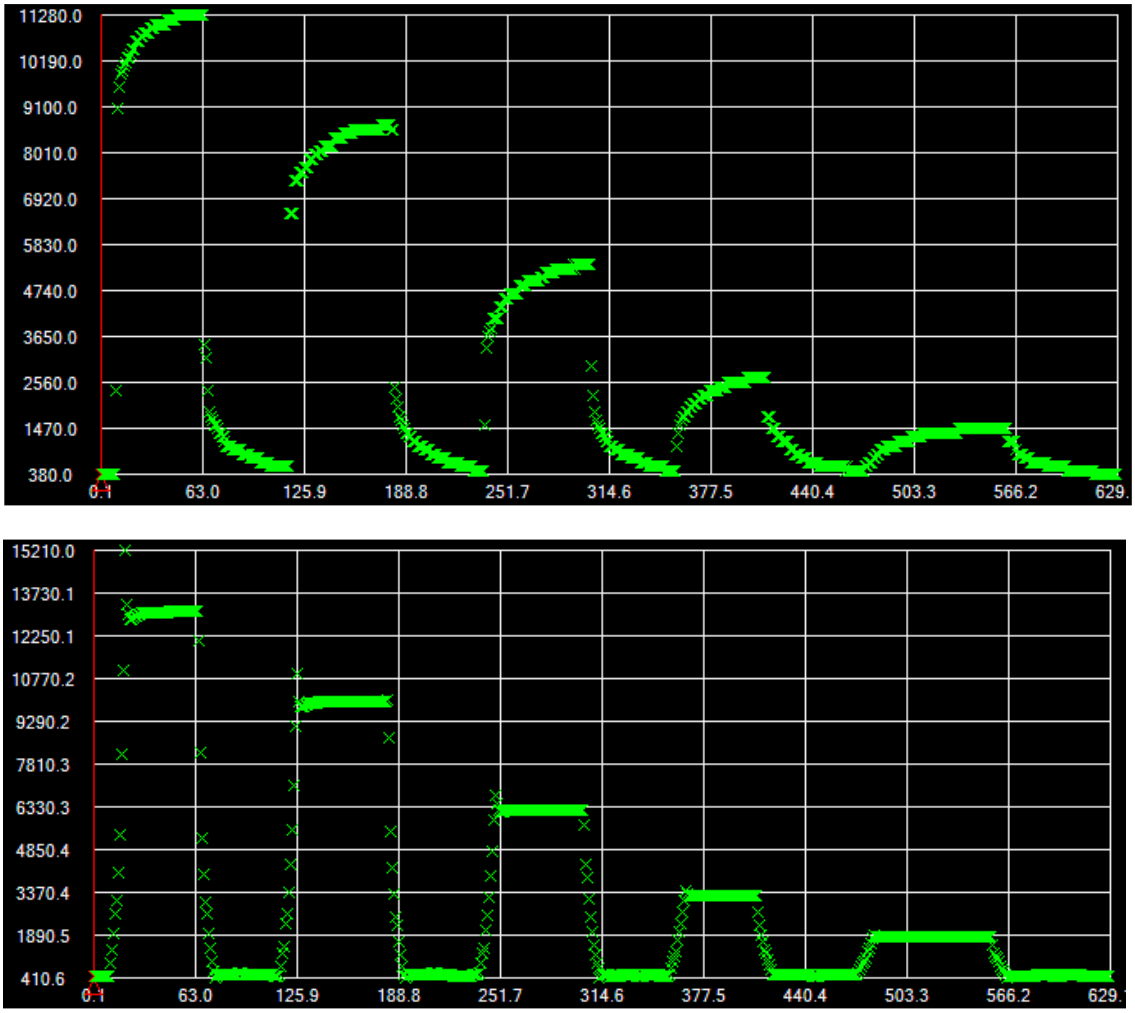

Figure 3.9 – Gas sample measurements of incremental dilutions with N_2. CO_2 measurements of the CO_2 sensor (top) and of the LI-COR (bottom). Time (s) and concentration (ppm) on horizontal and vertical axis respectively (Screenshot of the FluxRevision software.).

Comparing the measurements of the CO_2 sensor with the actual concentration of the different samples analyzed, the linear fit of the points returns an R^2 of 0.9999 and a slope of 1.145 (Figure 3.10). This can be used in the software as a calibration equation to adjust the CO_2 sensor readings in this range of concentrations.

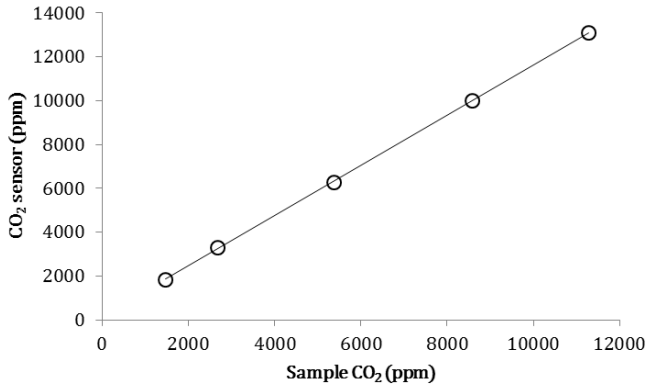

Figure 3.10 – Scatter plot of the measured and the actual CO_2 content of the standard gas progressively diluted.

In order to check for eventual sensor drifts from this linear relation due to sensor aging, the periodic repetition of this exercise is suggested. To date, no significant deviation of this value was observed.

At startup, the CO_2 sensor needs to be exposed to ambient air so that a one point calibration can be performed. For off-gas measurements this is advantageous, since reference measurements in ambient air are needed at least before the start of the measurement day. This can be considered as a zero point calibration, since in full-scale measurements there will be no case under this concentration.

Cross validation O2-C2 and CO_2 sensors, and evaluation of a CO_2 scrubber

The O2-C2 sensor is provided with very precise information on calibration curves and relations to be used over the whole range of the sensor's applicability (for temperature, pressure and humidity). These relations were implemented in the software of the off-gas analyzer. The linearity of the signal is ensured within the measuring range. However, a small verification of signal quality and sensor sensitivity in presence of different compounds concentrations was required. In this test the raw signal of the O2-C2 sensor in lab controlled environment (ambient pressure, 20°C) is shown.

In presence of only N_2 gas the sensor response was 4.38 mA which can be considered to be the zero point calibration. The small deviation from the theoretical zero of 4 mA is due to the excitation of the sensor parts by the power supplied, normally observed in every device. Thus the importance of a zero calibration.

The O2-C2 sensor was tested in parallel with the CO_2 sensor in ambient air (Figure 3.11) and with a gas mixture of 10500 ppm of O_2 10200 ppm of CO_2, 5000 ppm of CH_4 and N_2 for the remaining part (Figure 3.12). In order to crosscheck the quality of the CO_2 reading and the variations in O_2 reading due to the presence or absence of CO_2 (causing a change in O_2 partial pressure), an absorption column (1 L) with sodium hydroxide (NaOH) was used along with silica gel to trap the generated moisture. This solution of CO_2 trapping is largely used in off-gas measurements when a CO_2 sensor is not available (Caretti et al., 2014; Gori et al., 2014; Leu et al., 2009; Rosso et al., 2005) by filling

one third of a stripping column (generally of 0.5 L) with NaOH pellets. However, to the author's best knowledge, its grade of efficacy has not been reported.

In ambient air the response of the O2-C2 sensor (Figure 3.11, top) remains between 17.34 and 17.39 mA with small oscillations, both with and without the CO_2 absorption column (Figure 3.11, orange and yellow rectangles respectively). This is because the small amount of CO_2 removed (about 200 ppm, roughly 0.02% of the air composition) does not significantly impact the ambient concentration of O_2 to make visible variations in the O2-C2 sensor signal. Interestingly, the CO_2 absorption trap cannot remove all the CO_2 after 300 seconds, however, these are very small concentrations that are more than negligible for the purpose of off-gas testing.

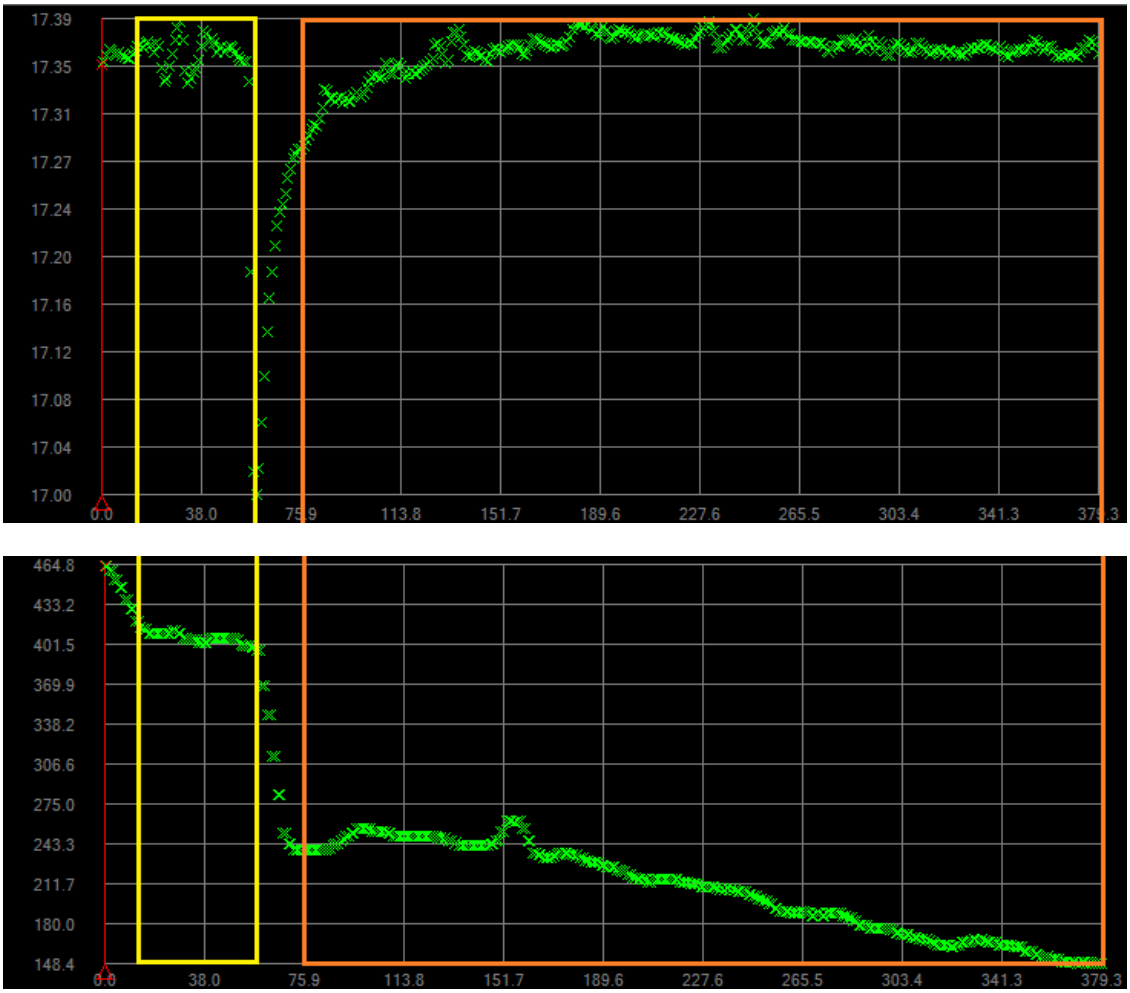

Figure 3.11 – Response of O2-C2 (top, in mA) and of CO_2 (bottom, in ppm) sensors in ambient air. The yellow and orange rectangles define the test without and with CO_2 scrubber respectively. Time (s) on the horizontal axis.

Before feeding the sensors with the gas mixture, the whole apparatus was restarted and initiated the measurement with ambient air in absence of a CO_2 scrubber (Figure 3.12, yellow rectangle) giving confirmation of the previous measurements. When the gas mixture was fed to the sensors passing through the CO_2 scrubber the O2–C2 sensor took about 20 s to arrive at equilibrium and

return 10.7 mA. This data confirms the linearity of the O2–C2 sensor behavior as it aligns with a 0.9998 R^2.

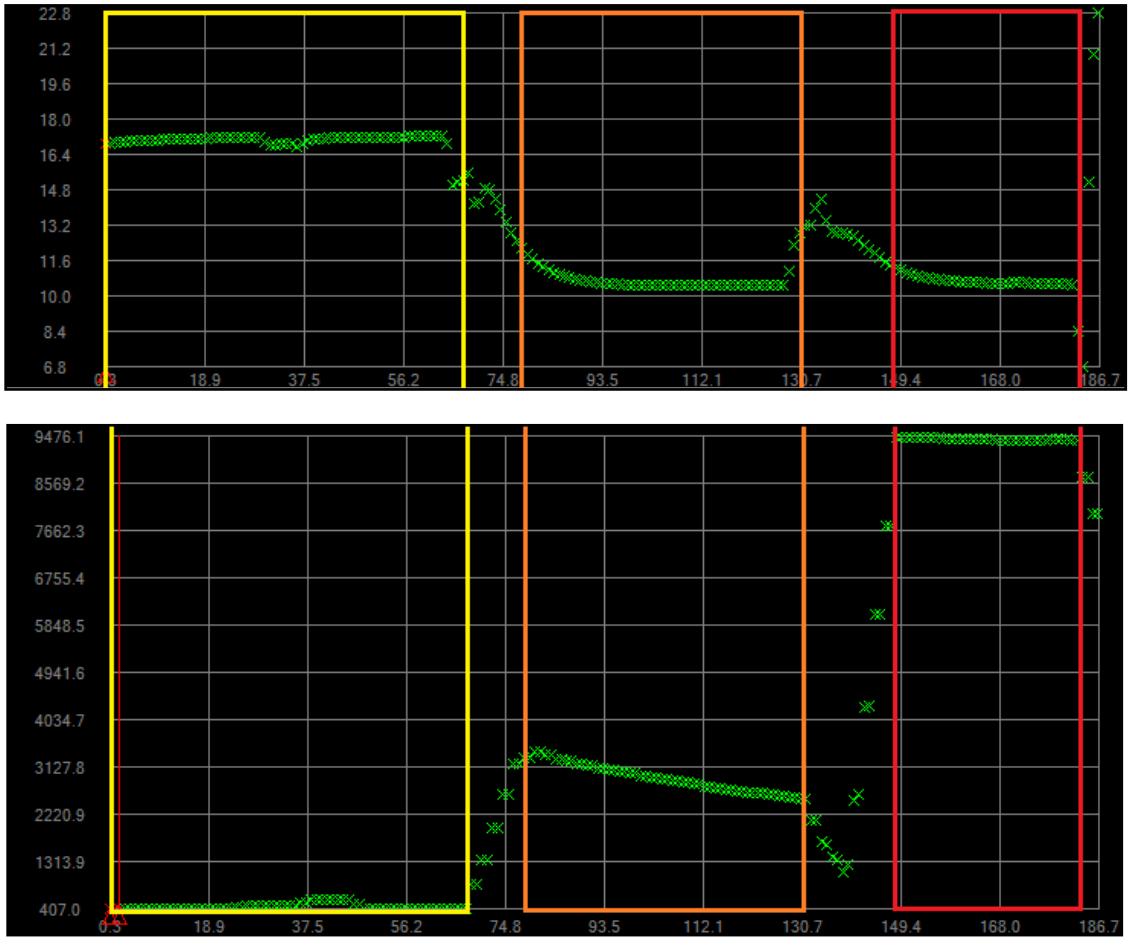

Figure 3.12 - Response of O2-C2 (top, in mA) and of CO_2 (bottom, in ppm) sensors in ambient air (yellow rectangle), and in the test sample with (orange rectangle) and without (red rectangle) the CO_2 scrubber. Time (s) on the horizontal axis.

Interestingly, the CO_2 scrubber could not capture all the CO_2, but only about 7000 pmm. When the CO_2 scrubber was excluded from the sampling line, the signal of the O2-C2 sensor was not sensibly affected and recovered its original equilibrium value. The expected increase of the O_2 percentage in the sample should have been of 0.12, which is within the accuracy of the sensor ($\pm$0.05). However, in full-scale measurements the CO_2 concentrations in the off-gas can reach 4% and leaks of CO_2 can be more relevant.

These measurements confirmed the linearity assumption of the O2-C2 sensor and the good performances of the CO_2 sensor. In addition to this, the tests revealed that CO_2 scrubbers might not be able to remove all the CO_2 and ultimately interfere with the aeration efficiency assessment. Thus, the importance of the presence of a CO_2 sensor in the off-gas analyzer or of a properly designed absorption column.

3.2. Calculation methods and results interpretation

Data acquired from the different sensors composing the off-gas analyzer and its floating hood are processed inside the controller of the off-gas analyzer. A software was designed and structured (then, hard coded in C++ with the help of West Systems) to include the various features of off-gas testing and sequence of operations for aeration efficiency in accordance with available testing guidelines but also integrating ameliorations where possible. In order to ease the operation of the analyzer, automation of both hardware (e.g. valves, pumps) and software (e.g. data acquisition and processing) was maximized as much as possible.

The data acquired by the off-gas analyzer are processed and recorded according to the different purposes of each measurement step of a complete aeration efficiency assessment. The data acquisition process, data flow and the calculation of the variables used for the final aim of calculating the efficiency of oxygen transfer are shown. The automated features of the off-gas analyzer are described in the next sections for each step of the aeration efficiency assessment.

3.2.1. Data acquisition and processing

The software of the off-gas analyzer needs a series of input values in order to be able to start the data acquisition and processing, and to safely operate the instrumentation. Some operational parameters of the off-gas analyzer are not directly changeable by a normal user but need to be modified by specialized programmers (Table 3.3). This is in order to reduce the amount of inputs needed at the GUI and discourage changes of control parameters important for the safety of the instrumentation.

Table 3.3 – Fixed parameters of the off-gas analyzer

Parameter	Description	Default value
P_{lim}	Limit of depression	200 mbar
t_{p2}	Time of action of the peristaltic pump	3 min
$Q_{air\ lim}$	Lower limit of airflow	2 L/min
C	Maximum number of consecutive drainage cycles	5
t_{max}	Max temperature of gas sample	55 °C

The off-gas analyzer allows the user to define some input parameters and information regarding environmental conditions, hood dimensions, and tank geometry, in order to be able to derive the necessary aeration efficiency measures, properly store output data, and define optimal alarm thresholds (Table 3.4).

Table 3.4 – User-defined parameters for initialization of the off-gas analyzer and their default value

Parameter	Description	Default value
β	DO saturation correction factor for process water conditions	0.99 *
θ	Geometric temperature correction coefficient	1.024 *
CF	Dimensional pressure correction factor	92.92 mbar/m *
h	Diffuser depth	6 m
P_0	Atmospheric pressure	1000 mbar
El	Elevation	0 m
$DO_{s\,20}^{*}$	Saturation concentration of DO in clean water in standard conditions	9.08 mg/L *
S_{hood}	Hood surface	2 m^2
L_{tube}	Length of sampling tube	30 m
D_{tube}	Diameter of sampling tube	6 mm
$D_{discharge}$	Diameter of off-gas discharge tube	60 mm
$L_{submergence}$	Level of hood immersion	30 cm
Logging Time	Time frequency of logged data	10 s
t_p	Point-by-point test duration	7 min
t_{Ref}	Reference test duration	5 min
t_s	Stationary test duration	7 days

* from Techobanoglous et al. (2014)

During the off-gas tests, the variables in Table 3.5 are measured and written in a text file as raw signals in order to allow the user to go back to the original mA signal and adjust for possible errors during the processing. These variables are used to derive all relevant relations for aeration efficiency assessment.

Table 3.5 – Measured variables during off-gas tests

Variable	Description	Unit
$O_{2\ Ref}$	O_2 concentration in ambient air	% (*)
$O_{2\ Off}$	O_2 concentration in the off-gas	%
$CO_{2\ Ref}$	CO_2 concentration in ambient air	% (*)
$CO_{2\ Off}$	CO_2 concentration in the off-gas	%
$CH_{4\ Ref}$	CH_4 concentration in ambient air	% (*)
$CH_{4\ Off}$	CH_4 concentration in the off-gas	%
DO	O_2 in the liquid phase	mg/L
$V_{anemometer}$	Gas speed at the anemometer	m/s
P	Pressure in the pipeline of the analyzer	mbar
T	Temperature in the pipeline of the analyzer	°C
$T_w = T_{air}$	Water temperature (same as the temperature of the gas exiting the tank)	°C

* measured during the reference test and fixed for the rest

In the signal processing of the off-gas analyzer, the MR of O_2 to inerts is calculated for both ambient air and off-gas (cfr. §2, Equation 2.1 and 2.2). By definition, inerts are all components that do not sensibly change in their concentration between the inlet and outlet of the air inflated in the AS tank. These components, can be considered to remain a constant fraction of the air for both ambient and off-gas. With this assumption, the only fractions that do change are the ones of O_2, CO_2 and water vapor, the latter being sequestered by the adsorption column.

Knowing the actual MR value of O_2 in the reference gas and the off-gas, the amount of O_2 transferred from the ambient air to the liquid phase is calculated as OTE (cfr. § 2, Equation 2.3) (Redmon et al., 1983).

The OTE is adjusted to standard conditions (of 0 mg/L DO, 1 atm pressure and 20°C temperature) according to Equation (3.1).

$$\alpha SOTE = \frac{OTE \cdot DO_{s20}^{*}}{\beta \cdot DO_{st}^{*} - DO}\,\theta^{(20-T)} \cdot 100 \qquad \text{Equation (3.1)}$$

Where the DO saturation concentrations at process temperature and at half depth, are reported to process water with Equation 3.2 and 3.3 respectively (Tchobanoglous et al., 2014).

$$DO_s = (14.62 - 0.398 \cdot T_w + 0.006969 \cdot T_w^2 - 0.00005897 \cdot T_w^3) \cdot (1 - 6.9 \cdot 10^{-6} \cdot El)^{5.167} \qquad \text{Equation (3.2)}$$

$$DO_{st}^{*} = DO_s \cdot \frac{P_0 + CF\frac{h}{2}}{P_0}$$ Equation (3.3)

The off-gas analyzer software converts the anemometer speed to flow rate with Equation 3.4.

$$Q_{Air} = \frac{V_{anemometer} \cdot \left(\frac{D_{discharge}{}^{2} \cdot \pi}{4}\right) \cdot 3600 \cdot 273.15}{273.15 + T_{Air}}$$ Equation (3.4)

The off-gas analyzer also calculates the time needed to renew the volume inside the hood and in the sampling line (Equation 3.5) so to be used to ensure the measurement on the correct sample.

$$t_{empty} = \frac{V_{hood}}{Q_{Air}} + D_{tube}{}^{2} \cdot \frac{\pi}{4} \cdot L_{tube} \cdot 1\ L/min$$ Equation (3.5)

Where V_{hood} is calculated as the difference between the hood volume and its submerged part ($L_{submergence}$) and 1 L/min is the fixed sampling speed of the sampling pump. This, retrieves an indicative time information on how much time is needed before a representative sample of a certain location can be measured.

3.2.2. Off-gas analysis

As the assessment of an aeration system can be divided in two types of tests, namely stationary measurements and point-by-point measurements, the software was structured accordingly. In addition to this, as a first step before the actual measurements, a reference test in ambient air is also considered in the software. The sequence of operations in each test is described.

Reference test

The reference measurement is needed in particular for O_2 and CO_2 sensors to be initialized and referenced to ambient air concentrations. A schematic flow diagram of the reference measurement is provided in Figure 3.13.

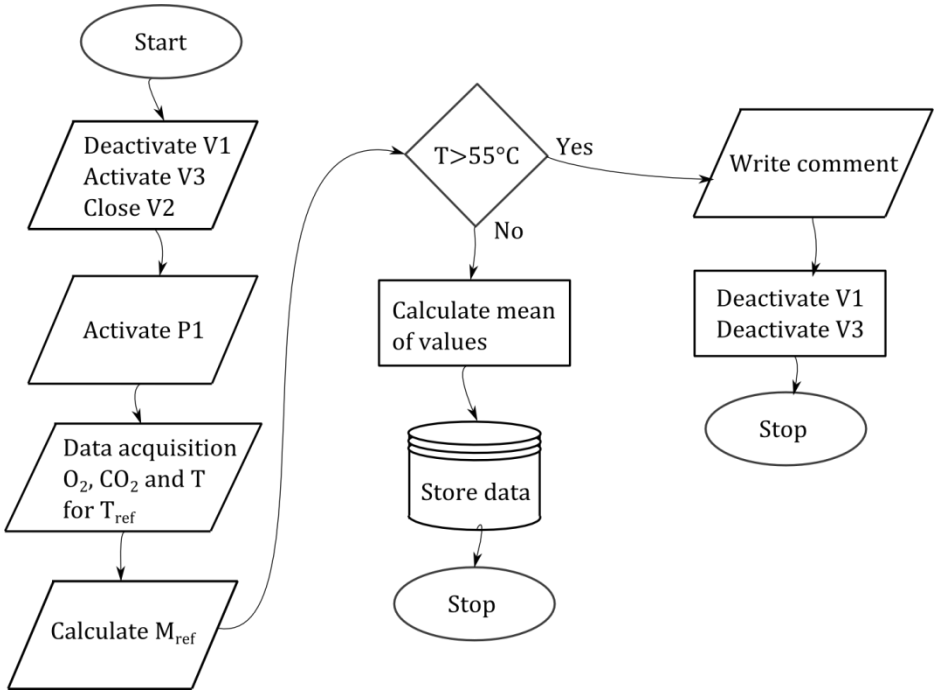

Figure 3.13 – Reference measurement flow diagram of the operations of the off-gas analyzer

As soon as the test is started, the valves are actuated in order to make the sample line take ambient air. The sampling pump is activated for a time (user-defined, default is 2min) necessary to renew the volume inside the sensors pipeline plus the actual measurement time (user-defined, default is 3min). During the measurement time, data of air temperature, O_2 and CO_2 concentrations are recorded. A temperature control on the equipment ensures safe operation below 55C. As reference for the actual aeration efficiency assessment the mass ratio of O_2 is calculated and stored in memory. Averages of acquired and calculated variables are stored in a text file including the raw signal.

Point-by-point and stationary tests

Off-gas measurement can be performed for assessing spatial or temporal dynamics of an aeration system efficiency. Both are important parts of the characterization of an aeration system and dedicated measurements have been developed over the years. The off-gas analyzer, offers the user the possibility of performing both a point-by-point test or a stationary test.

In the point-by-point test, in order to assess the efficiency of the aeration system over its area, spot measurements in different points of the aerated tank are performed. The hood is placed on pre-defined points on the tank surface and the point-by-point test is run on each of these locations.

In the stationary test, the aeration efficiency is monitored over one single location on the aerated surface. This allows to observe the effect of influent dynamics from a fixed point of view.

In terms of operation of the off-gas analyzer, the sequence of commands used for both the point-by-point and the stationary case differ only in the duration of the logging time. A schematic diagram of the operations actuated for each test is provided in Figure 3.14.

At the start of an off-gas test the valves are actuated to connect the hood with the sensor pipeline and the sampling pump is started. At this point, the data acquisition starts, but the analyzer holds-on the data logging for a time t_{empty} in order to allow the renewal of the hood and the sampling tube volumes. After this, online and calculated variables are logged for a specified time, i.e. t_p in case of a point-by-pint test or t_s in case of a stationary test.

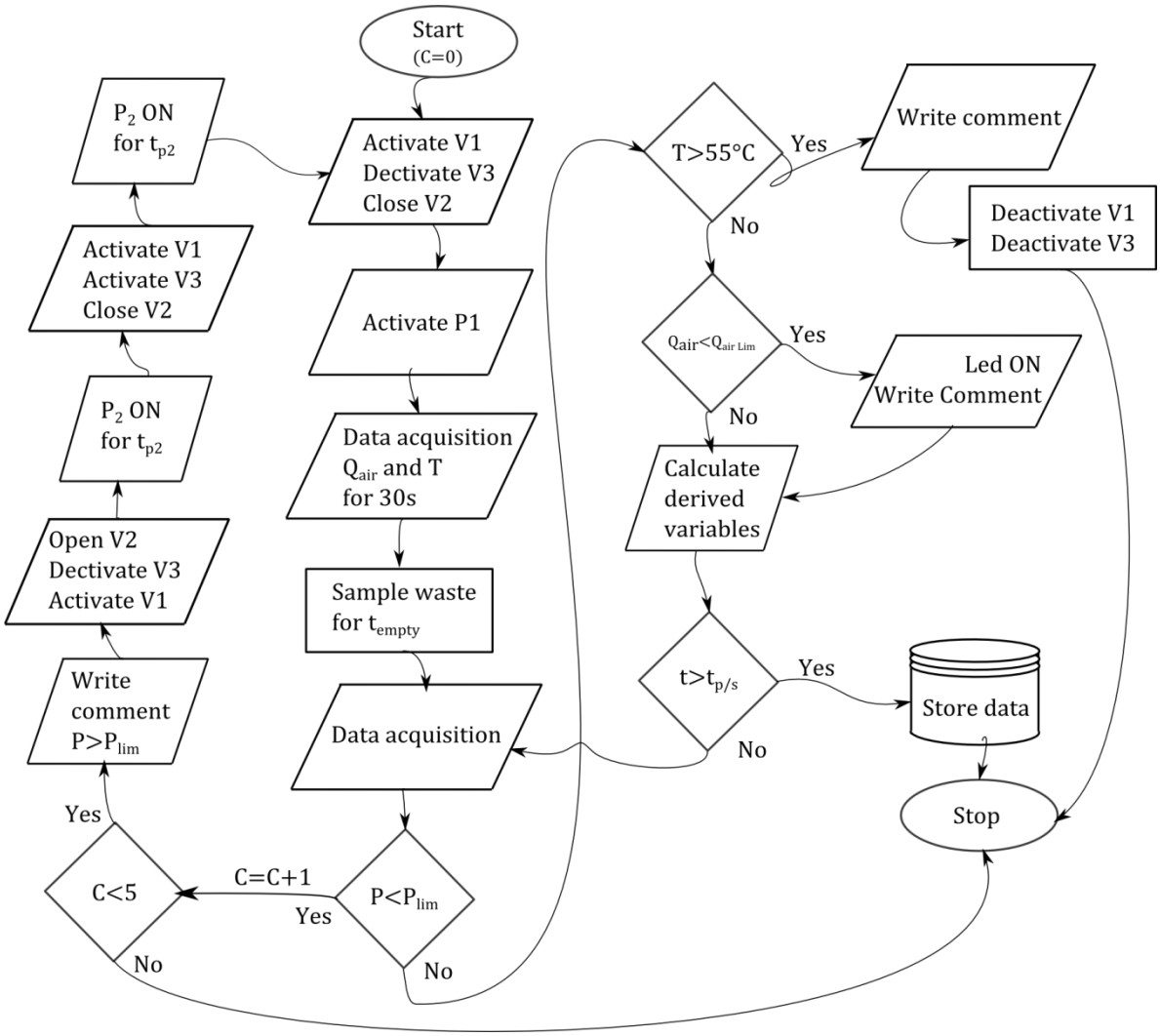

Figure 3.14 - Flow diagram of the operations of the off-gas analyzer during the point-by-point test

Pressure and temperature measurements inside the off-gas analyzer are used to ensure the good operation of the sensing devices. In particular, the pressure in the analyzer is monitored not to go below 200 mbar from the ambient pressure, and the temperature not to exceed 55°C (both values are actually dictated by the most sensitive device in the sensing pipeline, i.e. the O2-C2 sensor).

An additional control is set on a minimum flow rate leaving the monitored liquid surface, for which a comment is written on the output text file to label those measurements that are at risk of ambient air contamination. As the analyzer itself needs 1 L/min, in the waste hose of the hood there should pass at least 2 L/min for ensuring an unbiased sample.

3.2.3. Post-processing and interpretation of results

Results are stored by the off-gas analyzer in a raw data and a summary text file both of which in tab separated format. The header of each file returns the eventual description of the user, data frequency, duration, type of test, and time and date information of the test.

The raw data file contains the raw signals of all instruments inside the off-gas analyzer and the calculated variables. Therefore, all information of the relative measurement are stored in this file.

Separately from the raw files, and stored in separate dedicated folders depending on the type of test, are the summary files of reference, point-by-point and stationary tests. The summary files contain meaningful statistics of the single test. In specific, for reference measurements, average, standard deviation, minimum, and maximum of CO_2 and O_2 measurements are reported. For stationary and point-by-point tests, the same statistics are reported for αSOTE, OTE, Q_{Air}, O_2 and CO_2.

Effects of O_2 measurement error on calculated variables (error propagation)

Comparability of efficiency results among different tests and different WRRFs can be significantly affected by the accuracy of the O_2 sensor. In this regard, the measurement error of an O_2 probe is propagated to the final aeration efficiency measure.

The error of an O_2 sensor is propagated by the calculation of the MR (cfr. § 2, Equation 2.1, 2.2 and ultimately 2.3) to the OTE value. This effect is not linear as the error on the reading gains importance for low O_2 values. Defining a domain of O_2 measurements and a domain of possible sensor errors (sensor specific) enables to calculate the uncertainty around the MR values (Equation 3.6).

$$MR = \frac{O_2 \pm \Delta O_2}{1 - CO_2 - (O_2 \pm \Delta O_2)} \qquad \text{(Equation 3.6)}$$

From here, the reflection of the measurement error on the final OTE value can be calculated (Figure 3.15). The surface can be divided in isolines of OTE, defining different regions of uncertainty around a given O_2 value of a probe characterized by a given error. Since the measurement error becomes more important when O_2 values are low, its effect on the resulting OTE is more prominent with decreasing O_2 concentrations. Two sensors having different precision but operated at different O_2 levels, may have the same accuracy on the final OTE. On the other hand, the same sensor, does not have the same accuracy with respect to OTE, over the entire range of O_2 values.

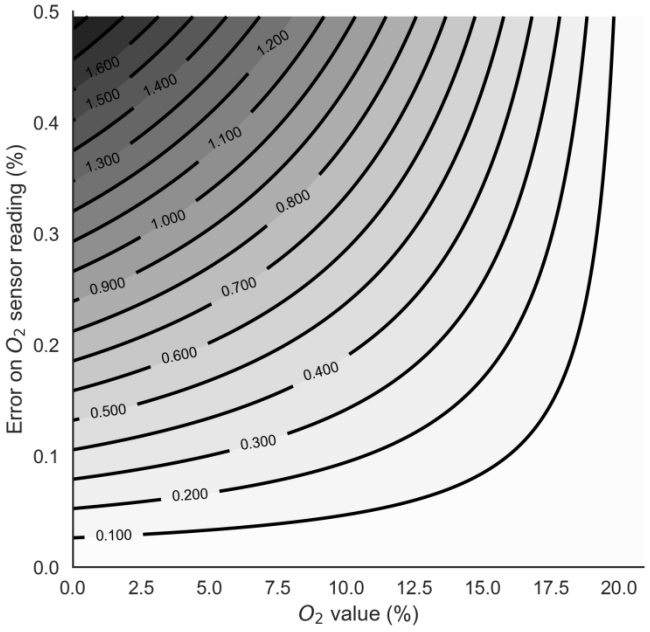

Figure 3.15 – Isoclines of OTE (%) for possible O_2 concentrations in off-gas samples and specific probe errors

The O2-C2 sensor, being characterized by a ± 0.052 error on its O_2 % reading (± 0.25% of full-scale), has a relative range of error on the OTE. For each value of OTE, the accuracy of the O_2 sensor causes the error in Figure 3.16. Given the low magnitude of the sensor error, its reflection on the OTE error is almost linear. Nonetheless, considering that normally the O_2 concentration in off-gas measurements does not go below 12%, the error on the final OTE reading for the O2-C2 sensor does not exceed 0.15 %.

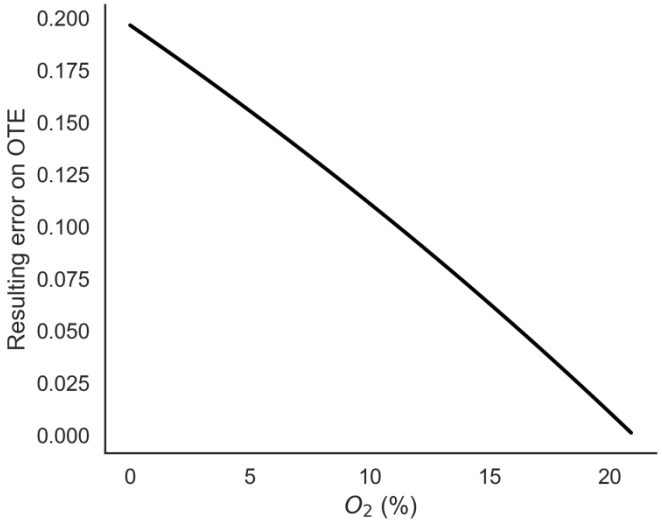

Figure 3.16 – Effect of the error of the O2-C2 sensor on the calculated OTE for the entire range of O_2 values

In full-scale measurements, this reflects in a varying uncertainty depending on OTE levels. Applying the results in Figure 3.16 to a time series of OTE measurements performed on a full-scale WRRF, it is possible to see how the measurement error of the O_2 probe reflects in terms of uncertainty on the final OTE readings (Figure 3.17). At each value of OTE (Figure 3.17, top) corresponds an uncertainty around it (Figure 3.17, bottom). However, the maximum OTE uncertainty that can be observed in the case reported does not exceed 0.14 %. This value was plotted as a $\pm$ 0.07 % shaded area around the OTE time series (Figure 3.17, top), but it is not even visible as compared to the normal variations observed in the biological tank dynamics.

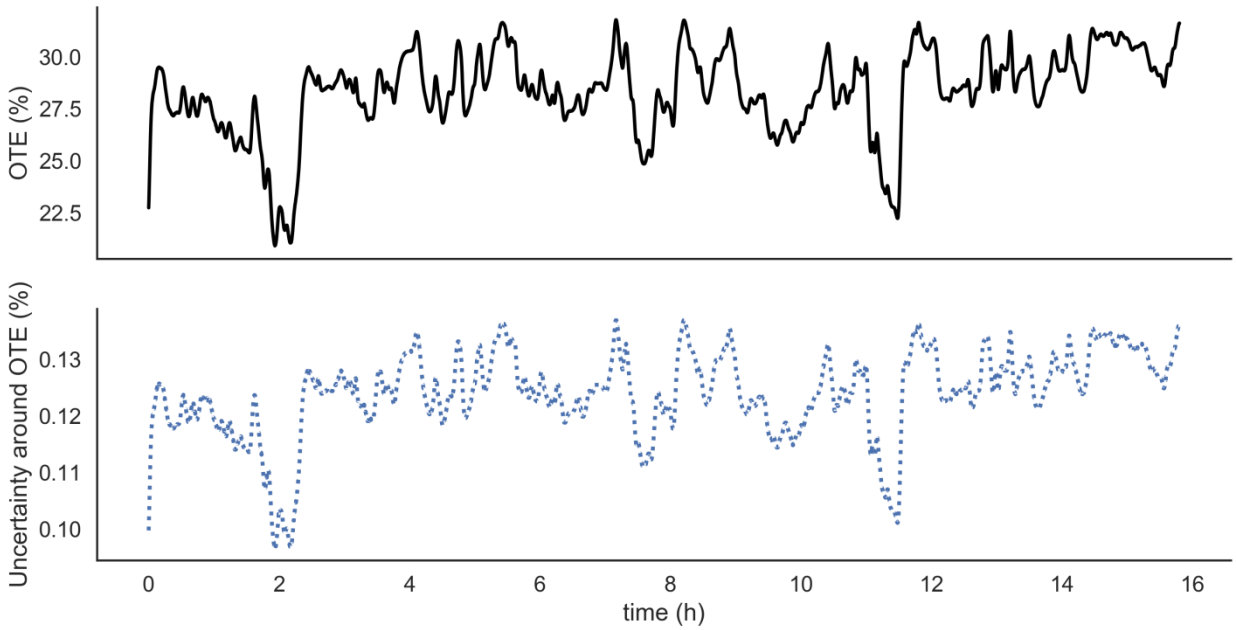

Figure 3.17 – Full-scale measurements of OTE (top) showing the uncertainty caused by the probe's error on the calculated OTE values (gray shadow at the top graph). Absolute values of uncertainty for each OTE reading (bottom graph)

For the case of the O2-C2 sensor, it can be stated that the accuracy of the probe does not significantly influence OTE calculation resulting in high accuracy in terms of efficiency measurements. The effect of the O2-C2 sensor error can be considered as negligible for the range of OTE considered. Unless OTE values increase significantly above 40 % (unfortunately almost unfeasible for current aeration devices using ambient air), the error of the O2-C2 sensor can be considered as non-influential. However, in case that comparisons, e.g. among different points of an aerated tank rather than among different tanks, concern differences in OTE similar to the observed uncertainty, the corresponding error cannot be ignored and should be considered.

Effect of errors of other sensors

The accuracy of the pressure and temperature sensor is much higher as compared to that of the O2-C2 sensor that its effect on the O2-C2 reading (and reflection on OTE) can be neglected. A similar conclusion can be stated for the CO_2 sensor, for which the accuracy can affect OTE for a maximum of 0.0063 %, even far below what was observed for the O2-C2 sensor. Therefore, the reflection of the other sensors used in the off-gas analyzer on the calculation of OTE can be considered as negligible.

Although the measurement accuracy of optical DO probes is nowadays extremely high as well as the one of temperature sensors, further research should focus on assessing the effect of DO and temperature error on the calculation of αSOTE.

3.3. Extensions for N_2O monitoring

The off-gas analyzer can be extended for measurements of N_2O emissions from the aerated compartments by coupling it with available N_2O sensors for gas and liquid phase as discussed earlier in this work (cfr. § 2.3.2).

To the best of the author's knowledge, yet there are no sufficiently small (and economically interesting) sensors for N_2O measurement in the gas phase that can be embedded in the off-gas analyzer sensors pipeline. Therefore, the use of a parallel N_2O analyzer is suggested along with the off-gas analyzer when N_2O emissions have to be monitored. As described earlier, current alternatives for measuring gaseous N_2O are IR and micro-GC technologies. These devices can be used in field applications and a selection over costs, benefits, and ease of use, can determine the most suitable choice for a specific user.

In the present work, the Model 46i (ThermoFisher Scientific, USA) N_2O analyzer was preferred over the micro-GC due to its reasonable measurement accuracy (0.02 ppm resolution), low calibration requirements, ease of use, no requirements for extra equipment onsite (e.g. gas cylinders), and automatic correction for temperature and pressure.

As stripping capabilities of aeration devices in WRRFs can substantially differ due to design features and tank geometry among the rest, it is also advisable to monitor dissolved N_2O measurements. As a matter of fact, the liquid measurements give a more precise indication of what is the actual production of N_2O for a certain location in the bioreactor while gas measurements quantify the actual emission, which is dependent on stripping by aeration devices and the degree of fluid surface motion. For this purpose, two full-scale N_2O sensors from Unisense Environment (Denmark) were used in the present work. The probes were calibrated before each measurement campaign.

3.3.1. Monitoring anoxic zones

The contribution of anoxic zones has been observed to be relevant in the assessment of the biological tank contribution to N_2O emissions in WRRFs (GWRC, 2011; Marques et al., 2016). Therefore, solutions for monitoring these environments are needed. In the present work, a floating hood was designed and tested in a full-scale measurement campaign (cfr § 4.2) with the aim of facilitating the assessment of N_2O emissions in non-aerated surfaces.

The floating hood developed for anoxic zones, here named FhAx for the ease of reading, is based on the principle of the Lindvall gas hood system (Lindvall et al., 1974). This method was firstly implemented for this purpose by Desloover et al. (2011), where they created a confined channel, opened at the bottom to allow exchange with the bulk liquid. The working principle wanted an air flow blown from one side to the other where a measuring device was placed. In this way, the air

sample along the length of the exchange chamber was enriched for diffusion at the liquid surface as it would naturally happen but causing high sample dilutions and wastage making the system applicable only for extremely high-emitting surfaces.

The FhAx (Figure 3.18) is designed to be used along with an auto-sampling analyzer so that the ambient air entering the channel can be minimized to minimize dilutions of the gas sample and maximize the capabilities of detection of the analyzer. This allows to extend its applicability to measure very low emissions from non-aerated surfaces minimizing the air travelling inside the channel and maximizing accumulation. The IR used in this work requires a flow of 1 L/min which leaves 1.7 minutes for the accumulation inside the FhAx (considering the floating line at half of the channel). The suction induced by the analyzer on one side of the channel, allows a clean sample of ambient air to travel in a confined space at the surface of the tank.

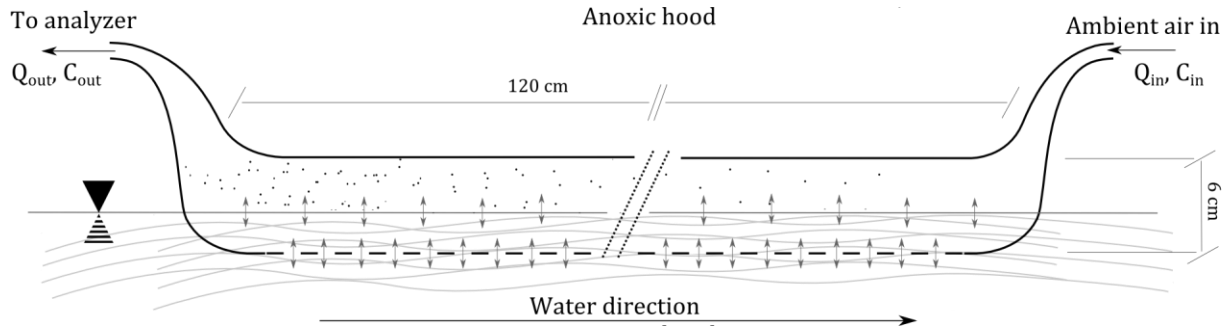

Figure 3.18 – Floating hood for anoxic zones (FhAx), schematic overview of the working principle and major quotes.

As the emissions from the tank surface can alter the baseline N_2O concentration of the air entering the FhAx, the inlet of the exchange channel should be connected to a sufficiently long tube to make sure the incoming air comes from unbiased ambient air. Also, the inlet air should be monitored to know the baseline concentration and accurately assess only the N_2O release from the tank surface. Knowing the ambient N_2O concentration, the size of the channel and the sampling airflow, it is possible to calculate the exchanged N_2O at the interface of non-aerated areas.

The quotes indicated in Figure 3.18, represent the apparatus developed in the present work, however, different dimensions can be used as far as the following points are satisfied.

- Ensure N_2O gas sample concentrations far below 900 ppm in order not to limit diffusion from the liquid; indicative value obtained assuming an oversaturation of 1.5 mg/L in the liquid and Henry's constant of 2.5 $mol \cdot m^{-3} \cdot Pa^{-1}$ (Sander, 2015)
- Ensure sufficient gas residence in order to allow exchange of a measurable amount of N_2O for the analyzer in use.

3.3.2. Calculating emissions

Once the concentration of the ambient sample and of the off-gas sample are known (for measurements on both aerated and non-aerated surfaces), the following equation can be used to calculate the EF.

$$EF = \left(\sum_1^j \frac{Q \cdot (C_{out} - C_{in})}{A_{hood\,j}} \cdot A_j\right) \cdot \frac{1}{NH_4 - N_r} \quad \text{(Equation 3.7)}$$

Where:

- j – the number of the area measured
- Q – the local airflow measured over the monitoring area or its best approximation. For the case of anoxic zones this is the sampling flow of the N_2O analyzer.
- C_{in} the N_2O-N concentration in the environment adjusted for temperature and pressure.
- C_{out} – the N_2O-N concentration in the sample adjusted for temperature and pressure.
- A_j – area j^{th} location.
- $A_{hood,j}$ – the area of the j^{th} hood.
- $NH_4 - N_r$ – removal of NH_4^+-N per unit time as the difference between the incoming NH_4^+-N to the bioreactor and the concentration exiting the plant.

Where available, online NH_4^+-N measurements (either from SCADA or manual sampling) should be used. As alternative, a known removal efficiency can be a valid substitute. The EF has the dimension of N_2O-N emitted per NH_4^+-N removed.

3.4. Conclusions

An off-gas analyzer was designed and assembled considering the most important requirements for off-gas testing and providing features crucial to be considered when assessing aeration efficiency in WRRFs. Its components were described in detail, tested and the most important results were shown proving the suitability of sensing devices on OTE assessment.

The off-gas analyzer contains automated features that are aimed at assuring a good implementation of the off-gas tests. The software considers the volume of sample to waste in order to renew both the internal analyzer volume and the hood volume based on the airflow from the liquid surface. All internal equipment is monitored for operating in optimal conditions. All the main aeration efficiency variables are calculated online and stored in the output files along with raw data.

The possibility to extend off-gas measurement to N_2O emission monitoring for full-scale application was provided for both gas and liquid phases. Most importantly, an additional floating hood was designed for assessing N_2O emissions from non-aerated surfaces.

3.5. References

Bellandi, G., Plano, S., Rosso, D., Maere, T., Keyser, W. De, Weijers, S., Flameling, T., 2011. Measuring oxygen transfer efficiency (OTE) at the Eindhoven WWTP using real-time off-gas analysis in circular aeration tank, in: IWA BeNeLux Regional Young Water Professionals Conference, 2nd.

Caivano, M., Bellandi, G., Mancini, I.M., Masi, S., Brienza, R., Panariello, S., Gori, R., Caniani, D., 2017. Monitoring the aeration efficiency and carbon footprint of a medium-sized WWTP: experimental results on oxidation tank and aerobic digester. Environ. Technol. 38, 629–638.

Caretti, C., Gori, R., Caffaz, S., Dugheri, S., Lubello, C., 2014. Monitoring of the oxygen transfer efficiency and greenhouse gas emissions in the oxidation tank of San Colombano WWTP, in: Proceedings IWA EcoSTP Conference in Verona.

Daelman, M.R.J., van Voorthuizen, E.M., van Dongen, L.G.J.M., Volcke, E.I.P., van Loosdrecht, M.C.M., 2013. Methane and nitrous oxide emissions from municipal wastewater treatment – results from a long-term study. Water Sci. Technol. 67, 2350.

Daelman, M.R.J., van Voorthuizen, E.M., van Dongen, U.G.J.M., Volcke, E.I.P., van Loosdrecht, M.C.M., 2012. Methane emission during municipal wastewater treatment. Water Res. 46, 3657–70.

Desloover, J., De Clippeleir, H., Boeckx, P., Du Laing, G., Colsen, J., Verstraete, W., Vlaeminck, S.E., 2011. Floc-based sequential partial nitritation and anammox at full scale with contrasting N2O emissions. Water Res. 45, 2811–2821.

Gori, R., Balducci, A., Caretti, C., Lubello, C., 2014. Monitoring the oxygen transfer efficiency of full-scale aeration systems: investigation method and experimental results. Water Sci. Technol. 70, 8–14.

Guo, L.S., Lamaire-chad, C., Bellandi, G., Daelman, M.R.J., Maere, T., Nous, J., Flameling, T., Weijers, S., Mark, C.M., Loosdrecht, V., Volcke, E.I.P., Nopens, I., Vanrolleghem, P.A., 2013. High frequency Field Measurements of Nitrous oxyde (N2O) Gas Emissions and Influencing Factors at WWTPs under Dry and Wet Weather Conditions, in: WEF/IWA Nutrient Removal and Recovery 2013.

GWRC, 2011. N2O and CH4 emission from wastewater collection and treatment systems. Lodon.

Leu, S.-Y., Rosso, D., Larson, L.E., Stenstrom, M.K., 2009. Real-Time aeration efficiency monitoring in the activated sludge process and methods to reduce energy consumption and operating costs. Water Environ. Res. 81, 2471–2481.

Lindvall, T., Noren, O., Thyseliu.L, 1974. Odor reduction for liquid manure systems. Trans. Asae 17, 508–512.

Marques, R., Rodriguez-Caballero, A., Oehmen, A., Pijuan, M., 2016. Assessment of online monitoring strategies for measuring N2O emissions from full-scale wastewater treatment systems. Water Res. 99, 171–179.

Porro, J., Kampschreur, M.J., Pijuan, M., Volcke, E.I.P., Daelman, M.R.J., Guo, L., Nopens, I., Vanrolleghem, P.A., Yuan, Z., Chandran, K., Murthy, S., 2014. Measuring nitrous oxide emissions from biological wastewater treatment, art or science?, in: IWA Specialist Conference on Global Challenges for Sustainable Wastewater Treatment and Resource Recovery. Kathmandu, Nepal.

Redmon, D.T., Boyle, W.C., Ewing, L., 1983. Oxygen transfer efficiency measurements in mixed

liquor using off-gas techniques. Water Pollut. Control Fed. 55, 1338–1347.

Rosso, D., Iranpour, R., Stenstrom, M.K., 2005. Fifteen years of off-gas tranfer efficiency measurements on fine pore aerators: key role of sludge age and normalized air flux. Water Environ. Res. 77, 266–273.

Sander, R., 2015. Compilation of Henry's law constants (version 4.0) for water as solvent. Atmos. Chem. Phys. 15, 4399–4981.

Tchobanoglous, G., Burton, F.L., H.D., S., 2014. Wastewater Engineering: Treatment and Reuse (5th ed), Metcalf and Eddy, McGraw-Hill series in civil and environmental engineering. McGraw-Hill, New York.

Chapter 4

4. Field measurements and sampling strategy

This chapter is redrafted from:
Bellandi G., Porro J., Senesi E., Caretti C., Caffaz S., Weijers S., Nopens I. and Gori R. "Multi-point monitoring of nitrous oxide emissions in three full-scale conventional activated sludge tanks in Europe" (2018) *Water Science & Technology, 77(4): 880-890*.

Abstract

Monitoring aeration efficiency and N_2O emissions from biological tanks requires adequate technology and methodologies in order to produce reliable and comparable results. Ideally, measurements performed in view of describing a certain process of a WRRF should be reproducible within the same facility and, at the same time, to be easily compared with other plants. This is particularly important for aeration efficiency and N_2O emission assessment.

Available standard guidelines for oxygen transfer testing and N_2O emission assessment have guided users towards obtaining reproducible measurements, reasonably comparable with results produced elsewhere by other groups. However, the variety of plant layouts, tank geometries and different aeration technologies used often induce variability in the results hindering their comparability. Hence, the continuous need of methods refinements suggesting best practice modalities and robust measuring equipment.

In this chapter some of the methodical bottlenecks in aeration efficiency testing and in N_2O emission assessment are discussed. For aeration efficiency, two critical points in performing spot measurements (point-by-point tests) are discussed, in particular the ASCE standard limit of 2% on the area to be covered, and the time issue linked to influent variability when monitoring a series of points in time. On the other hand, regarding N_2O emissions, as monitoring guidelines are fewer in this case, a monitoring technique is proposed.

4.1. Aeration efficiency

Methodological guidelines are of importance for every standard procedure. In full-scale aeration efficiency assessment there are well known difficulties for performing reliable unbiased measurements. In particular, according to ASCE standards, the amount of point-by point measurements is suggested to be set to a minimum of 2% of the basin's total surface area (ASCE, 1997). However, the background leading to this threshold is not explained and motivations remain vague.

Depending on the area of the hood, the number of points to be assessed can significantly impact the duration of the test. The total duration of a series of point-by-point measurements has currently no specific indication and the advantage of adding one spot measurement is not clear, while efforts can be substantial. Hence, the effort of this section is exploring the added value of increasing tank surface coverage.

In addition to this, as the number of point-by-point measurements increases, differences between the first and last points assessed can become considerable depending on influent dynamics. The extent of the effect of influent variability on the aeration efficiency of one location, can be noticed when stationary off-gas measurements are performed at a fixed airflow. The variability that can be observed during these measurements is still present when performing point-by-point tests, however, in this case difficult to isolate, making differences between points the lumped result of both the interaction between local influent characteristics and effective local efficiency. Therefore, the time issue on surface coverage is treated in this section.

4.1.1. Tank surface coverage

At the WRRF of Florence, aeration efficiency measurements were performed with the off-gas analyzer and the floating hood described in this work (cfr § 3). In order to cover 2 % of the total aerated surface with the floating hood of 2 m^2, 7 points-by-point measurement are sufficient. An additional 5 points were monitored for a total of 12 locations representing 3.40 % of the aerated surface (Figure 4.1), in order to largely exceed the minimum required monitored surface and evaluate the added value of including additional locations. The distribution of the points was defined in view of evenly covering the three zones in which the aeration tank is divided. The WRRF of Florence was chosen for this exercise as influent dynamics are much smoother compared to other plants given the diluted characteristics of the influent due to groundwater infiltration. This, minimizes the effect of influent load on aeration efficiency measurements as influent dynamics can potentially become important when a large amount of point-by-point measurements have to be performed.

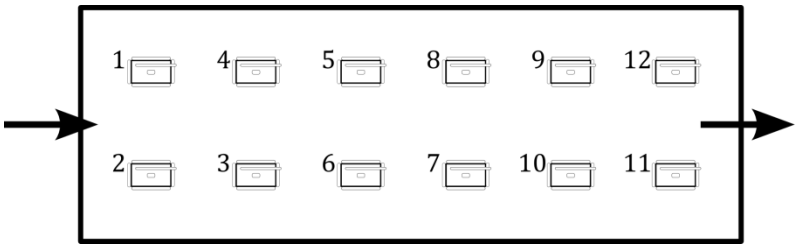

Figure 4.1 – Top view of the sequence of point-by-point measurements performed at the WRRF in Florence

In the literature, the efficiencies measured from different locations are often used to have both a more detailed average value of the overall efficiency of the system and an overview of the efficiency distribution of the aerated area (Amerlinck et al., 2016; Caivano et al., 2017; Gori et al., 2014).

As efficiency may substantially vary among different points due to hydrodynamics, contaminants concentration, and air distribution, the addition of a measurement spot can more or less contribute to the final aeration efficiency assessment. The decision of the amount of points to be monitored is often a trade-off between accuracy and the time needed for one single measurement. However, an a priori rule to be applied in the definition of the number and distribution of measurement locations is difficult to define.

Using the 12 measured efficiencies over the tank area and recursively discarding, at first one and then more and more locations, a recombination game of all possible configurations at decreasing number of available points could be performed. In particular, considering the availability of 12 measurements as a reference, a "*true mean*" of the efficiency over the tank area can be assumed. Initially, one of the 12 samples can be recursively discarded resulting in 12 possible combinations of groups. In a second instance, dropping all possible combinations of two samples from the 12 points, results in 66 possible combinations. This can be repeated until hypothetically all measurements except one can be dropped thus resulting in the 12 points measured. The recombination game was performed using the *Itertools* and *Combinations* modules of Python (Python Software Foundation, https://www.python.org).

The recombination game proposed, provides an overview of the degree of dispersion of the results with respect to a maximum number of measurements. To quantify this, in view of defining a possible threshold criterion for the definition of the minimum required measurement, the RMSE was used as indication of the deviation from the *true mean*.

The recombination game

The 12 locations were monitored for aeration efficiency between 12:00 and 15:00 with the modalities of the proposed off-gas analyzer and results are reported in Figure 4.2 in terms of αSOTE. The boxplot reports the efficiencies in the 12 locations and relative statistics. Also, the minimum required amount of points to cover the 2 % of the area is reported as a general indication. Each of the point-by-point measurement has a different mean value and range of efficiencies as local conditions vary around the tank. Overall, the efficiency varies between 15.1 and 29.2 % with average αSOTE at 22.6 %.

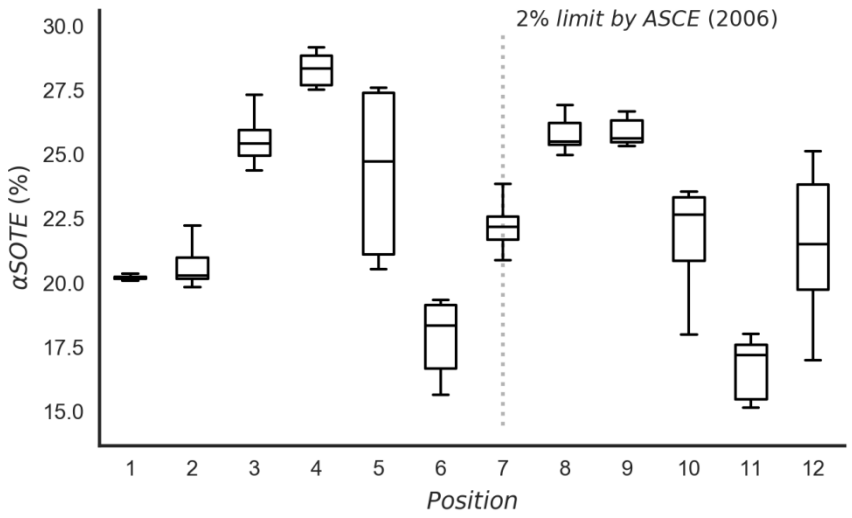

Figure 4.2 – Box plots of the OTE measured in the 12 locations and the indication of the ASCE recommended minimum for the hood used

The most efficient location in terms of oxygen transfer appears to be location 4, while location 11 reports the lowest efficiency. Locations closer to the inlet (i.e. 1, 2 and 3), and thus experiencing higher influent loadings and airflow (due to higher diffuser density), report a slightly higher efficiency as compared with locations close to the outlet (i.e. 10, 11 and 12) but only because location 3 is sensibly higher than 1 and 2, and location 11 is the lowest registered. The variability observed is the combined result of local differences in the air distribution, local concentrations, and different local diffuser aging. In order to properly assess the overall aeration efficiency, it is important to choose a sufficient amount of monitoring points that would give a proper representation.

A recombination game of the 12 locations can be performed dropping recursively 1 to 11 locations and performing all combinations of aeration efficiency for each possible combination of groups (Figure 4.3). The average αSOTE resulting from all the data contained in the 12 samples is the hypothetical t*rue mean* (black dot in Figure 4.3 left). This is used for evaluating the deviation resulting from a lack of a number of samples, increasing towards the right of Figure 4.3. In specific, if we would have chosen to work with 11 available samples (or point-by-point measurements), the 12 possible groups of samples return a cluster of mean values that deviates from the t*rue mean* with an RMSE of 0.316. As we decrease the number of samples available, the cloud enlarges and the RMSE as well. In final instance, having the availability of only one measured location among the 12 (1 available sample, Figure 4.3, right), we would have the largest cloud (and RMSE) possible. This means that measuring from only one location on the whole tank surface would bring a very high uncertainty as compared to the t*rue mean*.

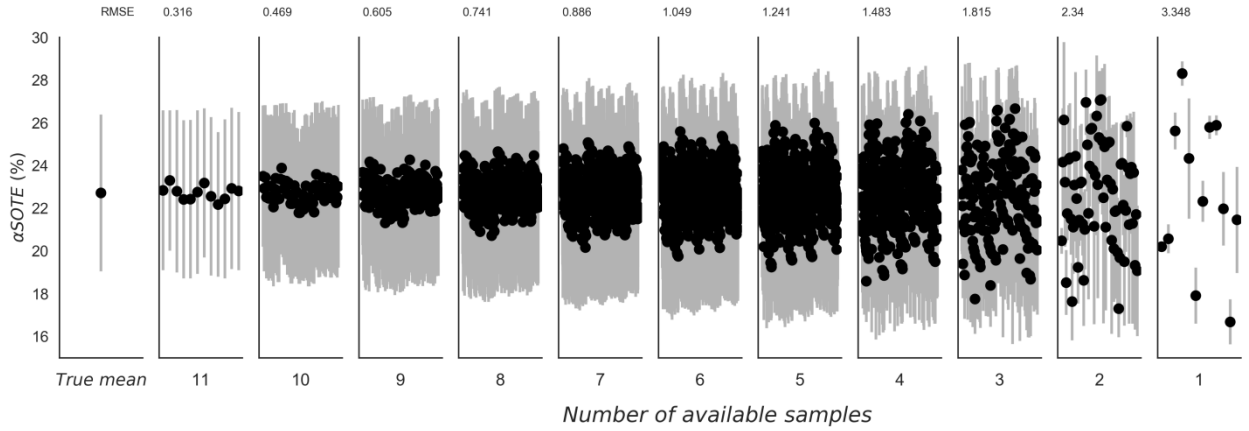

Figure 4.3 – Recombination game of the 12 locations. Each graph reports all possible hypothetical combinations of αSOTE that can be obtained discarding one part of the available samples. Mean and standard deviation of the samples are reported with black dots and gray lines respectively.

The overview provided in Figure 4.3 gives information on the number of effectively necessary point-by-point measurements. Interestingly, reaching the number of 7 available samples, the RMSE drops below 1 (Figure 4.3). In this sense, for an indication of the gain in accuracy of the aeration efficiency assessment at each additional sample, the shape of the RMSE curve provides better insight (Figure 4.4, left). For each additional point-by-point measurement on the tank surface, the RMSE decreases with a varying slope, meaning that the informative gain decreases as well. The slope of the RMSE curve (Figure 4.4, right) reaches its minimum with 9 available points, meaning that the 9th additional location returned very few information as compared with the others.

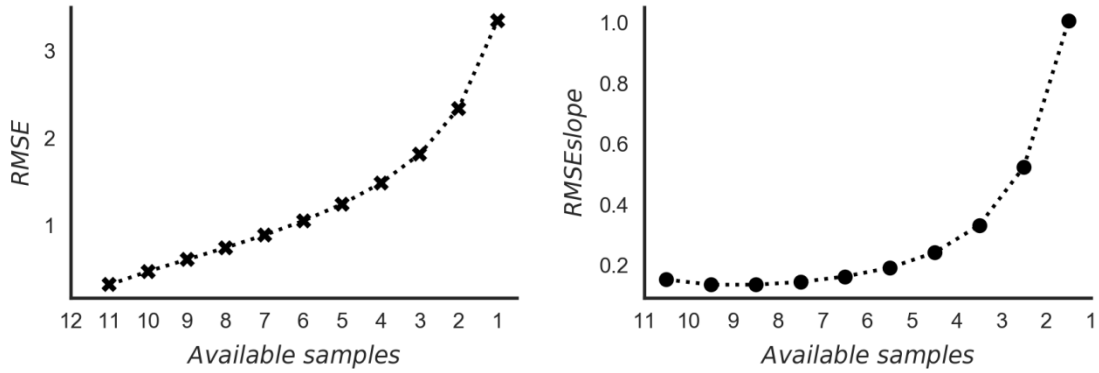

Figure 4.4 – RMSE deviation of the average OTE obtained using a number of samples from the average obtained with 12 samples (left). Slope of the RMSE curve showing the variation in RMSE at varying samples number (right)

For the case studied, in terms of % of aerated surface covered, reaching 2.27 % (8 points) reported an increment RMSE, while reaching 2.55 % (9 points) provided the minimum gain observed in RMSE (Figure 4.4, left). From these results it appears that measuring from 2.27 % of the tank area provides the most informative contribution to the real representation of the tank. Also, decreasing

the tank coverage below 1.7 % (6 points) reduces more importantly the precision of the aeration efficiency assessment.

In terms of deviation from the *true mean* (Figure 4.5), all points between 4 and 9 result in the same reduction of standard deviation (slope of the curve) confirming the observations above.

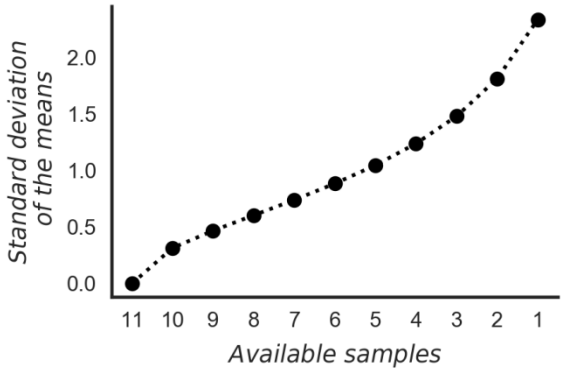

Figure 4.5 – Standard deviation of the means. Calculated for each cluster resulting from the recombination.

Increasing the number of point-by-point measurements reduces the standard deviation of the means more sensibly for the first 5 samples, after which a less steep decrement can be noticed confirming that the gain of overall information decreases for each additional point. The inclusion of the 11th point, and thus crossing the 3 % of area coverage, appear to increase again the informative gain (Figure 4.5), however, this might be an artifact of closely approaching what we have defined as *true mean.* In fact, it must be reminded that this involves the assumption that the 12 samples include all the information possible. Also, these 12 samples, and thus their 3.40 % coverage of the tank, can be considered as representative of this specific case study, but values may vary for other WRRFs. It must also be considered that, as hydrodynamics play an important role in the final local aeration efficiency, the distribution of the 12 points can have an impact on the results. With regards to this, the recombination game by itself uses all possible combinations of available samples, thus covering all possible cases that could be chosen among the 12 initially available locations. However, basing the initial choice of the 12 locations on a CFD study might provide more clues on the most appropriate strategy to cover the aerated area.

4.1.2. The time issue on coverage

When performing a series of point-by point tests, besides assessing an overall average efficiency over the tank surface, a parallel purpose is to compare the performance of the single points and compare them in relation with the rest of the locations. This is useful to eventually identify low efficiency zones in the tank area and define strategic actions on e.g. cleaning rather than adjusting the air distribution.

As influent dynamics are influencing the overall efficiency in time, it becomes difficult to properly define actual differences between different points. Each point-by-point measurement is performed

at different times and a reference for a fair comparison is missing with the current assessment method.

At the WRRF in Rome, a series of off-gas point-by-point measurements was performed moving the hood around 8 locations while keeping an additional hood and its dedicated analyzer (here named old analyzer), at a fixed location (Figure 4.6). The old analyzer measures O_2 partial pressure in the gas phase and airflow and its hood has a surface of 0.7 m^2 (Gori et al., 2014). It uses a Zirconium cell for measuring oxygen and an absorption column with NaOH pellets for CO_2, both having limitations as explained earlier (cfr. §3.1.1 and 3.1.3 respectively).

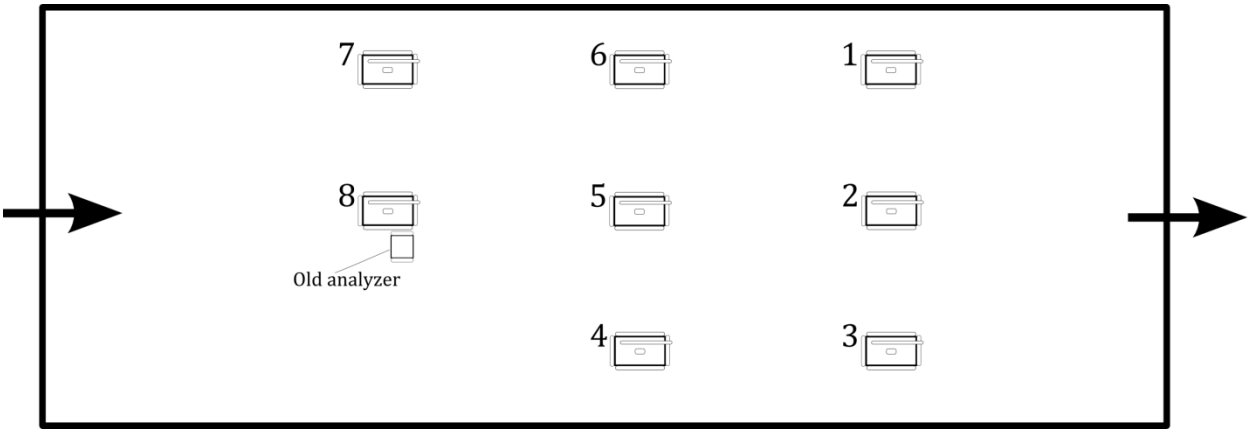

Figure 4.6 – Schematic of the hood positions over the tank surface and the fixed position of the old analyzer.

Keeping the old analyzer in a fixed position, i.e. performing a stationary test, allows to monitor aeration efficiency dynamics at location 8 while performing a point-by-point test. As aeration is kept constant within the day in this WRRF, the variability observed from a fixed position can be addressed to the influence of influent fluctuations only.

Referenced off-gas measurements

The αSOTE measured in the 8 points of the aerated tank with the analyzer developed in this work, is reported along with the stationary measurement performed with the old analyzer (Figure 4.7). Location 1 appears to be the most efficient in oxygen transfer, while αSOTE decreases as the hood approaches location 8. Even though location 8 shows a rather constant αSOTE, fluctuations from 14 to 20 % are visible within the time that the 8 point-by-point measurements were performed (Figure 4.7).

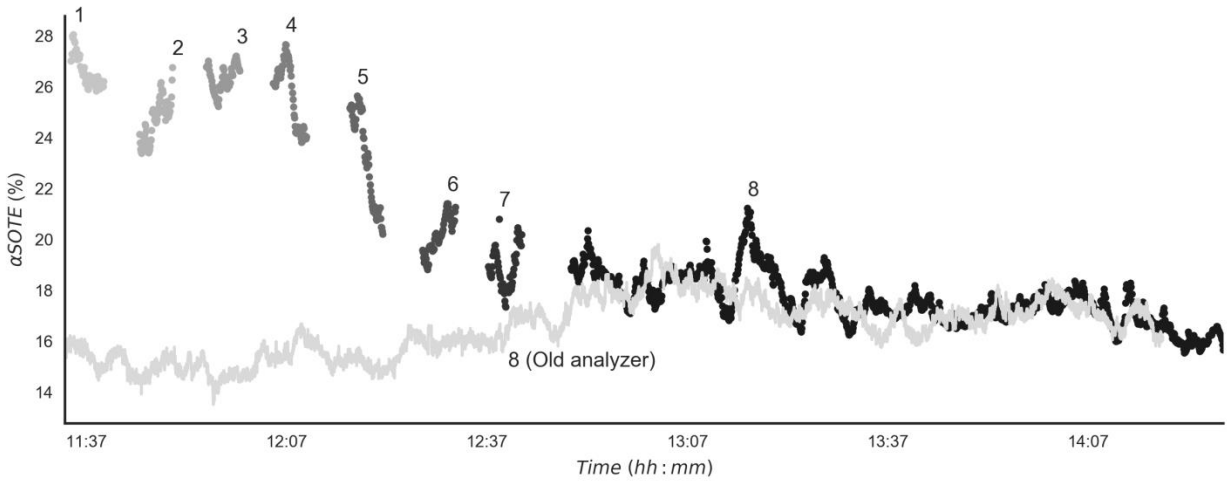

Figure 4.7 – αSOTE measurements with the developed analyzer (1-8) in grayscale and with the old analyzer (only 8) in lightest gray. Location number is reported close to the max of each point-by-point measurement, while for the old analyzer it is reported below the time series.

The stationary measurement in location 8 in fact, shows an αSOTE of about 16 % at the beginning of the measurements, then decreases around noon reaching its maximum of 20 % at 13:00, and stabilizing at 18 % for the rest of the time. As expected, the αSOTE profiles registered when both analyzers were in position 8 (*8* and *8 (Old analyzer)* series in Figure 4.7) nicely coincide. Small differences are to be addressed to the different sampling methods of the two analyzers (e.g. the old analyzer uses a long flexible hose of 60 mm ø to connect to the hood) making the old analyzer less responsive to changes as compared to the analyzer describe in this work. In addition to this, it must be considered that the old analyzer has a lower precision in measuring O_2 content in the off-gas as compared to the developed analyzer. This is due to the O_2 sensor itself and the CO_2 scrubbing column. Despite this, the parallel measurements in location 8 are generally deviating only up to 2 % at maximum.

In Figure 4.8 point-by-point measurement deviations relative to the average αSOTE in location 8 measured with the developed analyzer are shown. These measurements are only from the analyzer developed in this work, resembling what would normally be done if only one analyzer would be available. In fact, for comparing different locations, the general assumption of constant conditions during point-by-point measurements is necessary. However, this might not be the most sound comparison for measurements performed at different times. Location 1 shows up to 10 % difference in αSOTE as compared to the average of location 8 and seems to have the highest difference among all locations tested. Deviations at locations 2, 3 and 4 range between 6 to 10 % of difference as compared to location 8. Also, location 5 shows a rather large deviation between 3 and 8 % difference from location 8. Locations 6 and 7 do not report sensible differences from location 8. However, as these results are based on an average reference value, αSOTE fluctuations in time are not considered, which might bias the interpretation of the differences between locations.

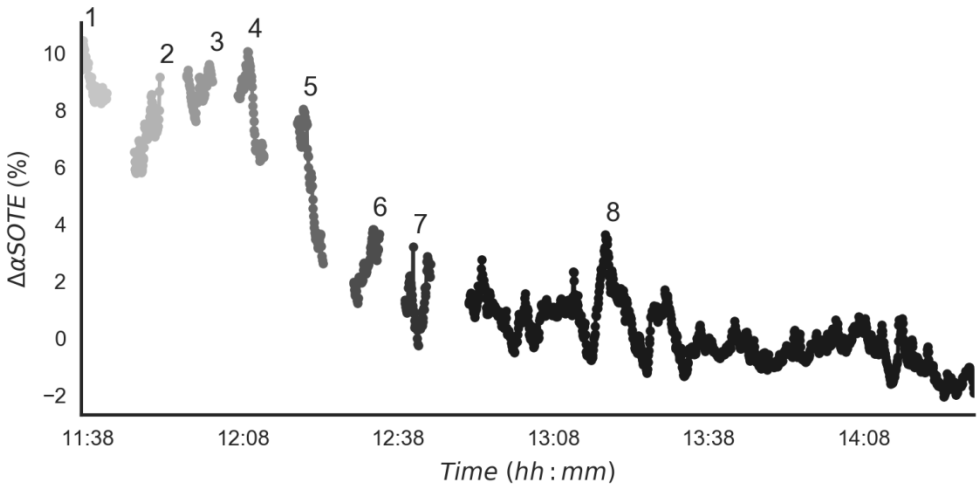

Figure 4.8 – Difference in αSOTE, using only data from the developed analyzer, between the average αSOTE of location 8 and the rest of the measurement points.

Using the real-time measurements of the old analyzer as the reference αSOTE from location 8, the difference with the rest of the locations is sensibly changing (Figure 4.9). Efficiency values from the different point-by-point measurements were subtracted at each measurement instant (i.e. not using the average but the actual instant value) from the αSOTE in location 8. As a result, location 1 reports a difference from location 8 of up to 12 %, and locations 2, 3 and 4 reach similar values. Location 5 still shows a variation of 5 % within its data points but the deviation with respect to location 8 is sensibly higher than in the former case. In addition to this, a difference between location 6 and 7 as compared to 8 is now visible in Figure 4.9.

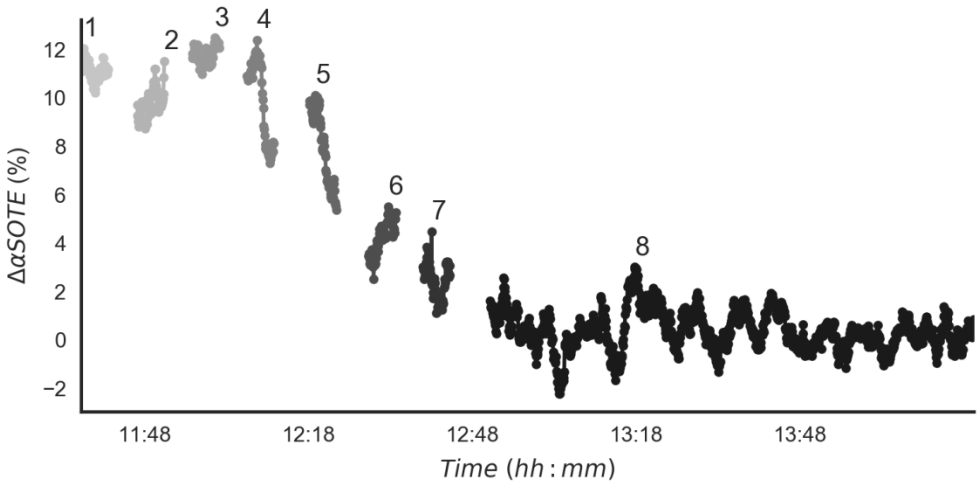

Figure 4.9 – Difference in αSOTE between the point-by-point measurements performed with the analyzer developed in this work and the stationary measurement with the old analyzer. All data points are the result of the difference between real-time data.

Actual differences as compared to location 8 are therefore better highlighted in the case that parallel off-gas measurements are used. Doing so, it is possible to compare the different efficiencies

of the different points at the net of αSOTE fluctuations due to influent dynamics. However, this statement has the major assumption that local fluctuations related to influent dynamics are the same at all locations. This is obviously not the case, but it is surely an improvement from the initial assumption of no αSOTE fluctuation during point-by-point tests.

4.2. N_2O emissions

In full-scale plants, local conditions are highly variable depending on process conditions and hydrodynamics, which will dictate which of the N_2O pathways will be dominant. The high variability of N_2O emissions has provided a fertile ground for the scientific debate on the correct definition and use of an EF. Temporal (seasonally and daily) variations are known to significantly impact the assessment of EFs (Bollon et al., 2016; Daelman et al., 2015; Masuda et al., 2015) and also local differences lead to important variabilities (cfr. §2.2.2) (Rehman, 2016).

N_2O is generally considered to be emitted in vast majority in aerated compartments of WRRFs where the enormous surface for exchange provided by aeration aid the passage from the liquid to the gas phase (Chandran, 2011). On the other hand, anoxic zones represent a central source of generation of N_2O (Ahn et al., 2010; Gabarró et al., 2014; Garrido et al., 1998). Although in anoxic zones the available gas-liquid surface for exchange is severely lower than in aerated compartments and emissions are more troublesome to measure, they are often reported in literature as emitting a non-negligible amount of N_2O (Marques et al., 2016).

As specific guidelines on how to define a sampling strategy in N_2O monitoring are currently lacking, also due to the elevated variability observed in literature, a parallel sampling approach was adopted. In order to contribute to the critical topic of the production dynamics and discrepancies among WRRFs, the biological tanks of three WRRFs (in Italy and The Netherlands) having similar configurations, but different hydrodynamics were monitored for N_2O emissions from different points simultaneously.

The multi-point simultaneous monitoring allowed to capture N_2O emission dynamics in both time and space domains. Spatial heterogeneities were highlighted for the three plants over time, helping to understand which location is more responsible for N_2O production at a given moment.

Spatial and temporal shifts in N_2O production were investigated to gain insight in the design of sampling strategies and to tackle the most timely issues in the assessment of the extent of N_2O emissions from WRRFs using AS biological nitrogen removal. Having a better understanding of this will facilitate strategies to ultimately reduce N_2O production and emissions.

4.2.1. Materials and methods

Three WRRFs were investigated, in Florence, Rome and Eindhoven. A schematic representation of each biological reactor is reported in Figure 4.10. For the case of Florence and Rome, the floating hood for aerated zones described in this work (cfr. § 3.1.2) was used in one of the locations. In particular, the hood was placed in location 5 in Florence, and in location 3 in Rome, with the

purpose of leaving the zone with fewer aeration per unit area to the biggest hood. For the rest of the aerated zones, simpler and smaller hoods were built.

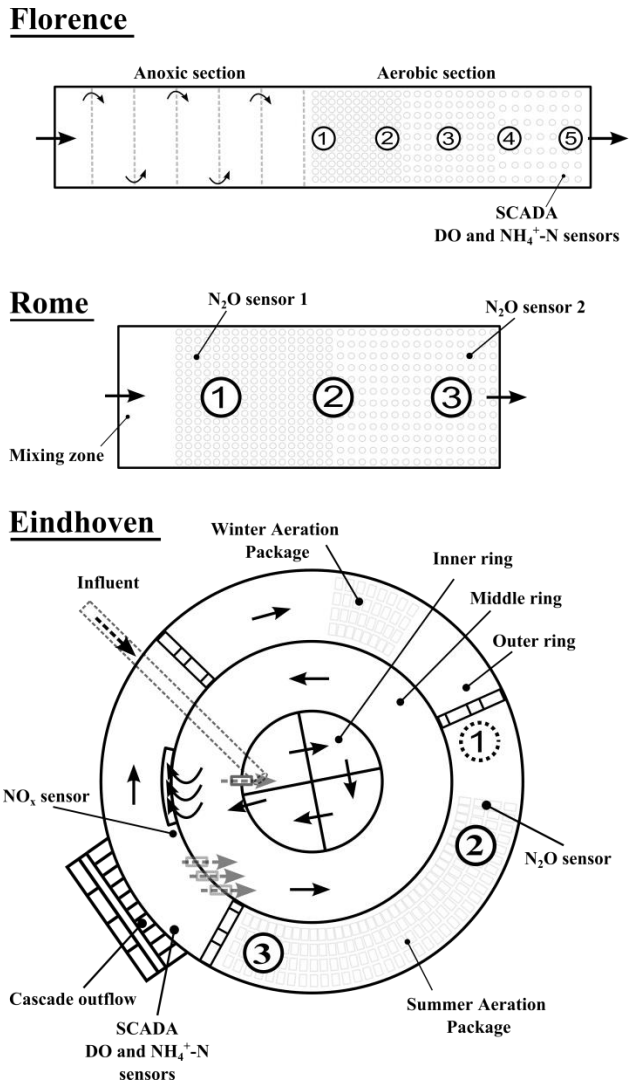

Figure 4.10 - Schematic overview of the biological tanks outline of the three plants. Locations of hoods are numbered in the direction of the flow according to the following graphs. The circle with the dotted line is the anoxic hood. Dimensions of tanks are only indicative.

N_2O measurements and emissions calculation

All hoods were connected via a Teflon tube (4 mm in diameter) to a multiplex sampler allowing to automatically switch among the different locations and control the monitoring time to spend on each hood. Two NDIR gas analyzers were used at the WRRFs of Rome (Thermo Scientific™, Model 46i) and Eindhoven (Teledyne API™, Model T320), while a photoacoustic IR (LumaSense, Inc., INNOVA 1412i) was used at Florence WRRF. For all WRRFs, due to the difference in diffusers distribution along the length of the aeration tanks, N_2O readings were corrected according to the locally supplied airflow.

Emissions from anoxic zones

Gaseous emissions of N_2O from the anoxic compartment were monitored with FhAx (cfr. §3.3) in the WRRFs of San Colombano and Eindhoven. In this way, the air sample along the length of the exchange chamber is enriched with the compounds that are released from the water surface as it would naturally happen. The inlet of the exchange channel was connected to a long tube to make sure the incoming air was unbiased ambient air. Knowing the ambient N_2O concentration, the size of the channel and the sampling airflow, it is possible to calculate the exchanged N_2O at the interface of non-aerated areas.

Emission Factor calculation

The N_2O EF was calculated as the N_2O emitted per unit NH_4^+-N removed (SM), which not only can account for N_2O production from AOB, but also from heterotrophic denitrification.

4.2.2. Results of the multipoint measurements

Florence

It must be pointed out that the diluted character of the influent of the WRRF in Florence shows very limited NH_4^+-N concentrations already at the entrance of the plant (Figure 4.11, bottom) due to a constant infiltration of groundwater in the sewer, which is most probably the reason why influent peaks are known to be uncommon for this WRRF. Due to sensor failure, only 6 of the 24h of gas sampling are shown in (Figure 4.11). NO_2^--N measurements in the bioreactor had no significant variation during the 24h (0.04 $\pm$0.02 mg/L).

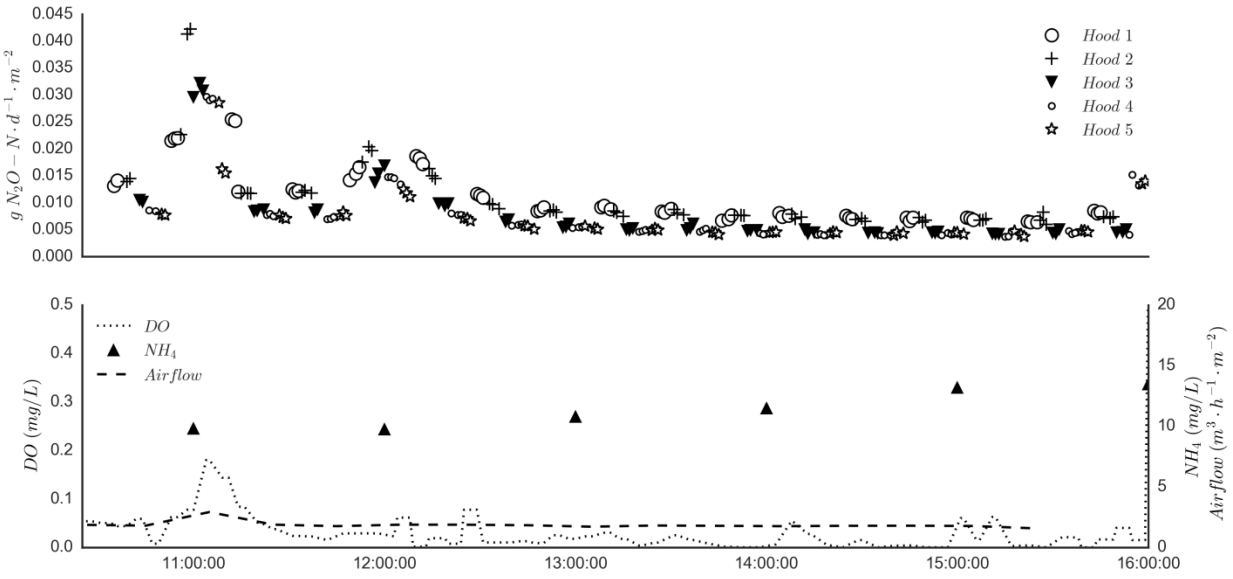

Figure 4.11 - N_2O emissions (top), total air flow and concentrations of DO from SCADA in the bioreactor and NH_4^+-N from automatic sampler before the AS tank (bottom) at the WRRF of San Colombano (Florence, Italy).

In terms of temporal variation, the data from the off-gas measurements show that at the beginning of the measurements, N_2O emissions were higher, as were the DO concentration peaks. This is most

likely the result of the slight increase in aeration and higher amount of stripping. However, this could also be from higher N_2O production. As the DO concentrations were generally low, it is unlikely that N_2O production was due to incomplete hydroxylamine oxidation based upon the DO concentrations reported by Peng et al. (2014). This means that N_2O production may have been via AOB denitrification in addition to heterotrophic denitrification, given that NO_2^--N and DO were consistently low and NH_4^+-N was relatively constant until the end of the campaign. Moreover, due to the difference in oxygen half-saturation indices between AOB and NOB (Mota et al., 2005), which results in higher NO_2^- with lower DO, the peaks in N_2O corresponding to peaks in air flow and DO are likely not due to peaks in NO_2^- at those moments, but rather due to more stripping of N_2O resulting from the baseline NO_2^- concentrations and related AOB denitrification prompted by low DO conditions. DO has been seen to inhibit heterotrophic denitrification at 0.21 mg O_2/L (Kester et al., 1997), and particularly the Nos enzyme responsible for reducing N_2O to N_2, which would result in incomplete heterotrophic denitrification and accumulation of N_2O (Von Schulthess et al., 1994). Since there is removal of ammonia, it is most likely that N_2O is being produced from both AOB denitrification and heterotrophic denitrification given the low DO conditions. Therefore, the temporal variation is most likely due to diurnal variation of DO, substrate, and corresponding variation in the degrees of AOB denitrification and heterotrophic denitrification N_2O production.

As far as spatial variation, locations 1 and 2 generally appear to be emitting more as compared to the other locations. Seeing that location 1 and 2 are at the beginning of the aeration tank, which would be the locations with a higher expected substrate availability, it makes sense that generally this area of the tank emits more than the rest. However, this seems to be valid for only low emission periods. When emissions are higher (Figure 4.11, top between 10:00 and 12:00), location 3, 4 and 5 gain importance, even emitting more than location 1. One possibility can simply be different local mixing conditions leading to significantly different DO concentrations at the different locations, keeping in mind that the DO data is from a sensor located at the end of the aeration tank (more representative of locations 4 and 5). Another possibility is different DO concentrations due to the diffuser grid layout. The normally very low DO conditions (at the limit of anoxia) of the locations close to the outlet of the aeration tank are likely prompting both AOB and heterotrophic denitrification N_2O production and overall greater N_2O production, which is not fully stripped at the downstream locations until the aeration increases. Airflow, as well as local DO and liquid N_2O data at each location could confirm which of these possibilities is most likely; however, the objective of the study was identifying the temporal and spatial variations and understanding possible factors for each.

Assessing the EF for each location separately using the respective average value results in very different estimations. In particular, as compared to location 1, estimating the EF in location 5 would result in an underestimation of about 37.5%. EFs estimated in Locations 3 and 4 show both 28.1% deviation from the EF calculated in location 1. On the other hand, location 2 has a similar EF as compared to location 1, showing only a 0.8% increase.

Rome

During low loading periods of the plant, there seems to be no relevant difference among the three locations in terms of N_2O emissions (Figure 4.12, top). However, discrepancies among hoods start

to increase when a peak load enters the AS tank and location 2 and 3 gain more importance compared to location 1 (the one closer to the inlet). This observation was confirmed by the liquid N_2O measurements (Figure 4.12, bottom). The two probes, located close to the entrance (N_2O liquid sensor 1) and close to the outlet (N_2O liquid sensor 2) of the aeration zone, detected very low or zero N_2O concentration in the liquid during periods of low gaseous N_2O emissions. Interestingly, the N_2O liquid sensor 2 was always detecting higher concentrations than sensor 1 and this difference increased during the peak of N_2O emissions in the gas, confirming that the production in the second half of the tank was more proficient.

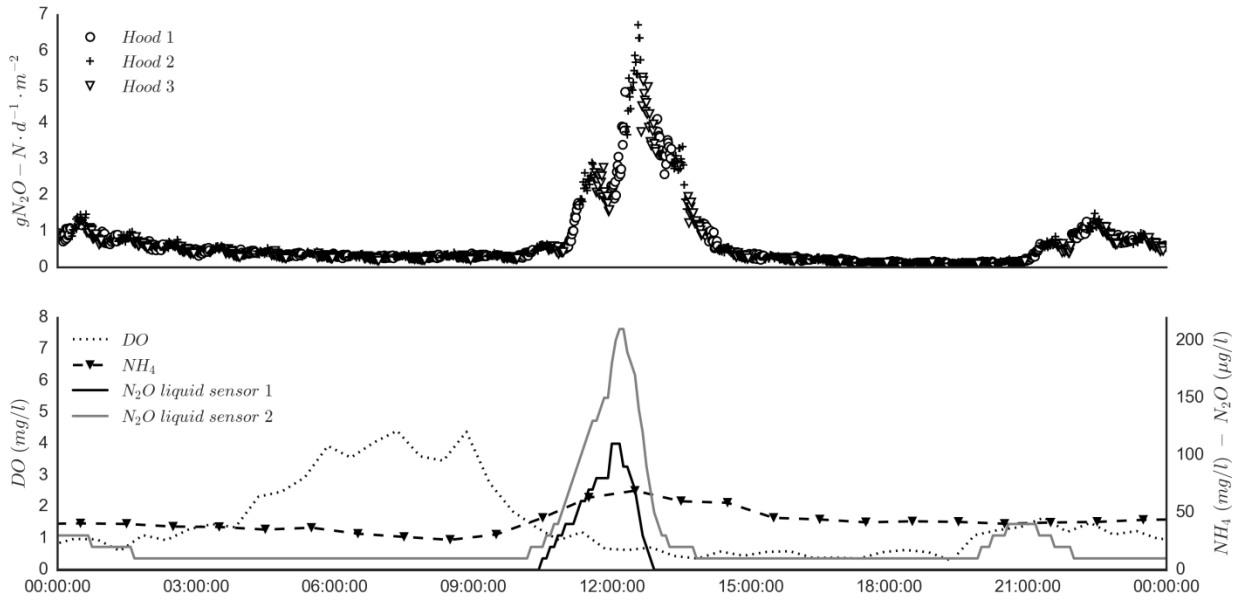

Figure 4.12 - N_2O gas emissions (top graph) and liquid measurements of DO, NH_4^+, and N_2O (bottom graph) at the WRRF in Rome (Italy)

The constant aeration flow rate characterizing this plant facilitates the understanding of DO fluctuations, allowing to directly connect them to influent load dynamics. The DO concentrations in Figure 4.12 (bottom), recorded at hood 1, show that increasing DO concentrations (around 4:00) did not influence N_2O emissions and neither its production in the liquid phase. However, as soon as the decrease in DO occurs (after 9:00), probably due to an increased biological activity resulting from the higher incoming load, N_2O production in the liquid and relative gaseous emissions start to increase. Interestingly, the DO concentration at which the N_2O production has its maximum rate is when it reaches below 1 mg/L, in accordance with literature results (Tallec et al., 2008). As DO approaches limiting conditions during the highest N_2O concentrations, N_2O is most likely produced via the AOB denitrification pathway. The daily composite sample of NO_2^--N (i.e. 0.21 mg/L) may indeed suggest that NOB-inhibition concentration can be reached. The maximum emissions are registered from hood 2 and 3, which are located further downstream towards the outlet, further confirming this last observation as NO_2^--N concentration may increase and DO is likely to maintain limiting values. In addition to this, since the diffuser density is lower in this area than in location 1, DO is likely lower, potentially resulting in greater N_2O production from AOB denitrification.

Eindhoven

NH_4^+-N loads (Figure 4.13, bottom) and relative fluctuations are more prominent for this plant as compared to the other cases since the sewer experiences sensibly lower infiltrations of groundwater. The temporal variation in N_2O emissions (Figure 4.13 top) appear to be mainly due to the diurnal effect of varying ammonia and corresponding DO concentrations. From the control, as NH_4^+-N increases, DO is increased until NH_4^+ -N is lowered, after which DO is lowered again. This pattern repeats throughout the day. The highest N_2O emissions occur when the daily ammonia peak arrives. NO_2^--N at the three locations showed similar values throughout the day (0.25±0.03 mg/L) and, although, it cannot provide specific information for the single location, may suggest the NOB-inhibitory effect in favor of the AOB denitrification pathway where DO is limiting.

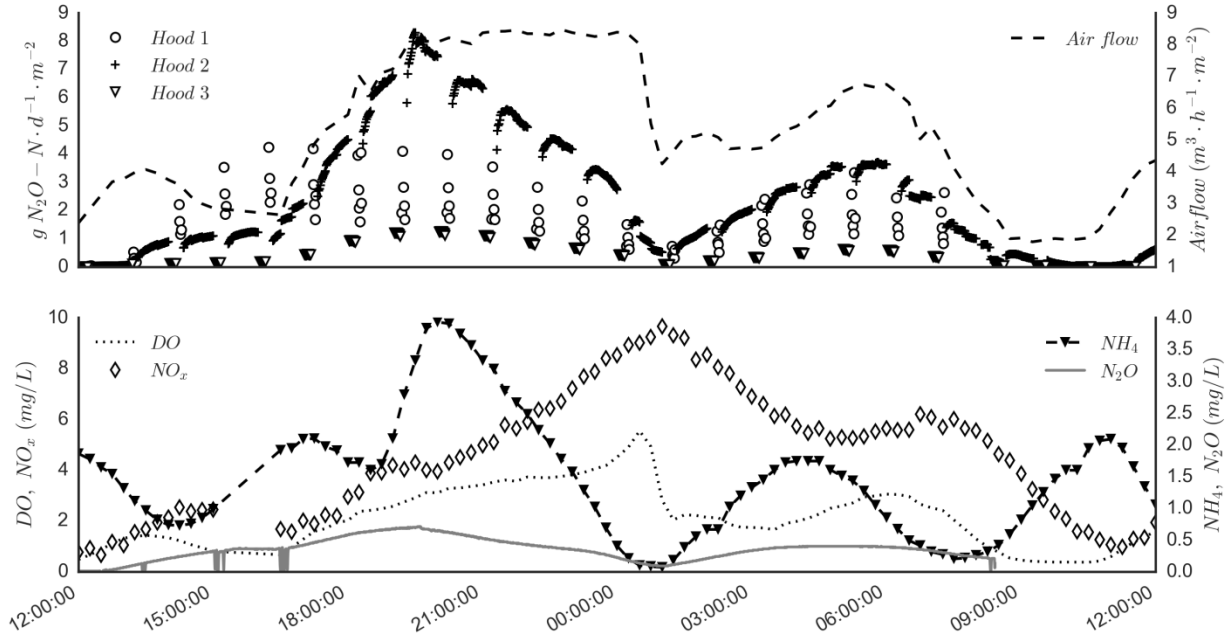

Figure 4.13 - N_2O gas emissions and air flow (top) compared with liquid concentrations of DO, NH_4^+-N NO_x–N and N_2O-N (bottom) at the WRRF of Eindhoven (The Netherlands). Due to unavailability of influent data, measurements of NH_4^+ are from the SCADA sensor in the bioreactor.

In terms of spatial variation, measurements from hood 1 (Figure 4.13, top) were generally lower than the ones observed in location 2, but higher than the ones registered from location 3. However, in the last part of the time series, there are missing data points from location 1. The N_2O emission from the anoxic zone appears to be more fluctuating (within the same group of measurement samples) than from other locations. This can be due to the fact that, unlike in the aerated zone, there is no constant stripping in the anoxic, and the occurrence of recirculations from deeper zones and eddies at the surface provide more variable instantaneous emissions. These variations from the anoxic zone are consistent but do not repeat similar patterns within the same cloud of data, reinforcing the previous observation.

Emissions from hood 1 were of the same magnitude as the ones registered from the other hoods even though location 1 was in the anoxic zone. Therefore, only diffusion at the surface could account for comparable emissions to the ones occurring for active stripping.

Peaks in N_2O emission from location 1 seemed to occur when relatively high NH_4^+ peaks appeared and DO values were close or even below 1 mg/L (17:00 and 5:00). The highest N_2O emission recorded from hood 1 occurred at 17:00 when DO was below 0.5 mg/L. These observations are suggesting that emissions from location 1, and thus production from the anoxic zone, are most likely to happen either due to the AOB denitrification pathway, or from incomplete heterotrophic denitrification.

Emissions from location 2 registered the highest peaks in correspondence of important NH_4^+ peaks. Interestingly, the first peak in N_2O emission from location 2 corresponds with a first peak of location 3 (Figure 4.13, bottom at 20:00) and, since at the same time N_2O emission from location 1 seems too decrease, it is likely that an important part of this production takes place in the aerobic compartment. This is also confirmed directly by the increase in liquid N_2O concentration. The rising DO in correspondence of these peaks (at 20:00 and 8:00), indicates that the dominating pathway in this particular moment can be the hydroxylamine oxidation, especially considering DO is non-limiting, approximately 3 mg O_2/L.

N_2O measurements in the liquid (sensor placed at location 2) (Figure 4.13, bottom), seem to corroborate this hypothesis. The highest rate of N_2O emission (steepness of the N_2O curves) for location 2 and 3 occurs in those moments when both increasing NH_4^+-N availability and increasing DO values above 1 mg/L occurred. The differences in emissions between location 2 and 3, both within the aerobic zone, but at the beginning and end, respectively, are most likely attributed to different local NH_4^+-N and DO concentrations.

Literature studies on the same WRRF confirm our observations. A qualitative comparison with the findings of the modelling work of Rehman (2016), performed on the same plant, corroborates with the distribution of emissions measured in this work. Although measured N_2O concentrations in this work are 3 orders of magnitude higher than the values observed by Rehman (2016), the qualitative pattern of liquid concentrations before and within the aerobic zone (Figure 4.14), interestingly matches the patterns observed in our gas measurements (Figure 4.13). In particular, in the work of Rehman (2016), the anoxic zone (location 1 in this work), has been shown to have higher N_2O concentration in the liquid as compared to the aerated zone in general (relative to location 2 and 3 of this work) (Figure 4.14, left). Only the very beginning of the aerated zone has shown the highest concentrations especially in the outer part of the ring, however, this is likely to be the result of the clockwise liquid flow dragging the concentrations of the anoxic part in the initial region where the aerators are installed. On the other hand, the actual aerated conditions occur few meters downstream from the first plate aerators (Figure 4.14, right). The beginning of the aerated zone shows significantly higher N_2O concentration as compared to the end (Guo et al., 2013; Rehman, 2016) further confirming our results.

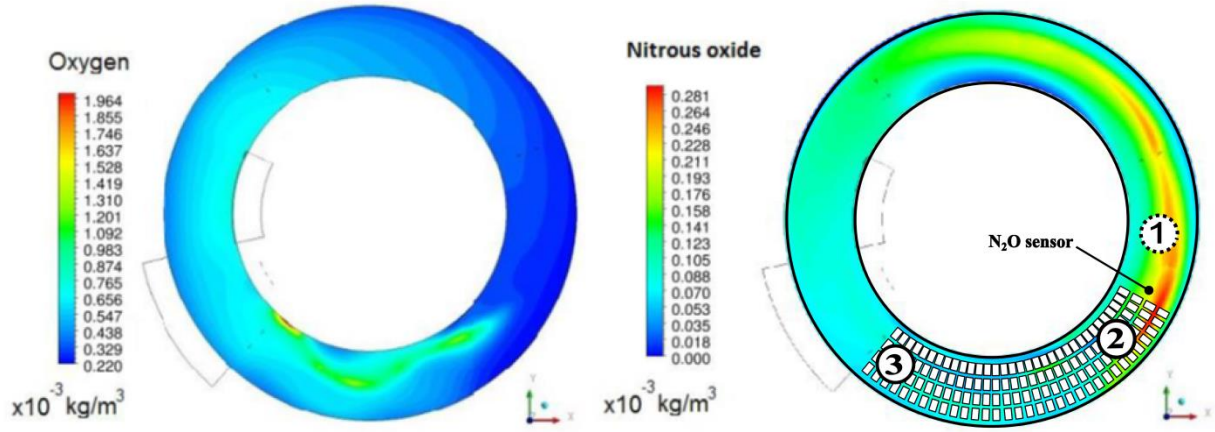

Figure 4.14 – Redrafted from Rehman (2016). Overlap of the locations monitored in this work with the horizontal section of Rehman (2016) for DO (a) and N_2O (left) concentrations in the liquid in the outer ring of the WRRF of Eindhoven.

Interestingly, given the good qualitative resemblance of the measurements performed in this work with the results of Rehman (2016), we could think that placing the hood few meters closer to the outer wall of the tank, would have likely resulted in even higher N_2O emission measured from location 1. Hence the relevance of the choice of measurement locations. This is an important point in view of defining a reliable monitoring strategy for N_2O emission assessment and providing guidelines on tank coverage.

Estimation of an EF

In order to further illustrate how the use of a single EF for describing the extent of emissions of different (although similar in AS technology used) WRRFs is not valid, an overview of EF from all the different locations in the three WRRFs studied is provided (Figure 4.15).

The case of the WRRF in Florence is reported in the top graphs of Figure 4.15. Selecting only the peak of N_2O emission (Figure 4.15, top, graph A) the average values of location 3 and 4 gain importance over the rest of the hoods. However, deviation bars around the data in location 1 and 2 hamper the strength of this observation.

Considering only the period outside the peak of N_2O emission for the case in Florence (Figure 4.15, top, graph B), emissions seem to be consistently low with location 1 showing a slightly higher EF than the rest.

A boxplot of the entire dataset from Florence (Figure 4.15, top, graph C) shows the higher emission of location 1 and 2, but also considerable overlapping variations from the rest of the hoods. However, this overall statistical description is hiding the importance that location 3, 4 and 5 gain when DO and ammonia increase. Location 1 and 2 show a tendency to be the highest emitting locations in comparison with 3, 4 and 5, from their mean values and their general behavior in the dataset. However, these initial locations also show the highest variability (up to 0.0002 N_2O-N / NH_4^+-N) and the unsuitability for the assessment of an EF from a sampling campaign shorter than a full day.

Isolating the N_2O emission peak from the WRRF in Rome (Figure 4.15, mid, graph A) it is noticeable how the highest emission values reached by hood 2 is not able to drag its mean value higher than hood 1, thus remaining the location of hood 1 emitting the most. Therefore, for the case of Rome location 1 remains the highest emitter of the AS tank.

During low emissions (Figure 4.15, mid, graph B), all locations appear to contribute to the same extent to the release of gaseous N_2O. Similarly, looking at the boxplot over the whole dataset from Rome (Figure 4.15, mid, graph C), differences among locations do not stand out.

For the case of Eindhoven (Figure 4.15, bottom) the picture is rather different. Location 2 and 3, have very different extent of emissions in all cases. During N_2O emission peak events (Figure 4.15, bottom, graph A), location 2 has EF values of more than one order of magnitude higher than location 3. When low emission of N_2O occurs (Figure 4.15, bottom, graph B), the contribution of location 3 practically disappears. In the overall picture (Figure 4.15, bottom, graph C), even considering the whole data set, the contribution of location 3 is sensibly lower than the rest, and hood 2 provided the highest emissions. Spatial differences along the aeration package are therefore very important.

In addition to this, also the contribution of the anoxic compartment resulted very relevant, comparable to location 2. This is due to the big surface available for exchange in the anoxic part of the outer ring of the WRRF in Eindhoven. As a matter of fact, overall hood 1 maintains EF values and deviations close to what occurs at hood 2.

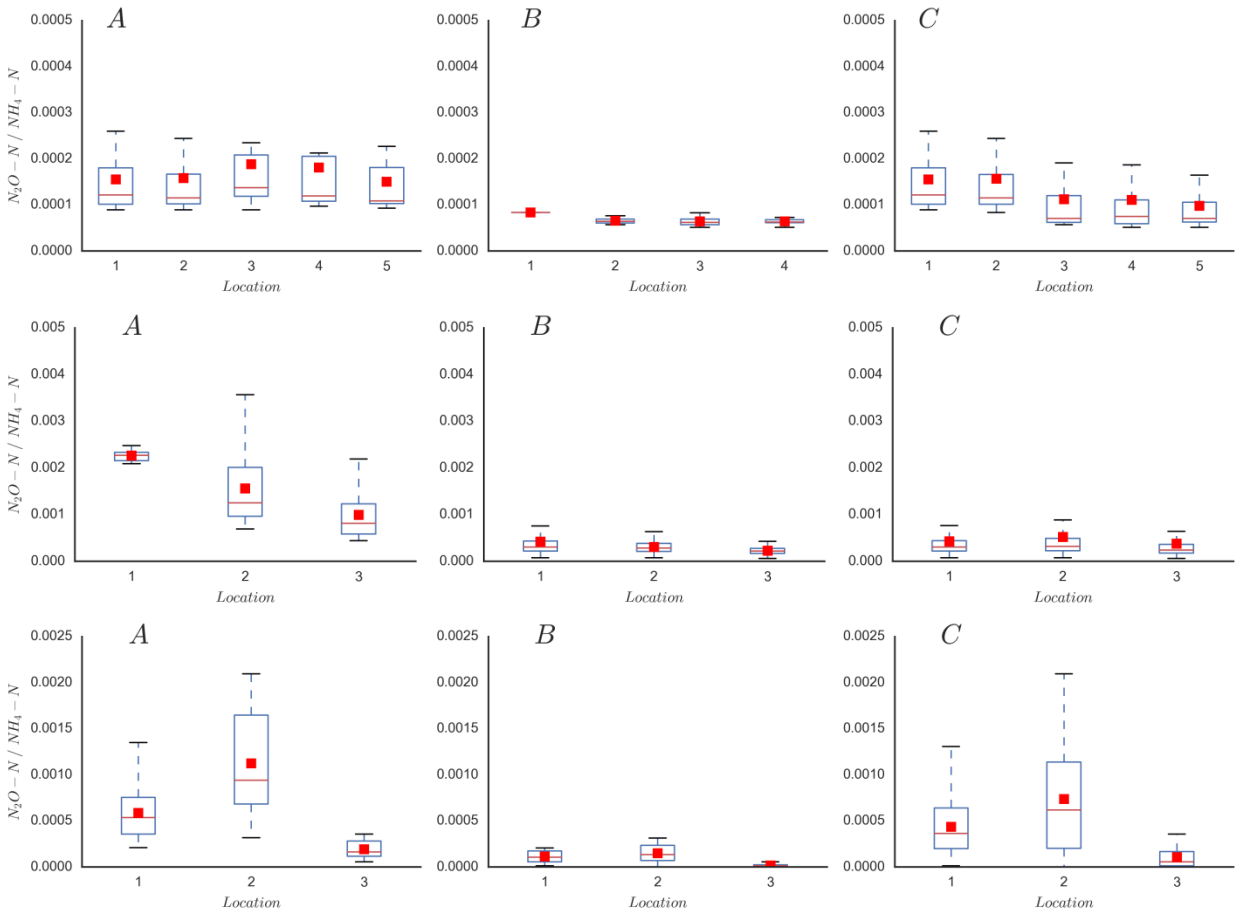

Figure 4.15 - Box plots of peak emission periods (A), low emission periods (B), and overall emission (C) for the case of Florence (top), Rome (middle), and Eindhoven (bottom)

Comparing the different WRRFs, the EFs of the WRRF in Florence are in general one order of magnitude lower than for the other plants. This fact can be mainly attributed to its highly diluted influent, preventing to have sudden N peak loads to be converted. Interestingly, despite the known diluted influent character also for the case in Rome, higher EFs than the one in Eindhoven were observed.

One important detail to notice is that all EFs provided in Figure 4.15 represent the EF of the plant that one would have calculated only measuring from a specific hood. In this view, variations among the locations represent the error that would have been made in judging EF by an operator measuring N_2O emissions from only one single location.

Adding the contribution of each location

Clearly, single point calculation measurements of EFs are usually not representative of the different contributions from all locations of a bioreactor. Given the availability of parallel measurements, it is possible to add up the contributions from each of the hoods and calculate a more refined EF for the three cases studied. In particular, this is possible addressing a specific portion of the surface area of

the tank to each hood based on their location. The main assumption is that the given surface area behaves in a similar fashion, which is still a better approach than assuming it for the whole reactor.

For the WRRF in Florence the overall EF calculated with the contributions from all hoods becomes 0.012 % (±0.007 %), which is not far from what was already observed in the boxplots. However, the sole average might not be exhaustive in this case as a consistent standard deviation is present.

For the case of Rome the three hoods contributed to give an average of 0.064 % (±0.078 %) which is also in the range observed in the box plots. A relevant deviation is observable also in this case.

For the WRRF in Eindhoven the overall EF accounting for both contributions of aerobic and anoxic zones is 0.110 % (±0.047 %). Interestingly, if one would have neglected the contribution of anoxic zones the estimated mean EF would have been 0.035% (±0.031 %). Therefore, neglecting the contribution of anoxic zones in the case of the WRRF in Eindhoven leads to an underestimation of the EF of 68.18 %. However, as reported by Rehman (2016) location 1 might be one of the most emitting parts of the whole AS tank, therefore, leading to an overestimation of the anoxic contribution of the EF. Nonetheless, this confirms the necessity of different sampling locations to reasonably represent the behavior of a tank and the need of a solid strategy for designing their distribution.

Since the purpose of these assessment is the classification of WRRFs, based on the evaluation of the extent of their emission of N_2O, using the average value of a 24h monitoring of the plant's dynamics could diminish or neglect important contributions to the assessment of an EF and a statistical representation of the emissions is surely more valuable than the use of a single number. However, in those cases in which a unique representative number has to be used (e.g. for policy makers and regulatory purposes), the EF should represent by definition the amount of N_2O typically emitted from a WRRF. In this view, the 24h measurements, inclusive of the contribution of all the different locations as described, were integrated over time. Equation 4.1 can be used for this purpose once the EF time series from n different locations are available.

$$EF = \sum_{1}^{n} \int EF_i \, dt \tag{4.1}$$

Doing so, the integral calculated for the WRRFs of Florence and Rome resulted in the same EF as for the case of the average, i.e. 0.012 % and 0.064 % respectively. The EF calculated for the case of Eindhoven resulted 0.129 %, slightly higher than the average calculated earlier. Therefore, in cases in which seldom and sharp peaks are occurring, the average EF practically coincides with the integral. On the other hand, in cases in which different and extended peaks are occurring throughout the monitoring time, averaging the EF can result in an underestimation. Hence, the use of a cumulative daily EF, integrating over time the 24h multi-point measurements, is suggested. Finally, considering the findings of Daelman et al. (2013) for a sound assessment of the EF, a single 24h campaign is likely to be poorly representative, and repetitions of the 24h assessment in different periods of the year are suggestable.

4.3. Conclusions

With the results evidenced in this work, the general rule of thumb of the 2 % area suggested by ASCE standards can now be assumed as a reasonable indication for off-gas testing. However, from these results it can be stated that increasing the number of point-by-point measurements so to cover up to 2.27 % can significantly contribute to the precision of the assessment. On the other hand, as measurements can be time consuming, a reduction below the 2 % can be also pondered. From our results, a lower limit in surface coverage of 1.7 % was suggestible. Below this lower limit, a considerable amount of information starts to be missing for each point not assessed.

For a fair comparison between the different locations of a point-by-point off-gas test, one should ideally perform all parallel measurements. This is unfortunately not feasible. The results show that differences among locations can be better quantified if a parallel stationary off-gas measurement is performed. However, as equipment is expensive, it is difficult to have the availability of two analyzers on the same plant. On the other hand, the advantage of making more robust and reliable observations should be considered when organizing an aeration efficiency assessment. Using an older and cheaper version of the analyzer proposed in this work, provided interesting clues on the effect of influent fluctuations on the tank αSOTE. Even though less precise as compared with the analyzer developed, its information could be used to refine actual local efficiencies and improve comparability among points. A simple method was proposed to refer local efficiencies to a reference location, however, further improvements will be needed. Hopefully, these considerations will rise attention when evaluating differences among locations. To the best of the author's knowledge this is the first time that this level of attention is provided to local aeration efficiency assessment. This in view of bringing more precision and confidence in the output that the analyst provides to the client in off-gas testing.

The assessment of the contribution of anoxic zones to N_2O emissions should be a normal procedural approach. A method for accounting for the contribution of anoxic zones via direct gas emission measurements was proven. The anoxic hood effectively allowed the detection of N_2O emissions from non-aerated surfaces of an AS tank with an economic, practical and user friendly approach. Both the temporal domain, relative to influent dynamics, and spatial domain, relative to hydrodynamics, are crucial to understand N_2O emission dynamics. More than one measurement location should be foreseen for assessing anoxic zones contribution. However, the exact number with respect to the tank surface, cannot be provided from the available data. The spatial distribution of measurement location should be planned considering hydrodynamic studies when available, or related concepts to gain insights on liquid flow patterns.

For the case of the WRRF in Florence the diluted influent (groundwater infiltration) is the most probable reason for which the EFs are so low. The plant in Rome showed higher N_2O emissions in the locations closer to the outlet of the AS tank when a peak load was experienced. Higher DO levels may be maintained to mitigate N_2O production. The carousel configuration of the AS tank of the WRRF in Eindhoven seems to result in anoxic N_2O emissions comparable to the ones from the aeration compartment. This validates with literature studies on hydrodynamics on the same plant. Tuning the DO control to lower DO levels during peak loads may reduce production from both

anoxic (removing limiting DO conditions that favor AOB denitrification) and aerobic zones (removing high DO levels that may favor hydroxylamine oxidation).

From the N_2O measurements performed in the three plants, results show that the aerated area should be monitored in at least two points, one at the beginning of the aerated zone and one at the end. However, this is valid for tanks resembling plug-flow behavior. Recommendations on the % of area to be covered as for the case of off-gas measurements, are not possible at this stage, but information on hydrodynamics were indicating important clues in this regard.

The experimental method used for assessing N_2O emissions allowed to simultaneously monitor different locations in full-scale AS tanks and highlighted the wide range in EF values from plant to plant and within the same facility. Spatial variabilities are heavily influencing emission results and the use of a single EF describing the entire WRRF operation or classifying a treatment technology is once more discouraged. The EF measurements performed in WRRFs using similar AS tanks differed more than one order of magnitude. Therefore, when a WRRF needs to be evaluated in terms of its environmental impact, the use of an EF should be accompanied with information regarding its variability and potential extents of emissions to better understand the WRRF potential and refine its classification. However, in e.g. the definition of regulatory thresholds and eventually legislation, a single number has to be used for classifying WRRFs or set emission reduction targets. In this case, given that an EF should represent the amount of N_2O typically emitted from a plant, the recommendation is the use the result of an integration of the EF measurements over a significant period of time that should include representative plant dynamics. As municipal WRRFs are characterized by observable daily patterns, this means that the assessment of an EF for a municipal WRRF should at least be calculated over an observation of 24h. In addition to this, for a fully sound assessment of an EF, keeping in mind the observations of Daelman et al. (2013) on the effect of sampling strategies for N_2O emission assessment, the 24h multi-point monitoring should be repeated different times over the year.

To our knowledge, this is the first time that spatial N_2O emissions are made visible at this resolution comparing similar configurations of AS tanks from different WRRFs.

4.4. References

Ahn, J.H., Kim, S., Park, H., Rahm, B., Pagilla, K., Chandran, K., 2010. N2O Emissions from Activated Sludge Processes, 2008—2009: Results of a National Monitoring Survey in the United States. Environ. Sci. Technol. 44, 4505–4511.

Amerlinck, Y., Bellandi, G., Amaral, A., Weijers, S., Nopens, I., 2016. Detailed off-gas measurements for improved modelling of the aeration performance at the WWTP of Eindhoven. Water Sci. Technol. 74, 203–211.

ASCE, 1997. Standard Guidelines for In-Process Oxygen Transfer Testing (18-96). American Society of Civil Engineers, New York, NY.

Bollon, J., Filali, A., Fayolle, Y., Guerin, S., Rocher, V., Gillot, S., 2016. N2O emissions from full-scale nitrifying biofilters. Water Res. 102, 41–51.

Caivano, M., Bellandi, G., Mancini, I.M., Masi, S., Brienza, R., Panariello, S., Gori, R., Caniani, D., 2017. Monitoring the aeration efficiency and carbon footprint of a medium-sized WWTP: experimental results on oxidation tank and aerobic digester. Environ. Technol. 38, 629–638.

Chandran, K., 2011. Protocol for the measurement of nitrous oxide fluxes from biological wastewater treatment plants. Methods Enzymol. 486, 369–85.

Daelman, M.R.J., De Baets, B., van Loosdrecht, M.C.M., Volcke, E.I.P., 2013. Influence of sampling strategies on the estimated nitrous oxide emission from wastewater treatment plants. Water Res. 47, 3120–3130.

Daelman, M.R.J., van Voorthuizen, E.M., van Dongen, U.G.J.M., Volcke, E.I.P., van Loosdrecht, M.C.M., 2015. Seasonal and diurnal variability of N2O emissions from a full-scale municipal wastewater treatment plant. Sci. Total Environ. 536, 1–11.

Gabarró, J., González-Cárcamo, P., Ruscalleda, M., Ganigué, R., Gich, F., Balaguer, M.D., Colprim, J., 2014. Anoxic phases are the main N2O contributor in partial nitritation reactors treating high nitrogen loads with alternate aeration. Bioresour. Technol. 163, 92–99.

Garrido, J.M., Moreno, J., Méndez-Pampín, R., Lema, J.M., 1998. Nitrous oxide production under toxic conditions in a denitrifying anoxic filter. Water Res. 32, 2550–2552.

Gori, R., Balducci, A., Caretti, C., Lubello, C., 2014. Monitoring the oxygen transfer efficiency of full-scale aeration systems: investigation method and experimental results. Water Sci. Technol. 70, 8–14.

Guo, L.S., Lamaire-chad, C., Bellandi, G., Daelman, M.R.J., Maere, T., Nous, J., Flameling, T., Weijers, S., Mark, C.M., Loosdrecht, V., Volcke, E.I.P., Nopens, I., Vanrolleghem, P.A., 2013. High frequency Field Measurements of Nitrous oxyde (N2O) Gas Emissions and Influencing Factors at WWTPs under Dry and Wet Weather Conditions, in: WEF/IWA Nutrient Removal and Recovery 2013.

Kester, R.A., De Boer, W., Laanbroek, H.J., 1997. Production of NO and N2O by Pure Cultures of Nitrifying and Denitrifying Bacteria during Changes in Aeration. Appl. Environ. Microbiol. 63, 3872–7.

Marques, R., Rodriguez-Caballero, A., Oehmen, A., Pijuan, M., 2016. Assessment of online monitoring strategies for measuring N2O emissions from full-scale wastewater treatment systems. Water Res. 99, 171–179.

Masuda, S., Suzuki, S., Sano, I., Li, Y.Y., Nishimura, O., 2015. The seasonal variation of emission of greenhouse gases from a full-scale sewage treatment plant. Chemosphere 140, 167–173.

Mota, C., Head, M., Ridenoure, J., Cheng, J., de los Reyes, F., 2005. Effects of Aeration Cycles on Nitrifying Bacterial Populations and Nitrogen Removal in Intermittently Aerated Reactors. Appl. Environ. Microbiol. 71, 8565–8572.

Peng, L., Ni, B.J., Erler, D., Ye, L., Yuan, Z., 2014. The effect of dissolved oxygen on N2O production by ammonia-oxidizing bacteria in an enriched nitrifying sludge. Water Res. 66, 12–21.

Rehman, U., 2016. Next generation bioreactor models for wastewater treatment systems by means of detailed combined modelling of mixing and biokinetics. Ghent University.

Tallec, G., Garnier, J., Billen, G., Gousailles, M., 2008. Nitrous oxide emissions from denitrifying

activated sludge of urban wastewater treatment plants, under anoxia and low oxygenation. Bioresour. Technol. 99, 2200–2209.

Von Schulthess, R., Wild, D., Gujer, W., 1994. Nitric and nitrous oxides from denitrifying activated sludge at low oxygen concentration. Water Sci. Technol. 30, 123–132.

Chapter 5

5. The N_2O risk model for WRRF knowledge based N_2O model selection

This chapter is redrafted from:
Bellandi G., Porro J., Caretti C., Rodriguez-Roda I., Comas J., Nopens I. and Gori R. "Use of artificial intelligence for WRRF knowledge based N2O model selection" (2016) 5*th* *IWA/WEF Wastewater Treatment Modelling Seminar (WWTmod2016) Annecy, France. Papers.*

Abstract

Given its high global warming potential, N_2O can represent the majority of the carbon footprint in WRRFs. N_2O is produced from the biological nitrogen removal processes of WRRFs via different pathways, which have been seen to vary among different plants and different conditions. Detailed mechanistic or physical-based mathematical models have been developed to represent the different pathways, however, as different pathways can alternate or coexist in AS tanks, appropriate methods for selecting the correct pathway models are still lacking. To facilitate this, in this chapter, the application of a qualitative knowledge-based risk assessment model (N_2O risk model, cfr. § 2.2.4.) to infer risk of WRRF N_2O production is presented. The N_2O risk model was applied to lab-scale literature studies and full-scale datasets to prove the concept of its use for mathematical model selection. Results show that the N_2O risk model was effective in helping to unravel the dynamics behind N_2O production, was able to give valuable insights in the mechanisms of N_2O generation, and proved to be useful for guiding the selection of N_2O mathematical models representing different N_2O production pathways.

5.1. Introduction

Wastewater treatment processes can be considered to contribute to global warming in different ways, one of which is through the emission of N_2O. The latter can be produced during biological nitrogen removal in WRRFs using AS technology. Therefore, there has been increasing concern regarding N_2O in the water sector over the past few years. Efforts were concentrated in understanding the specific bio-chemical processes responsible for N_2O production (Schreiber et al., 2012) and the WRRF design and operational factors impacting its emission (Daelman et al., 2013; Kampschreur et al., 2009; Monteith et al., 2005).

The different biological mechanisms responsible for the production of N_2O (i.e. heterotrophic denitrification, nitrifier denitrification, and the incomplete NH_2OH oxidation pathway) are favoured by different operational conditions, which strongly depend on the technology used, the wastewater treated and the control strategy of the WRRF. DO and NO_2^- concentrations along with COD/N ratio appear to be the key influencing factors for N_2O production pathways (Kampschreur et al., 2009).

Field measurements showed that N_2O emissions can represent more than 78% of the WWTP carbon footprint (Daelman et al., 2015) and as much as 7% of the influent nitrogen load can be emitted as N_2O (Kampschreur et al., 2008b). However, N_2O emission data show important variations in the fraction of influent N that is emitted as N_2O (Kampschreur, 2008; Mampaey, 2011). In this view, site-specific emission assessments are more and more needed and, in order to quantitatively determine the contribution of N_2O emission on the WWTP carbon footprint, as well as its reduction from mitigation, the California Wastewater Climate Change Group recommended modeling rather than the use of emission factors (CH2MHILL, 2008).

Considerable efforts have been put into modeling the AOB pathways either with a single-pathway solution (*inter alia:* Law et al., 2012; Mampaey et al., 2013) or considering both AOB pathways (*inter alia:* Ni et al., 2014). Recently, Peng et al. (2015) suggested a selection of AOB single-pathway models according to DO and NO_2^- concentrations and their performance measured against a validated two-pathway model (Ni et al., 2014) to arrive at recommendations for use of the different models under different process regimes. Regarding the N_2O heterotrophic pathway, the model from Hiatt and Grady (2008) is generally accepted as common base. However, given the heterogeneity of WRRF process conditions, the potential variability of N_2O emissions, and the diversity of available models, consensus on model selection, dominant pathways and on how to implement these pathways is yet to be reached. In this chapter we present a practical application of the knowledge-based N_2O risk assessment model (N_2O risk model) (Porro et al., 2014b) to full-scale data to prove its applicability for selecting appropriate N_2O production pathways, and thus, relative mechanistic models. To the best of our knowledge, this is the first time model selection has been made based on full-scale data.

5.2. Materials and methods

5.2.1. The N_2O risk model principle

The construction of the N_2O risk model was inspired by a similar AI-based risk model developed to diagnose the risk of WRRF settling problems from filamentous bacteria (Comas et al., 2008) where knowledge of AS bulking, foaming and rising sludge, was applied to diagnose the risk of settling problems by processing ASM output data.

The N_2O risk model has been applied for demonstrating the implication of specific N_2O production pathways in the risk diagnosis of WRRF simulation data (Porro et al., 2014a). The N_2O risk model, is based on the selection of variables thresholds known to affect N_2O production (e.g. DO, nitrite, pH, COD:N, etc.) in the different process steps (i.e. denitrification, nitrification, and transition zones where rapid changes occur). These variables are then classified in terms of low, medium, and high risk according to values found in the literature correlating to lower, medium, and higher N_2O production, respectively. This knowledge base system gathers information from either full-scale or lab-scale studies.

The representation of this knowledge is summarized in Table 5.1, with the risk parameters categorized by process step, the low, medium, and high risk classification for different values of each variable's threshold, the pathway implicated by the risk parameter, and the relative references for linking operational control and threshold values (Porro et al., 2014a). For the purpose of the risk model, variables' thresholds are applied independently since risk for N_2O production can be signaled with just one of the factors present, regardless of whether they are linked to other factors. Overall risk is defined as the maximum risk value of all risk parameters evaluated for each time step.

Table 5.1 - N_2O Risk Model knowledge base - adapted from Porro et al. (2014).

Process step	Operational conditions	Variable	Type	(Inversely) Proportional to Risk	Main pathway	Reference linking operation to N2O risk	Reference for thresholds
Nitrification	High NO_2^-	NO_2^-	Conc.	Prop.	AOB denit.	(Ahn et al., 2010; Foley et al., 2010; GWRC, 2011; Kampschreur et al., 2009)	(GWRC, 2011)
	Low DO	DO	Conc.	Inv.	AOB denit.	(Kampschreur et al., 2009, 2008a)	(Tallec et al., 2008)
	High DO	DO	Conc.	Prop.	Inc. NH_2OH oxid.	(Ahn et al., 2010; Chandran, 2011; Law et al., 2012b)	(Law et al., 2012b)
Denitrification	High NO_2	NO_2^-	Conc.	Prop.	Het. denit. AOB denit.	(Ahn et al., 2010; Foley et al., 2010; GWRC, 2011; Kampschreur et al., 2009)	(GWRC, 2011)
	pH	pH	Conc.	Inv.	Het. denit.	(Pan et al., 2012)	(Pan et al., 2012)
	Low COD/N	COD/N	Value	Inv.	Het. denit.	(Ahn et al., 2010; Foley et al., 2010; Kampschreur et al., 2009)	(Itokawa et al., 2001)
	High DO	DO	Conc.	Prop.	Het. denit. AOB denit.	(Kampschreur et al., 2009)	(Tallec et al., 2008)
Internal recycle	Internal recycle rate	xQ	Value	Inv.	AOB denit.	(Foley et al., 2010)	(Foley et al., 2010)
Anoxic/ oxic transitions	Transition zones	Delta DO between reactors	Value	Inv.	AOB denit.	(Chandran, 2011; Yu et al., 2010)	(Yu et al., 2010)
Rapid process changes	Spikes in NH_4, flow, COD/N	Delta	Value	Inv.	AOB denit. Het. denit Inc. NH_2OH oxid.	(Foley et al., 2010; Kampschreur et al., 2009)	Arbitrary

Therefore, the N_2O risk model uses known relations between operational variables/parameters and N_2O emissions to qualitatively classify risk of WRRF N_2O production. In order to process this knowledge and produce a qualitative classification response, fuzzy logic and rule-based systems are applied. More specifically, fuzzy logic assigns degrees of truth (i.e. between 0 and 1), by assigning numerical values to membership functions. Specific values are used to define membership functions (degree of low, medium, and high risk) for the qualitative risk classification of each parameter based upon the input value (i.e. online DO concentration), which are then converted to a numerical output on a scale of 0 (low risk) to 1 (high risk) for the ultimate risk outcome in the fuzzy logic process. As the operational variables implicate different pathways, the scores give direct

indications about which pathways are relevant and, as a result, which model would be useful to select.

5.2.2. Case applications

To prove the concept of using the N_2O risk model for N_2O model selection, it was first applied to two lab scale cases (Case 1 and Case 2) used in Ni et al. (2013b) to compare the N_2O risk model pathway selection versus the model performance. The DO data for Case 1 were taken from Yang et al. (2009) while for Case 2 they were taken from Kim et al. (2010), as referenced by Ni et al. (2013b). For Case 1, five batch laboratory experiments for nitritation were carried out at different controlled DO levels, varying from 0.5 to 2.5 mg DO/L starting with not limiting NH_4 concentrations 35 mg/L. In Case 2, Kim et al. (2010) examined N_2O production by AOB in two nitrification batch experiments with enriched nitrifying AS treating piggery wastewater using both NH_4 and NH_2OH as substrates without allowing N-limiting conditions.

The N_2O risk model was then applied to two full-scale modelling cases from Ni et al. (2013a), i.e. an OD and a SBR, Cases 3 and 4, respectively. DO data for these two full scale plants were available from Ni et al. (2013a) along with plant descriptions. Finally, the N_2O risk model was applied to data from measurement campaigns performed at the WRRFs in Florence and Eindhoven. These plants are known to have different influent and operating conditions (cfr. § 2.3). The WRRF in Florence is a CAS system characterized by 12 tanks loaded by very low-strength wastewater due to water infiltrations in the sewer. The WRRF in Eindhoven is a modified-UCT layout for nitrogen and phosphorous removal, employing a carrousel type bioreactor with concentric rings for alternating anaerobic, anoxic and aerobic conditions.

5.3. Results and discussion

Table 5.2 shows that the N_2O risk model's inference of pathways corresponds with the performance of the mathematical models in Cases 1 and 2 treated in Ni et al. (2013b); thereby, proving the concept at least for known laboratory conditions created so as to favor AOB denitrification. The N_2O risk model inferred the AOB denitrification pathway as being more relevant where the AOB denitrification pathway mathematical models have been reported to perform better. At the same instance, the incomplete (or partial) NH_2OH oxidation pathway models performed not as well.

Table 5.2 - N_2O risk model pathway selection versus N_2O model performance on two lab scale studies of Ni et al. (2013b). Models are labelled according to Ni et al. (2013b).

		Mechanistic model performance "+" indicates good and "-" poor performance			
	N_2O Risk Model pathway selection	Model I (AOB denitrification)	Model II (AOB denitrification)	Model III (Partial NH_2OH/NOH oxidation)	Model IV (Partial NH_2OH/NO oxidation)
Case 1	AOB denitrification	+	- *	-	-
Case 2	AOB denitrification	+	- **	-	-

*Did not perform as well as Model I because model does not include oxygen inhibition term.
**Did not perform as well as Model I because model does not include NH_2OH, the true electron donor for AOB denitrification (Ni et al., 2013b).

Figure 5.1 (left) reports the N_2O risk model (nitrification rules) results applied to Case 1 data from Yang et al. (2009). The increase in DO values decreases the *Low DO* risk, but this transition appears to increase the liquid N_2O concentration which start to decrease in the middle of the phase of no *Low DO* risk. However, as DO decreases again at limiting conditions, N_2O liquid concentration remains constant for the rest of the experiment along with the *Low DO* risk at its maximum. This confirms the presence of a predominant activity of the AOB denitrification pathway in the production of N_2O and corroborates with the findings of Ni et al. (2013b) and Yang et al. (2009) who demonstrated that nitrifier denitrification was mainly responsible for N_2O production by AOB.

In Figure 5.1 (left) data of N_2O production and DO from the laboratory experiment of Kim et al. (2010) are reported along with the results of this work from the application of the N_2O risk model. The *Low DO* risk stays at its maximum level for the first three hours indicating that the conditions of the reactor are likely to favor the AOB denitrification pathway. N_2O production sensibly increases from 0.5 hours and reaches until its maximum at 1.5 hours. At this point, DO is increased to non-limiting conditions and, as a consequence, *Low DO* risk drops to zero. Interestingly, also N_2O production decreases to zero, confirming that AOB denitrification can be addressed as the most responsible pathway for N_2O production in this laboratory experiment. This nicely corroborates with the findings of the laboratory tests of Kim et al. (2010) and of the modelling work of Ni et al. (2013b).

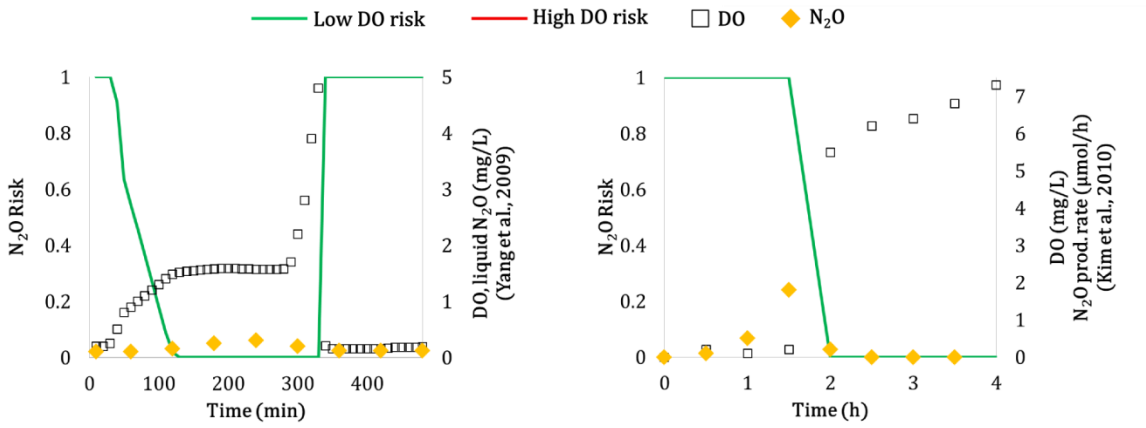

Figure 5.1 - N_2O risk model results (this study) for Case 1 (left) and Case 2 (right). Empty squares (DO) and yellow diamonds (measured N_2O) are adapted from Yang et al. (2009) and Kim et al. (2010) respectively.

Table 5.3 reports the model selections based on the N_2O risk model using the data from the OD (Case 3) and from the SBR (Case 4) full scale installations, as compared with the results of three models implemented by Spérandio et al. (2016) on the same datasets. Both model B and C were able to reasonably reproduce the N_2O production, but clearly showing the likelihood of the presence of both N_2O pathways. It must be pointed out that model C required important adjustment of the NO and NH_2OH affinity indices (Spérandio et al., 2016). However, the fact that both models were able to reproduce the datasets can be considered as a proof of concept that both pathways take place, corroborating with the findings of Ni et al. (2013b). The risk model in fact validates the possibility that both processes can occur.

Table 5.3 - N2O risk model pathway selection versus N2O model performance on two full scale studies in Spérandio et al. (2016). Models are labeled according to Spérandio et al. (2016).

		Mechanistic model performance "+" indicates good and "-" poor performance		
	N_2O Risk Model pathway selection	Model A (AOB denitrification + DO inhibition)	Model B (AOB denitrification)	Model C (NH_2OH oxidation)
Case 3	AOB denitrification and NH_2OH oxidation pathways	-	+	+
Case 4	AOB denitrification and NH_2OH oxidation pathways	-	+	+

Figure 5.2 (left) reports the N_2O risk model results for OD Case 3 (WWTP A location d5 from Ni et al. (2013a)), demonstrating the model selection approach with full-scale WRRF data. In Case 3, peaks in *Low* DO risk immediately precede the peaks in N_2O concentration alternating with peaks in *High DO* risk. This could express the presence of both AOB denitrification and NH_2OH oxidation

pathways for N_2O production. Starting at time zero, and going from left to right, we can see a large peak in *Low DO* risk followed by a large peak of N_2O when DO is raised. This first large peak in N_2O seems to be initially generated under *Low DO* risk conditions and then co-produced by the alternation of both *Low* and *High DO* risk again suggesting the concomitance of AOB denitrification and NH_2OH oxidation pathways. Around the 12^{th} hour, N_2O comes down until there is a new peak of *Low DO* risk, and at the same time N_2O starts to go up again and peaks immediately after *High DO* risk appears to kick in. Finally, N_2O reaches its minimum while the second small peak in *High DO* risk appears, following more closely the shape of the *Low DO* risk profile. Finally N_2O goes up again as *Low DO* risk goes up again. As *High DO* risk is marginally present during this whole period and there is an obvious link between the measured N_2O and the *Low DO* risk, which supports the strong likelihood that the N_2O production is largely due to AOB denitrification, the logical N_2O mathematical model selection would be an AOB denitrification pathway model based on this location (d5 from Ni et al. (2013a)). Interestingly, the other location (d4) from Ni et al. (2013a) exhibited high DO concentrations (> 4 mg O_2/L), which would obviously lead to *High DO* risk (> 1.8 mg/L) and N_2O production via NH_2OH oxidation as suggested by Ni et al. (2013a) since the DO is above 2 mg/L. This rises considerations on the effect of sensor location and on the different conditions occurring in AS tanks. The use of a dual-AOB pathway model for N_2O production might be considered as appropriate in this case for representing the entire OD. However, seen the difficulties reported by Spérandio et al. (2016) in finding a consistent set of calibration parameters, the use of a CM approach should also be evaluated in those cases where a number of different conditions occur and a finer spatial understanding of the biokinetics is required (Rehman et al., 2017). As seen in Figure 5.2 (left) the data confirm that the risk model can be applied to identify the likely mechanisms and help select the most appropriate mechanistic model(s).

In the SBR case (Case 4) (Figure 5.2, right), DO during the SBR aeration cycles varies and results in cycles with both *Low DO* and *High DO* risk, indicating the likelihood of both AOB denitrification and NH_2OH oxidation N_2O pathways occurring. Therefore, a dual-pathway model for AOB N_2O production is suggested for representing Case 4, since we know the SBR can operate with varying DO regimes.

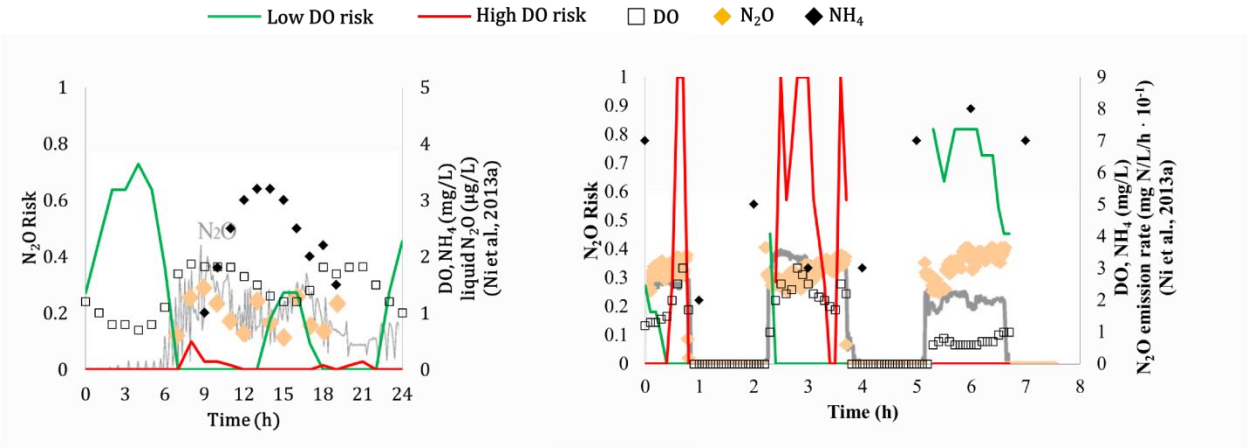

Figure 5.2 – N_2O risk model results for Case 3 (left) and Case 4 (right). Empty squares (DO), black diamonds (NH_4), and shaded yellow diamonds (measured N_2O) and lines (modelled N_2O) are adapted from Ni et al. (2013a).

Moving to the full-scale WRRFs investigated in this study, Figure 5.3 shows the case of Florence and the N_2O risk model's use as it is intended for model selection, and as if we knew nothing else other than the DO to run the risk model. This is to give a glimpse of how model selection would look like using this approach in practice or research. As shown in Figure 5.3, the N_2O production pathway suggested by the N_2O risk model in this case is AOB denitrification due to a consistently high *Low DO* risk and zero *High DO* risk. Since the actual N_2O emissions are known for this case from the measurements, in Figure 5.4 the risk is shown again, but with measured N_2O and DO to validate the model selection.

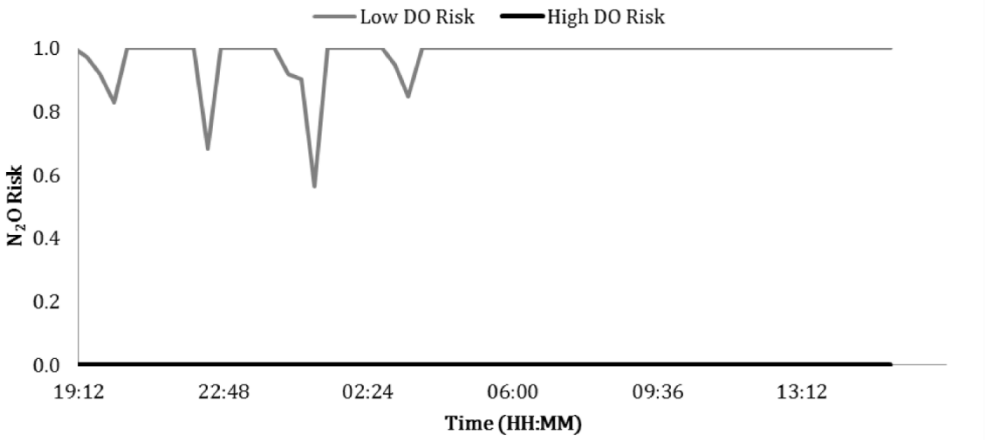

Figure 5.3 – Risk model results for the case of the WRRF of Florence

Figure 5.4 shows dips in *Low DO* risk (due to a rise in DO) corresponding with N_2O peaks. Similar to Case 3 in Figure 1, the *Low DO* risk indicates that the increase in DO likely results mainly in stripping rather than the production of the N_2O. Furthermore, the actual DO concentrations confirm that the DO is mostly very low, favoring AOB denitrification N_2O production due to oxygen limited

conditions (Kampschreur et al., 2009). Therefore, the risk model selection of an AOB denitrification single-pathway model appears to be valid based upon the field measurements.

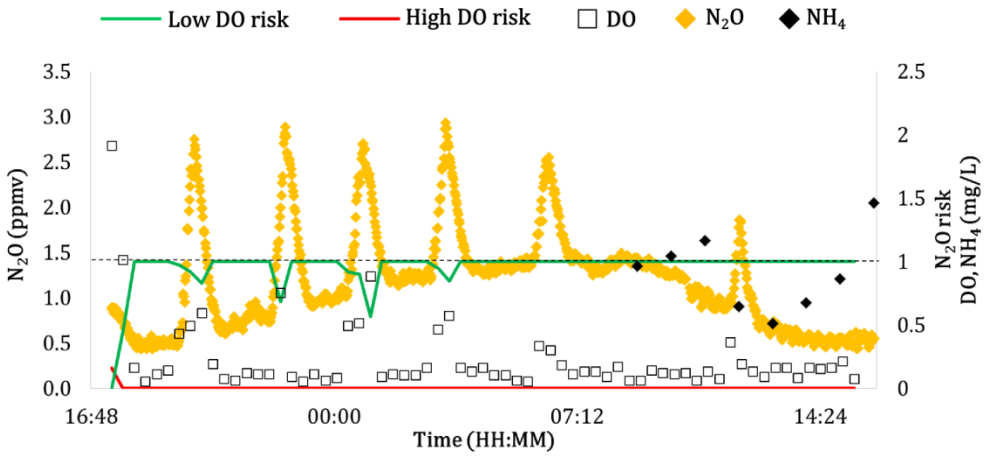

Figure 5.4 - Concentrations of N_2O in the gas phase, DO and ammonia (NH_4) in the liquid for the WRRF in Florence

Again, showing how the N_2O risk model is intended to be used for model selection, Figure 5.5 shows just the N_2O risk results for the WRRF of Eindhoven included in this study. The N_2O risk results in this case indicate that both AOB N_2O pathways can take place and interchange dynamically with process conditions, as there are clear predominant periods of *Low DO* risk (implicating AOB denitrification) with alternations of *High DO* risk (implicating NH_2OH oxidation pathway). Therefore, the risk model could indicate that ideally a dual-AOB pathway model could be selected. However, there is a large predominance of the *Low DO* risk suggesting the AOB denitrification pathway as the main contribution.

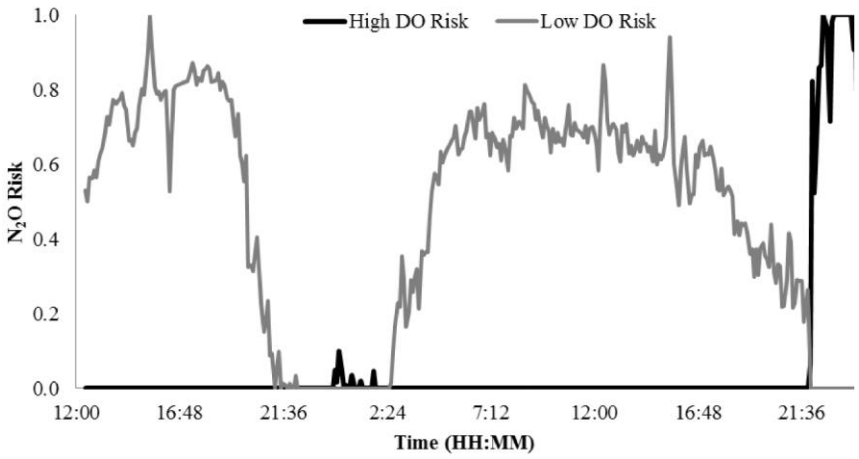

Figure 5.5 – N_2O Risk levels for the WRRF of Eindhoven during the measurement campaign

To test this selection, Figure 5.6 shows the risk with the measured data. Starting at the beginning of the period on the left side and going from left to right, N_2O emissions were seen to decrease and increase during *Low DO* risk conditions, were subsequently seen to decrease and then increase

with small peaks of *High DO* risk, then decrease with decreasing *High DO* risk, then increase with an increase in *Low DO* risk, then decrease and finally peak with *High DO* risk. This confirms that increases in N_2O production are related to conditions favoring N_2O production by both AOB denitrification (low DO conditions) and incomplete NH_2OH oxidation (higher DO and higher ammonia conditions) pathways. However, the large predominance of *Low DO* risk zones suggests a major responsibility of the AOB denitrification pathway. It must also be noticed that the peaks in N_2O concentration occur where a transition between the two risk levels can be observed. In particular, peaks in N_2O concentration appear when the *Low DO* risk reaches half of its range in its way up or down. This would most likely address N_2O production responsibilities to the AOB denitrification pathway. In this view, the use of the sole single pathway AOB denitrification model could be a suitable solution, however, we cannot say the same for a single pathway NH_2OH oxidation model. The selection of a dual-AOB pathway mathematical model would most probably be the best accurate choice based on the N_2O risk model.

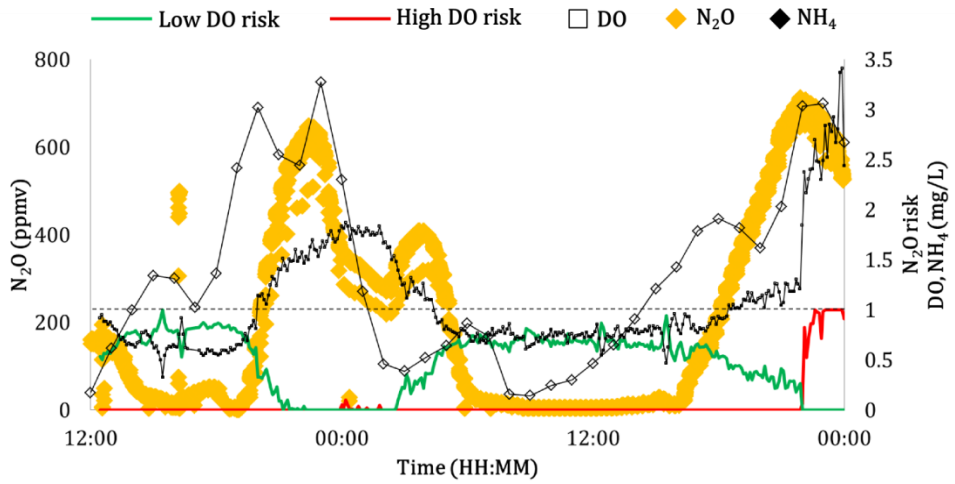

Figure 5.6 – Concentrations of N_2O in the gas phase, ammonia (NH_4^-) in the liquid and the resulting N_2O risk for the WRRF of Eindhoven. Dashed line is the upper risk limit.

5.4. Conclusions

A N_2O risk modelling tool was tested for its capability in selecting mathematical N_2O AOB pathway models based on our knowledge of conditions leading to N_2O production by AOB. Using lab-scale data and corresponding mathematical modelling results based on the same lab-scale data from literature (Kim et al., 2010; Ni et al., 2013a; Yang et al., 2009), the concept was proven by the risk model's selection of single-pathway models that best described the measured N_2O data. This approach was then validated using full-scale data from previous experimental campaigns available in the literature (Ni et al., 2013a) and found to be valid by the risk model's selection of single or dual pathway models that correspond with measured data and observed dynamic production of N_2O. Finally, confronting the N_2O risk model with two full-scale measurements collected as part of this study, the single-pathway mathematical model selections (AOB denitrification pathway for the Florence case study, and dual-AOB pathway model for the Eindhoven case study) using the risk

model were seen to be valid after examining the dynamic risk results with the corresponding process and N_2O data.

More generally, the results indicate that the N_2O risk model can essentially be applied for selecting mathematical models to describe N_2O emissions from a wide range of WRRFs, as the configurations tested were quite different from each other and we know the conditions leading to N_2O production can vary significantly, even between WRRFs of the same configuration. Furthermore, we see that although looking at just the risk results can properly indicate which pathways are relevant for the WRRF, we also see the added value of aligning the risk with the process data, which can only help give a more informed decision. Therefore, it is recommended to align the risk results with process or measured data when selecting models, even if there is no N_2O data. Overall, the use of the N_2O risk model to apply our *real* knowledge of N_2O production in WRRFs has been demonstrated successfully for selecting N_2O pathway mathematical models. However, as these results clearly highlight the capability of the N_2O risk model to identify the mechanisms and conditions leading to higher N_2O emissions for model selection, they also reinforce its utility in identifying possible mitigation strategies. This is important to keep in mind for instances where it is not feasible to implement mathematical models due to various practical reasons.

The current unavoidable limitation of a user's observation to local measurements should however be kept in mind as sensors location drive our conclusions. Results based on local sensor readings reflect only local conditions and not the ones of an entire AS tank where different processes are likely to take place simultaneously. This is not only valid for the risk model used in this section, but for all applications of similar tools and interpretations of local data.

5.5. References

Ahn, J.H., Kim, S., Park, H., Rahm, B., Pagilla, K., Chandran, K., 2010. N2O Emissions from Activated Sludge Processes, 2008—2009: Results of a National Monitoring Survey in the United States. Environ. Sci. Technol. 44, 4505–4511.

CH2MHILL, 2008. Discussion paper for a wastewater treatment plant sector greenhouse gas emissions reporting protocol, Final report prepared for California Wastewater Climate Change Group, 2008.

Chandran, K., 2011. Protocol for the measurement of nitrous oxide fluxes from biological wastewater treatment plants. Methods Enzymol. 486, 369–85.

Comas, J., Rodriguez-roda, I., Gernaey, K. V., Rosen, C., Jeppsson, U., Poch, M., 2008. Risk Assessment Modeling of Microbiology-Related Solids Separation Problems in Activated Sludge Systems. Environ. Model. Softw. 23, 1250–61.

Daelman, M.R.J., De Baets, B., van Loosdrecht, M.C.M., Volcke, E.I.P., 2013. Influence of sampling strategies on the estimated nitrous oxide emission from wastewater treatment plants. Water Res. 47, 3120–3130.

Daelman, M.R.J., van Voorthuizen, E.M., van Dongen, U.G.J.M., Volcke, E.I.P., van Loosdrecht, M.C.M., 2015. Seasonal and diurnal variability of N2O emissions from a full-scale municipal wastewater treatment plant. Sci. Total Environ. 536, 1–11.

Foley, J., de Haas, D., Yuan, Z., Lant, P., 2010. Nitrous oxide generation in full-scale biological nutrient removal wastewater treatment plants. Water Res. 44, 831–844.

GWRC, 2011. N2O and CH4 emission from wastewater collection and treatment systems. Lodon.

Hiatt, W.C., Grady, C.P.L., 2008. An updated process model for carbon oxidation, nitrification, and denitrification. Water Environ. Res. 80, 2145–2156.

Itokawa, H., Hanaki, K., Matsuo, T., 2001. Nitrous oxide production in high-loading biological nitrogen removal process under low cod/n ratio condition. Water Res. 35, 657–664.

Kampschreur, M.J., Tan, N.C.G., Kleerebezem, R., Picioreanu, C., Jetten, M.S.M., Loosdrecht, M.C.M. van, 2008a. Effect of Dynamic Process Conditions on Nitrogen Oxides Emission from a Nitrifying Culture. Environ. Sci. Technol. 42, 429–435.

Kampschreur, M.J., Temmink, H., Kleerebezem, R., Jetten, M.S.M., van Loosdrecht, M.C.M., 2009. Nitrous oxide emission during wastewater treatment. Water Res. 43, 4093–4103.

Kampschreur, M.J., van der Star, W.R.L., Wielders, H. a., Mulder, J.W., Jetten, M.S.M., van Loosdrecht, M.C.M., 2008b. Dynamics of nitric oxide and nitrous oxide emission during full-scale reject water treatment. Water Res. 42, 812–826.

Kim, S.-W., Miyahara, M., Fushinobu, S., Wakagi, T., Shoun, H., 2010. Nitrous oxide emission from nitrifying activated sludge dependent on denitrification by ammonia-oxidizing bacteria. Bioresour. Technol. 101, 3958–3963.

Law, Y., Ni, B.J., Lant, P., Yuan, Z., 2012a. N2O production rate of an enriched ammonia-oxidising bacteria culture exponentially correlates to its ammonia oxidation rate. Water Res. 46, 3409–3419.

Law, Y., Ye, L., Pan, Y., Yuan, Z., 2012b. Nitrous oxide emissions from wastewater treatment processes. Philos. Trans. R. Soc. B Biol. Sci. 367, 1265–1277.

Mampaey, K.E., Beuckels, B., Kampschreur, M.J., Kleerebezem, R., van Loosdrecht, M.C.M., Volcke, E.I.P., 2013. Modelling nitrous and nitric oxide emissions by autotrophic ammonium oxidizing bacteria. Environ. Technol. 34, 1555–66.

Monteith, H.D., Sahely, H.R., MacLean, H.L., Bagley, D.M., 2005. A rational procedure for estimation of greenhouse-gas emissions from municipal wastewater treatment plants. Water Environ. Res. a Res. Publ. Water Environ. Fed. 77, 390–403.

Ni, B.J., Peng, L., Law, Y., Guo, J., Yuan, Z., 2014. Modeling of Nitrous Oxide Production by Autotrophic Ammonia-Oxidizing Bacteria with Multiple Production Pathways. Env. Sci Technol 48, 3916–3924.

Ni, B.J., Ye, L., Law, Y., Byers, C., Yuan, Z., 2013a. Mathematical modeling of nitrous oxide (N2O) emissions from full-scale wastewater treatment plants. Environ. Sci. Technol. 47, 7795–803.

Ni, B.J., Yuan, Z., Chandran, K., Vanrolleghem, P. a., Murthy, S., 2013b. Evaluating four mathematical models for nitrous oxide production by autotrophic ammonia-oxidizing bacteria. Biotechnol. Bioeng. 110, 153–163.

Pan, Y., Ye, L., Ni, B.J., Yuan, Z., 2012. Effect of pH on N 2 O reduction and accumulation during

denitrification by methanol utilizing denitrifiers. Water Res. 46, 4832–4840.

Peng, L., Ni, B.J., Ye, L., Yuan, Z., 2015. Selection of mathematical models for N2O production by ammonia oxidizing bacteria under varying dissolved oxygen and nitrite concentrations. Chem. Eng. J. 281, 661–668.

Porro, J., Milleri, C., Comas, J., Rodriguez-roda, I., Pijuan, M., 2014a. Risk assessment modelling of N2O production in activated sludge systems: Quality not Quantity, in: 4th IWA/WEF Wastewater Treatment Modelling Seminar (WWTmod2014). pp. 351–357.

Porro, J., Milleri, C., Comas, J., Rodriguez-Roda, I., Pijuan, M., Corominas, L., Guo, L.S., Daelman, M.R.J., Volcke, E.I.P., van Loosdrecht, M.C.M., Vanrolleghem, P.A., Nopens, I., 2014b. Risk assessment modelling of nitrous oxide in activated sludge systems: Quality not Quantity., in: 4th IWA/WEF Wastewater Treatment Modelling Seminar, WWTmod 2014. Spa, Belgium.

Rehman, U., Audenaert, W., Amerlinck, Y., Maere, T., Arnaldos, M., Nopens, I., 2017. How well-mixed is well mixed? Hydrodynamic-biokinetic model integration in an aerated tank of a full-scale water resource recovery facility. Water Sci. Technol. 76, 1950–1965.

Schreiber, F., Wunderlin, P., Udert, K.M., Wells, G.F., 2012. Nitric oxide and nitrous oxide turnover in natural and engineered microbial communities: biological pathways, chemical reactions, and novel technologies. Front. Microbiol. 3.

Spérandio, M., Pocquet, M., Guo, L., Ni, B.J., Vanrolleghem, P.A., Yuan, Z., 2016. Evaluation of different nitrous oxide production models with four continuous long-term wastewater treatment process data series. Bioprocess Biosyst. Eng. 39, 493–510.

Tallec, G., Garnier, J., Billen, G., Gousailles, M., 2008. Nitrous oxide emissions from denitrifying activated sludge of urban wastewater treatment plants, under anoxia and low oxygenation. Bioresour. Technol. 99, 2200–2209.

Yang, Q., Liu, X., Peng, C., Wang, S., Sun, H., Peng, Y., 2009. N2O Production during Nitrogen Removal via Nitrite from Domestic Wastewater : Main Sources and Control Method. Environ. Sci. Technol. 43, 9400–9406.

Yu, R., Kampschreur, M.J., van Loosdrecht, M.C.M., Chandran, K., 2010. Oxide and Nitric Oxide Generation during Transient Anoxia. Environ. Sci. Technol. 44, 1313–1319.

Chapter 6

6. Tanks in series versus compartmental model configuration: Considering hydrodynamics helps in parameter estimation for an N_2O model

This chapter is redrafted from:
Bellandi G., De Mulder C., Van Hoey S., Amerlinck Y., Guo L., Vanrolleghem, P., Weijers S., Gori R. and Nopens, I. "Tanks in series VS compartmental model configuration: considering hydrodynamics helps in parameter estimation for a N2O model" (2018) *WRRmod2018, Québec, Canada. Papers.*

Abstract

The choice of the spatial submodel of a WRRF model should be one of the primary concerns in WRRF modelling. However, currently used mechanistic models are too often limited by a too simplified representation of local conditions. This is illustrated by the general difficulties in calibrating the latest N_2O models and the large variability in parameter values reported in the literature. The use of CM developed on the basis of accurate hydrodynamic studies using CFD can much better take into account local conditions and recirculation patterns in the AS tanks that are important with respect to the modelling objective. The conventional TIS configuration does not allow this. The aim of the present work is to compare the capabilities of two model layouts (CM and TIS) in defining a realistic domain of parameter values representing the same full-scale plant. A model performance evaluation method is proposed to identify the good operational domain of each parameter in the two layouts. Already at the steady state phase, the CM was found to provide better defined parameter ranges than TIS. Dynamic simulations further confirmed the CM capability to work in a more realistic parameter domain, avoiding unnecessary calibration to compensate for flaws in the spatial submodel.

6.1. Introduction

N_2O emissions are of great concern in WRRFs and modelling tools have been largely used to date in order to understand its production and define possible reduction strategies. The heterotrophic denitrification pathway model from Hiatt and Grady (2008) is currently the only generally accepted model. However, the pathways responsible for N_2O production are different and contributing to different extents to the emission depending on wastewater characteristics, plant dynamics and environmental conditions (cfr. § 2.2.1). Especially in full-scale applications, modelling is a fundamental tool for understanding N_2O production and emission dynamics. Mechanistic models have been applied to define general operational recommendations aimed at N_2O reduction (Ni and Yuan, 2015) but still case-specific recommendations are necessary and more in depth process understanding is needed for an effective minimization of emissions.

A number of kinetic N_2O models describing very detailed biological processes have recently been developed (Mannina et al., 2016; Ni and Yuan, 2015; Pocquet et al., 2015). In particular, models describing both AOB pathways (i.e. AOB denitrification and incomplete NH_2OH oxidation) have shown important advances in describing the contribution to N_2O production of the different consortia in laboratory controlled conditions (Ni et al., 2014; Pocquet et al., 2015; Spérandio et al., 2016). These mechanistic models are highly descriptive of the known biological processes responsible for N_2O production and have been calibrated and validated in laboratory controlled conditions. However, despite the suggestion of Ni et al. (2013b) for using the dual pathway AOB models, Ni et al. (2013a) discouraged this implementation due to the risk of over-parametrization of the model and the possible creation of strong parameter correlations. In addition to this, the application of both dual pathway and single pathway models in full-scale is still troublesome due to recognized difficulties in identifying proper parameter sets (Ni et al., 2013b; Spérandio et al., 2016). In particular, Spérandio et al. (2016) observed high variability of different parameters, among the different case studies and the different models applied, with related high influence on N_2O and NO emission results. In one case, the ηAOB has been set to a high value making K_{FNA} poorly identifiable, while the opposite has been observed for another full-scale application. These large variations of parameters from one system to another are likely the result of concurring reasons e.g. micro-organisms history and adaptation, defaults in the structure of the models, undescribed local heterogeneities in reactor (Spérandio et al., 2016).

The large variations of parameters values among different full-scale case studies considerably limit the predictive power of the models, as parameters cannot be extrapolated to other plants, and probably not even for different periods in the same plant. This reduced predictive power will also hamper the usage of such models in search for mitigation strategies. Given the detailed structure of available models with regards to the conversion processes involved, the considerable differences in parameters values among different (full-scale) applications are likely due to an unrealistic representation of local conditions in AS tanks, to which these conversion processes are highly sensitive (much more than the traditional ASM processes).

The design of proper WRRF layouts (with respect to spatial submodel) is an important step in plant-wide modelling and for understanding complex process dynamics such as the ones

responsible for N_2O production (Rehman et al., 2014a). In current TIS configurations, recirculation and more detailed local concentrations were assumed to be negligible, and the use of plug-flow-CSTR configurations was preferred to reduce overall model complexity and computational demand. In view of the latest issues in N_2O modelling in WRRFs, it is to date necessary to analyze the possibility and effect of the inclusion of more detailed descriptions of local concentrations in AS tanks by means of more detailed spatial submodels. The development of layouts designed for resembling more accurately hydrodynamic behavior of the internal volume layout, is currently bringing an additional level of detail that can reflect in improved predictive power of available mechanistic models, which is key in optimization and control. Currently, the use of CMs developed upon detailed CFD studies is gaining interest from the modelling community (Le Moullec et al., 2010; Rehman et al., 2017, 2015, 2014b).

In this chapter, a comparison of the performance of a CM and a TIS spatial submodel of the same full-scale WRRF on identifying a domain of good parameters values for the most sensitive parameters using the ASMG2d model (Guo, 2014; Guo and Vanrolleghem, 2014) is provided. Based on literature, each model parameter was sampled in a specific range for generating a number of simulation scenarios. Each simulation scenario was ranked for its performance in predicting measured variables based on different criteria suggested by Van Hoey (2016). The latter returns the good performing scenarios in the form of a distribution of parameter values for both the CM and TIS.

6.2. Materials and methods

6.2.1. Model layouts

Two model layouts of the WRRF of Eindhoven were used, differing in terms of spatial submodel (Figure 6.1). The TIS layout of the Eindhoven WRRF (Figure 6.1, top) is a well consolidated model obtained after years of research of the facility (Amerlinck, 2015; Cierkens et al., 2012; De Keyser et al., 2014) (See Annex I). On the other hand, the CM version (Figure 6.1, bottom) is a recent development of the WRRF model layout resulting from a thorough hydrodynamic study based on CFD simulations in a three-phase (i.e. gas, solid, liquid) model integrated with an ASM for resembling the biological activity (Rehman, 2016) (See Annex I). In particular, the volumes in which the biological tank was initially divided for the case of the TIS, were further partitioned by means of the cumulative species distribution concept that led to the development of the compartmental network currently in use.

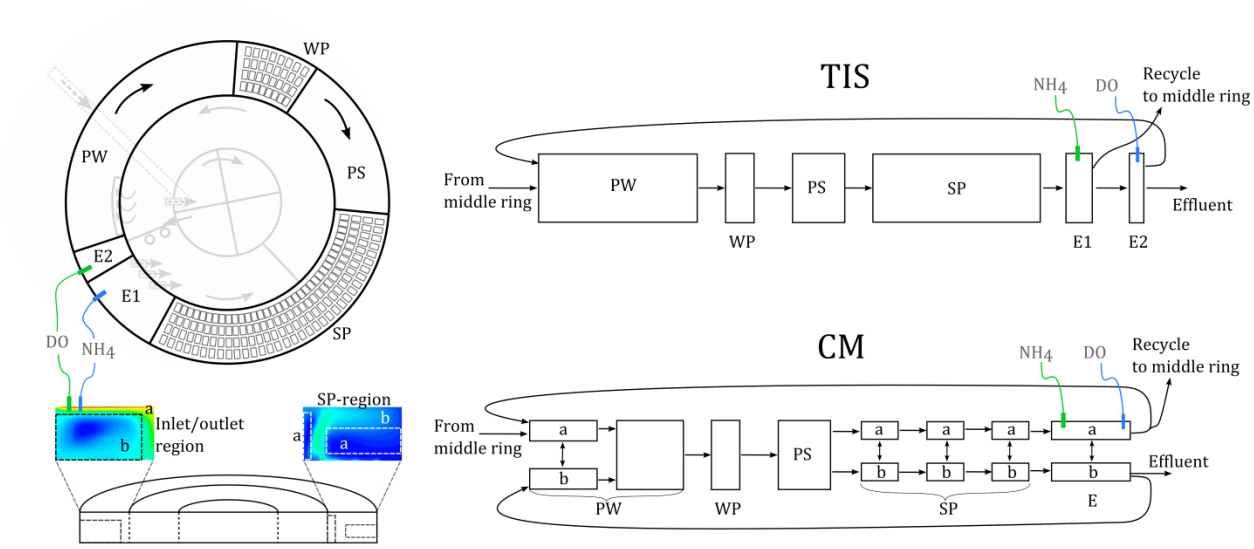

Figure 6.1 – Schematic representation of the partitioning of the AS tank volume according to the TIS (top) and CM (bottom) layouts. The planar representation of the AS tank (top left) is divided for the TIS (top right) in pre-winter (PW), winter package (WP), pre-summer (PS), summer package (SP), effluent (E1 and E2) zones. The CM follows the same concept of TIS in the general division of the volumes, but includes *a* and *b* recirculation zones according to Rehman (2016).

For comparing the two model layouts, a common mechanistic model was chosen with which comparison of the results was performed. Seen the results from § 5 an AOB dual-pathway model can result problematic for its application on this plant. Also, seen the efforts on calibrating the ASMG1 and ASMG2d on the same plant, the biokinetic model chosen for this work was the ASMG2d (Guo, 2014). This model is one of the most popular in full-scale applications and is also implemented in the WEST® platform. In addition to this, the ASMG2d has been considered in other studies in literature, representing an added value for further comparison of the results (Spérandio et al., 2016). It must be specified that, as other N_2O mechanistic models, the ASMG2d is far from being widely applicable to full-scale WRRFs due to the discussed difficulties that these models show in the calibration step. However, for the purpose of this study and for the application to this plant, the ASMG2d represents the most suitable choice.

As input to both the TIS and CM models, a dataset of validated SCADA data from May 2016 was used during which also N_2O measurements in the liquid (Unisense Environment, Denmark) were available. For the steady state simulations a period of 100 days was simulated and the last 30 days were used for averaging output variables. For the dynamic simulations, a 24h dataset of validated input data was used. In order to compare simulation output with measured values, dissolved N_2O measurements and SCADA data from the sensors present on the AS tank were used. The output data of the simulations were taken from the (CSTR) model block resembling most closely the location of the relative sensor in reality (Figure 6.2).

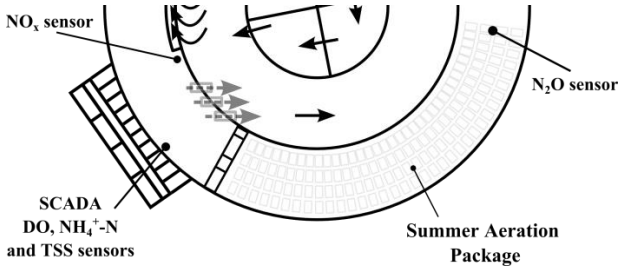

Figure 6.2 – SCADA sensors location in the outer ring of the biological tank of Eindhoven.

For the comparison of the two model layouts, three fundamental steps were followed: I) parameter selection and definition of parameters ranges, and ranking; II) steady state simulation of n-sampled parameters sets to confirm or redefine current parameter ranges; III) dynamic simulations of n-sampled parameters sets to evaluate whether CM can better define the parameter domain than TIS. Throughout steady state and dynamic simulations, 12 model fit metrics were assessed to evaluate the quality of the model output.

6.2.2. Parameter selection and sensitivity ranking (Step I)

A literature selection of the most influencing parameters for N_2O production contained in ASMG2d was performed. Screening the literature, a first set of 25 most uncertain parameters was selected (Gernaey and Jørgensen, 2004; Guo, 2014; Hiatt, 2006; Mampaey et al., 2013; Ni et al., 2013b; Spérandio et al., 2016; Van Hulle et al., 2012) and is reported in Table 6.1. Some of the parameters show up to 140% deviation from different calibration exercises (Spérandio et al., 2016).

Table 6.1 – Initial parameter selection showing extreme values of the domain used in literature.

Parameter	Description	Minimum value	Maximum value
$K_{O\_A1Lysis}$ [g/m³]	Sat/inhibition coefficient for O_2 in lysis, AOB	0.2	1.6
$K_{O\_A2Lysis}$ [g/m³]	Sat/inhibition coefficient for O_2 in lysis, NOB	0.2	0.69
b_{A1} [1/d]	Rate constant for lysis of X_BA1	0.028	0.28
b_{A2} [1/d]	Rate constant for lysis of X_BA2	0.028	0.28
$n_{NOx\_A1\_d}$	Anoxic reduction factor for decay, AOB	0.006	0.72
K_{FA} [g/m³]	Half-saturation index for Free Ammonia	0.001	0.005
K_{FNA} [g/m³]	Half-saturation index for FNA	5.00E-07	5.00E-06
K_{I10FA} [g/m³]	FA inhibition coefficient, NO_2 oxidation by NOB	0.5	1
K_{I10FNA} [g/m³]	FNA inhibition coefficient, NO_2 oxidation by NOB	0.036	0.1

K_{I9FA} [g/m³]	FA inhibition coefficient, NH_4 oxidation by AOB	0.1	1
K_{I9FNA} [g/m³]	FNA inhibition coefficient, NH_4 oxidation by AOB	0.001	0.1
K_{OA1} [g/m³]	O_2 half-saturation index for AOB	0.4	0.6
K_{OA2} [g/m³]	O_2 half-saturation index for NOB	1	1.2
Y_{A1} [g COD/g N]	Yield for AOB	0.15	0.24
Y_{A2} [g COD/g N]	Yield for NOB	0.06	0.24
K_{FA_AOBden} [g/m³]	NH half-saturation for AOB denit	0.001	1
K_{FNA_AOBden} [g/m³]	FNA half-saturation for AOB denit	1.00E-06	0.002
K_{IO_AOBden} [g/m³]	Inhibition coefficient for O_2 in AOB denit	0	10
K_{SNO_AOBden} [g/m³]	NO saturation coefficient for AOB denit	0.1	3.91
K_{SO_AOBden} [g/m³]	O_2 sat coefficient for AOB denit	0.13	12
$n1_{AOB}$ [-]	Growth factor for AOB in denitr step 1	0.08	0.63
$n2_{AOB}$ [-]	Growth factor for AOB in denitr step 2	0.08	0.63
K_{A1} [g/m³]	SA sat coefficient for heterotrophs aerobic growth	4	20
K_{F1} [g/m³]	SF sat coefficient for heterotrophs aerobic growth	4	20
K_{O1_BH} [g/m³]	Sat/inhibition coefficient for heterotroph growth	0.2	1

In order to ensure a sampling of the entire domain without excluding the maximum and minimum limits of each parameter, the domains reported in Table 6.1 were enlarged by 10% of the difference between the relative maximum and minimum values.

A GSA was performed on this set of parameters using the LH-OAT approach (van Griensven et al., 2006) with different perturbation factors. As the choice of the perturbation factor can have an important effect on the numerical stability and thus on the sensitivity results, different magnitudes were investigated (De Pauw and Vanrolleghem, 2006). Also, the impact of the number of samples was observed in order to check whether the increase of one or two orders of magnitude impacted the final ranking. These tests resulted in consistent ranking of the outputs, with the only exception

of the tests with the perturbation factors smaller than 10^{-5}, which resulted in numerical instabilities.

6.2.3. Simulations process

By means of a LH-OAT sampling approach on the most sensitive parameters resulting from Step I, the scenarios for the analysis in Step II and III were created. For each case 2k points on the domain of each parameter were uniformly sampled.

Step II
Steady state simulations were used to compare the model output concentrations with known normal operation conditions in the biological tank. This allowed to make a first ranking of the scenarios based on the proximity of the model output and the known measured values of NH_4, DO and TSS. As a result, this allowed to evaluate the domain of each parameter considered and eventually provide adjustments repeating the steady state simulations. This iterative approach allowed to define a domain for each parameter with "good" parameter values, so that no possibly good parameters values were left out and, at the same time, excluding zones of undoubtedly bad parameter values in order to proceed with Step III.

Step III
Once the last parameter domains after the steady state were defined, the LH-OAT sampling on 2k points was repeated for creating the scenarios for the dynamic simulations. Parameters were uniformly sampled on the eventually reduced domain after the steady state analysis. In this case, the outputs of the model were compared with a day of measured SCADA data (i.e. DO, NO_3, NH_4) and liquid N_2O measurements.

6.2.4. Scenario ranking using 12 different metrics

Different metrics can be used to score a model fit according to a variety of methods to describe the similarity between a modelled and an objective function, therefore, different are the criterion with which scores are assigned. Dissimilarity between metrics depends not only on their mathematical structure but also on the system behavior and objective. Hence, the need of an assortment of criteria to evaluate the performance of a model from different perspectives. For instance, RMSE is a commonly chosen metric to evaluate a model fit, however, it gives emphasis to the fit of peaks and high values. Therefore, its combination with RVE, from the total relative error category, is advisable when variables with a wide range of values are compared (Hauduc et al., 2015).

In this view, for both the steady state and the dynamic simulation step, the outputs were evaluated by means of 12 metrics (Table 6.2). These metrics were selected based on the classification of Hauduc et al. (2015) as the combination of different metrics from different classes have been observed to be more effective than choosing metrics from one class only (Van Hoey, 2016a). All metrics were chosen also based on their response range of values, all metrics (including RVE) indicate the best fit possible with 0. The metrics were selected based on their input requirements so that only values of observed and modelled results could be used as input. In this way, the response

value of each metric chosen, can be rescaled based on its output from a minimum of 0 (best fit) to a maximum of 1 (worst fit).

Table 6.2 – Summary table of the metrics considered for scenario ranking (Hauduc et al., 2015; Van Hoey, 2016a).

Metric	Category	Output range	Main feature
MAE	Absolute	[0, inf]	Indicates the average magnitude of the model error
RMSE	Absolute	[0, inf]	Emphasizes large errors
MSE	Absolute	[0, inf]	Emphasizes high errors
MSLE	Absolute	[0, inf]	Emphasizes low magnitude errors
RRMSE	Absolute	[0, inf]	Low values suggest good agreement
SSE	Absolute	[0, inf]	Low values suggest good agreement
AMRE	Relative	[0, inf]	Low values suggest good agreement
MARE	Relative	[0, inf]	Low values suggest good agreement
SARE	Relative	[0, inf]	Low values suggest good agreement
MeAPE	Relative	[0, inf]	Less affected by outliers and errors distribution
MSRE	Relative	[0, inf]	Emphasizes larger relative errors
RVE	Total Relative error	[-inf, inf]	Measures an overall adequacy

Finally, the different scenarios were ranked based on the 0 to 1 value of each metric separately. Subsequently, an overall ranking can be derived based on the score that each scenario has in each of the metrics. In this way, each metric is scalable within its own domain to a 0 to 1 domain, and addressing to each scenario a value from 0 to 1 allows the ranking of the scenarios according to the single metric (Figure 6.3, left). The value that each scenario collects from each metric, can then be summed up with the rest of the scores obtained from the rest of the metrics to obtain a final overall score used for the final ranking of a given scenario (Figure 6.3, right). The scenarios performing the best for all metrics, i.e. scoring nearly 0 for each different metric, result in the lowest overall score. The best one third of all the scenarios was selected as the *good scenarios*.

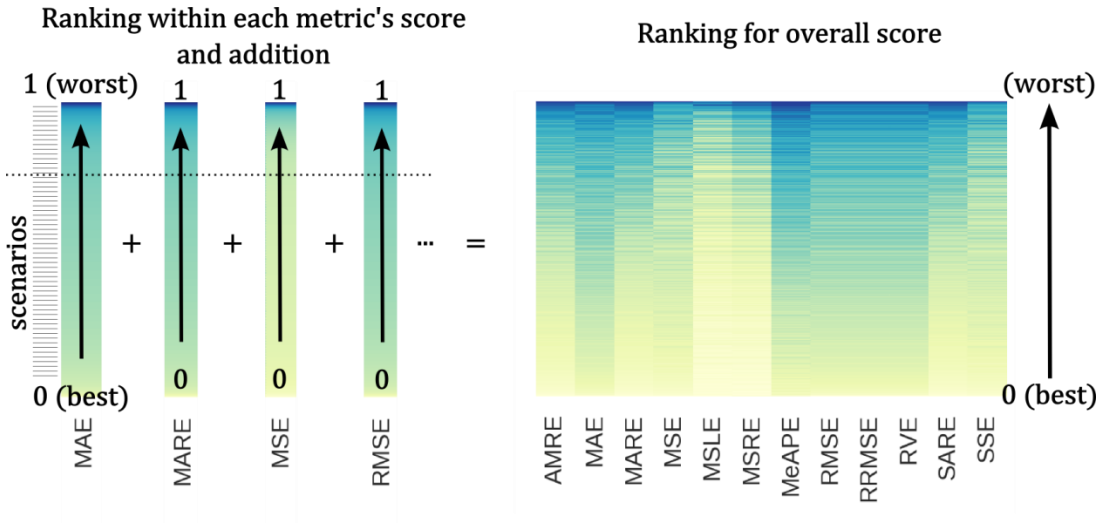

Figure 6.3 – Schematic representation of the scenario ranking method used in Step II and Step III. The initial ranking according to the single metric (left) allows to sum the scores of all metrics for each scenario and have a final score that is used for the overall ranking (right).

For the steady state case, the average output of the last part of the 100 days simulation (about 100 data points), were compared against an objective value. Therefore, for the evaluation of the steady state simulation outputs, the metric evaluation is only based on the proximity of two single values, i.e. the modelled mean and the relative reference value for NH_4, DO and TSS.

For the case of dynamic simulations, the model output of NH_4, NO_3, N_2O, and DO, were compared against measured values. In this case, the metric evaluation becomes more complex due to the different nature of the metrics involved. Each metric will return an estimation of the performance of the model output giving more emphasis to different aspects of a model fit. Hence, the necessity of using a ranking strategy summarizing the different aspects of the evaluation of a fit.

6.3. Results and discussion

6.3.1. Parameter ranking (Step I)

After the selection of the parameters and the definition of the respective range from the literature, a ranking exercise was done. A GSA was performed on this set of parameters using the LH-OAT approach with different perturbation factors. As the choice of the perturbation factor can have an important effect on the numerical stability and thus on the sensitivity results, different magnitudes were investigated (De Pauw and Vanrolleghem, 2006) resulting in a good performance of a perturbation factor of 10^{-3} for all the parameters (see Annex 1 for the test examples run with higher or lower perturbation factors). The suggested minimum sample size in the parameter space is in the range of 10k samples which sensibly impacts the practical possibility of repeating the GSA test due to the high computational effort making the experiment highly time demanding (Van Hoey, 2016b).

The GSA results provided a ranking of the most influential parameters for N_2O, O_2, NO_3, NH_4, TSS, X_{BA1}, X_{BA2} and X_H. For the case of the TIS layout (Figure 6.4), the influential parameters seemed to be the same among the different variables tested overall showing similar importance with few variations in the ranking.

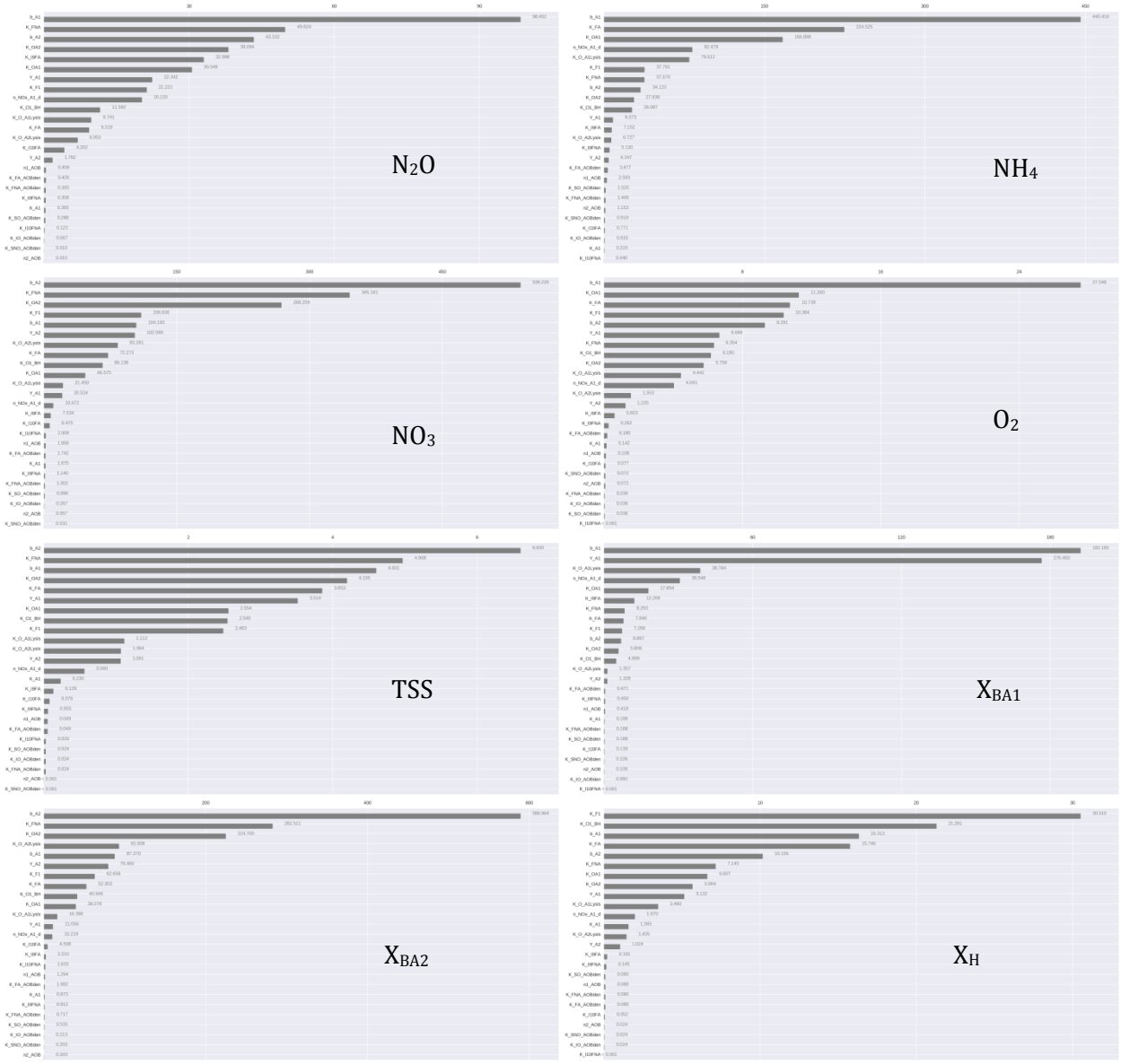

Figure 6.4 – Tornado plots resulting from the GSA (LH-OAT sampling with 10k samples) ranking the most influencing parameters for the case of TIS.

The GSA exercise was repeated in the same fashion for the case of the CM layout (Figure 6.5). Interestingly, the relevant parameters were very similar to the case of the TIS showing very few variations and negligible differences from the previous ranking exercise. In particular, the TIS model seems to address less importance than the CM to K_{A1_lysis} in terms of N_2O, but in general there is agreement between the two layouts. K_{FA} is reputed more sensitive than b_{A1} in the TIS layout in

terms of NO_3, but in both cases they are ranked in the top 5. The CM attributes a relevant position in the ranking for DO to the $n_{NOx\_A1\_d}$, while this is ranked lower in the case of the TIS configuration.

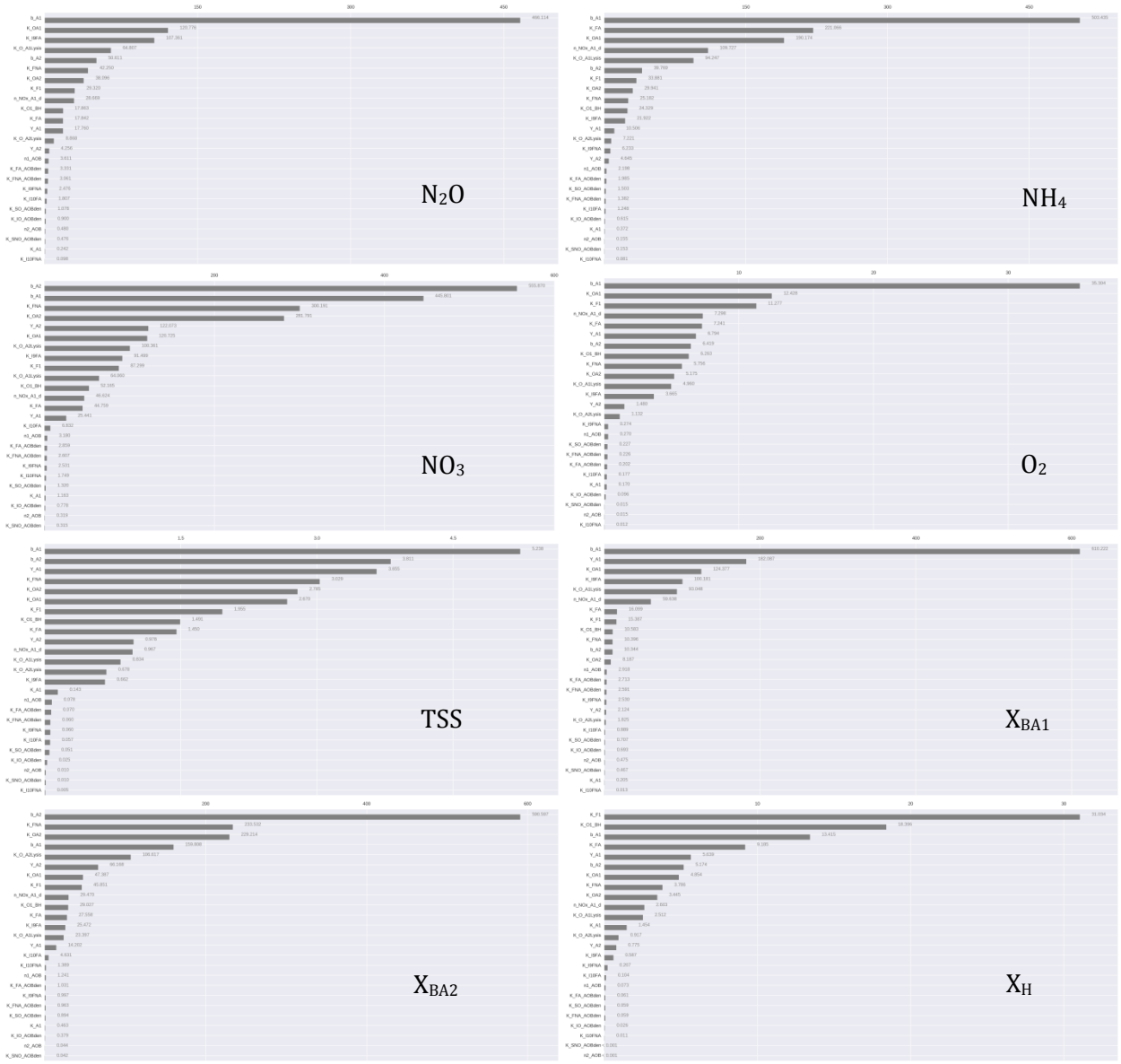

Figure 6.5 - Tornado plots resulting from the GSA (LH-OAT sampling with 10k samples) ranking the most influencing parameters for the case of CM.

In order to define an overall set of parameters suitable for both the TIS and the CM cases, it was decided to give a score to each parameter according to its position in the tornado plot of each variable (i.e. position 1 scores 1, position 2 scores 2, etc.). In this way, the parameters could be ranked from the lowest score to the highest resulting in the order in Table 6.3.

Table 6.3 – Final ranking of the parameters. Shaded are the most sensitive parameters selected by GSA ranking from both TIS and CM configurations.

Rank	
1	b_{A1}
2	b_{A2}
3	K_{OA1}
4	K_{FA}
5	K_{FNA}
6	K_{F1}
7	K_{OA2}
8	K_{O1_BH}
9	Y_{A1}
10	$n_{NOx\_A1\_d}$
11	$K_{O\_A1Lysis}$
12	K_{I9FA}
13	Y_{A2}
14	$K_{O\_A2Lysis}$
15	K_{I9FNA}
16	K_{A1}
17	K_{I10FA}
18	K_{SO_AOBden}
19	K_{I10FNA}
20	K_{FA_AOBden}
21	$n1_{AOB}$
22	K_{FNA_AOBden}
23	K_{IO_AOBden}
24	$n2_{AOB}$
25	K_{SNO_AOBden}

Initially, 10 parameters were selected according to the score and visual analysis of the tornado plots (i.e. b_{A1}, b_{A2}, K_{OA1}, K_{FA}, K_{FNA}, K_{F1}, K_{OA2}, K_{O1_BH}, Y_{A1}, $n_{NOx\_A1\_d}$). Given the presence of Y_{A1}, the proximity in the ranking of Y_{A2}, and the attention that this parameter received in literature, it was chosen to include also Y_{A2}. In a similar fashion, given the importance given to $K_{O\_A1Lysis}$ and the respective $K_{O\_A2Lysis}$ in the literature and their proximity to the cut-off threshold, it was decided to include also these parameters. Finally, given that K_{I9FA} was not the worst positioned in this new GSA ranking, it was also included. This selection resulted in a total of 14 parameters (highlighted in grey in Table 6.3) to be passed to step II and III.

In general, it is interesting that decay parameters for autotrophs are the most sensitive, and that a relevant quantity of half-saturation indexes (K-values) are present in relevant positions of the ranking. This highlights the importance of the correct definition of half-saturation indexes (Arnaldos et al., 2015).

6.3.2. Steady state simulations (Step II)

The aim of Step II was to define the best scenario (i.e. set of parameters) for initializing the model for dynamic simulation (Step III) and verify that the domain chosen for the different parameters was still valid, i.e. not indicating clear clues of a need for a modification of the domain.

With the selected set of parameters 5k scenarios were generated with the LHS method in both cases, i.e. the TIS and CM layout, and steady state simulations of 100 days were run. The output of the simulations was compared against average typical concentrations of NH_4, DO and TSS at the end of the summer package aeration compartment (1.01 mg N/L, 1.02 mg/L and 3200 g/m^3 respectively) obtained from averaging measured data of known good plant operation in dry conditions during summer 2012. Model outputs were scored from 0 (best) to 1 (worst) using the 12 metrics described and ranked accordingly in order to isolate the best performing scenarios. Each metric returns an internal ranking according to the score given to each scenario. An overall ranking among the scenarios is possible summing up the contribution of all metrics for each scenario (cfr. § 6.2.4 in this chapter).

TIS

The steady state simulations performed with the TIS model were ranked for the average output of NH_4, DO and TSS against an objective value. The ranking strategy used places the scenario with the lowest score overall (best performing) at the bottom of the graph (near value 0) in Figure 6.6, while the worst performing are ranked towards the top (near value 1). This visualization allows to qualitatively check both the overall ranking and the contribution of each metric. In particular, Figure 6.6 indicates that, for the scenario tested, the variation of the output TSS (Figure 6.6, right) as compared to the objective value is more pronounced than for DO or NH_4 (Figure 6.6, center and left respectively), the latter showing the smallest variations. Therefore, TSS seems particularly sensitive to variations in the selected parameters values as compared to DO and at last to NH_4, i.e. a deviation in color to the darker tones is visible already close to the bottom of Figure 6.6 (right). It must be also pointed out that, among the scenarios, the magnitude of variation between NH_4, DO and TSS values is largely different due to the different units. Therefore, the transition in color must be considered only as an indication of how fast the outputs of the different scenarios go far from the objective values and what is the contribution of each metric chosen. As an example, from the ranking graph relative to NH_4 (Figure 6.6, left), given the small absolute differences between the model output and the objective value, it can be noticed that the most sensitive metric is MSLE. MSLE is very sensitive to smaller differences as compared to the rest of the metrics due to the fact that it treats both modelled and objective values with a logarithm, thus emphasizing small differences and particularly values smaller than 1. On the other hand, the rest of the metrics need bigger absolute differences between modelled and objective values. Hence, the need of a variety of metrics evaluating a model fit from different points of view. In particular, for the case of NH_4, MSLE

provides most of the input for the final ranking as the rest of the metrics are showing very little variation.

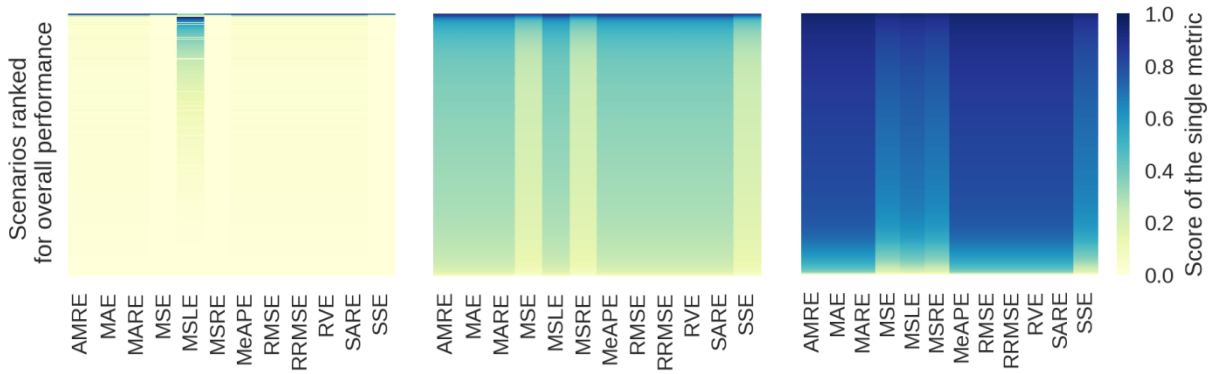

Figure 6.6 – Ranking of the scenarios (rows) according to the 12 metrics (columns) from the best performing (bottom) to the worst (top) (for NH_4, DO and TSS respectively from left to right). Each metric is colored according to its internal ranking from 0 (bright) to 1 (dark).

At this point the best performing scenarios (Figure 6.6, light colors) were selected from each of the cases, i.e. NH_4, DO and TSS. All the distributions for all the parameters resulting from the selection of the best performing scenarios are reported in Annex I, here only the most relevant results are summarized and discussed.

Distribution plots of the parameter values relative to the best performing scenarios, selected according to NH_4 ranking, showed that b_{A1} and K_{FA} appear to perform the best in the higher range of the respective domains (Figure 6.7). The rest of the parameters did not return a particular shape suggesting that there is not a preferred subrange in the tested range. This is an indication for possible reduction or modification to the conservative parameter ranges adopted for these simulations before moving to Step III.

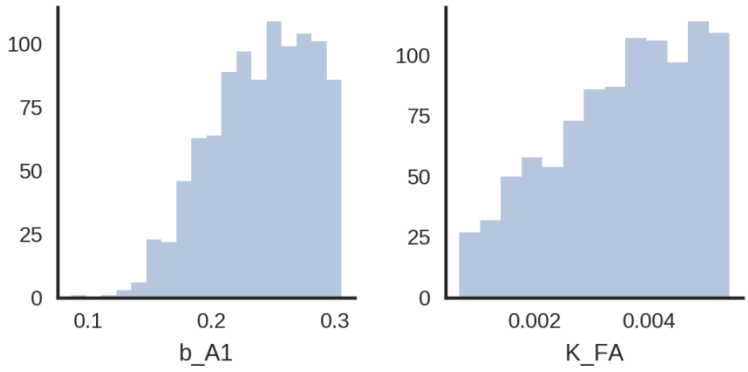

Figure 6.7 – Distribution of the parameter values resulting from the selection of the best performing scenarios for NH_4 in the TIS layout.

For the case of DO there is a confirmation of the good performance returning from the use of the higher range of b_{A1}, once again suggesting that for Step III a reconsideration of the sampling range

for this parameter is useful (Figure 6.8, upper left). Interestingly, the range of b_{A1} is also corroborating with the one observed for NH_4. Also b_{A2} shows a defined tendency in its distribution, showing a relevant preference for values in the lowest range of its domain (Figure 6.8, upper right). In addition to this, K_{F1} and K_{FNA} show a higher density of good performing scenarios close to zero (Figure 6.8, bottom left and right graphs). This reflects the general tendency of abating K_{FNA} to very low values (normally in the order of 10^{-6}) and confirms the reported difficulties in the calibration of this parameter (Spérandio et al., 2016). Similarly, K_{FA} shows a perceivable preference towards lower values in its range, although less pronounced than for the previous cases (Figure 6.8, bottom center) and with opposite tendency.

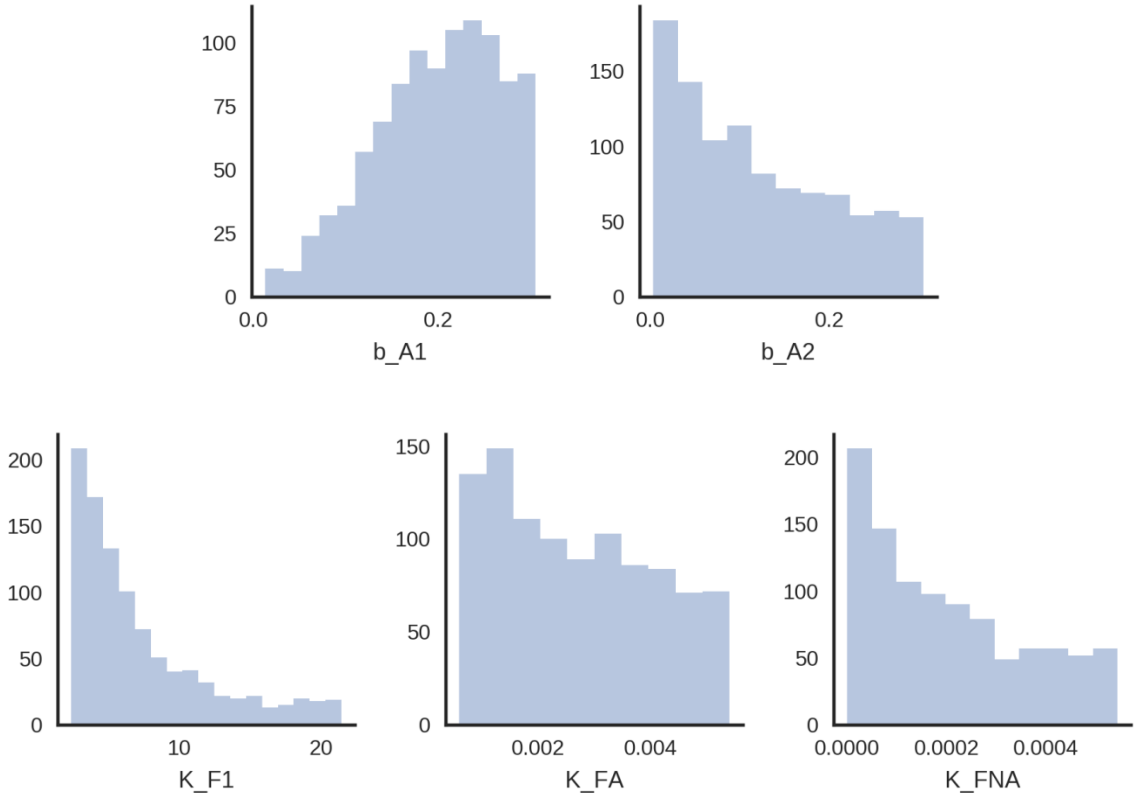

Figure 6.8 – Distribution of the parameter values resulting from the selection of the best performing scenarios for DO in the TIS layout.

From the isolation of the best performing scenarios according to the analysis of the modeled TSS, the distributions of parameters values show interesting shapes for b_{A1}, b_{A2}, K_{FA} and K_{FNA} (Figure 6.9). In contrast to the previous results, parameter b_{A1} shows the highest frequency peak in the lowest range of its domain (Figure 6.9, upper left). However, this distribution appears to be approaching a bimodal case as a noticeable peak in frequency is also visible in the highest part of the b_{A1} domain. This is particularly interesting as the peak on the right occurs very similar to the cases observed for NH_4 and DO. This confirms the necessity of shifting the parameter range towards bigger values for b_{A1} for the model to both comply for DO and NH_4.

For the first time b_{A2} shows a noticeable shape of its distribution pronounced towards the lower values of its domain (Figure 6.9, upper right). A similar shape is returned by the distributions of K_{FA} and K_{FNA} (Figure 6.9, bottom graphs) corroborating with the observations reported for the case of DO. The rest of the parameters selected using the metric ranking with the TSS modeled output, do not show other relevant distributions. They are summarized in Annex I.

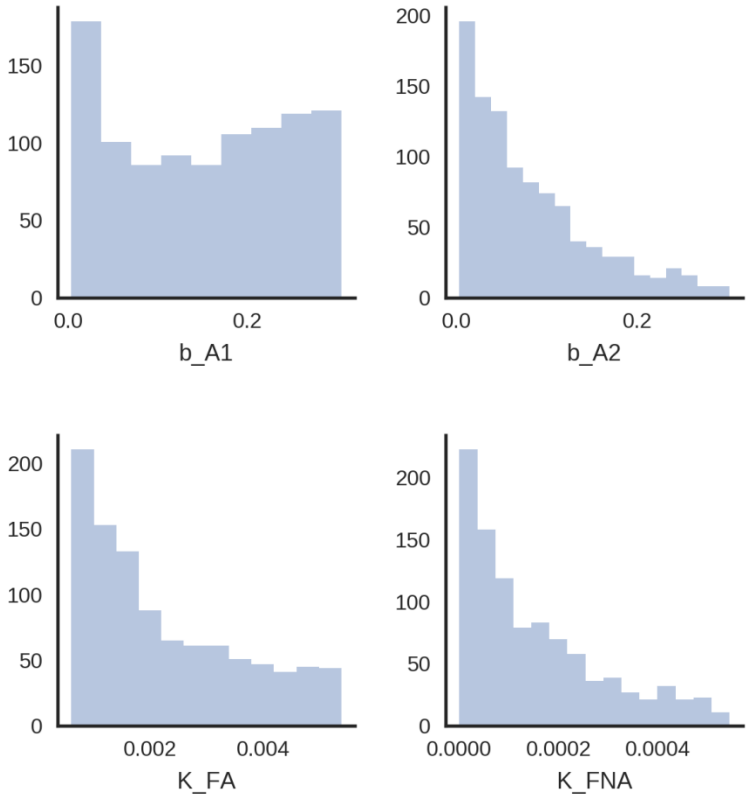

Figure 6.9 – Distribution of the parameter values resulting from the selection of the best performing scenarios for TSS in the TIS layout.

By merging the three groups of best performing scenarios (i.e. for NH_4, DO, and TSS) it was possible to obtain an overall group containing all selected best performing scenarios. This overall group was used as ultimate check on whether the working domain of the parameters needed to be modified before passing to Step III or not. Using an overall dataset including the parameter domains isolated for NH_4, DO, and TSS, helps in defining whether the information gathered from the singular cases still holds when considering multiple parameters simultaneously.

As b_{A1} demonstrated a remarkable tendency for NH_4, DO, and TSS selections to have higher density of best performing scenarios in the higher range of its domain, this is obviously reflected in the overall distribution of best performing scenarios (Figure 6.10, top left). A similar observation is made for K_{FNA} which confirms a strong preference for the very low range of its domain (Figure 6.10, bottom right) while YA_1 suggest the same but with a mild tendency of its frequency distribution (Figure 6.10, top right).

Although b_{A2} was not providing a definite shape for the case of NH_4, its preference for the lower range of its domain in the cases of DO and TSS remains consistent and is reflected in its overall view (Figure 6.10, top center). In the case of K_{F1}, even though it only showed a defined shape of its best performing values for the case of DO, this strong preference still holds in the overall picture (Figure 6.10, bottom left). Finally, K_{FA} seems to maintain a higher frequency of best performing values close to the lower range of its domain (Figure 6.10, bottom center), although this being the result of opposite behaviors observed among NH_4, DO and TSS.

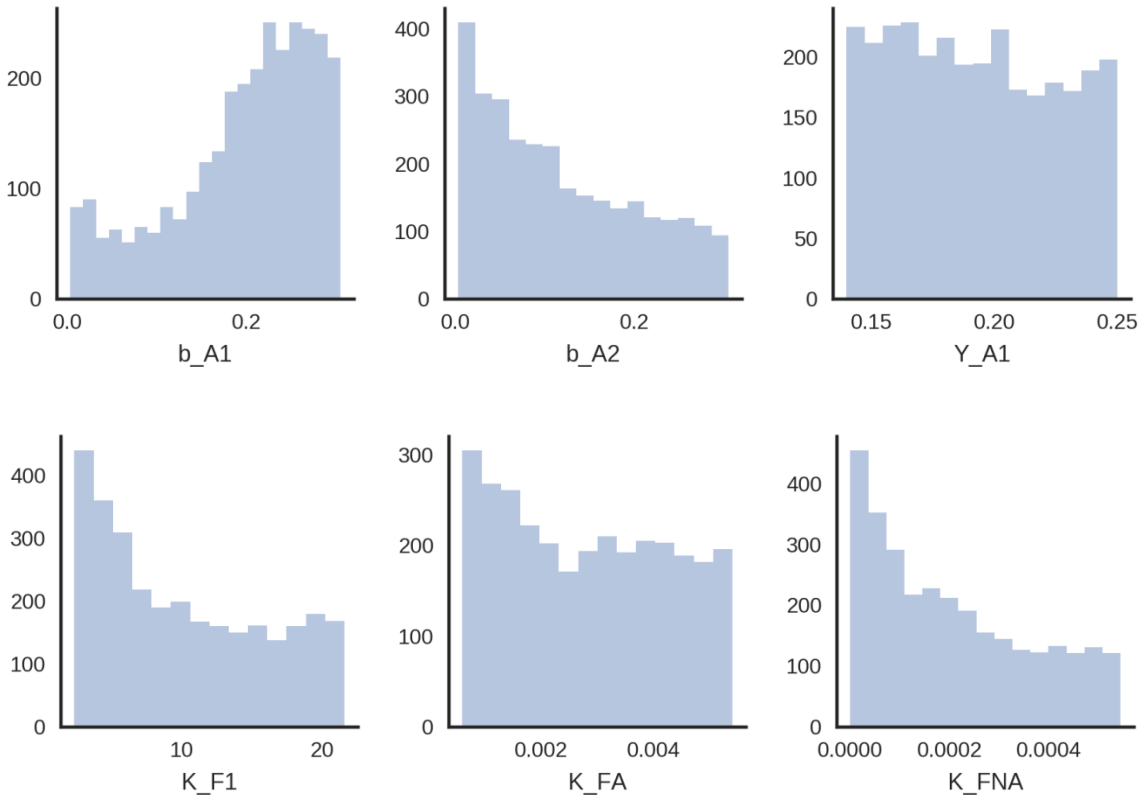

Figure 6.10 – Distribution of the parameter values resulting from the selection of the best performing scenarios overall in the TIS layout.

As a result of these observations, the range of the parameters to be used for Step III (i.e. dynamic simulations) could be modified. However, as the first target of this work is the comparison of the TIS layout with the CM, for a fair comparison the two case studies should use the same parameter range. In this view, the CM output was examined in the same fashion.

CM

The visual ranking of the scenarios for the steady state simulations with the CM layout (Annex I) resembles very closely the one observed for the case of the TIS layout (Figure 6.6). This means that the absolute variation of the model output for the different scenarios from the objective value, are similar for the two layouts for NH_4, DO and TSS.

Similarly to what was observed in the results of the TIS layout, distribution plots of the parameter values relative to the best performing scenarios for NH_4 ranking, showed that b_{A1} and K_{FA} perform the best in the higher range of their domains (Figure 6.11). This is an important aspect in view of identifying which parameter's domain needs adjustment before passing to the dynamic simulations (Step III).

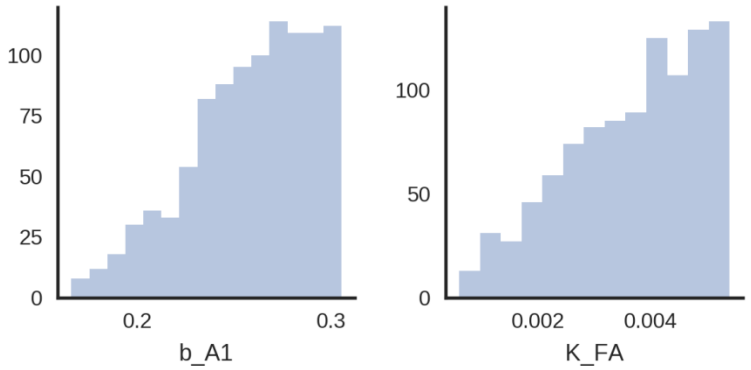

Figure 6.11 – Distribution of the parameter values resulting from the selection of the best performing scenarios for NH_4 in the CM layout.

Plotting the best performing scenarios relative to DO ranking (Figure 6.12), there is again full agreement with what already observed in the case of the TIS layout. The frequency of the best performing scenarios is highest in the higher range of b_{A1}'s domain, while b_{A2}, K_{F1} and K_{FNA}, show a clear preference for their lowest limit. A similar pattern can be observed for K_{FNA} (Figure 6.12, bottom center) although with less definite shape than for the other parameters, and very similar to what observed in the TIS results. In the same way, K_{FA} shows a perceivable preference towards lower values in its range, although opposite and less definite than was observed for NH_4, matching the results of the TIS layout.

Again these are important clues for the modification of the domain of certain parameters before passing to Step III. At the moment all results between TIS and CM seem to corroborate rather closely and no clear difference can be noticed.

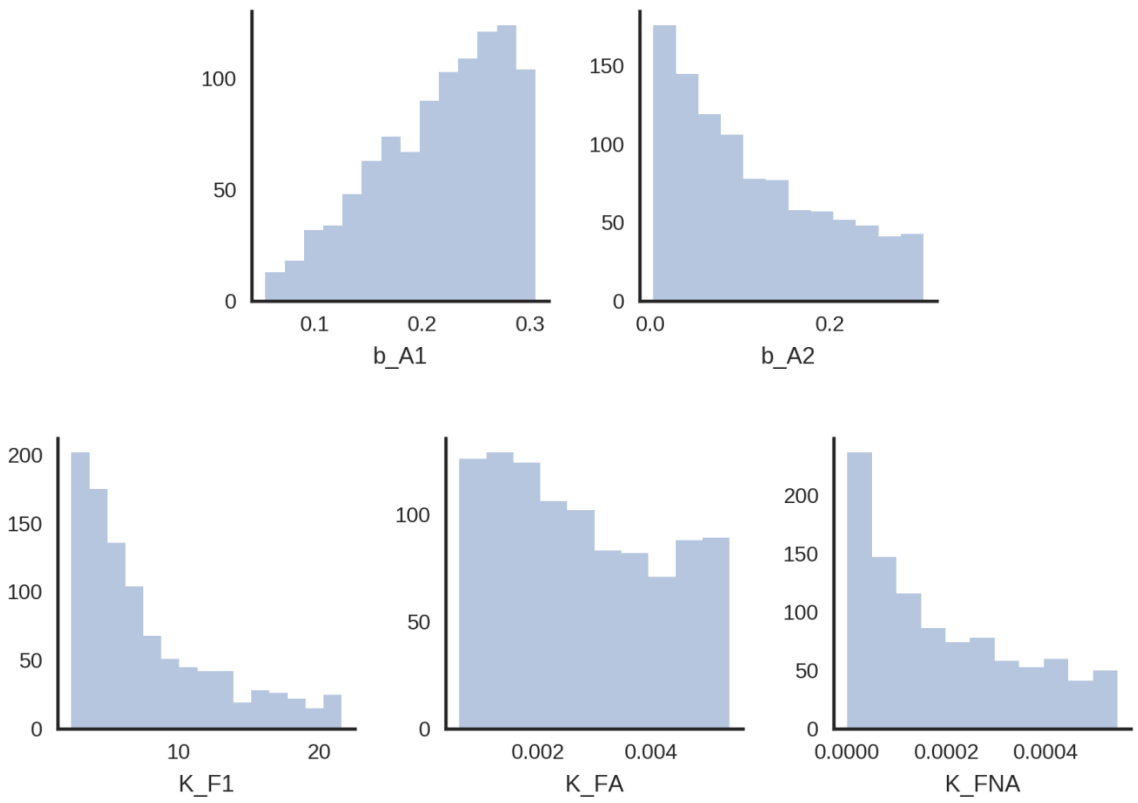

Figure 6.12 – Distribution of the parameter values resulting from the selection of the best performing scenarios for DO in the CM layout.

The best performing scenarios ranked according to TSS returned a well-defined shape of the b_{A1} distribution with high frequency value at the highest edge of its domain (Figure 6.13, top left). In the case of the TIS layout, i.e. where two peaks were observed in correspondence of both the highest and the lowest edges of the domain, this was less clear than for the CM. This is an important point in the evaluation of the performances of the two layouts as the case of b_{A1} for the TSS ranking is the first clue of the gain in definition of the CM as compared to the TIS layout. In addition to this, regarding the modification of the parameter's domain for Step III, this is confirming what was observed in the previous results and corroborating the observation of the TIS case.

As for the rest of the parameters, b_{A2}, K_{FA}, and K_{FNA}, are showing a higher frequency of best performing scenarios in the lowest range of their domain (Figure 6.13). These observations are resembling the results of the TIS layout confirming a potential for modifying the domain of some parameters for Step III.

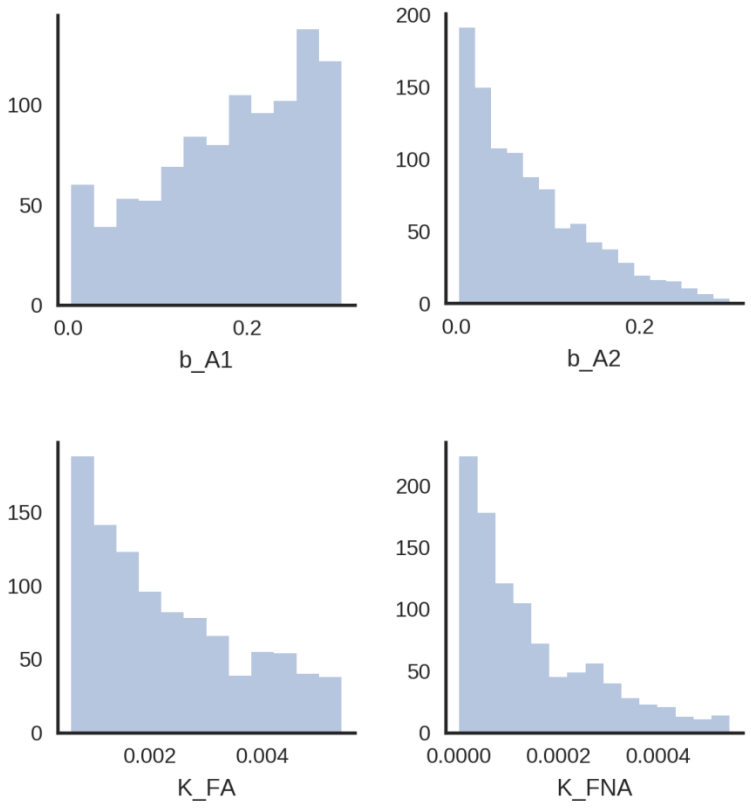

Figure 6.13 - Distribution of the parameter values resulting from the selection of the best performing scenarios for TSS in the CM layout.

In the overall view, merging the three groups of best performing scenarios resulting from the ranking for NH_4, DO, and TSS, a clear tendency of b_{A1} to show higher frequency in the highest part of its domain can be noticed until the distribution gets truncated (Figure 6.14, top left). This is a clear indication of the need for a redefined domain for b_{A1} before passing to Step III, given also the corroborating results of the TIS case. As compared to the case of TIS, the results of the CM layout for b_{A1} show a more defined shape suggesting the presence of a normal distribution with the highest frequency at the maximum edge of its domain. This is obviously the effect of grouping the NH_4, DO, and TSS results, which, for the CM, yielded more defined shapes of the distributions.

Similarly, b_{A2}, K_{F1}, and K_{FNA}, return a clear preference of the highest frequency of their distribution plot for the lower edge of their domain (Figure 6.14). On the other hand, K_{FA} shows also a tendency to prefer lower values of its domain but with a less clear intensity (Figure 6.14, bottom center) as well as Y_{A1} (Figure 6.14, top right). However, in both the cases of K_{FA} and Y_{A1}, there is absence of an outspoken maximum over the range of the parameter to clearly define a definite tendency. These observations agree with what was already observed for the TIS case for the same parameters.

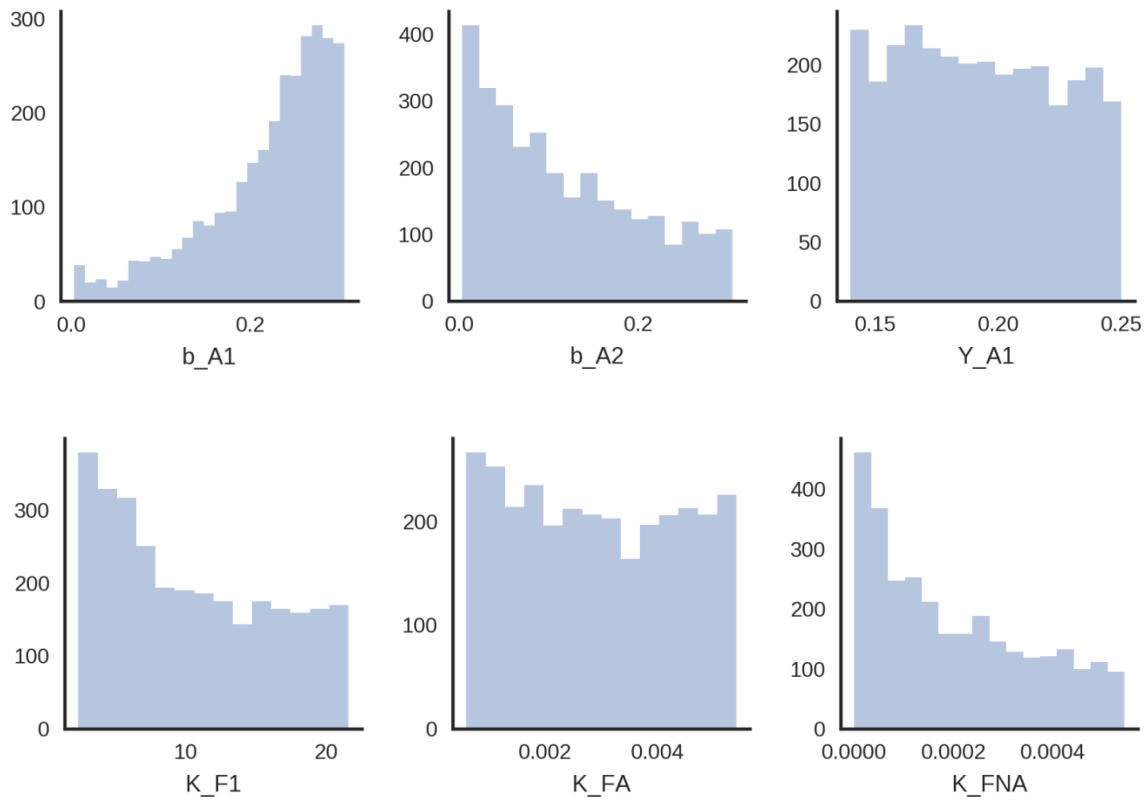

Figure 6.14 – Distribution of the parameter values resulting from the selection of the best performing scenarios overall in the CM layout.

Redefinition of parameter domains

According to the results of Step II for the cases of the TIS and CM layouts, some of the parameters show a clear potential for the modification of their sampling domain before passing to Step III. For those parameters showing truncated distributions and high frequency of best performing values close to an edge of their domain, the modification was considered. This will reduce the number of experiments that likely result in a less goof prediction and are not very useful in the analysis anyway.

In particular, the domains of b_{A1} , Y_{A1} , K_{FA}, and K_{F1}, were modified as indicated in Table 6.4. b_{A1} needed a sensible shift towards higher values and its domain was modified considering a normal distribution with mean value in correspondence of 0.26 and reducing part of the tail that was showing very little frequencies of good performing values (Figure 6.15). In order to ensure that no important information was lost in this passage, a double check plotting the distribution of the top 100 scenarios (Figure 6.15, dark distribution) was done for each parameter with the domain to be redefined. For Y_{A1}, K_{FA}, and K_{F1}, the domains were modified especially at the lowest edge allowing to reach smaller values than what was originally set.

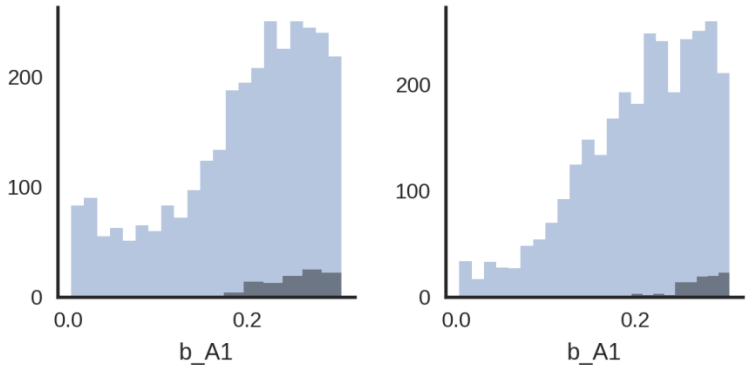

Figure 6.15 – Distribution of the parameter values of the overall best performing scenarios for the case of the TIS (left) and CM (right) layouts. In dark, the b_{A1} distribution of the top 100 best performing scenarios for checking that important information was not lost in the definition of new domain.

In addition to this, the domain of Y_{A1} was also modified given that small but consistent indications of the tendency of higher frequency of best performing scenarios at its lower limit of the domain for both the TIS and CM layouts was observed.

Table 6.4 – New domains for the selected parameters derived from the results of both the TIS and CM layouts results.

Parameter	Minimum value	Maximum value
b_{A1}	0.15	0.40
Y_{A1}	0.04	0.20
K_{FA}	0.001	0.005
K_{F1}	2.4	21.6

Given the known tendency reported in literature for abating K_{FNA} values close to zero in order to accomplish a model fit, and given that those values are recognized to be unrealistic, the domain of K_{FNA} was not modified. In addition to this, the modification of four parameters domains could already have a positive effect on K_{FNA}.

6.3.3. Dynamic simulations (Step III)

The model was initialized with a steady state simulation of 100 days for performing the dynamic simulations. For doing this, the choice of a scenario for initialization was needed. Using the intersection of the three groups of best performing scenarios, i.e. the scenarios considered the best

at the same time for NH_4, DO, and TSS cases, the best scenario according to all three cases could be identified.

Step III was targeted at defining the best performing scenarios analyzing the dynamic simulations output against measured data in specific locations on the bioreactor. The aim of this phase was to compare the capabilities of the TIS and CM layouts in defining a good set of scenarios best resembling the full-scale measured data. In this view, the scenarios were ranked according to the 12 metrics and compared, as in Step II, in terms of the capability of providing a realistic and observable parameters range of best performing values. Therefore, the ranking used the same method as for Step II, but using online measured data as objective functions of the metric comparison (i.e. NH_4, DO, N_2O and NO_3).

It must be pointed out that for the case of N_2O it was not possible to use all 12 metrics. This is due to the fact that some metrics use the value of the objective function at the denominator of a fraction, which returns an infinite solution if a variable can report zero concentration which is the case for N_2O. Therefore, of the original set or metrics AMRE, MARE, MSLE, MSRE, and SSE were not considered for ranking the scenarios according to the N_2O output.

The scenarios were ranked in the same fashion as for Step II but using different variables of comparison depending on the availability of the online datasets.

For the TIS layout, the ranking according to the measured NH_4 (Figure 6.16) showed an interesting behavior of the MSLE metric which at first sight seems to rank the scenarios inversely to the rest of the metrics. This is true for some of the worst performing scenarios for MSLE (darker color), which are not considered as bad by the rest of the metrics. The reason lays in the high sensitivity of the MSLE to small differences between modelled and measured values. In particular, when both measured and modelled variables are smaller than 1, the discrepancy is enhanced by the effect of the logarithm and the quadratic term in the MSLE. Thus, the importance of using multiple metrics is illustrated once more. Using multiple metrics of different nature allows to analyze and rank the scenarios from different points of view, but also to compensate for particular behavior of a single metric. Nonetheless, the visualization proposed in this work highlights the contribution of the single metric and relative potential limits.

Concerning the ranking according to DO, all metrics resulted behaving similarly and overall agreeing in a common final ranking.

Although the ranking according to N_2O was forced to have fewer metrics, those metrics used were still coming from different categories, thus ensuring a ranking according to different approaches. All metrics appear to rank accordingly, although the fast transition towards the darkest colors suggests the presence of few scenarios performing significantly better than the rest. In a similar picture the ranking according to NO_3 can be observed, where, for most of the metrics, a fast transition to darker colors indicates a fast deviation of the modelled results away from the objective measured dataset.

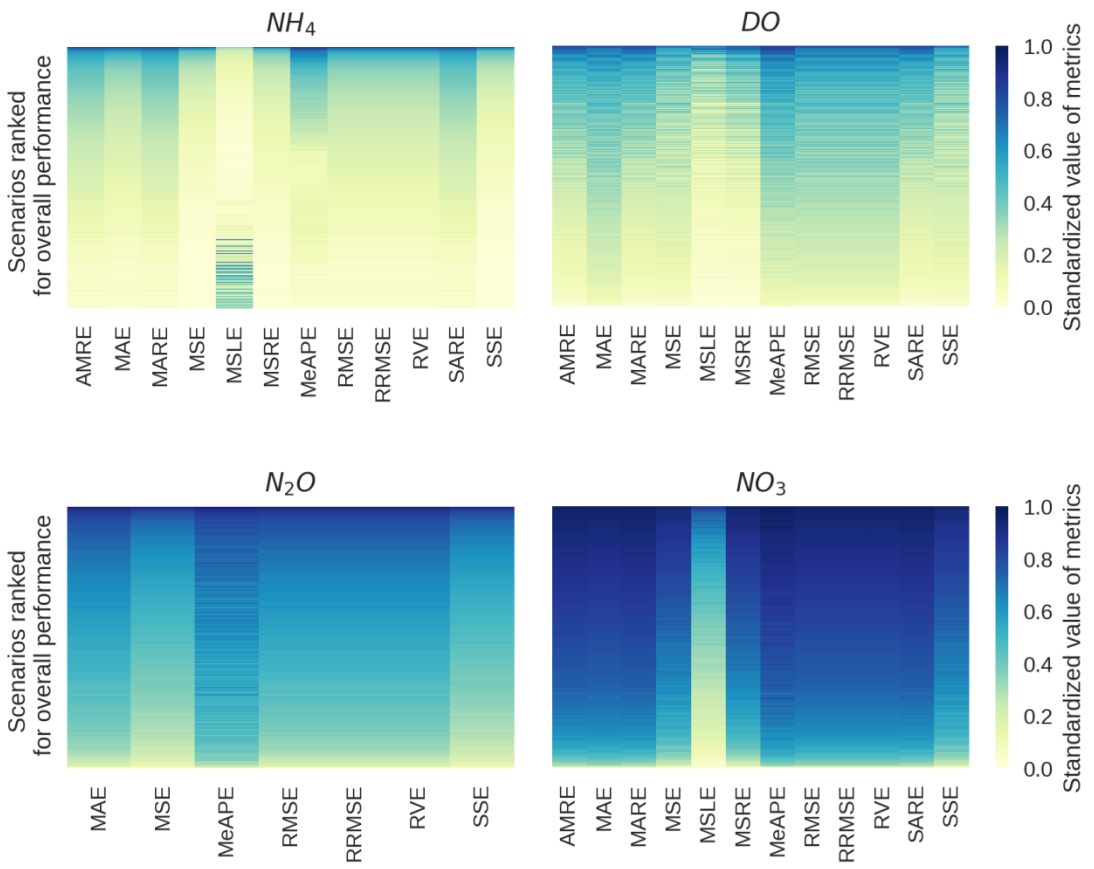

Figure 6.16 - Ranking of the scenarios (rows) according to the metrics (columns) from the best performing (bottom) to the worst (top). Each metric is colored according to its relative ranking from 0 to 1. Results of the TIS layout.

Figure 6.17 shows the ranking for the scenarios of the CM layout. Small differences can be observed among the metrics for the ranking according to NH_4 in which MSLE seems to behave slightly different from the rest of the metrics, although generally agreeing with the rest of the metrics for the best performing scenarios (lighter colors).

For the case of DO there is faster transition to the darker tones of the ranking for all metrics, indicating probably that few scenarios are providing an output close to the measured dataset while the rest is fastly deviating away of it.

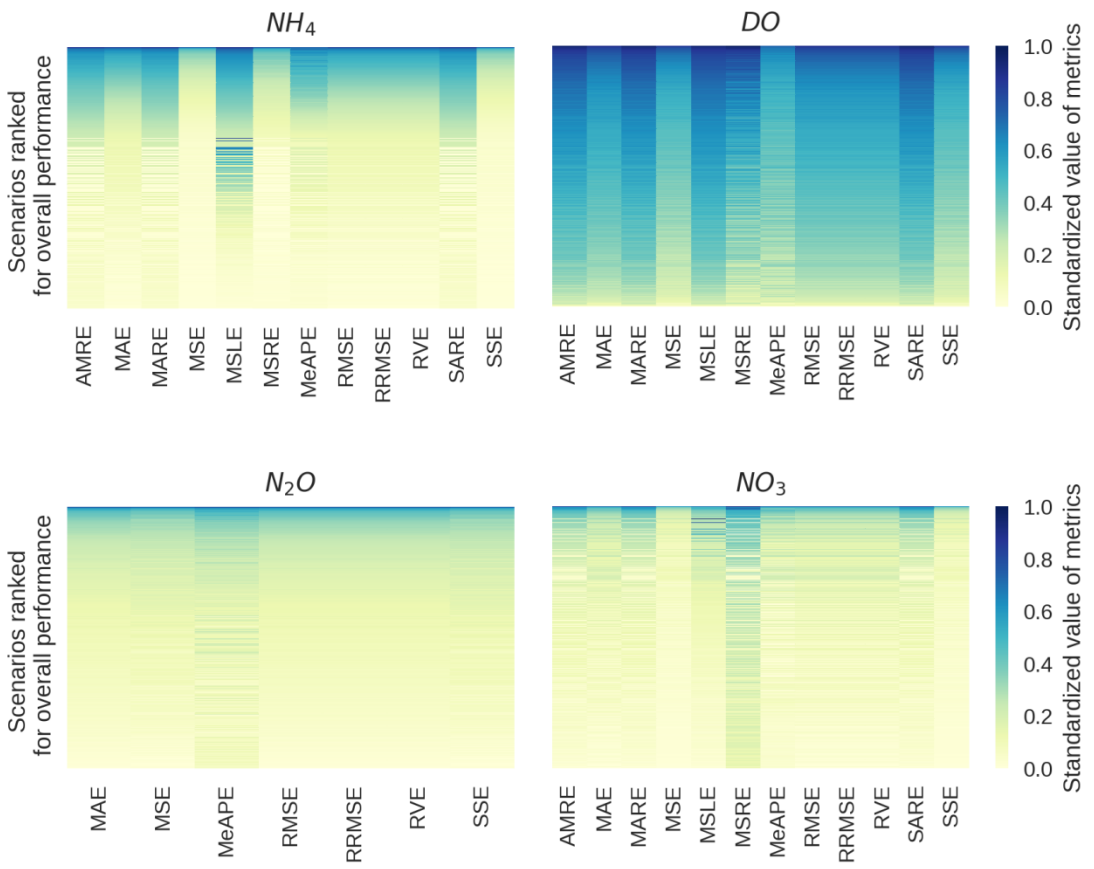

Figure 6.17 – Ranking of the scenarios (rows) according to the metrics (columns) from the best performing (bottom) to the worst (top). Each metric is colored according to its relative ranking from 0 to 1. Results of the CM layout.

Differently from the case of DO, the case of N_2O and NO_3 present a very gradual shift away from the objective function making all metrics generally providing the same ranking (for N_2O fewer metrics are considered).

Comparison between TIS and CM

The overall distributions of the parameter values for the best performing scenarios derived from the ranking for NH_4, DO, N_2O, and NO_3 are reported to make a global comparison of the performances of both model layouts in defining ranges of parameter values that are best performing. Specific distribution of parameters according to NH_4, DO, N_2O, and NO_3 rankings can be found in Annex I.

For the case of Y_{A1} (Figure 6.18), the CM configuration (right) returned a clearly defined range of acceptable parameter values as compared to the case of the TIS layout. The Y_{A1} distribution of the CM appears to define a normally shaped curve which encounters a maximum frequency around the value of 0.1 g COD/g N. The TIS model (Figure 6.18, left) identifies the best performing scenarios in the lowest range of Y_{A1}, which are less realistic values as compared to the case of the CM.

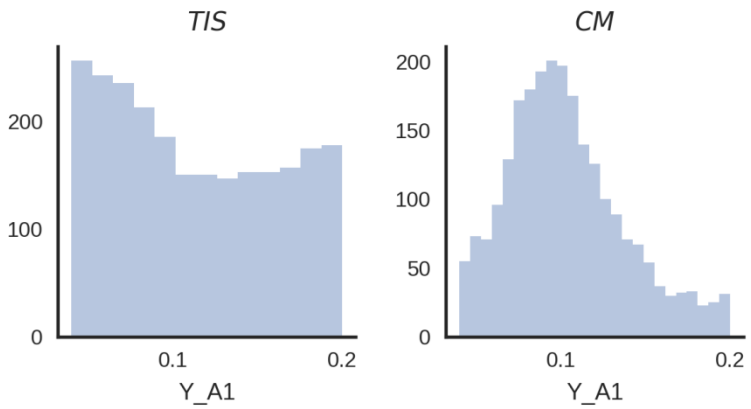

Figure 6.18 – Distributions of overall best performing scenarios for the case of the parameter values of Y_{A1} in the dynamic simulations with the TIS (left) and CM (left) layouts.

K_{FNA} (Figure 6.19), is a known difficult parameter to calibrate which is often abated to values very close to zero to force calibration fit (Spérandio et al., 2016). The CM results (Figure 6.19, right) show a more pronounced shape of a distribution as compared to the TIS, peaking in frequency around the value of 3E-4 g/m^3. This is an important indication finally proposing more realistic values for this parameter and to revert the general tendency of abating this parameter down to 1E-6. On the other hand, the TIS layout does not show a definite distribution having almost everywhere the same frequency. However, it must be pointed out how the far right edge of the distribution for the TIS is slightly increasing in frequency suggesting the possibility of a need for a modification of the K_{FNA} domain.

In this view, it is interesting to consider that, despite the literature studies generally reporting very low values of K_{FNA}, the TIS layout reverts this tendency showing this time a propensity for more realistic values. Furthermore, it is interesting to point out how the CM model confirms the same tendency but with a more pronounced shape of the distribution. This is another confirmation that the higher hydrodynamic accuracy of the CM significantly increases the identifiability of some parameters.

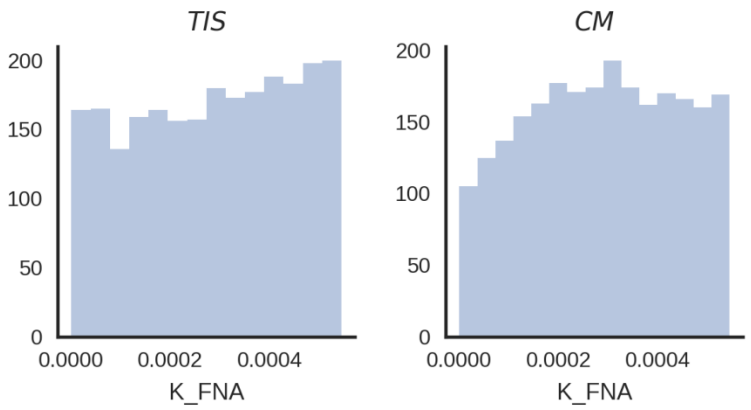

Figure 6.19 – Distributions of overall best performing scenarios for the case of the parameter values of K_{FNA} in the dynamic simulations with the TIS (left) and CM (left) layouts

Finally, looking at K_{F1}, it is interesting how both distributions have a similar shape (Figure 6.20), though more pronounced for the case of the CM layout. The distribution of K_{F1} returned by the TIS layout is noticeably flatter than the one returned by the CM. This can be considered another indication of the increased identifiability of the K_{F1} by means of the CM layout.

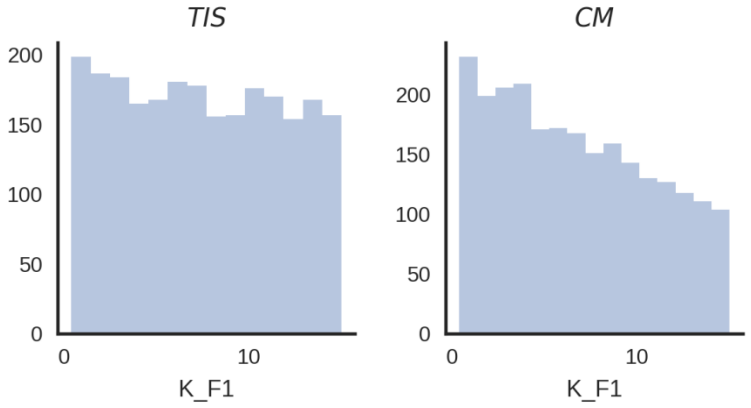

Figure 6.20 – Distributions of overall best performing scenarios for the case of the parameter values of K_{F1} in the dynamic simulations with the TIS (left) and CM (left) layouts

Model fits

The fitting of a model against measured values is the primary target of every calibration and modelling exercise. However, before that, the modeler should consider to be working as close as possible to an accurate representation of the reality, regarding both physical and biological aspects. Thus, firstly aiming to working with realistic parameter values.

It must be pointed out that the present work does not represent a calibration exercise and model fits against measured data were yet not shown with the purpose of focusing the reader's attention in evaluating the ability of a model layout to select its suitable parameter domains. However, for completeness, model fits using the best performing scenario are shown in this section for a qualitative assessment of the model performances.

For the TIS and the CM both layouts the best performing scenario was selected. The best performing scenario was chosen according to all variables considered in Step III (NH_4, DO, N_2O, and NO_3) using the intersection of the four groups of best performing scenarios. Therefore, this results in a trade-off in precision among the different variables used for comparison. In the end, the scenario selected for a layout is not the best fitting according to the single variable, but the best performing overall.

For the case of TIS, the intersection group resulted empty, meaning that there is no scenario putting in accordance the four groups of best performing scenarios. In particular, the group relative to the best performing scenarios for NO_3, appears not to have a common scenario with the rest of the groups. Enlarging the size of the best performing scenarios for NH_4, DO, N_2O and NO_3, and repeating the intersection, a common scenario for all can be found, however, results are reasonably better for NO_3 but sensibly worst for the rest of the measured variables (not shown). Excluding the NO_3 from the intersection of the four groups, results in few scenarios of reasonably good performance. The best scenario of this selection, was used to show the results of the TIS (Figure 6.21, left).

For the case of CM, the selection of an overall best performing scenario was less problematic. The different groups of best performing scenarios from for NH_4, DO, N_2O and NO_3, were in accordance for 39 scenarios. The overall best performing scenario (i.e. scoring the minimum for all the variables of comparison) was selected for the simulation results in Figure 6.21 (right).

Table 6.1 reports the parameter values for the scenario selected for the TIS and CM layouts respectively. It is interesting to notice that the difference in Y_{A1} corroborating with what observed earlier in the parameter distribution. The same seems to be shown for the K_{FNA} parameter. The parameter b_{A1} is also reported in both the CM and TIS cases as in the range of highest frequency of best performing parameters. On the other hand, b_{A2} assumes in this scenario for the case of the TIS layout, higher values than what was observed to be the range of highest frequency of best performing scenarios.

Table 6.5 – Parameter values for the scenario performing the best according to all variables of comparison for the TIS and for the CM layout.

Parameter	TIS	CM
$K_{O\_A1Lysis}$	0.116767	0.103970
$K_{O\_A2Lysis}$	0.319499	0.623322
b_{A1}	0.254775	0.177371
b_{A2}	0.211606	0.031296
Y_{A1}	0.06097	0.103379
Y_{A2}	0.2377	0.126444
$n_{NOx\_A1\_d}$	0.498316	0.565986
K_{FA}	0.005617	0.003866
K_{FNA}	0.000292	0.000206
K_{I9FA}	0.660808	0.703306
K_{OA1}	0.394944	0.550270
K_{OA2}	1.217972	1.145907
K_{F1}	2.230151	6.928328
K_{O1_BH}	0.758667	0.505318

In Figure 6.21 are reported the model results of the TIS (left) and CM (right) in comparison with the measured time series. The TIS model initially accumulates NH_4 until DO reaches a reasonably high concentration, not matching the measured values. In its final part the modelled NH_4 seems to approach better the measured profile in its last small peak, however, as soon as DO decreases sensibly below 1 mg / L, the modelled NH_4 gives a final spike. On the other hand, although the CM over predicts DO while the TIS gives its best fit with it, the CM maintains NH_4 levels closer to what are the measured values.

In terms of N_2O, the CM misses the first peak but maintains a concentration that seems to resemble the measured one with reasonable accuracy. On the other hand, the TIS results are showing a slightly better detection of the highest N_2O peak, while in the second part the modelled profile fades away from the second peak.

The TIS model layout gives the worst performance in terms of NO_3, where modelled concentrations remain at very low values as compared to the measured profile. The CM layout appears to provide modelled NO_3 results closer to the reality. Despite the fact that NO_3 levels are resulting pretty constant from the CM and the peak in the measured NO_3 is not detected, the NO_3 concentration appears closer to the measured NO_3 than for the case of the TIS layout.

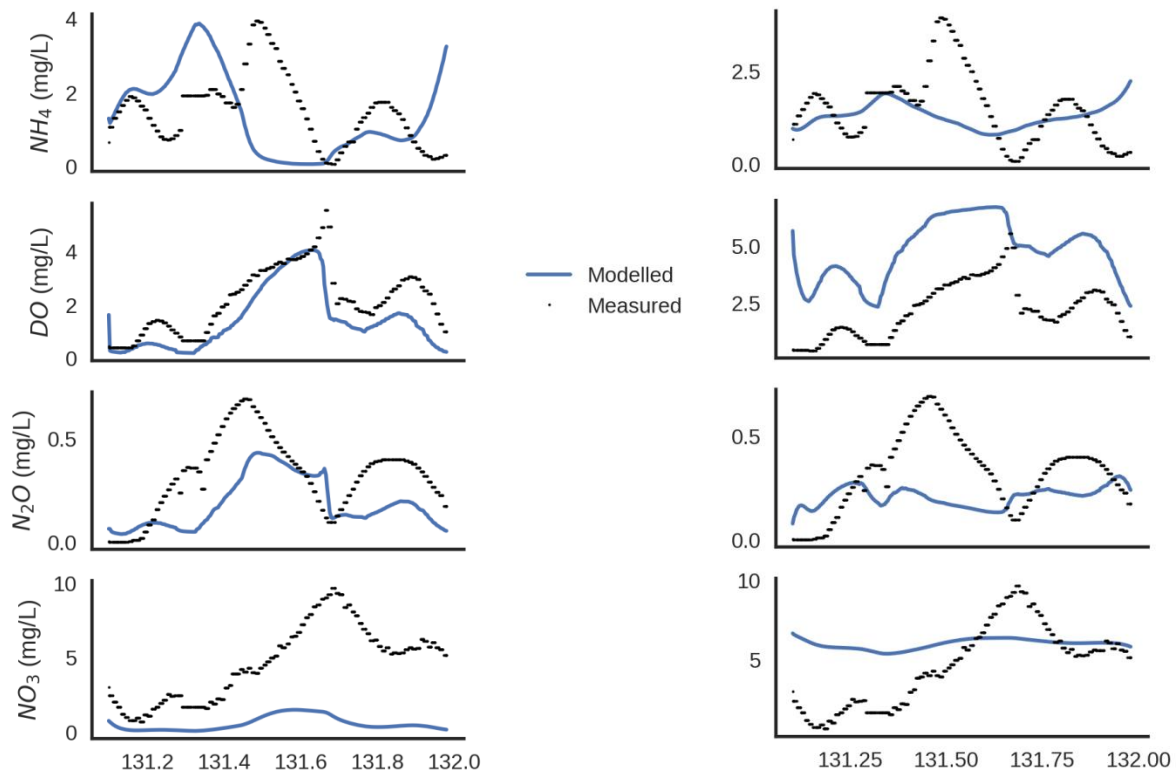

Figure 6.21 – Model outputs of the TIS (left) and CM (right) layouts in comparison with the full-scale measurements.

As specified earlier, this work does not want to be a calibration exercise, and model fits are reported for a more complete view. However, the benefits of the use of the CM layout have been evidenced once more.

Considering that the CM is a recent development of the more exploited TIS layout, the performances of the CM are showing an important potential and the advantage of increasing the level of accuracy of local recirculation and concentrations with respect to the reality.

The actual calibration exercise targeting a good model fit should require more iterative work. In a calibration exercise, the same procedure shown in this work can be used for evaluating the performances of each scenarios and refining the parameter ranges.

6.4. Conclusions

In the present work, a ranking method and a visualization were proposed for selecting the best performing scenarios and providing a qualitative indication of the performance and contribution of each metric used. The advantage of the use of different metrics coming from different categories was visually proven corroborating the indications from the literature.

The visual representation of the ranking of the different scenarios in both steady state and dynamic simulations, returned interesting clues on the necessity of considering multiple metrics of different

nature. Also, the performance of each metric was highlighted in its ranking and the relative effect on the overall arrangement of the scenarios providing information on the contribution of the single metric and as a whole.

Plotting the parameter values obtained through the selection of the best performing scenarios, it was possible to directly compare the performance of the CM and TIS layouts. The two layouts were compared in terms of capability of distinguishing a good operational range for specific parameters. In this way the ability of a model layout to resemble the reality by a more detailed description of recirculation patterns and hydrodynamics in general is compared in terms of ability for parameter identification.

The use of the CM increases the level of detail in the representation of local concentrations. The volume containing the sensors (and therefore providing local concentrations) is much better represented in the case of the CM. This improves results significantly. This implies a relevant gain in accuracy that allowed to redefine some of the key parameters to acceptable values and obtain more defined distributions.

The CM generally returned a more narrow parameter domain of good values with respect to the TIS layout. This indicates that the more detailed description of local concentrations helps in defining a narrower domain of key parameters, which will upon calibration improve the model predictive power.

For reaching more precision in the identification of important parameters, more iterative work is needed. Nonetheless, important clues were already provided regarding the informative gain from the use of CM layout as compared to the canonical TIS configuration. Improvements from the use of the CM configuration are already visible at this stage and the potential gain with increasing hydraulic details is a tangible result.

Further developments of the CM will consider the possibility of varying the volumes of the different compartments according to the influent flow. This will sensibly increase the level of detail in representing local concentrations enhancing the descriptive power of the model. Using variable volumes is per se an improved representation of what is the real behavior of the different small volumes.

6.5. References

Amerlinck, Y., 2015. Model refinements in view of wastewater treatment plant optimization: improving the balance in sub-model detail. Ghent University.

Arnaldos, M., Amerlinck, Y., Rehman, U., Maere, T., Van Hoey, S., Naessens, W., Nopens, I., 2015. From the affinity constant to the half-saturation index: Understanding conventional modeling concepts in novel wastewater treatment processes. Water Res. 70, 458–470.

Cierkens, K., Nopens, I., De Keyser, W., Van Hulle, S.W.H., Plano, S., Torfs, E., Amerlinck, Y., Benedetti, L., Van Nieuwenhuijzen, A., Weijers, S., de Jonge, J., 2012. Integrated model-based optimisation at the WWTP of Eindhoven. Water Pract. Technol. 7, 1–9.

De Keyser, W., Amerlinck, Y., Urchegui, G., Harding, T., Maere, T., Nopens, I., 2014. Detailed dynamic pumping energy models for optimization and control of wastewater applications. J. Artic. 5, 299–314.

De Pauw, D.J.W., Vanrolleghem, P. a, 2006. Practical aspects of sensitivity function approximation for dynamic models. Math. Comput. Model. Dyn. Syst. 12, 395–414.

Gernaey, K. V., Jørgensen, S.B., 2004. Benchmarking combined biological phosphorus and nitrogen removal wastewater treatment processes. Control Eng. Pract. 12, 357–373.

Guo, L., 2014. Greenhouse gas emissions from and storm impacts on wastewater treatment plants: Process modelling and control. LAVAL University.

Guo, L.S., Vanrolleghem, P. a., 2014. Calibration and validation of an activated sludge model for greenhouse gases no. 1 (ASMG1): Prediction of temperature-dependent N2O emission dynamics. Bioprocess Biosyst. Eng. 37, 151–163.

Hauduc, H., Neumann, M.B., Muschalla, D., Gamerith, V., Gillot, S., Vanrolleghem, P.A., 2015. Efficiency criteria for environmental model quality assessment: A review and its application to wastewater treatment. Environ. Model. Softw. 68, 196–204.

Hiatt, W.C., 2006. Activated sludge modeling for elevated nitrogen conditions. Clemson University.

Hiatt, W.C., Grady, C.P.L., 2008. An updated process model for carbon oxidation, nitrification, and denitrification. Water Environ. Res. 80, 2145–2156.

Le Moullec, Y., Gentric, C., Potier, O., Leclerc, J.P., 2010. Comparison of systemic, compartmental and CFD modelling approaches: Application to the simulation of a biological reactor of wastewater treatment. Chem. Eng. Sci. 65, 343–350.

Mampaey, K.E., Beuckels, B., Kampschreur, M.J., Kleerebezem, R., van Loosdrecht, M.C.M., Volcke, E.I.P., 2013. Modelling nitrous and nitric oxide emissions by autotrophic ammonium oxidizing bacteria. Environ. Technol. 34, 1555–66.

Mannina, G., Ekama, G., Caniani, D., Cosenza, A., Esposito, G., Gori, R., Garrido-Baserba, M., Rosso, D., Olsson, G., 2016. Greenhouse gases from wastewater treatment - A review of modelling tools. Sci. Total Environ.

Ni, B.J., Peng, L., Law, Y., Guo, J., Yuan, Z., 2014. Modeling of Nitrous Oxide Production by Autotrophic Ammonia-Oxidizing Bacteria with Multiple Production Pathways. Env. Sci Technol 48, 3916–3924.

Ni, B.J., Ye, L., Law, Y., Byers, C., Yuan, Z., 2013a. Mathematical modeling of nitrous oxide (N2O) emissions from full-scale wastewater treatment plants. Environ. Sci. Technol. 47, 7795–803.

Ni, B.J., Yuan, Z., 2015. Recent advances in mathematical modeling of nitrous oxides emissions from wastewater treatment processes. Water Res.

Ni, B.J., Yuan, Z., Chandran, K., Vanrolleghem, P. a., Murthy, S., 2013b. Evaluating four mathematical models for nitrous oxide production by autotrophic ammonia-oxidizing bacteria. Biotechnol. Bioeng. 110, 153–163.

Pocquet, M., Wu, Z., Queinnec, I., Spérandio, M., 2015. A two pathway model for N2O emissions by

ammonium oxidizing bacteria supported by the NO/N2O variation. Water Res. 88, 948–959.

Rehman, U., 2016. Next generation bioreactor models for wastewater treatment systems by means of detailed combined modelling of mixing and biokinetics. Ghent University.

Rehman, U., Audenaert, W., Amerlinck, Y., Maere, T., Arnaldos, M., Nopens, I., 2017. How well-mixed is well mixed? Hydrodynamic-biokinetic model integration in an aerated tank of a full-scale water resource recovery facility. Water Sci. Technol. 76, 1950–1965.

Rehman, U., Maere, T., Vesvikar, M., Amerlinck, Y., Nopens, I., 2014a. Hydrodynamic-biokinetic model integration applied to a full-scale WWTP, in: 9th IWA World Water Congress and Exhibition. Lisbon.

Rehman, U., Maere, T., Vesvikar, M., Amerlinck, Y., Nopens, I., 2014b. Hydrodynamic - biokinetic model integration applied to a full-scale, in: IWA World Water Congress & Exhibition. Lisbon, Portugal.

Rehman, U., Vesvikar, M., Maere, T., Guo, L., Vanrolleghem, P.A., Nopens, I., 2015. Effect of sensor location on controller performance in a wastewater treatment plant. Water Sci. Technol. 71, 700.

Spérandio, M., Pocquet, M., Guo, L., Ni, B.J., Vanrolleghem, P.A., Yuan, Z., 2016. Evaluation of different nitrous oxide production models with four continuous long-term wastewater treatment process data series. Bioprocess Biosyst. Eng. 39, 493–510.

van Griensven, A., Meixner, T., Grunwald, S., Bishop, T., Diluzio, M., Srinivasan, R., 2006. A global sensitivity analysis tool for the parameters of multi-variable catchment models. J. Hydrol. 324, 10–23.

Van Hoey, S., 2016a. Development and application of a framework for model structure evaluation in environmental modelling. Ghent University.

Van Hoey, S., 2016b. Development and application of a framework for model structure evaluation in environmental modelling.

Van Hulle, S.W.H., Callens, J., Mampaey, K.E., van Loosdrecht, M.C.M., Volcke, E.I.P., 2012. N2O and NO emissions during autotrophic nitrogen removal in a granular sludge reactor--a simulation study. Environ. Technol. 33, 2281–90.

Chapter 7

7. Towards a mitigation strategy for N_2O emissions through Principal Components Analysis

This chapter is redrafted from:
Bellandi G., Weijers S., Nopens I. and Gori R. "Towards a mitigation strategy for N_2O emissions through Principal Components Analysis" (2017) *IWA BeNeLux Young Water Professionals Conference, Ghent, Belgium. Papers.*

Abstract

The emission of N_2O is a relevant issue in wastewater treatment in particular for its large contribution to the plant's CFP. In view of the potential introduction of more stringent regulations regarding wastewater treatment plants' CFP, the availability of a tool allowing the development of mitigation strategies for N_2O emissions is required. Mechanistic kinetic modelling in full-scale applications often appears to be still not mature as some dynamics are not sufficiently understood and emissions are strongly plant specific. In particular plant-wide modelling is too often represented by a very detailed representation of the biological mechanisms but, at the same time, limited by both a poor representation of hydrodynamics and model calibrations on tens of global parameters based on few local process variables. This is particularly true for current N_2O kinetic models. In this chapter, an alternative approach for understanding N_2O production related to process dynamics is proposed. For the first time a data mining approach was tested on full-scale data along with different clustering techniques to identify eventual process criticalities in view of developing a tool for N_2O emission control.

7.1. Introduction

Wastewater treatment processes can be considered to contribute to global warming in different ways, one of which is through the emission of N_2O (cfr. 2.2.1). At a global level, N_2O is a greenhouse and ozone depleting gas of major concern (IPCC, 2013; Ravishankara et al., 2009). Efforts were concentrated in understanding the specific bio-chemical processes responsible for N_2O production (Schreiber et al., 2012) and the WRRF design and operational factors impacting its emission (Daelman et al., 2013; Kampschreur et al., 2009; Monteith et al., 2005).

Measurements on full-scale WRRFs showed that N_2O emissions can represent more than 78% of a wastewater resource recovery facility (WRRF) CFP (Daelman et al., 2015). In addition to this, literature studies show the emission of up to 7% of the influent nitrogen load in the form N_2O (Kampschreur et al., 2008). However, the fraction of influent N that is emitted as N_2O show important variations among plants (Kampschreur et al., 2008; Mampaey et al., 2013).

Considerable efforts have been put into modeling the AOB pathways known to be responsible for N_2O production (i.e. AOB denitrification and NH_2OH) either with a single-pathway solution (Law et al., 2012; Mampaey et al., 2013) or considering both AOB pathways (Ni et al., 2014). However, given the heterogeneity of WRRF process conditions, the potential variability of N_2O emissions, and the diversity of available models, consensus on model selection, dominant pathways and on how to implement these pathways is yet to be reached.

At present, most advanced WRRFs have the availability of a large amount of data from sensors scattered over the plant, which is largely underexploited. Modern small WRRFs generate up to 500 signals, whereas larger ones typically register over 30k (Olsson et al., 2014). These data are in some sense lost in most of the cases, as they are stored in databases and not transformed into actionable knowledge for system optimization. As a result, the investments made for these sensors is only marginally payed back. Resources are thus dissipated on installing and maintaining on-line sensors without making proper use of potentially hidden information. Sub-optimal operation of WRRFs is still the norm rather than the exception (Villez et al., 2016).

In the literature several applications of data mining tools to wastewater treatment for process understanding, monitoring (fault detection), and control of industrial processes such as wastewater treatment are reported (Gernaey et al., 2004). Clustering techniques have been applied to characterize industrial wastewaters (Dürrenmatt and Gujer, 2011), while Pareto efficiency algorithms have been proven to be effective in defining the optimal sensor placement (Villez et al., 2016). Several variants of PCA have been proven to be effective in the control of different aspects of SBRs (Villez et al., 2008). However, to the best of the author's knowledge, there is neither research nor applications of a data mining technique for N_2O production monitoring in WRRFs yet.

In this work, we present a practical application of PCA applied with different clustering techniques with the aim of deriving possible relations relatively to N_2O production among the variables that are normally measured on a full-scale WRRF.

7.2. Materials and methods

7.2.1. Full-scale data

A dataset of one moth of data from one of the biological reactors of the plant of Eindhoven (The Netherlands) (cfr. § 2.3) was used to identify potential clues related to the emissions of N_2O from this treatment step. The dataset, with a frequency ranging from 1 to 15 minutes, was collected during an extensive field measurement campaign. SCADA data available from database of the WRRF of Eindhoven and measured N_2O concentrations in the liquid, were used to unravel possible relations between variables that are normally measured in WRRFs and N_2O concentrations measured in the liquid phase. The variables monitored from the SCADA system were NH_4, NO_x, DO and Q_{air}, while concentrations of N_2O in the liquid phase were measured by means of two full-scale probes (Unisense Environment, Denmark) located at the beginning and the end of the summer aeration package (Figure 7.1).

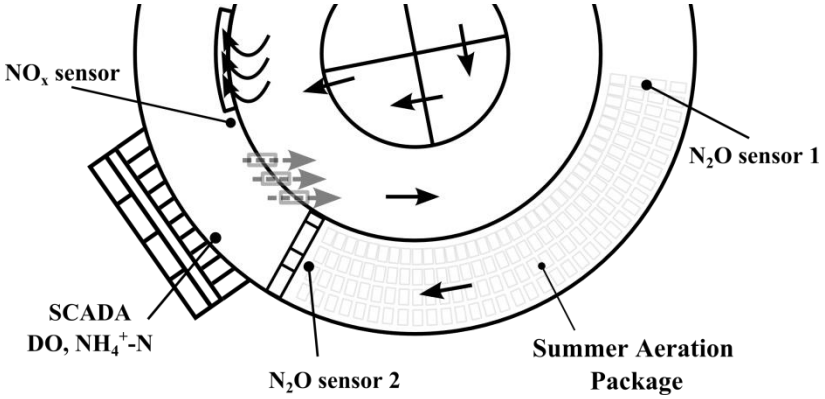

Figure 7.1 – Sensors location in the outer ring of the bioreactor of Eindhoven

The sensors of NH_4, NO_x, DO and the N_2O sensor 2, were located reasonably close to one another, whereas N_2O sensor 1 was located about 70 m upstream, at the beginning of the aeration compartment. This ensured a high resolution of information at the end of the aeration compartment, and at the same time a monitoring location for the N_2O concentration entering the aerated zone.

7.2.2. Data reduction

PCA is one of the most flexible and widely accepted multivariate statistical methods for data mining and is often used for process understanding, monitoring (fault detection), and control of industrial processes such as wastewater treatment (Gernaey et al., 2004; Villez et al., 2008). The principle of PCA is to reduce the amount of information available to a smaller number of variables (PCs) capable of explaining most of the variance of the dataset. In this way, it is possible to unravel hidden dependencies among known key variables.

A set of variables describing a certain process can be represented by a two dimensional matrix Z composed of N samples and M variables (NxM) (Equation (7.1).

$$\boldsymbol{X} = \begin{bmatrix} x_{1,1} & x_{1,2} & \cdots & z_{1,j} & \cdots & x_{1,M} \\ x_{2,1} & x_{2,2} & \cdots & x_{2,j} & \cdots & x_{2,M} \\ \vdots & \vdots & & \vdots & & \vdots \\ x_{i,1} & x_{i,2} & \cdots & x_{i,j} & \cdots & x_{i,M} \\ \vdots & \vdots & & \vdots & & \vdots \\ x_{N,1} & x_{N,2} & \cdots & x_{\cdot N,j} & \cdots & x_{N,M} \end{bmatrix} \tag{7.1}$$

By calculating the scatter matrix (Equation (7.2) of this dataset, or the covariance matrix (Equation (7.3) of the standardized data $\tilde{X}$, it is possible to generate a newly referred dataset expressed by a new set of variables which are linear combinations of the original variables (Equation (7.4).

$$S = \sum_{1}^{N} (x_j - \bar{x})(x_j - \bar{x})^T \tag{7.2}$$

$$\sum = cov(\tilde{X}) = \frac{\tilde{X}^T \cdot \tilde{X}}{N} \tag{7.3}$$

Of this new set of variables, the coefficients are the principal components, i.e. the new reference system is defined.

$$\begin{aligned} t_{i,1} &= \widetilde{\boldsymbol{X}}_{i,\cdot} \cdot \boldsymbol{p}_{\cdot,1} = \tilde{x}_{i,1} \cdot p_{1,1} + \tilde{x}_{i,2} \cdot p_{2,1} + \cdots + \tilde{x}_{i,2} \cdot p_{M,1} \\ t_{i,2} &= \widetilde{\boldsymbol{X}}_{i,\cdot} \cdot \boldsymbol{p}_{\cdot,2} = \tilde{x}_{i,1} \cdot p_{1,2} + \tilde{x}_{i,2} \cdot p_{2,2} + \cdots + \tilde{x}_{i,2} \cdot p_{M,2} \\ &\vdots \\ t_{i,C} &= \widetilde{\boldsymbol{X}}_{i,\cdot} \cdot \boldsymbol{p}_{\cdot,C} = \tilde{x}_{i,1} \cdot p_{1,C} + \tilde{x}_{i,2} \cdot p_{2,C} + \cdots + \tilde{x}_{i,2} \cdot p_{M,C} \end{aligned} \tag{7.4}$$

An interesting property of the $\boldsymbol{p}_{\cdot,c}$ vectors is that they are the eigenvectors of the covariance matrix S and the corresponding eigenvalues λ_c (Equation (7.5) are equal to the variance of the corresponding linear combinations (Johnson and Wichern, 1992).

$$\lambda_c = var(\boldsymbol{t}_{\cdot,c}) = var(\boldsymbol{p}_{\cdot,c} \cdot \widetilde{\boldsymbol{X}}) \tag{7.5}$$

Thus, by sorting the eigenvectors according to their eigenvalues and selecting the first c of them, one has exactly determined the order of the PCs. Another important characteristic of the eigenvalues is that the RV captured by the c^{th} component can be expressed as in (Equation (7.6):

$$RV = \frac{var(\boldsymbol{t}_{\cdot,c})}{tr(\boldsymbol{S})} = \frac{\lambda_c}{\sum_{b=1}^{\max(M,N)} \lambda_b} \tag{7.6}$$

The equation can be explained as the proportional amount of variance captured by the c^{th} PC, and is equal to the ratio of its corresponding eigenvalue to the sum of all eigenvalues (Johnson and Wichern, 1992). The RCV of all components is the sum of the relative variances of each component (Equation (7.7).

$$RCV = \frac{\sum_{c=1}^{C} var(\boldsymbol{t}_{.,c})}{tr(\boldsymbol{S})} = \frac{\lambda_b}{\sum_{b=1}^{\max(M,N)} \lambda_b} \quad (7.7)$$

Once the PCs are identified there are different methods used for data reduction, but the common target is to capture a maximal amount of variance with a minimum number of dimensions. For this reason a scree plot of the eigenvalues is normally an accepted solution. By plotting the eigenvalues corresponding to the PCs in decreasing order, similarly to plotting RV values, the PCs that together explain at least 70 % of the variance of the original dataset (Villez et al., 2008) are selected, which is a general recommendation as no definite threshold exists to the best of author's knowledge.

7.2.3. Clustering

Most commonly applied clustering techniques are based on two popular methods, i.e. the iterative square-error partitional clustering and the agglomerative hierarchical clustering. Clustering algorithms in literature can generally be classified into two types: hierarchical clustering and partitional clustering. Hierarchical clustering methods include agglomerative algorithms and are more efficient in handling noise and outliers than partitional algorithms. On the other hand, partitional clustering admit relocation of points from a different cluster thus allowing to correct initial partitions in later stages.

In addition to hierarchical and partitional clustering, a large number of methods are available from the literature (Han and Kamber, 2001). One example among the most implemented solutions alternative to hierarchical and partitional clustering, is the density-based clustering. This method groups a dataset based on specific criterion of the density functions, defining density as the number of objects in a particular neighborhood of a dataset.

Three of the most spread clustering techniques were applied (Pedregosa et al., 2011) in order to evaluate the capabilities of grouping relevant information selected by the PCs. In particular, *K*-means and the agglomerative clustering are two well-known algorithms already tested in wastewater treatment (Dürrenmatt and Gujer, 2011; López García and Machón González, 2004), while HDBSCAN is a recent improvement of a density based method which, to the author's best knowledge, has never been used in wastewater treatment applications.

K-means

The *K*-means algorithm normally divides the dataset in a number of pre-defined clusters (K) and iteratively minimizes the sum of squared errors within the cluster. For doing so, at the ith iteration each point x is assigned to a cluster based on the following relation.

$$x \in c_j(k)\ if\ x - z_j(k) < x - z_i(k) \quad (7.8)$$

With $c_j(k)$ the set of samples with center $z_j(k)$. At this point, the sum of squared distances for all points belonging to the new cluster center is minimized with the sample mean of $c_j(k)$ (Han and Kamber, 2001; López García and Machón González, 2004).

Agglomerative

This algorithm uses a bottom-up approach, therefore starting with each sample being a separate cluster itself. Successively, groups are merged according to a distance measure, similarly to the *K*-means case, this is done minimizing the sum of squared differences between two clusters (Ward's method) or using the maximum distances between all observations of the different sets (maximum linkage method), but tackling the objective with a hierarchical approach. This recursively merges the pair of clusters that minimally increase a given linkage distance (Murtagh and Legendre, 2014). The clustering may stop when all samples are in a single group or when the required number of clusters is reached.

HDBSCAN

Campello et al. (2013), demonstrated that extending the original density based method (DBSCAN) (Tan et al., 2005) with a hierarchical clustering algorithm, it was possible to achieve an improved application of the DBSCAN. This is one of the latest developments in clustering algorithms providing improvements in the results of a wide variety of data (McInnes et al., 2017; Melvin et al., 2016). HDBSCAN has been observed to be useful for determining a system's stability by grouping stable systems in few bins (Melvin et al., 2016). In this work, HDBSCAN is considered for classification of the PCA output given its exceptional results reported in the literature.

7.3. Results and discussion

Figure 7.2 shows the time series of the variables acquired from the WRRF of Eindhoven for this study. It is noticeable how the peaks in N_2O concentration in the liquid phase (and therefore its actual production) correspond to peaks in NH_4, however, the contrary cannot be stated. The production of N_2O is in fact related to multiple interchanging factors (cfr. §2.2.1) and therefore qualifies as a multivariate problem.

The N_2O sensor 1 (Figure 7.2, top graph), located at the beginning of the aerated compartment and the first sensor according to the flow direction, always shows a higher concentrations compared to the N_2O sensor 2. This is mostly due to the stripping effect of the aeration package, but the high concentration of N_2O at the end of the anoxic zone confirms its production prior to entering the aerobic zone.

Given the known high volatility of N_2O (Weiss and Price, 1980) and the relevant concentrations observed by the N_2O sensor 2 about 70 m downstream at the end of the aerated compartment, it can be stated that the production also occurs within the aerated zone.

In this view, this is an additional confirmation that multiple pathways of N_2O production occur in the different zones of a biological tank. The concentrations recorded by the N_2O sensor 1 are most likely caused by the activity of AOB in DO limiting conditions, while the signal recorded by the N_2O sensor 2, given the non-limiting levels of DO also during N_2O peaks, are most likely to be caused by autotrophic NH_2OH oxidation. In this picture, another relevant element is the NO_2 concentration, reported here together with NO_3 as NO_x, which is strongly influencing the N_2O production (cfr § 2.2.1).

Also included in this dataset is Q_{air} supplied as m^3/h over the aeration package surface (Figure 7.2, bottom). Q_{air} is obviously strongly linked primarily with DO, and then with NH_4, given that the aeration control is primarily based on the NH_4 concentration in the tank.

These variables are potentially containing most of the information required to develop a monitoring tool for N_2O aimed at minimizing its emission.

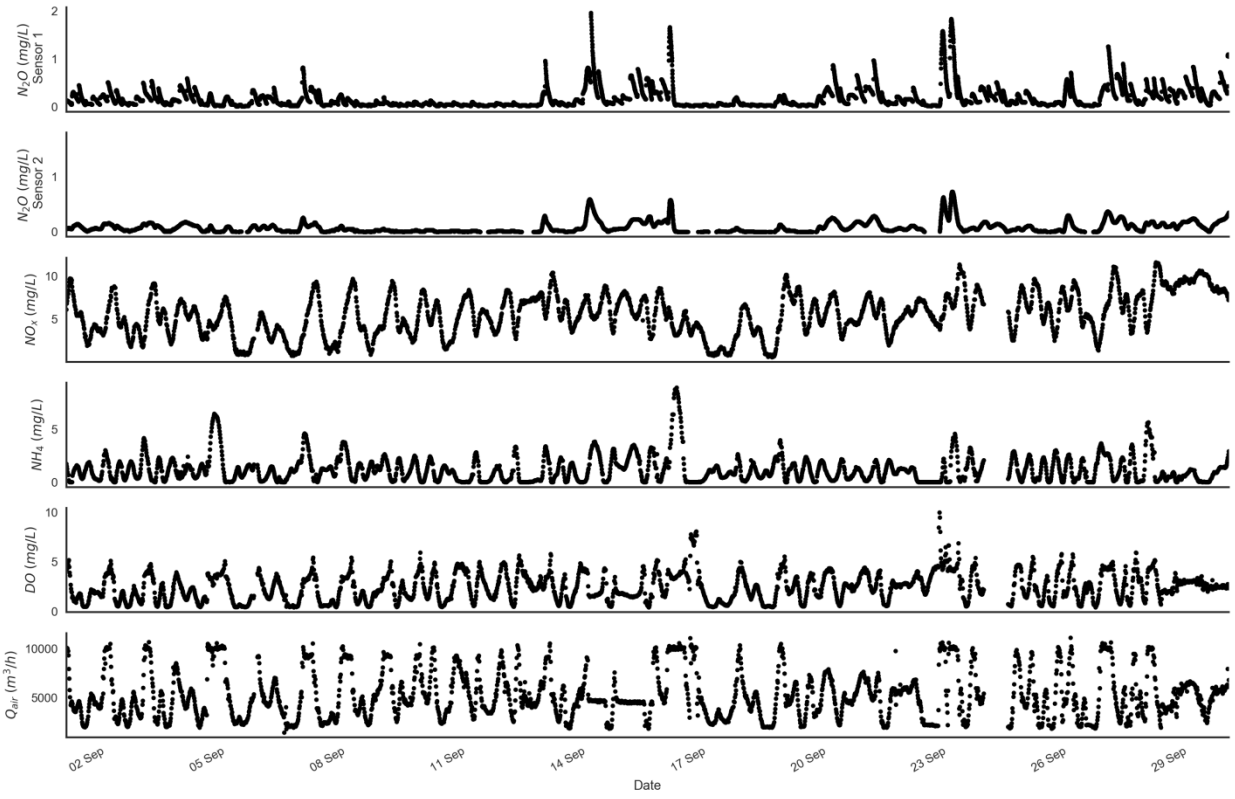

Figure 7.2 – Dataset of an entire month for a bioreactor of the WRRF of Eindhoven.

The dataset reported in Figure 7.2 contains data of high quality in terms of time frequency and sensor status. This is not common for a general WRRFs data stream since periods of missing data for maintenance or failures of probes are rather frequent. The dataset shows a period of regular operation of the plant, good data quality of the sensors without major failures (only exception between 24 and 25th September), and was acquired during a month of good dry weather. This represents a good example of training dataset for the application of a data mining technique.

7.3.1. Data preparation

Preliminary evaluation

Pre-processing of the dataset is important in order to clean the time series from outliers, known to potentially bias the PCA step, and thus ensure good quality input data for training the model. However, in view of a realistic full-scale application, data preparation should be minimized to ease automation and generalization of the algorithm in future practice. However, despite the regular

operation of the plant under dry weather over the whole month, feeding the entire dataset to the PCA did not return a meaningful output. This means that at least a minimal data preparation is needed before implementing the PCA. Therefore, it was decided to use the information contained in the entire dataset to build a representative daily pattern for each of the variables.

Definition of a typical daily pattern

In order to work with the same time frequency for all variables, seen that the lowest frequency was given by the 15 minutes of the SCADA system, a moving window was used to average the N_2O measurements and report all variables at the same time frequency. In this way, the problem of how to fill missing data points from the removal of outliers could also be easily solved.

Each quarter of an hour contained in a day was grouped in a distribution over the whole month from which the 70^{th} percentile was extracted. The 70^{th} percentile of each quarter of an hour of each day in the month considered, was observed to return a close representation of a typical daily pattern for every variable. Thus, the resulting dataset was composed of representative data points describing a characteristic day for each of the variables (Figure 7.3).

It must be mentioned that a higher percentile, although maintaining the general daily pattern of a variable, was observed to discard too much information resulting in less suitable input for the PCA step due to the fact that it would return smoother time series limiting the intrinsic variability of each variable. Basically, this makes all variables look very similar after passing to the correlation matrix, resulting in a PC with very little information.

On the other hand, using smaller percentiles than the 70^{th} favoured the appearance of less frequent daily dynamics and emphasised the noise component of the datasets. After different trials, the 70^{th} percentile was observed to be the most realistic representation of what is a typical daily pattern.

Finally, running a KMO test on the resulting daily pattern, returned a score of 0.53, which confirms the suitability of this dataset for the application of the PCA. The same cannot be confirmed for the raw data as the KMO scored 0.41.

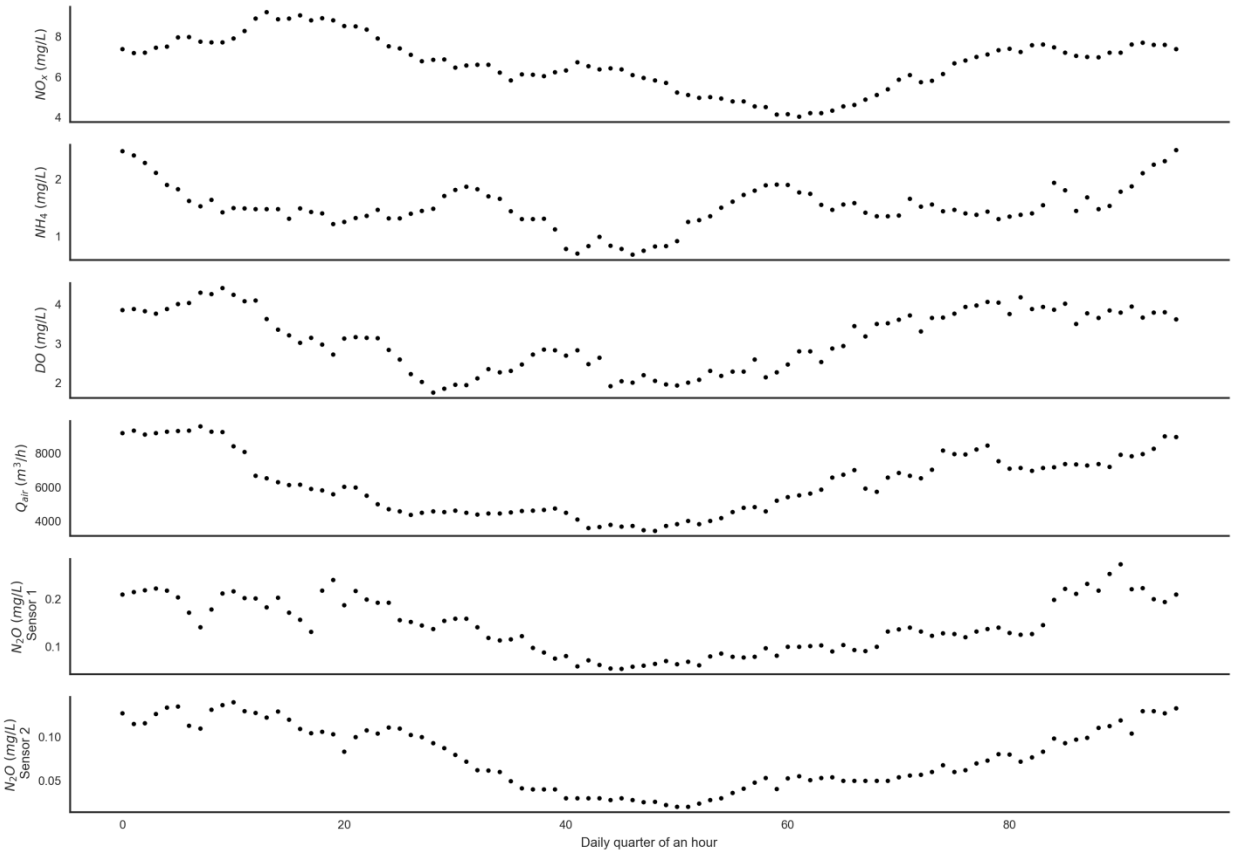

Figure 7.3 – 15 minutes 70th percentile of the raw dataset. This represents a typical daily 24h pattern of the WRRF dynamics, and is the input of the PCA.

By definition, the 70th percentile of a distribution returns the value below which can be found 70 % of the observations. This eliminates the most infrequent absolute daily peaks and valleys, but leaves the general daily pattern of the dataset and its internal variability. This is the reason why the relative concentrations of NH_4, NO_x and DO in Figure 7.3 are somewhat higher than one would normally expect in a correctly managed bioreactor, i.e. concentrations of NO_x and NH_4 peak above 8 and 2 mg/L. In this way, treating all variables the same means maintaining the intrinsic information of a daily pattern for all variables even though relative values are slightly higher that in reality. However, this rises no concern in terms of the application of the PCA since this technique uses the correlation matrix (or the scatter matrix) to derive relations between standardized variables and therefore is not affected by the relative value of a variable (otherwise Q_{air} would be the most influencing seen that its values are in the order of magnitude of 10^3).

7.3.2. Application of the Principal Component Analysis

All variables were fed to the PCA with the exception of the N_2O measurements in order to create a model composed exclusively of variables that are normally measured in a WRRF and increase its applicability on full-scale. In this way, the information contained in those variables can be effectively tested for its capability of predicting N_2O production.

Prior to analysing the PCA response, the contribution to the explained variance for each PC needs to be evaluated. The contribution of each PC is reported in the bar chart in Figure 7.4 along with the cumulative step curve. From this plot it can be noticed that two PCs are explaining together more than 90 % of the variance of the entire dataset, with the first PC containing about 70 % and 20 % for the second PC, while the variance explained by the third PC is below 10 %. Therefore, two PCs can be considered to describe most of the variability of the four original variables.

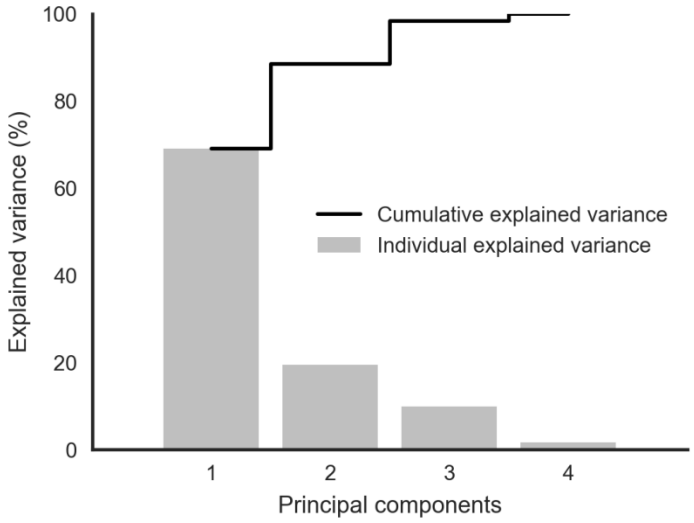

Figure 7.4 – Explained variance of the PCA

The results of the first two PCs are reported in Figure 7.5. It is interesting to notice that two main groups of data points can be already distinguished at the positive and negative sides of the x axis. The measurements of the liquid concentrations of N_2O were used to color the data points according to the concentration measured, so to ease the visualization of highly emitting clusters. The left graph reports the values of the PCs colored according to the N_2O sensor 1, while the data points in the right graph were colored according to the concentration measured by the N_2O sensor 2.

The red vectors reported on the scatterplot indicate the degree of correlation (variance explained) by a certain PC with respect to each original variable. PC1 is more correlated with Q_{air} and DO while PC2 describes the behavior of the nitrogen species. A small correlation of PC1 with NH_4 and NO_x was expectable, given the effect of DO on the nitrogen transformation, as well as the small correlation between Q_{air} and PC2 in the direction of NH_4, as a result of the NH_4 based control. Finally, it is important to mention that in the direction of each vector the values of the respective variable increase, hence, the expectable opposite directions of NH_4 and NO_x. The vicinity of the vectors relative to Q_{air} and DO suggests that they bring very similar information to the results.

Both N_2O sensors' highest concentrations are mostly clustered on the positive side of PC1, indicating that Q_{air}, and ultimately DO, has a high impact on N_2O production. However, the cluster forming for both graphs in Figure 7.5 at the negative side of PC2 indicates that NO_x has also a strong importance on N_2O formation. These two groups of data are already suggesting two main types of pathways possible for N_2O production. Interestingly, the N_2O sensor 2, being physically closer to the

rest of the sensors in the tank considered for the PCA, is returning a better defined separation between high and low N_2O concentrations (Figure 7.5, right).

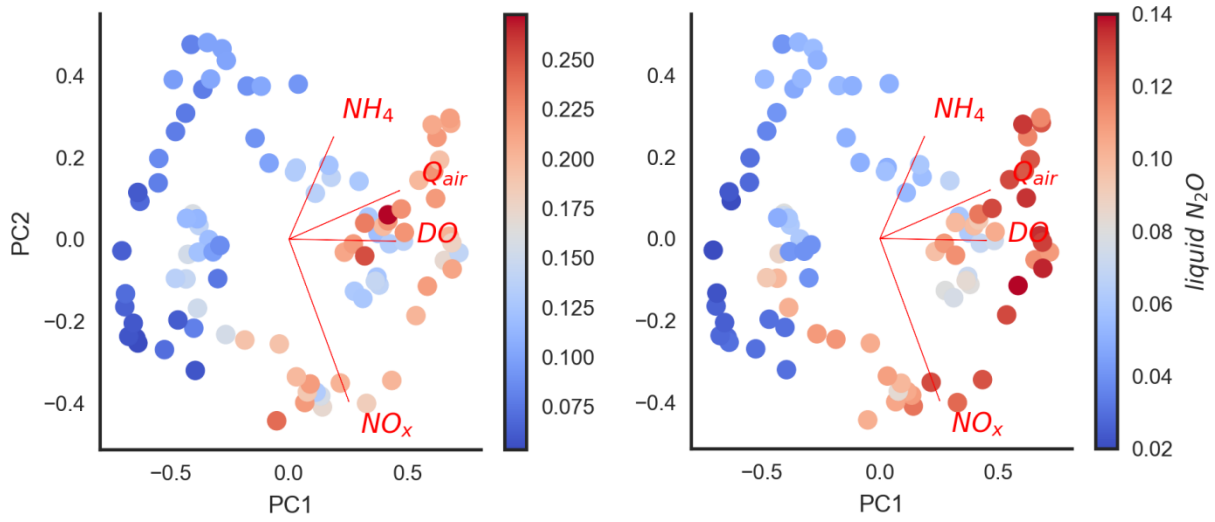

Figure 7.5 – Scatterplot of the first two PCs labeled according to the N_2O concentrations in the liquid of sensor 1 (left) located at the beginning of the aeration compartment and sensor 2 (right) located at the end of the aeration compartment.

The two groups of data points identifiable for high N_2O concentrations, can be interpreted as the interchange of the two main pathways already observed to be occurring in this plant (cfr. § 5), i.e. AOB denitrification and NH_2OH oxidation pathways. The data grouping close to the tip of the DO and Q_{air} vectors are related to the highest DO concentrations observed in the time series, and therefore most likely to be linked to the NH_2OH oxidation pathway.

The data grouping close to the tip of the NO_x axis and closer to the zero of PC1, are more likely to correspond to high NO_2 concentrations as NO_2 is also inherently linked to DO (Peng et al., 2015) since lower DO concentrations can lead to higher NO_2 concentrations due to the difference in oxygen half-saturation index between AOB and NOB (Hanaki et al., 1990; Mota et al., 2005) (cfr. § 2.2.1). This suggests a possible AOB preference of NO_2 as the electron acceptor over DO (Bock et al., 1995; Kampschreur et al., 2009) and the production of N_2O due to AOB denitrification. In addition to this, since red dots of N_2O sensor 2 reach to the negative side of PC2, this can correspond to more limiting DO concentrations associated with the AOB denitrification pathway.

7.3.3. Clustering

In view of applying the PCA results on a full-scale control, a clustering technique is necessary for automating the recognition of the different N_2O production pathways. The three clustering methods introduced were applied to the PCA results with the aim of recognizing the different clusters in terms of N_2O formation and possibly extract more information.

The different clusters are colored differently to distinguish the different groups. Colors are not specific of a single cluster.

***K*-means**

The main input of the *K*-means clustering method is the number of clusters. The minimum number of interesting groups for the purpose of this study is 3 if we focus on the recognition of the two main N_2O production pathways (i.e. AOB denitrification and NH_2OH oxidation) and the zone of low N_2O production. A number of 4 clusters was also used to further test the algorithm.

Initializing *K*-means with 3 clusters (Figure 7.6, left), it is interesting to see how the resulting clusters at equilibrium are already nicely divided among the groups previously indicated, corroborating with the initial interpretation of the raw PCA results. However, the points closer to the NH_4 vector should not belong to the cluster of high emissions for NH_2OH oxidation. The cluster relative to AOB denitrification is instead rather well defined, including also one of the points in the negative side of PC1 known to have elevated N_2O concentration.

When 4 clusters were used for initialization (Figure 7.6, right), the resulting cluster responsible for N_2O formation due to NH_2OH oxidation was defined better than in the previous case, although some of the points close to the NH_4 vector are still included. The cluster attributable to AOB denitrification remains the same, while the low emission cluster, closer to the PC2 axis is divided in two as expected from the need of dividing the space in 4.

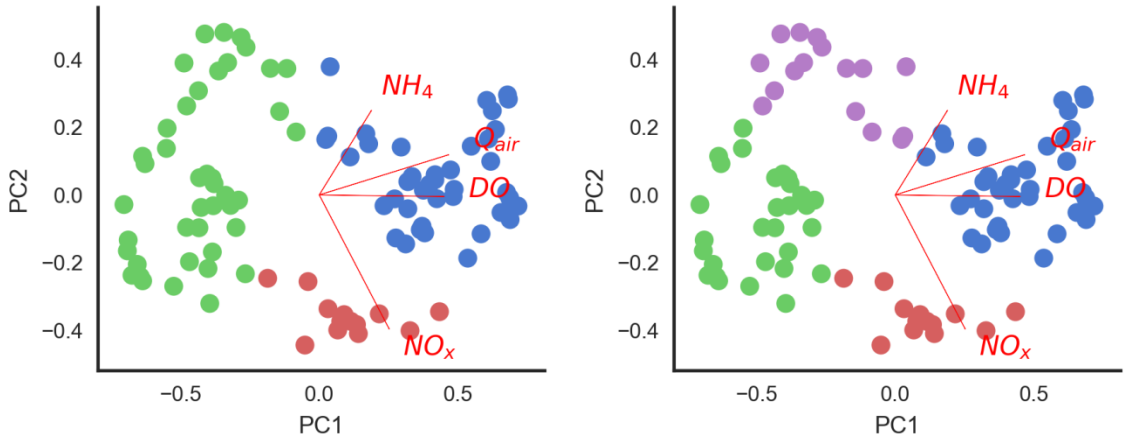

Figure 7.6 – *K*-Means with 3 clusters (left) and 4 clusters (right). Colors are randomly assigned only to distinguish clusters.

Agglomerative

Using the Ward's method, four clusters were needed for initialization in order for the algorithm to distinguish the two groups of data known to describe the two main N_2O production pathways, i.e. AOB denitrification and NH_2OH oxidation (Figure 7.7, right). Without the initialization of the algorithm to target four final clusters, it was not possible to achieve this distinction. This resulted also in the division in two clusters of the group of data linked to small N_2O concentrations in the same fashion as for the *K*-means method.

Initializing the agglomerative clustering to target 3 clusters with the maximum linkage method for the iterated merging of initial clusters, the algorithm isolated all three main groups of data, i.e. the AOB denitrification, the NH_2OH oxidation and the area of low N_2O production (Figure 7.7, right).

The Ward's algorithm performed better in terms of time, taking only 1/3 of the time needed for the maximum linkage method. The difference in time is probably due to the fact that the Ward's method was able stop one iteration earlier (ending with 4 clusters instead of 3). However, although each algorithm performs in the order of few milliseconds, in terms of efficiency for future implementation this can be a useful selection criterion to choose between the algorithms.

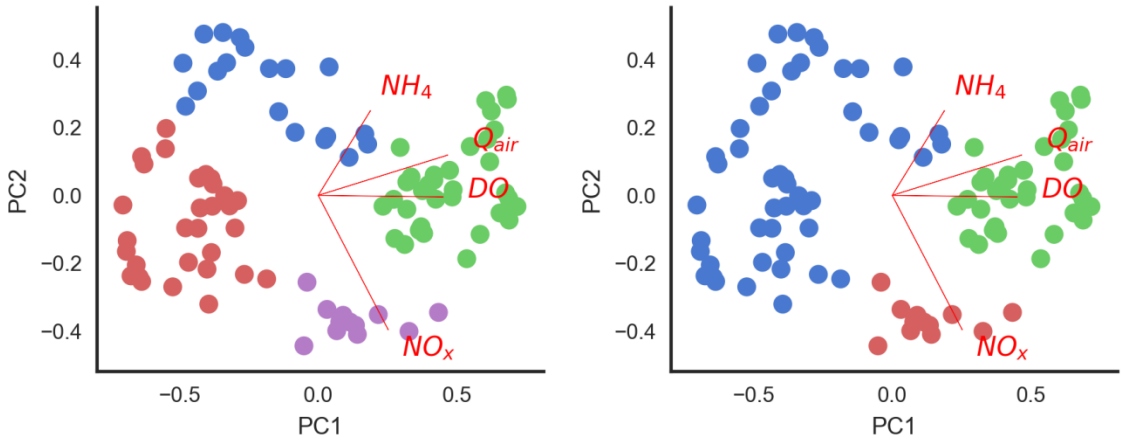

Figure 7.7 – Agglomerative clustering with Ward's (left) and maximum linkage (right) methods. Colors are randomly assigned only to distinguish clusters.

Interestingly, for both merging algorithms, the data points close to the NH_4 vector are correctly grouped with the cluster of data relative to low N_2O concentration, corroborating with the results discussed in the PCA section. However, few data points corresponding to the negative part of PCs and characterized with a rather high N_2O concentration by the N_2O sensors, were included in the low N_2O concentration cluster by both algorithms. Finally, the two clusters relative to high N_2O concentrations coincide for the two methods.

HDBSCAN

This clustering method, diversely from the former ones, requires as input the minimum number of points to be considered as a cluster. With this feature, the HDBSCAN output can also consider the existence of data points not belonging to any of the clusters (reported in black).

With a minimum cluster size of 4 data points (Figure 7.8, left) the HDBSCAN distinguishes between the two clusters of known high N_2O concentration. Interestingly, between these two clusters there are two black data points not belonging to either of the clusters. This is an interesting result since it allows for the existence of points of transition between one cluster and another. However, the data points close to the NH_4 vector, known to belong to low N_2O concentrations or at least expected to be classified in a transition zone, are instead grouped with the high N_2O concentration due to the NH_2OH oxidation pathway.

In the negative part of both PC1 and PC2, the high N_2O concentration cluster linked to AOB denitrification, and the rest of the clusters close to the PC2 axis, are divided by three black data points that the previous clustering methods grouped uncertainly. In fact, these three data points seem to lay in a transition zone that only the HDBSCAN is able to detect.

The low N_2O concentration zone, in the negative side of PC1, is divided into four clusters (Figure 7.8, left). Although this subdivision is allowed by the minimum cluster size, no physical meaning could be found for these different clusters. This granularity of clusters in this part of the graph disappears when increasing the minimum cluster size to 9 (Figure 7.8, right).

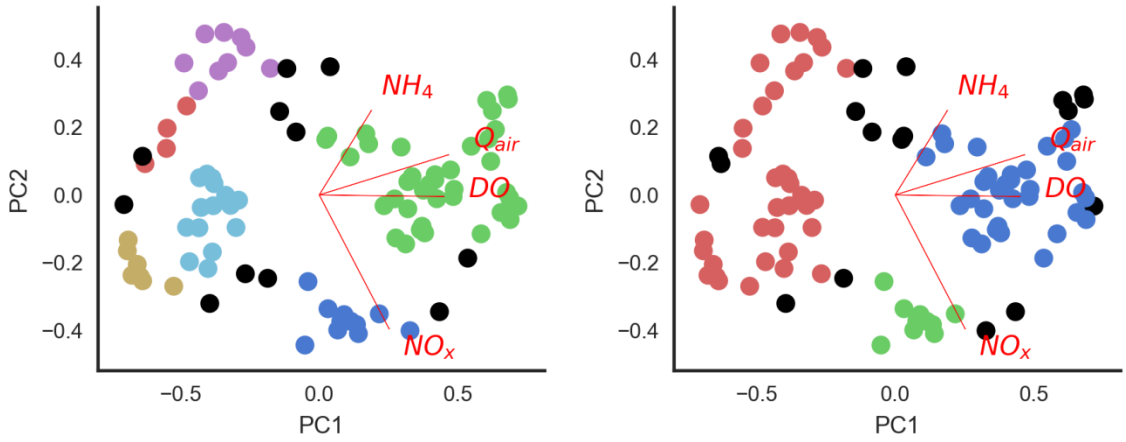

Figure 7.8 – HDBSCAN with minimum clusters size 4 (left) and minimum clusters size 9 (right). Colors are randomly assigned only to distinguish clusters. In black the data points not attributed to any cluster.

Increasing the minimum cluster size to 9 (Figure 7.8, right), sensibly decreases the number of clusters on the left part of the plot (corresponding to the lowest concentrations of N_2O) while maintaining the two clusters relative to high N_2O concentration (center and right of PC1). Interestingly, the points close to the NH_4 vector are still classified within the cluster of high N_2O concentration for NH_2OH oxidation, but more data points were addressed (in black) to the transitional points. Therefore, this initialization performed slightly better than the minimum cluster size of 4.

Overall evaluation

All clustering methods were able to recognize differences among those clusters generated by the two PCs resulting from the application of the PCA. The *K*-means method could sufficiently isolate the correct main clusters, however, some imprecisions in the classification of data points close to the edge of two neighboring clusters were observed. In this view, the agglomerative method was able to identify with more precision those data points that were erroneously addressed by *K*-means to the clusters of higher emission. On the other hand, the HDBSCAN method does not coerce the attribution of boundary data points to a cluster and allows to consider the existence of transitional zones. This is an important point in monitoring full-scale WRRFs as conditions in AS tanks are highly dynamic and transitions from one state to another are continuously happening.

For an online application, based on their good performances, at the moment both the agglomerative method and the HDBSCAN are equally applicable. For discriminating between one method or the other would need more testing.

For a practical online application, the clustering method chosen, could be initially integrated in a supervisory system to alert operators on the possibility of an important N_2O production. Based on the PCA model built with the training dataset, the online data stream can be projected on the PCs space, thus, potentially revealing in which of the clusters related to N_2O production the system is. Based on the cluster, specific instructions can be proposed. For instance, in the case that the system would be directing to the cluster responsible for N_2O production due to NH_2OH oxidation, the operator could evaluate the option of reducing the DO, thus limiting this reaction. On the other hand, if the system would reveal to be shifting towards the cluster responsible for N_2O production due to AOB denitrification, the operator could be prompted to evaluate the possibility of increasing the DO concentration. Simple instructions or suggestions deriving from a thorough analysis of WRRF data.

7.4. Conclusions

PCA was applied to a dataset of the WRRF of Eindhoven for detecting a possible relation between variables known to be highly related to N_2O production. A PCA model was defined after a small pre-processing step defining the most typical behavior observed in one entire month for all variables. The PCA model could separate the two main N_2O production pathways by using two PCs. The results show that the two PCs could isolate the main known relations between N_2O production and plant operation. Both the AOB denitrification and NH_2OH oxidation N_2O production pathways were nicely identifiable.

In view of applying these results to full-scale, three clustering methods were tested for automating the identification of the different regions of the PCA scatterplot. The *K*-means method could sufficiently separate between the two main N_2O production pathways, although some of the edges of the clusters included data points that could be questionable. Both the HDBSCAN and the agglomerative methods successfully differentiated between the two N_2O production pathways excluding irrelevant points that were difficult to detect.

Results confirm the potential for defining a new monitoring system for N_2O emissions based on historical plant data. Operators could be provided with important information deriving from a thorough analysis of the AS tank, this in view of a full integration in a SCADA system. Future implementations should consider the introduction of MPCA to increase the informative content of the original dataset and limit the loss of information in the pre-processing step.

7.5. References

Bock, E., Schmidt, I., Stuven, R., Zart, D., 1995. Nitrogen loss caused by denitrifying Nitrosomonas cells using ammonium or hydrogen as electron donors and nitrite as electron acceptor. Arch. Microbiol. 163, 16–20.

Campello, R.J.G.B., Moulavi, D., Sander, J., 2013. Density-Based Clustering Based on Hierarchical Density Estimates. pp. 160–172.

Daelman, M.R.J., De Baets, B., van Loosdrecht, M.C.M., Volcke, E.I.P., 2013. Influence of sampling strategies on the estimated nitrous oxide emission from wastewater treatment plants. Water

Res. 47, 3120–3130.

Daelman, M.R.J., van Voorthuizen, E.M., van Dongen, U.G.J.M., Volcke, E.I.P., van Loosdrecht, M.C.M., 2015. Seasonal and diurnal variability of N2O emissions from a full-scale municipal wastewater treatment plant. Sci. Total Environ. 536, 1–11.

Dürrenmatt, D.J., Gujer, W., 2011. Identification of industrial wastewater by clustering wastewater treatment plant influent ultraviolet visible spectra. Water Sci. Technol. 63, 1153.

Gernaey, K. V., Van Loosdrecht, M.C.M., Henze, M., Lind, M., Jørgensen, S.B., 2004. Activated sludge wastewater treatment plant modelling and simulation: State of the art. Environ. Model. Softw. 19, 763–783.

Han, J., Kamber, M., 2001. Data Mining: concepts and techniques. Los Atos, CA.

Hanaki, K., Chalermraj, W., Shinichiro, O., 1990. Nitrification at low levels of dissolved oxygen with and without organic loading in a suspended-growth reactor. Water Res. 24, 297–302.

IPCC, 2013. Climate Change 2013: The Physical Science Basis. Contribution of Working Group I to the Fifth Assessment Report of the Intergovernmental Panel on Climate Change. Cambridge.

Johnson, R.A., Wichern, D.W., 1992. Applied Multivariate Statistical Analysis, New York.

Kampschreur, M.J., Temmink, H., Kleerebezem, R., Jetten, M.S.M., van Loosdrecht, M.C.M., 2009. Nitrous oxide emission during wastewater treatment. Water Res. 43, 4093–4103.

Kampschreur, M.J., van der Star, W.R.L., Wielders, H. a., Mulder, J.W., Jetten, M.S.M., van Loosdrecht, M.C.M., 2008. Dynamics of nitric oxide and nitrous oxide emission during full-scale reject water treatment. Water Res. 42, 812–826.

Law, Y., Ni, B.J., Lant, P., Yuan, Z., 2012. N2O production rate of an enriched ammonia-oxidising bacteria culture exponentially correlates to its ammonia oxidation rate. Water Res. 46, 3409–3419.

López García, H., Machón González, I., 2004. Self-organizing map and clustering for wastewater treatment monitoring. Eng. Appl. Artif. Intell. 17, 215–225.

Mampaey, K.E., Beuckels, B., Kampschreur, M.J., Kleerebezem, R., van Loosdrecht, M.C.M., Volcke, E.I.P., 2013. Modelling nitrous and nitric oxide emissions by autotrophic ammonium oxidizing bacteria. Environ. Technol. 34, 1555–66.

McInnes, L., Healy, J., Astels, S., 2017. HDBSCAN: Hierarchical density based clustering. J. Open Source Softw. 2, 205.

Melvin, R.L., Godwin, R.C., Xiao, J., Thompson, W.G., Berenhaut, K.S., Salsbury, F.R., 2016. Uncovering Large-Scale Conformational Change in Molecular Dynamics without Prior Knowledge. J. Chem. Theory Comput. 12, 6130–6146.

Monteith, H.D., Sahely, H.R., MacLean, H.L., Bagley, D.M., 2005. A rational procedure for estimation of greenhouse-gas emissions from municipal wastewater treatment plants. Water Environ. Res. a Res. Publ. Water Environ. Fed. 77, 390–403.

Mota, C., Head, M., Ridenoure, J., Cheng, J., de los Reyes, F., 2005. Effects of Aeration Cycles on

Nitrifying Bacterial Populations and Nitrogen Removal in Intermittently Aerated Reactors. Appl. Environ. Microbiol. 71, 8565–8572.

Murtagh, F., Legendre, P., 2014. Ward's Hierarchical Agglomerative Clustering Method: Which Algorithms Implement Ward's Criterion? J. Classif. 31, 274–295.

Ni, B.J., Peng, L., Law, Y., Guo, J., Yuan, Z., 2014. Modeling of Nitrous Oxide Production by Autotrophic Ammonia-Oxidizing Bacteria with Multiple Production Pathways. Env. Sci Technol 48, 3916–3924.

Olsson, G., Carlsson, B., Comas, J., Copp, J., Gernaey, K. V., Ingildsen, P., Jeppsson, U., Kim, C., Rieger, L., Rodríguez-Roda, I., Steyer, J.-P., Takács, I., Vanrolleghem, P.A., Vargas, A., Yuan, Z., Åmand, L., 2014. Instrumentation, control and automation in wastewater – from London 1973 to Narbonne 2013. Water Sci. Technol. 69, 1373.

Pedregosa, F., Varoquaux, G., Gramfort, A., Michel, V., Thirion, B., Grisel, O., Blondel, M., Prettenhofer, P., Weiss, R., Dubourg, V., Vanderplas, J., Passos, A., Cournapeau, D., Brucher, M., Perrot, M., Duchesnay, E., 2011. Scikit-learn: Machine Learning in Python. J. Mach. Learn. Res. 12, 2825–2830.

Ravishankara, A.R., Daniel, J.S., Portmann, R.W., 2009. Nitrous Oxide (N2O): The Dominant Ozone-Depleting Substance Emitted in the 21st Century. Science (80-.). 326, 123–125.

Schreiber, F., Wunderlin, P., Udert, K.M., Wells, G.F., 2012. Nitric oxide and nitrous oxide turnover in natural and engineered microbial communities: biological pathways, chemical reactions, and novel technologies. Front. Microbiol. 3.

Tan, P.., Steinbach, M., Kumar, V., 2005. Introduction to data mining. Addison-Wesley.

Villez, K., Ruiz, M., Sin, G., Colomer, J., Rosén, C., Vanrolleghem, P.A., 2008. Combining multiway Principal Component Analysis (MPCA) and clustering for efficient data mining of historical data sets of SBR processes. Water Sci. Technol. 57, 1659–1666.

Villez, K., Vanrolleghem, P.A., Corominas, L., 2016. Optimal flow sensor placement on wastewater treatment plants. Water Res. 101, 75–83.

Weiss, R.F., Price, B.A., 1980. Nitrous oxide solubility in water and seawater. Mar. Chem. 8, 347–359.

Chapter 8

8. General conclusive remarks and future work

The importance of preserving natural resources is (one of) the main challenge(s) of this century as global warming and (related) economic/population growth are threatening our renewable, but limited, most important resources, i.e. water and air. Preserving the environment is ensuring the safety of our water reserves and thus of our health. Surface and groundwater stocks as well as atmosphere quality need to be guarded and protected from an uncontrolled and indiscriminate economic growth.

Research efforts and resources are nowadays largely focused on understanding complex human-environment interactions for providing the most suitable approaches/methods/tools in view of limiting the effects of anthropogenic pollution. Environmental awareness has in fact changed the human perception of economic growth, driving the new targets of current community evolution to ensure the continuation of all human activities but abating their environmental costs at the same time. More and more human activities are developed and ameliorated for an improved integration in the surrounding environment aiming at very limited or no impact.

WRRFs are the last point in which we can significantly tackle our environmental impact, the last step with which the environment can be preserved from anthropogenic pollution. With improved WRRFs our society can gain sustainability and be integrated in the surrounding nature by preserving both water and air.

The research presented in this manuscript, focused on two timely issues that are currently important for improved WRRFs, i.e. aeration efficiency and N_2O emission. These aspects of water treatment have severe effects on both liquid effluent and air qualities. Limiting N_2O emission and maximizing aeration efficiency means significantly reducing WRRFs CFP while coping with high standards of effluent quality limits and improve WRRFs' sustainability.

In order to develop proper strategies for optimizing aeration devices use and reducing N_2O emission, current monitoring methods showed major lacks and the need to be updated and improved. As a matter of fact, as it is very challenging to control something that is not fully understood ([…] *like the sailor who boards ship without a rudder and compass* […], if I may paraphrase da Vinci), improved methods are needed to comprehend the most effective strategies.

In processes such as AS tanks, in which the complexity of several concurrent biological activities is joined nonetheless by the intricate hydrodynamic behavior of large liquid volumes, suitable monitoring strategies are particularly important for understanding spatial and temporal heterogeneities and develop insights for targeting appropriate solutions. At the same time, for developing appropriate solutions, improved modelling tools are essential.

In this work, the complexity of aeration efficiency and of the several N_2O production processes responsible for its emission in the intricacy of biological tanks were investigated. The current work focused on improving practical field-monitoring methods, and, regarding N_2O emissions, on the application of knowledge-base, stochastic and kinetic modelling tools. Nonetheless, the need of improved modelling methods for hydrodynamic patterns and gas-liquid oxygen transfer in AS sludge tanks is a clear evidence of this work from which N_2O mechanistic modelling can significantly benefit.

Sound measurements can provide fertile ground for solid modelling and further improved understanding. At the same time, as modelling is improved, more clues on relevant monitoring strategies for limiting human efforts and maximizing the informative input can be produced. A synergistic approach between modelling and monitoring represents the most valuable and effective strategy for improved understanding and effective control.

8.1. Conclusions

8.1.1. Field measurements

Instrumentation

The first part of this work focused on improving the applicability, replicability and reliability of off-gas measurements. The design, assembling and testing phases of an improved off-gas analyzer were reported in consideration of the most important requirements for off-gas testing and providing crucial features to be considered when assessing aeration efficiency in WRRFs. Suitability and reliability of the new instrument were assessed through deep testing carried out at both lab and field scale.

The off-gas analyzer was provided with the possibility to extend off-gas measurement to N_2O emission monitoring, examining the most suitable tools for N_2O measurements in full-scale application in both gas and liquid phases. Nonetheless, a first implementation of an additional floating hood was proposed for assessing N_2O emissions from non-aerated surfaces.

Off-gas analysis and N_2O emission monitoring methodologies

Possible improvements to current methods used in off-gas testing and N_2O emission assessment were provided. As for aeration efficiency measurements, indications on the surface coverage of the aerated tank of a point-by-point test were provided with a confidence deviation from the generally accepted 2 % rule. A user is provided with an evaluation case of the significance of missing rather than additional points. To the user remains the final decision of the most suitable set of measurements depending on a trade-off between accuracy and time limitation/costs.

The effect of plant dynamics on the variability of αSOTE in time and its effect on the assessment of local efficiencies was discussed. The time needed for performing a set of off-gas measurements has an effect on the local efficiency and a method to consider this variability for a more solid comparison of the αSOTE among the different locations was provided as a first step towards a more conscious and reproducible assessment of point-by-point off-gas tests.

A multi-point method for N_2O emission assessment was proposed for understanding the dynamics of emissions and responsible patterns. This is important especially considering that heterogeneity of N_2O emissions is a known issue in the determination of a representative EF. Given the heterogeneity of AS tanks conditions and the need for validation of current CFD models, a synergistic approach between field measurements and advanced modelling can be very useful in defining suitable monitoring strategies in both temporal and spatial domain.

A user friendly method for assessing the contribution of non-aerated zones to N_2O emission, was provided. Considerations and proposals on the modalities of EF assessment, calculation and analysis, were given as a proposal for a proper WRRF classification. The proposed approach allows to provide a better understanding of the responsible pathways for N_2O production and address the most suitable reduction strategies. Reduction strategies need to be plant specific.

8.1.2. Modelling emissions from WRRFs

Different types of modelling strategies were proven to be suitable to the purpose of understanding and developing reduction strategies for WRRFs. In this work, the availability of different solutions to modelling N_2O was highlighted, showing advantages and limitation of different approaches. The differentiation of modelling tools is an important aspect of process analysis given the diversity of WRRF technologies.

The large literature knowledge available on N_2O production dynamics was proven to be applicable to full-scale plants by means of a knowledge-based model. The N_2O risk model effectively helped in unraveling the dynamics behind N_2O production and to identify responsible pathways. The risk model was shown to effectively indicate the most probable N_2O production pathway based on few measurements that are normally available on most WRRFs and difficult to interpret from a naked eye. This facilitates the selection of the most appropriate mechanistic model for a given facility and helps in defining N_2O reduction strategies.

The level of detail of available mechanistic models has reached a very valuable level. The application of this level of kinetic detail to over-simplified spatial representation risks to dissipate the informative potential of mechanistic models. The significant discrepancy between biological and physical representation of AS tanks is currently the most limiting factor in N_2O emission modelling.

Finally, given the large availability of extensive quantities of information from the most advanced WRRFs, data mining was proven to be a suitable tool for understating N_2O emissions. A large amount of information can be condensed in fewer, most informative, variables which can help to unravel responsible pathways and possible reduction strategies.

8.2. Perspectives

As instrumentation continuously experiences improvements, currently available monitoring devices can be periodically updated aiming at reducing capital investments, maintenance, space requirements and maximizing automation. In this view, the recent start of the LESSWATT EU-founded project (LIFE16 ENV/IT/000486), of which the University of Florence is leading and Ghent University supports with an important partnership, gives the possibility of continuing the improvement of the current off-gas analyzer. In particular, major advancements are regarding the fully-automated aspect of the device with an integrated referenced GPS system, reduced dimensions of the equipment, full integration of all measuring devices on board, and the availability of recent small solutions for integrating on-board the IR technology for N_2O measurements in the off-gas.

In the short term, focus should be put on improving the methods provided for both aeration efficiency and N_2O emission assessment. In particular, as for aeration efficiency, an embedded system for defining the accuracy gain in the addition of a new point measurement should be included in a new version of the software of the analyzer. Also, improved referencing strategies are needed for addressing differences among point-by-point measurements. Regarding N_2O emissions,

additional multi-point measurements are needed in order to define a suitable number of surveyed locations especially for anoxic zones. In this view, the development of advanced models can be a very valuable aid.

Further research in the development of field monitoring strategies for aeration efficiency will consider the evaluation of the impact of off-gas sampling locations in case of uneven distribution of aerators. In this view, the optimization of off-gas testing methods should involve the use of calibrated CFD models to understand the most suitable distribution of point-by-point measurements over a tank's surface. Also, seen the diversity of DO levels in depth, the methodology for aeration efficiency assessment should consider to exploit the impact of the DO sensor depth in the calculation of αSOTE. Also this investigation could be boosted by hydrodynamic insights as completely mixed conditions are nowadays to be considered non existing. On the other hand, as CFD models often need robust validations, they could benefit of information coming from off-gas testing to consolidate results.

In addition to this, the αSOTE equation currently in use should be further discussed as the β factor is known to be variable and the applicability of this equation to very low DO can be problematic. Furthermost, as in conditions of standard temperature, pressure, and zero DO, OTE should equal αSOTE, the choice of an appropriate formula for calculating DO at saturation can significantly impact reproducibility.

There are evidences that mechanistic modelling requires more detailed descriptions of hydrodynamics. In addition to this, also the oxygen transfer process needs a more refined description. These are currently the most limiting features of current physic-chemical modelling of WRRFs. Future work should focus on developing better representation of the physical aspects which are most influencing the correct biological and chemical representation. In this view, near-future work should focus on using aeration efficiency measurements as model input in order to increase the predictive power of mechanistic models, in view of the availability of more refined aeration models.

The informative potential of WRRFs' data flow should be further exploited since promising results were shown also in case of very complex phenomena such as N_2O production and emission. Given that the promising results of the data mining application shown in this work were dug out of locally measured variables, the possibility of integrating data mining of full-scale measurements with a better representation of local conditions might be a new target for future projects.

Annex .I

This annex reports complementary information concerning the modelling part of §6 on the comparison of the TIS and CM spatial model layouts.

Step I

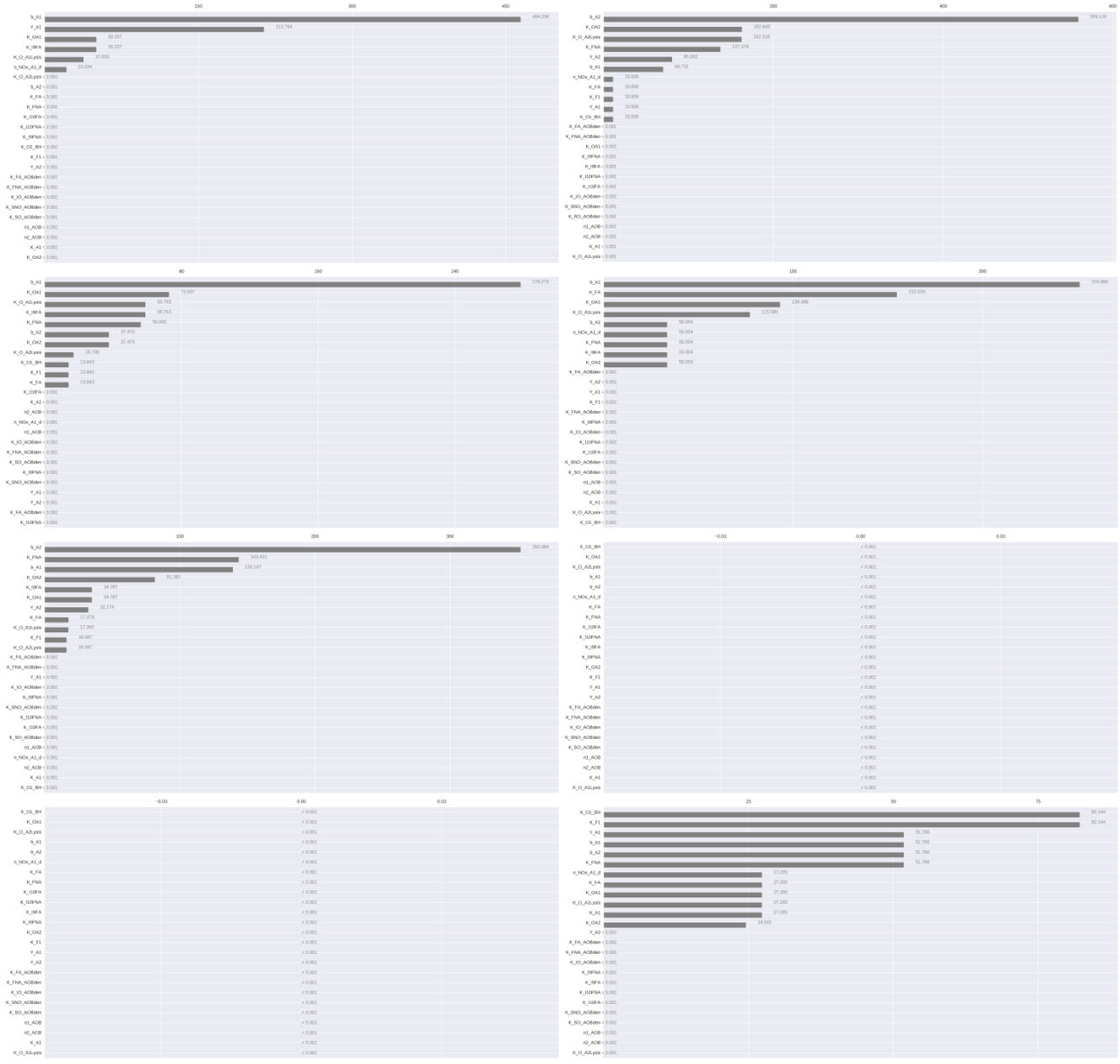

Annex I. 1 – GSA for the TIS layout with perturbation factor of 10^{-6}.

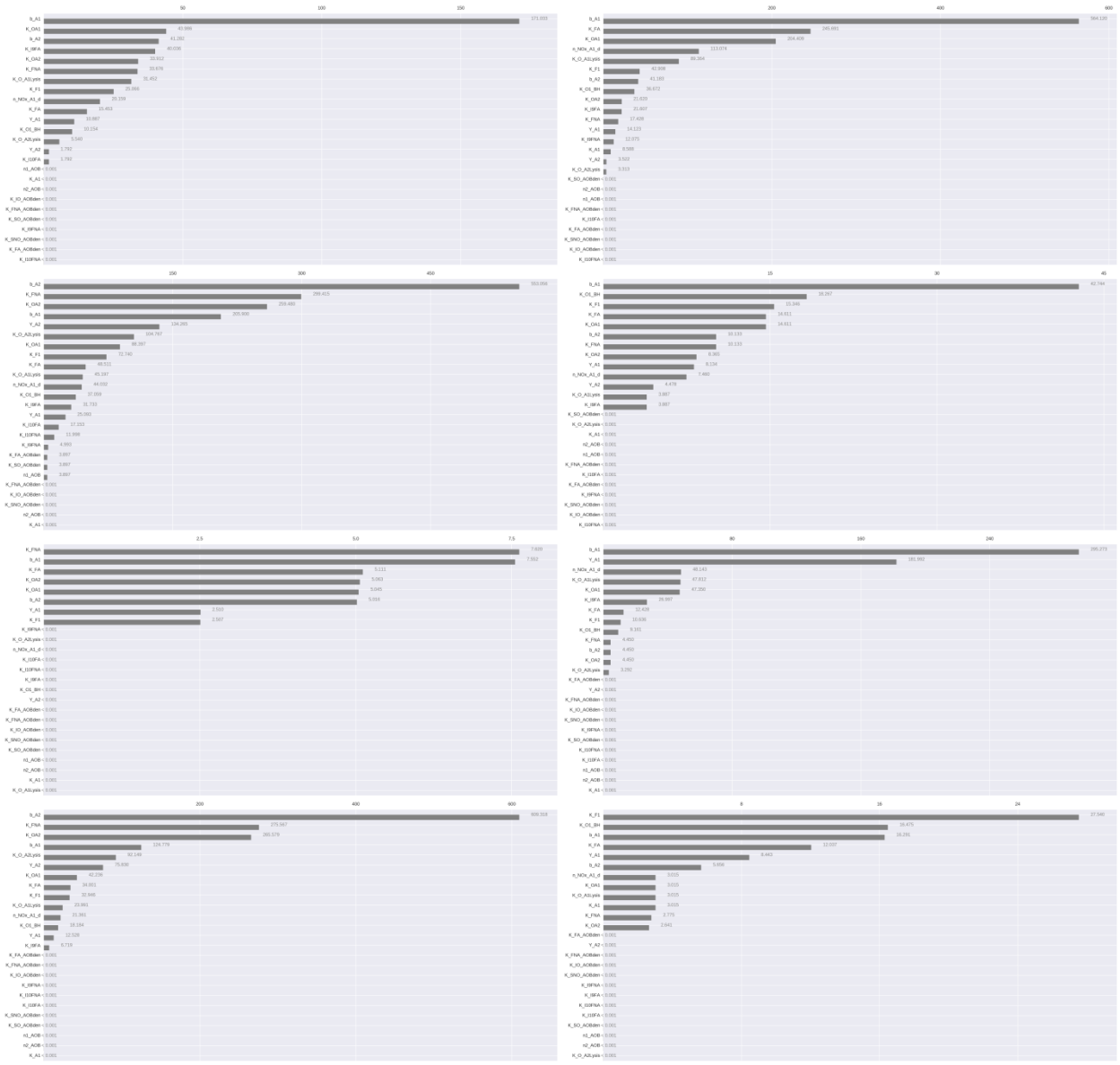

Annex I. 2 - GSA for the CM layout with perturbation factor of 10^{-6}.

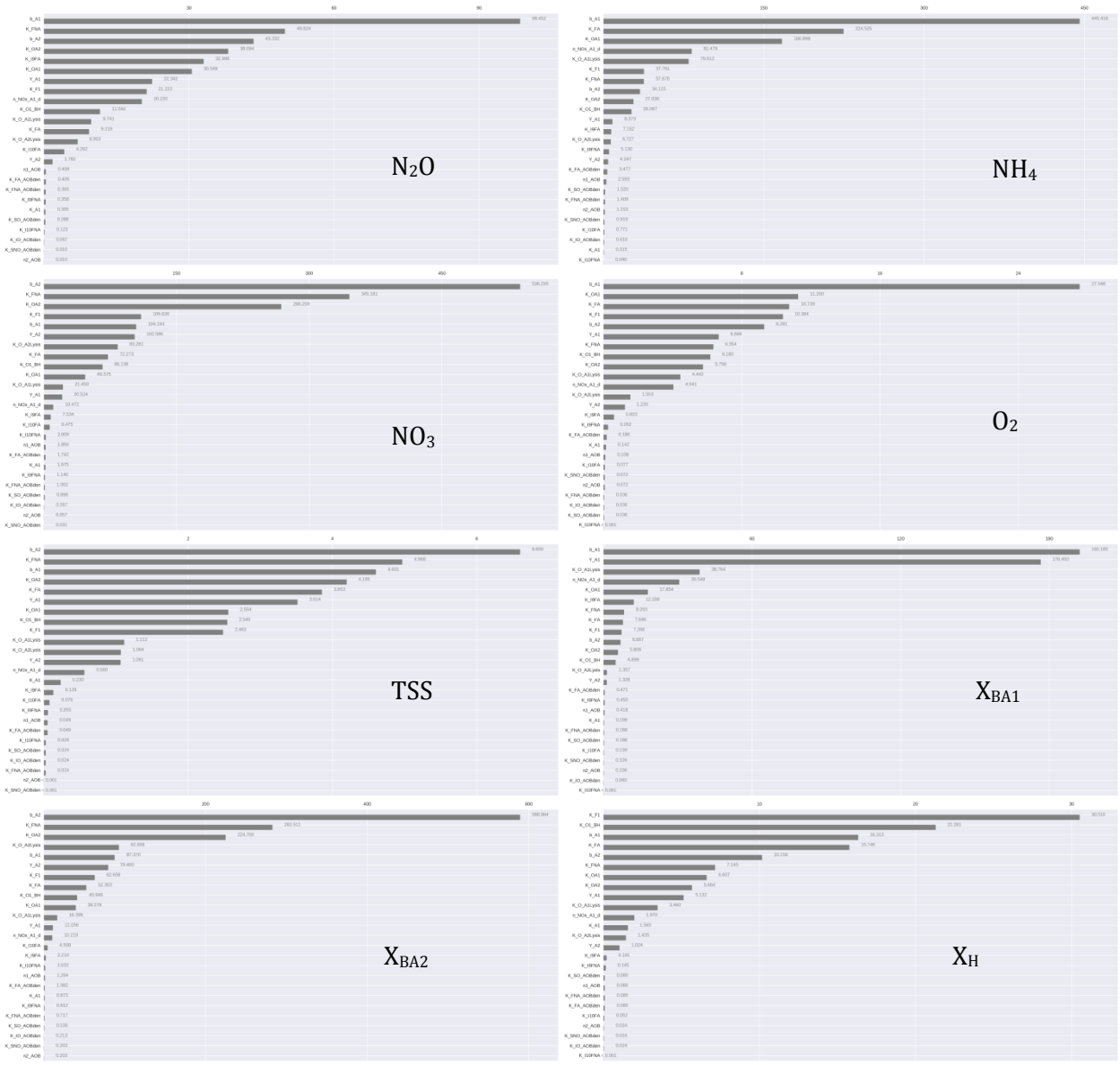

Annex I. 3 – GSA for the TIS layout with perturbation factor of 10^{-3}.

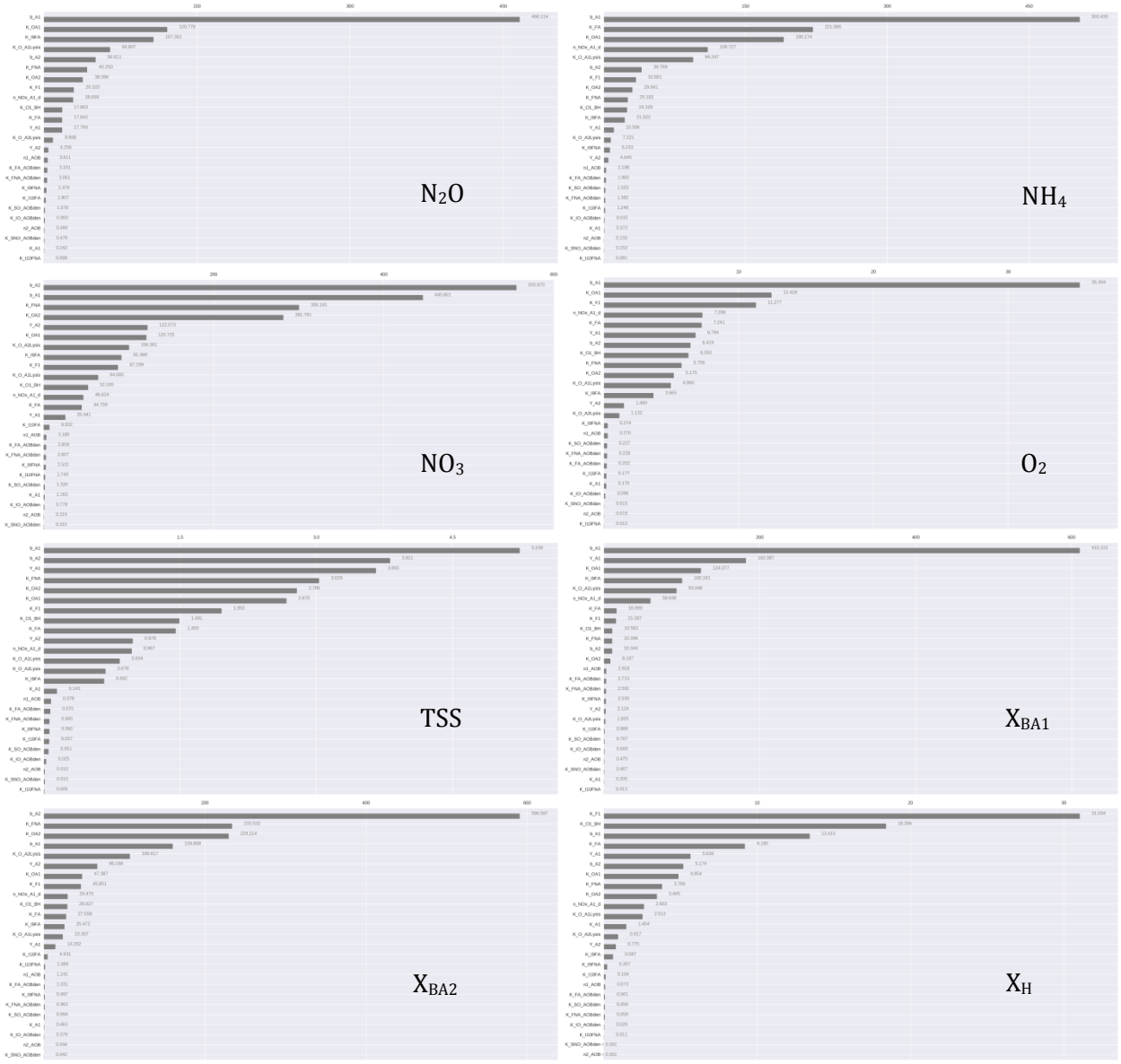

Annex I. 4 - GSA for the CM layout with perturbation factor of 10^{-3}.

Step II

Annex I. 5 – Check of the correctness of the uniform LH sampling method over the different parameters ranges

TIS

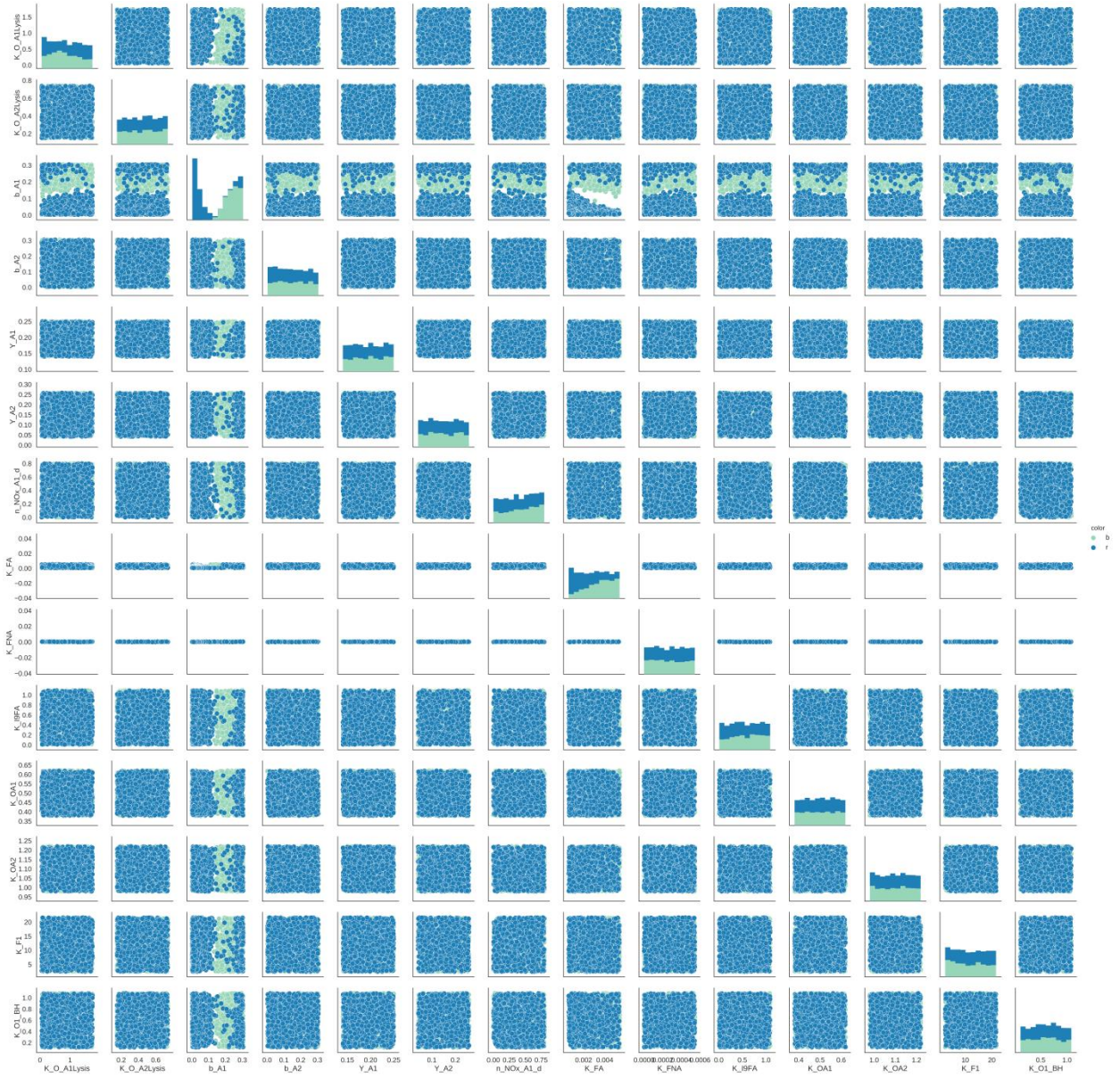

Annex I. 6 – Scatterplot of the parameters reporting both the best (light) and the worst performing scenarios (dark) for the case of NH_4 with the TIS layout

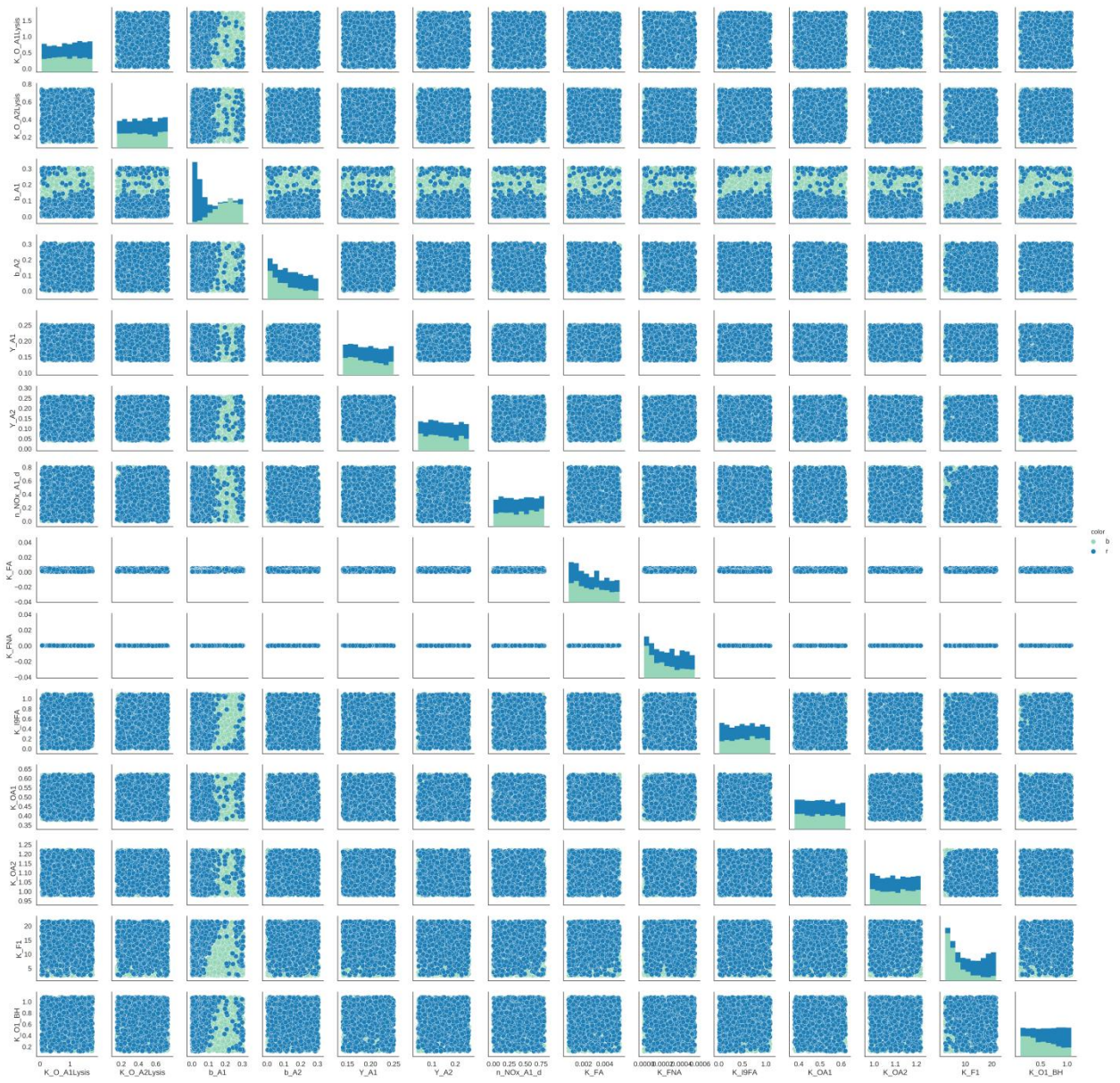

Annex I. 7 – Scatterplot of the parameters reporting both the best (light) and the worst performing scenarios (dark) for the case of DO with the TIS layout.

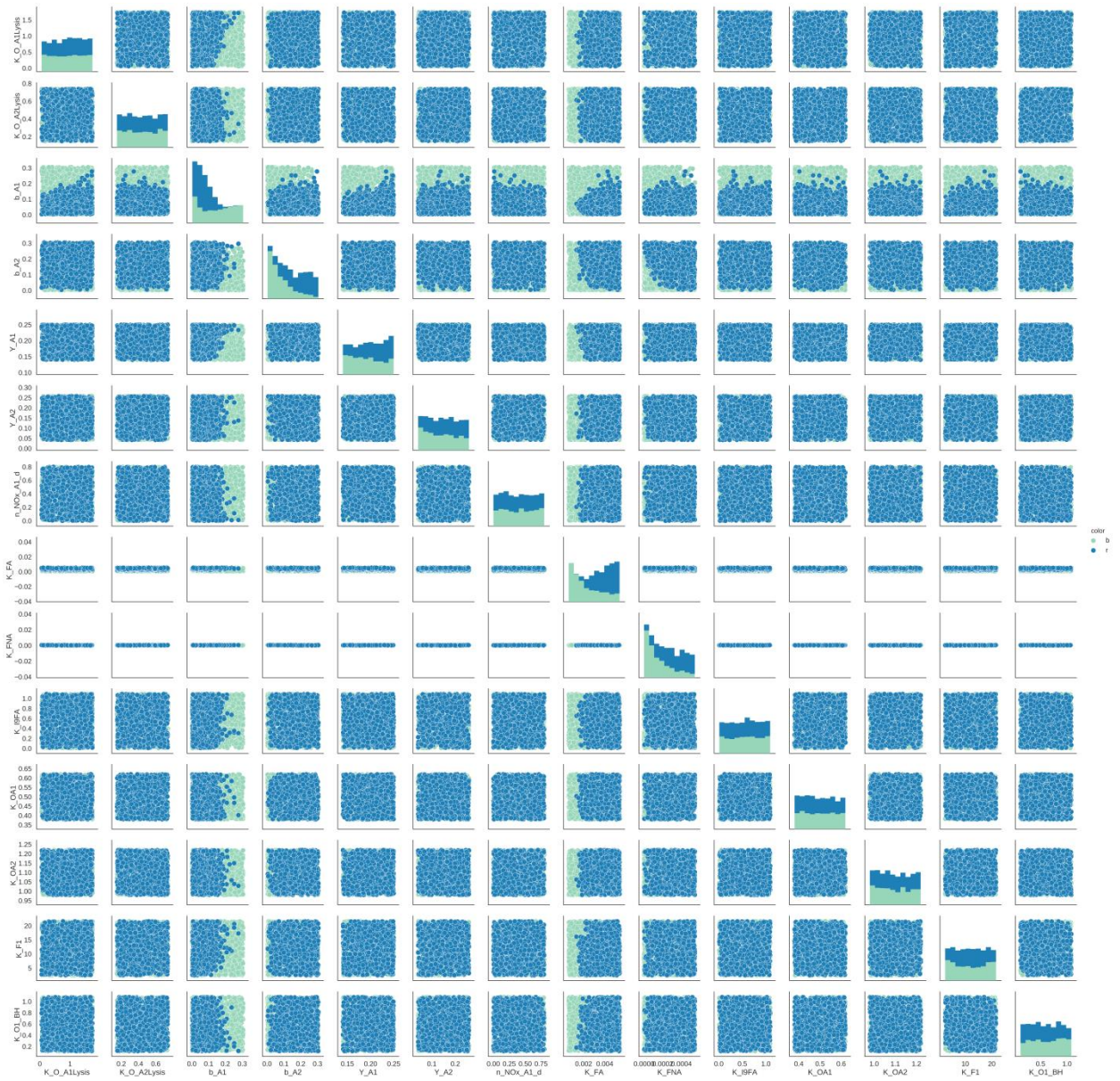

Annex I. 8 – Scatterplot of the parameters reporting both the best (light) and the worst performing scenarios (dark) for the case of TSS with the TIS layout.

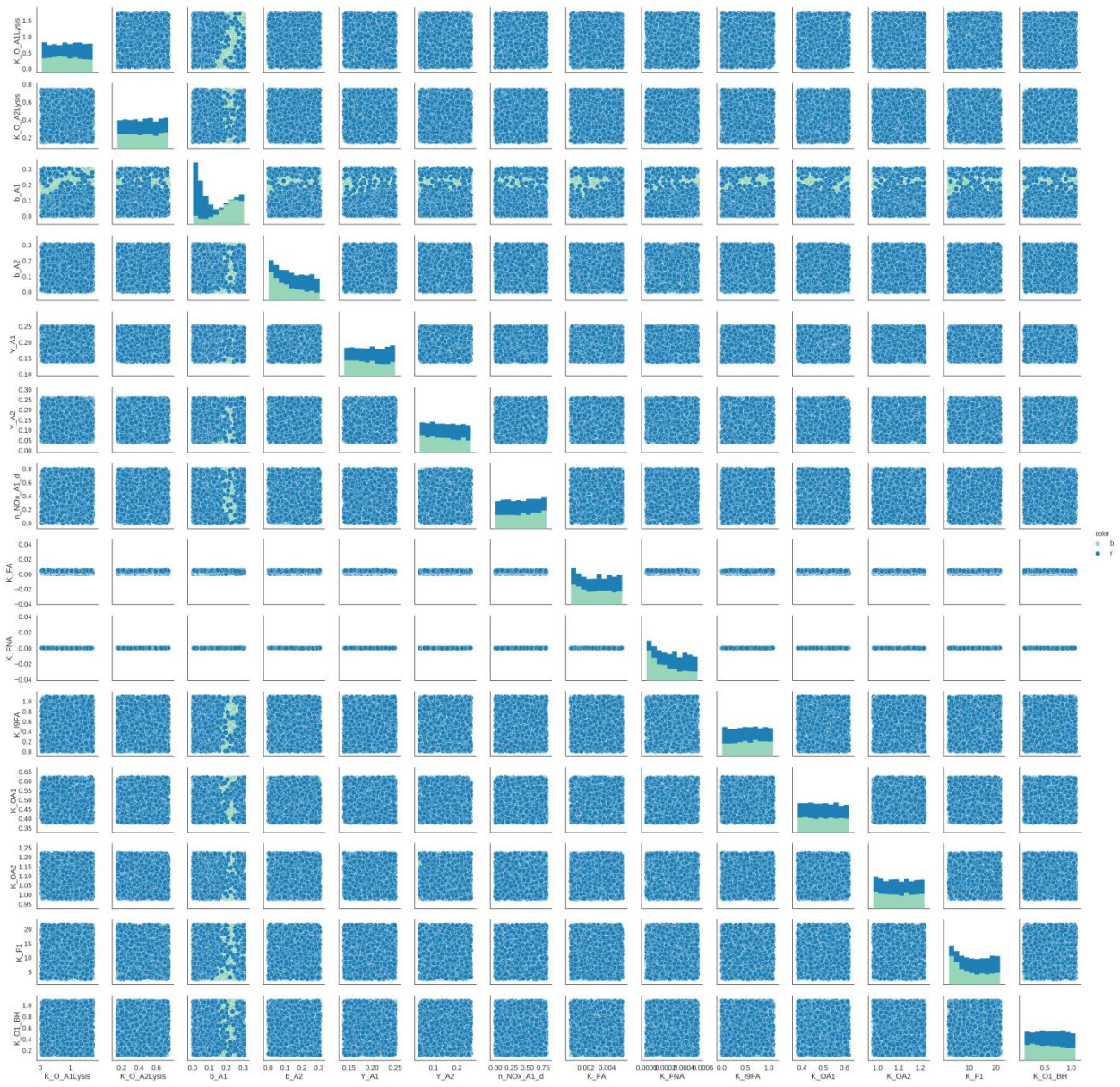

Annex I. 9 - Scatterplot of the parameters reporting both the best (light) and the worst performing scenarios (dark) for the overall case with the TIS layout.

CM

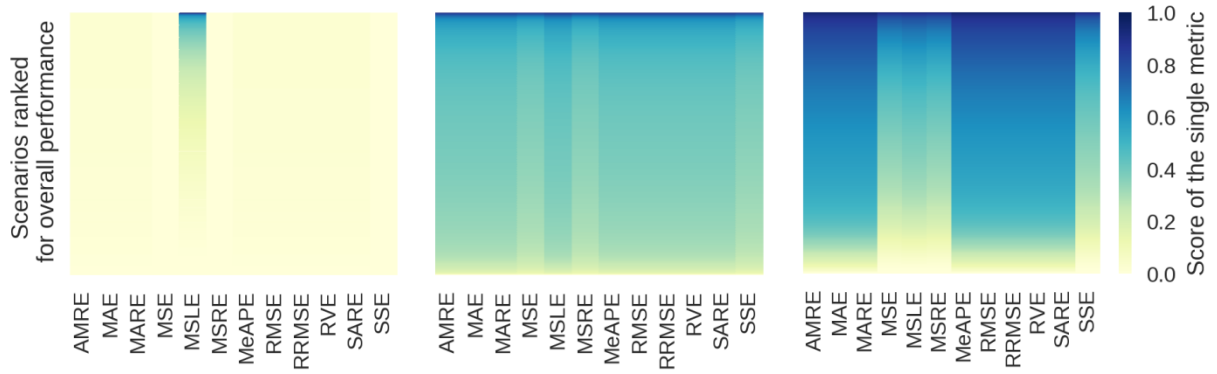

Annex I. 10 – Steady state simulations with the CM layout. Ranking of the scenarios (rows) according to the 12 metrics (columns) from the best performing (bottom) to the worst (top) (for NH_4, DO and TSS respectively from left to right). Each metric is colored according to its internal ranking from 0 to 1.

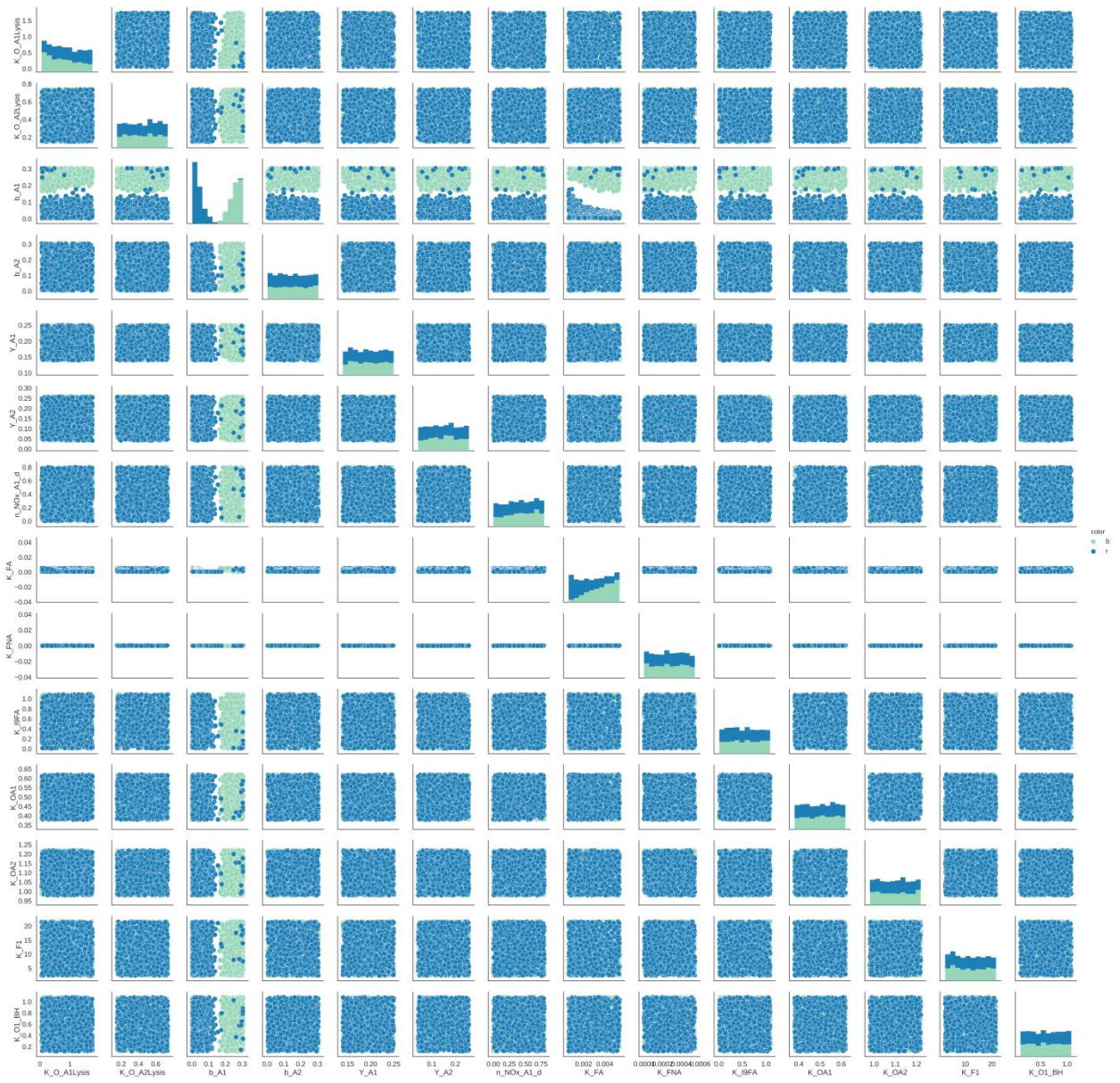

Annex I. 11 - Scatterplot of the parameters reporting both the best (light) and the worst performing scenarios (dark) for the case of NH_4 with the CM layout

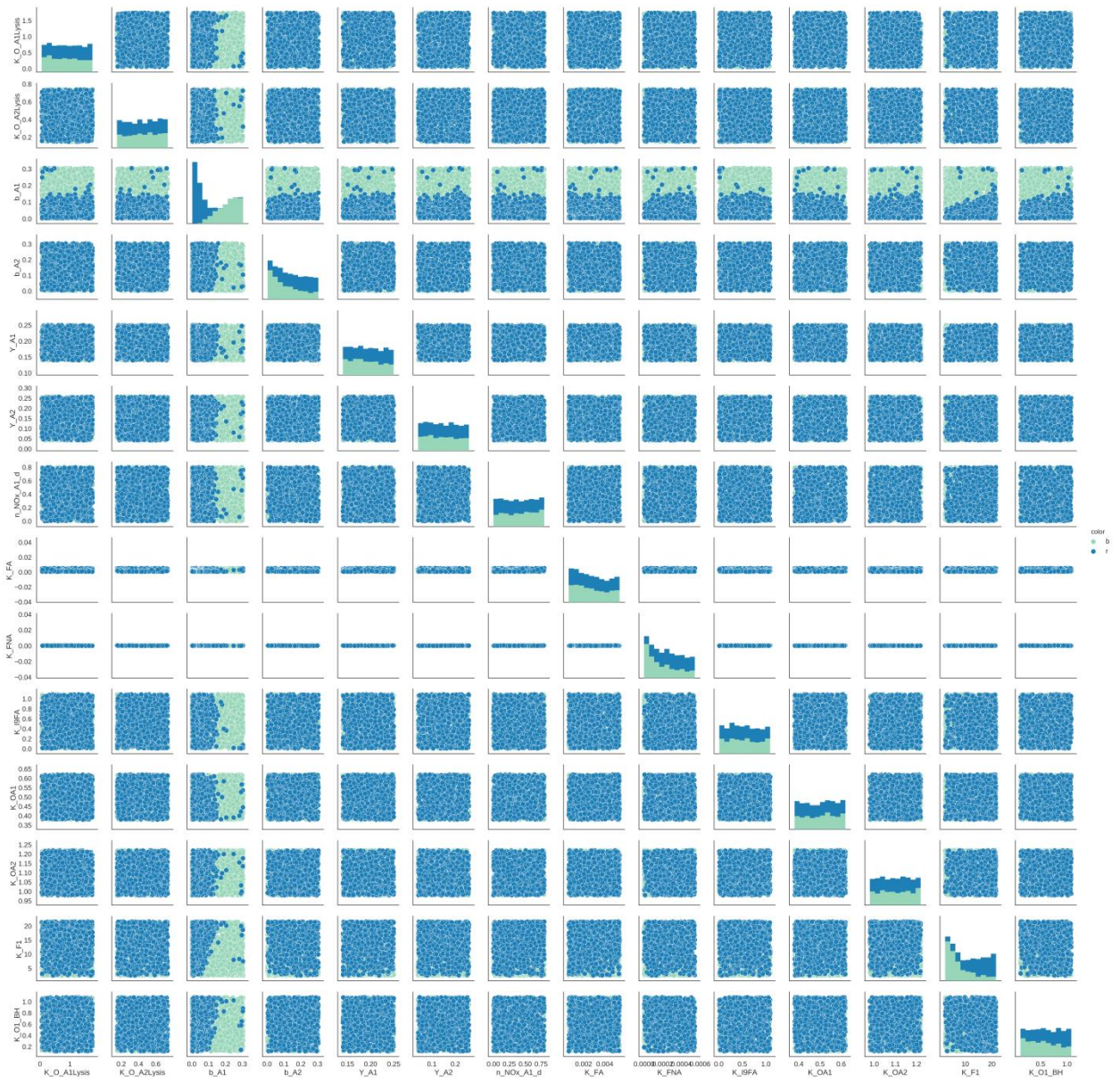

Annex I. 12 – Scatterplot of the parameters reporting both the best (light) and the worst performing scenarios (dark) for the case of DO with the CM layout

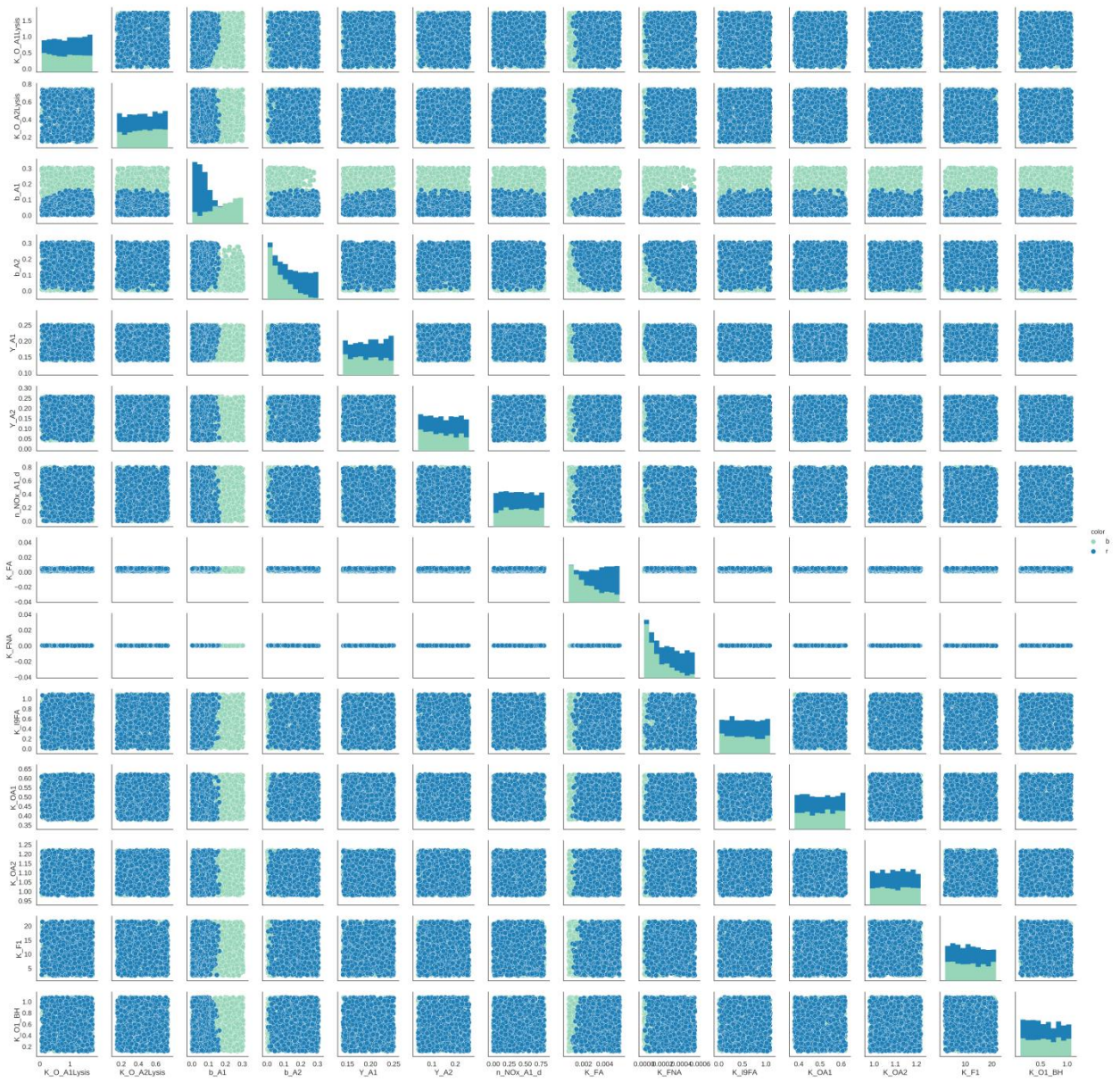

Annex I. 13 – Scatterplot of the parameters reporting both the best (light) and the worst performing scenarios (dark) for the case of TSS with the CM layout

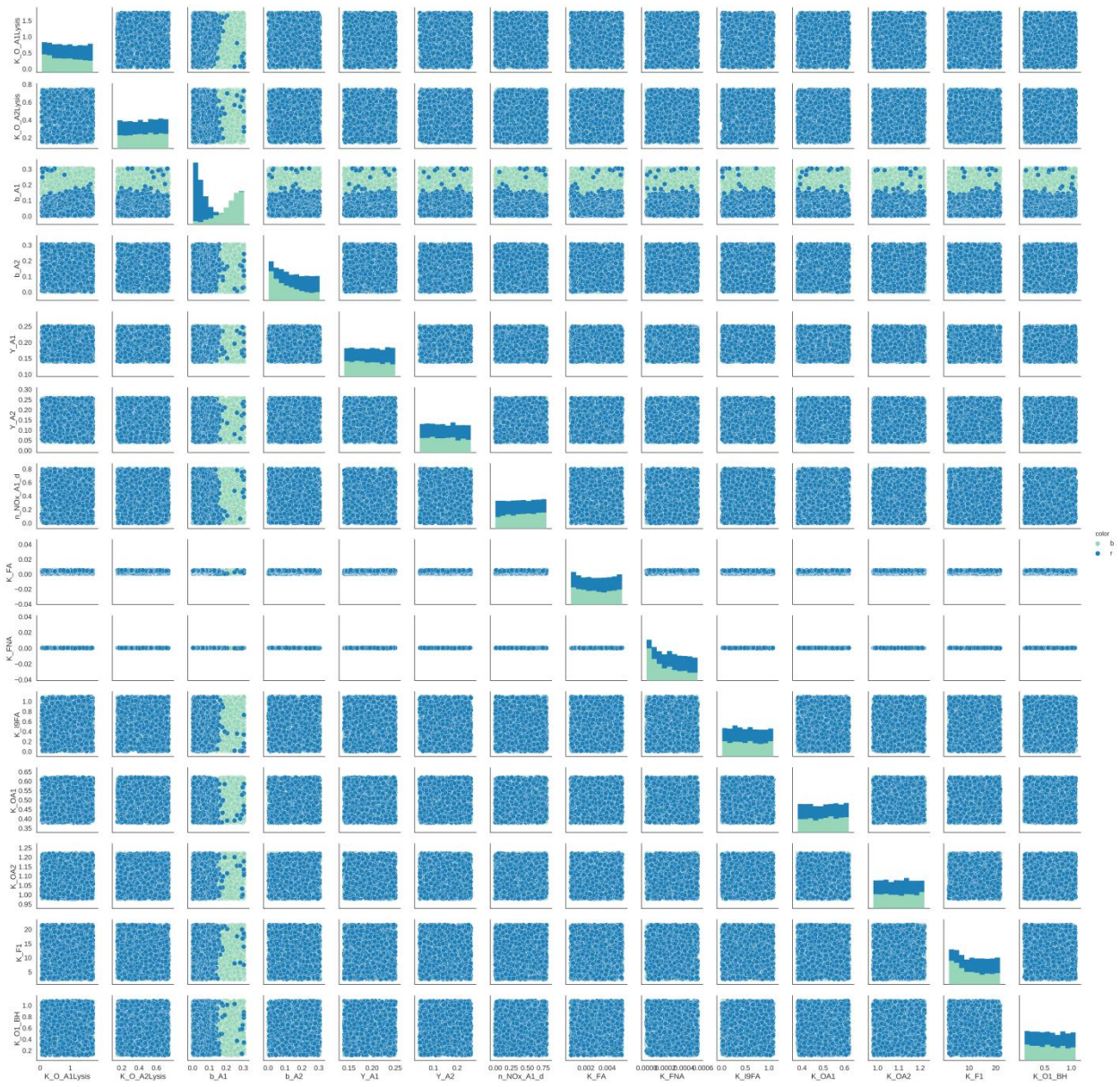

Annex I. 14 - Scatterplot of the parameters reporting both the best (light) and the worst performing scenarios (dark) for the overall case with the CM layout

Step III

TIS

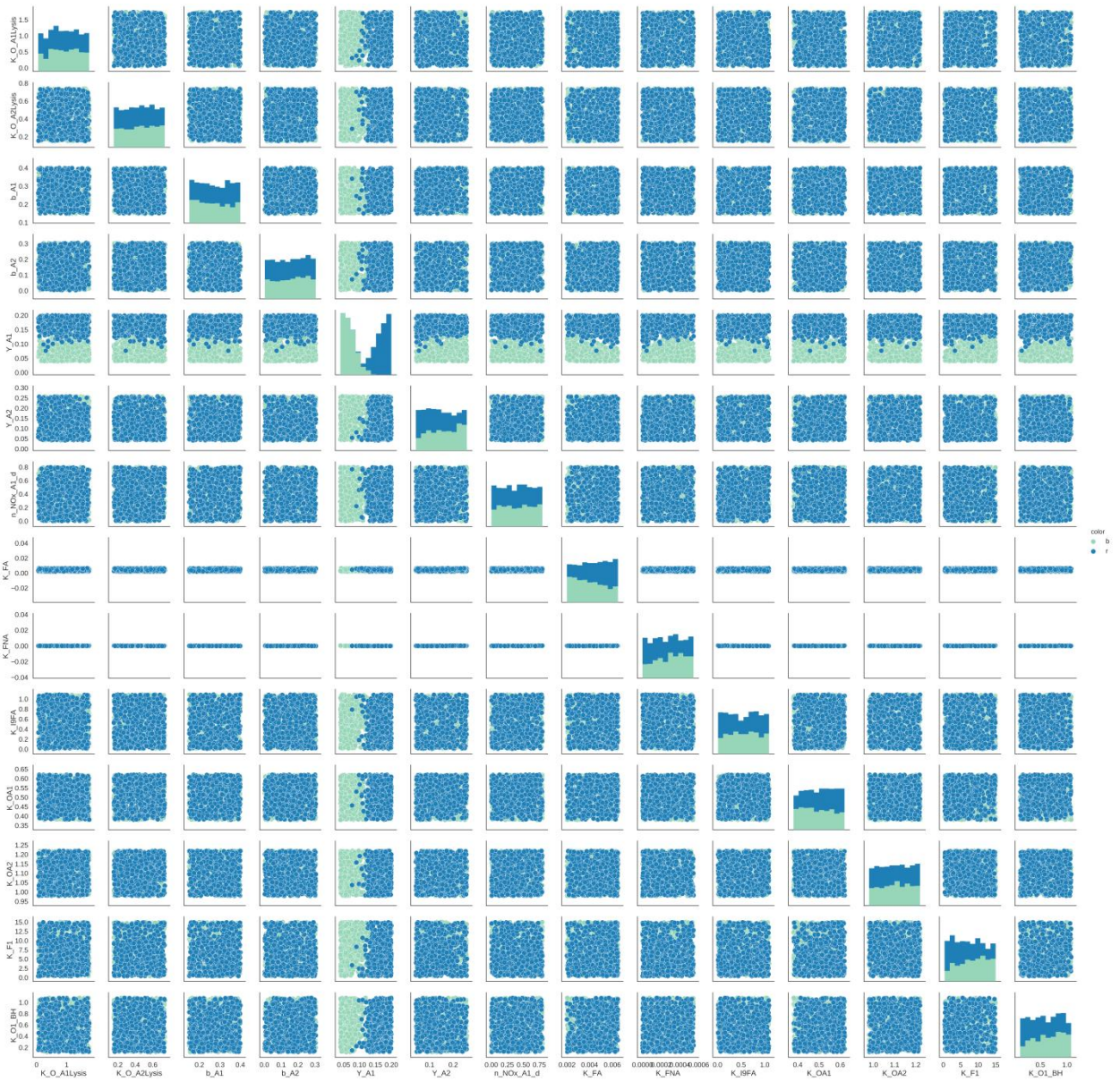

Annex I. 15 – Scatterplot of the parameters reporting both the best (light) and the worst performing scenarios (dark) for the case of NH_4 with the TIS layout

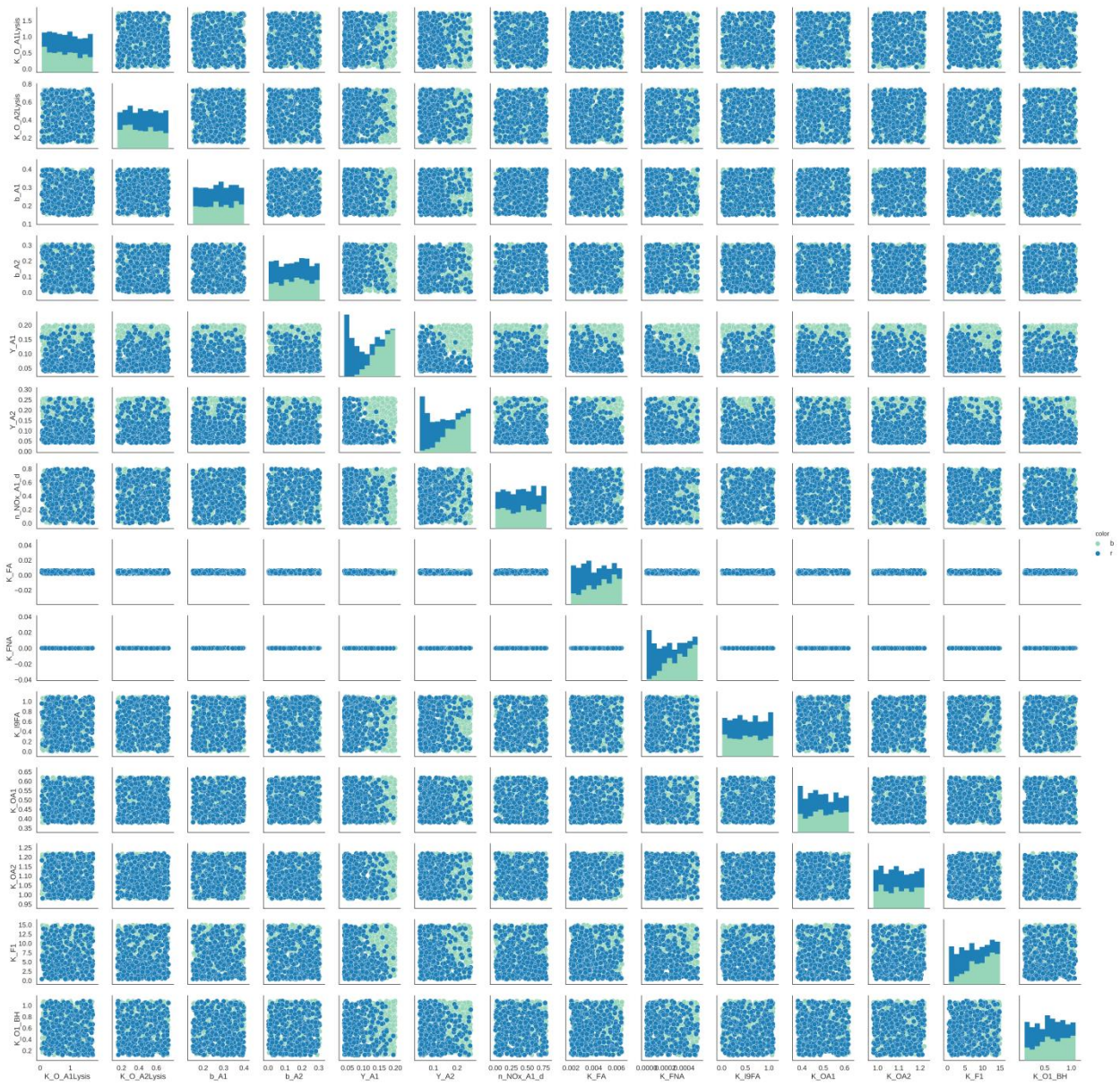

Annex I. 16- Scatterplot of the parameters reporting both the best (light) and the worst performing scenarios (dark) for the case of DO with the TIS layout

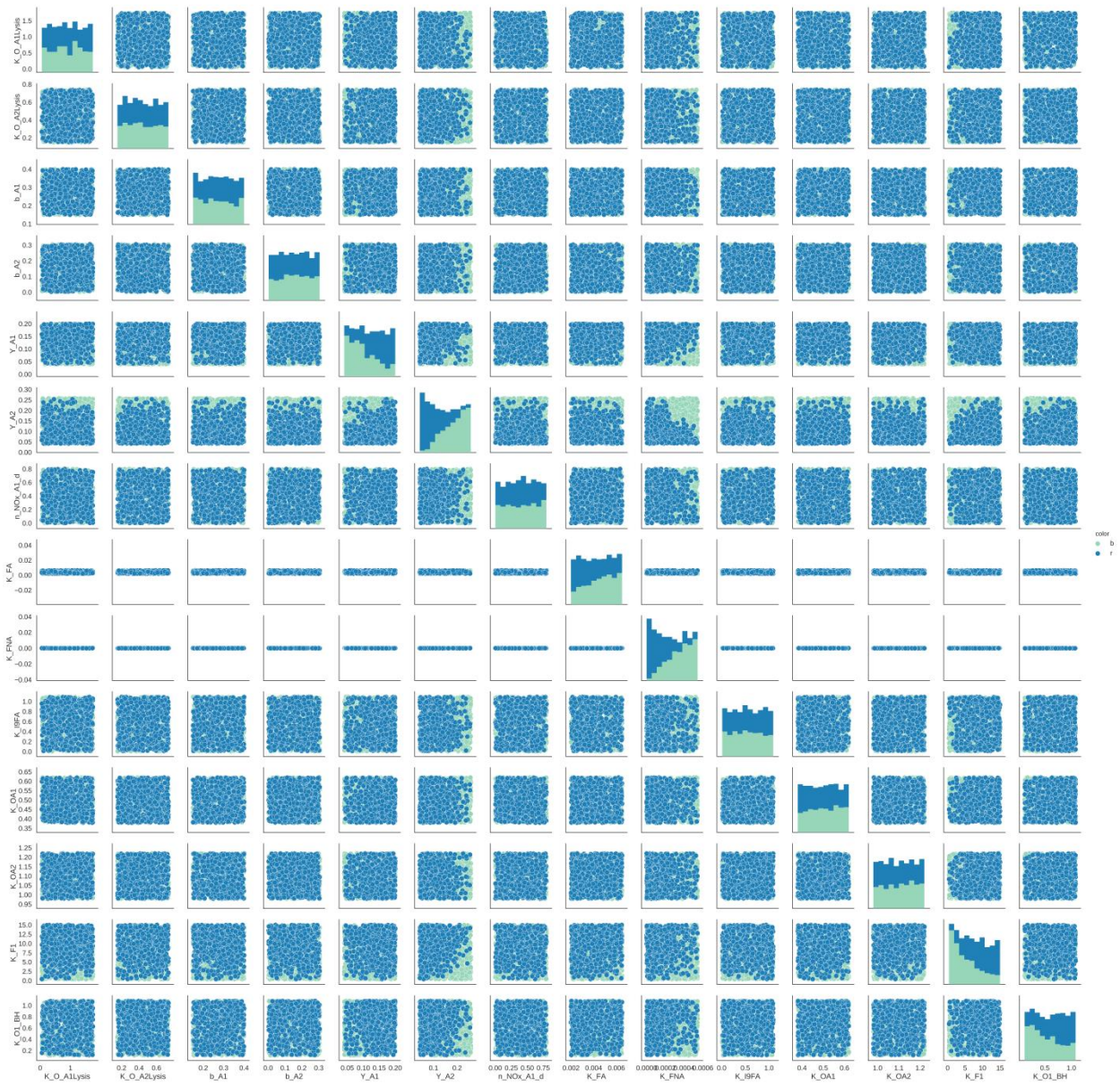

Annex I. 17 - Scatterplot of the parameters reporting both the best (light) and the worst performing scenarios (dark) for the case of N_2O with the TIS layout

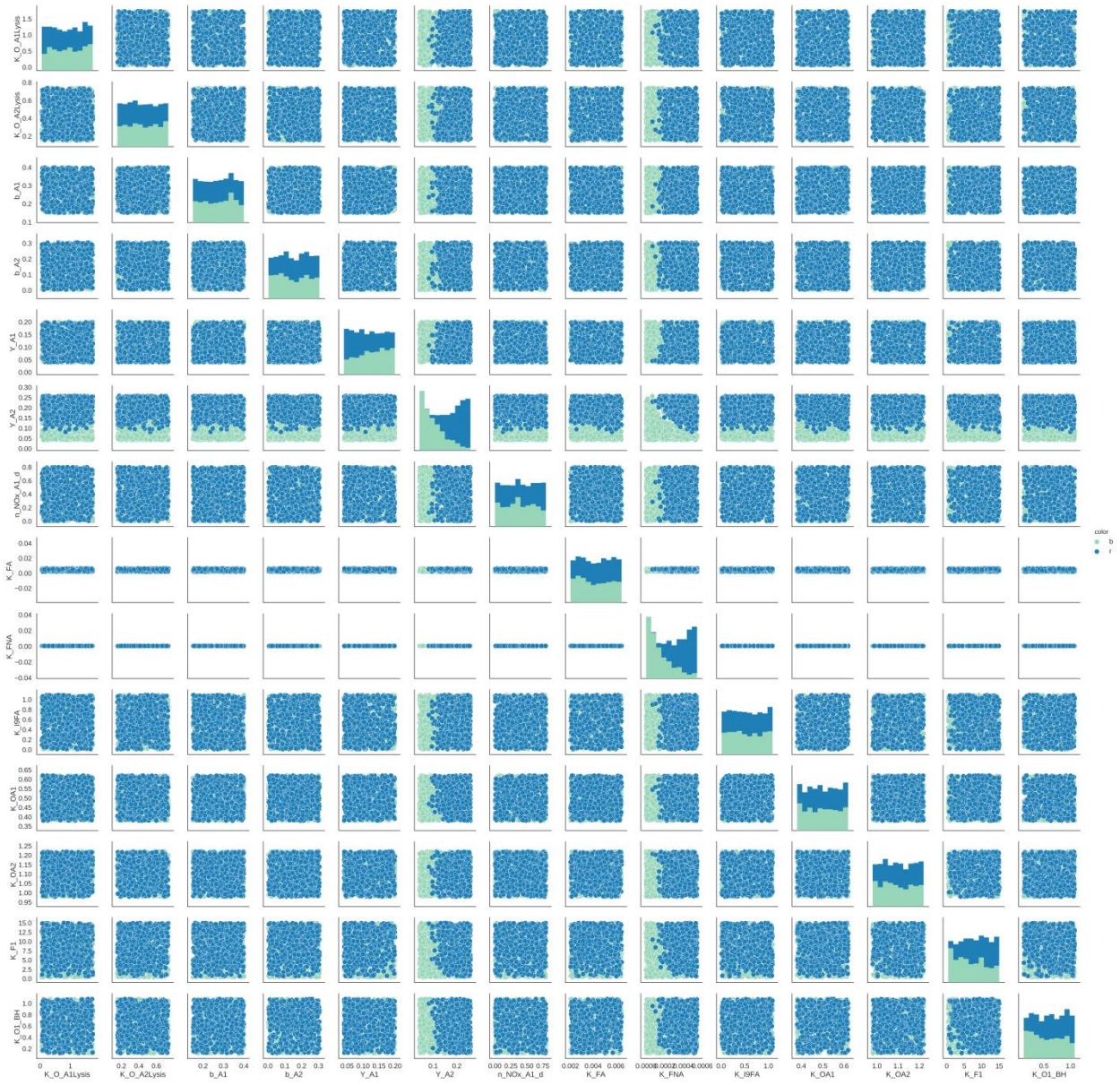

Annex I. 18 - Scatterplot of the parameters reporting both the best (light) and the worst performing scenarios (dark) for the case of NO_3 with the TIS layout

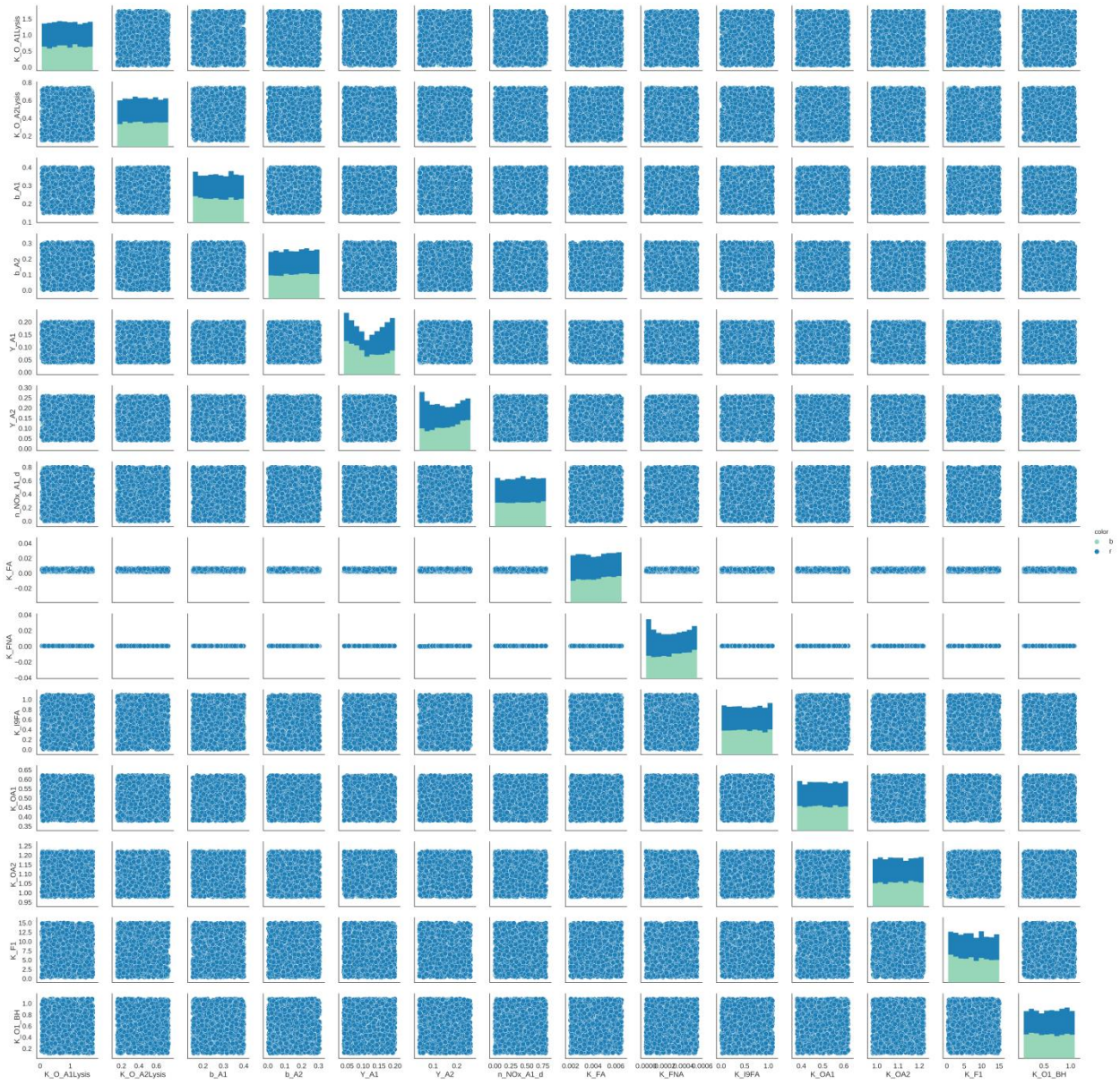

Annex I. 19 - Scatterplot of the parameters reporting both the best (light) and the worst performing scenarios (dark) for the overall case with the TIS layout

CM

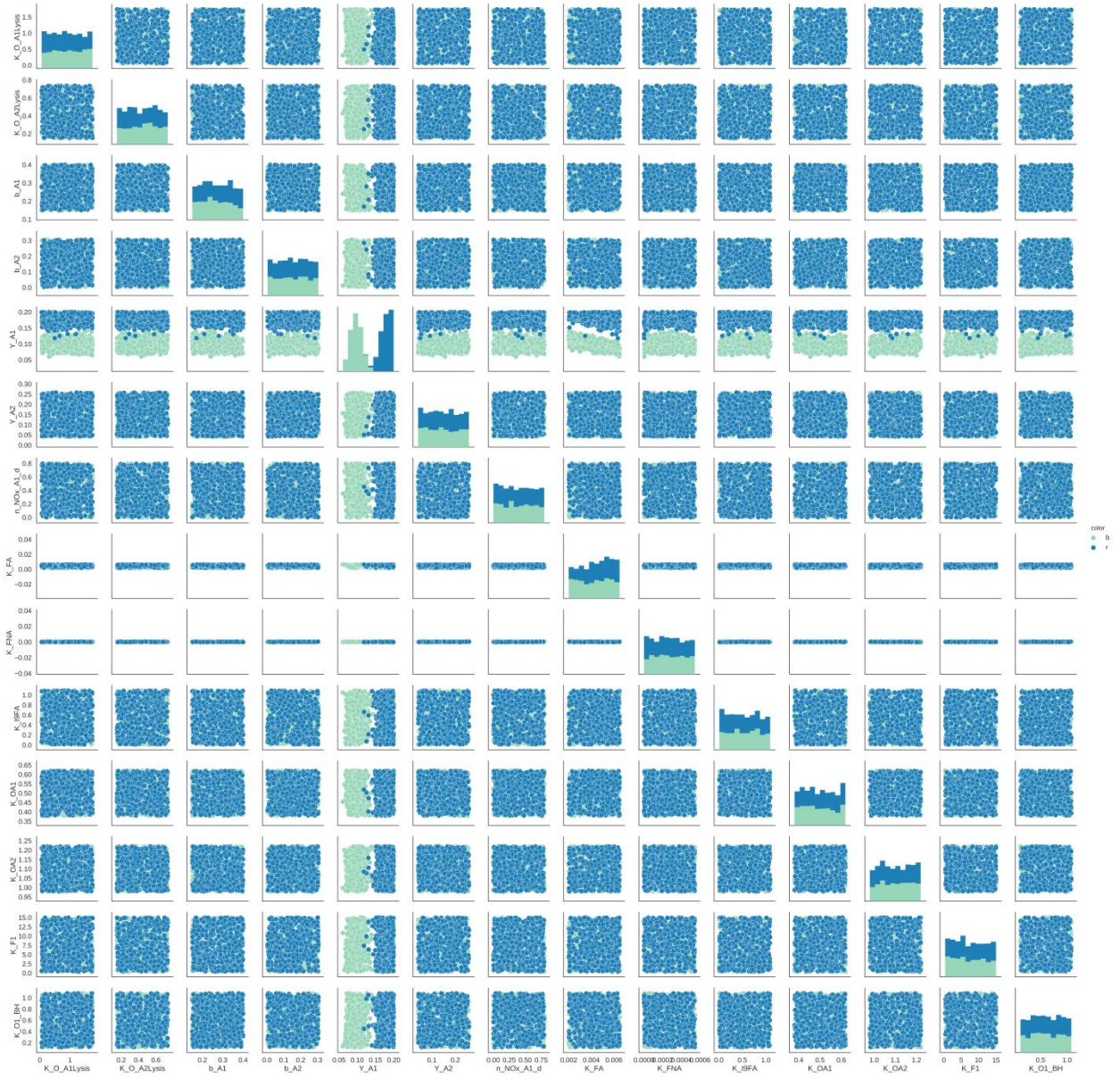

Annex I. 20 – Scatterplot of the parameters reporting both the best (light) and the worst performing scenarios (dark) for the case of NH4 with the CM layout.

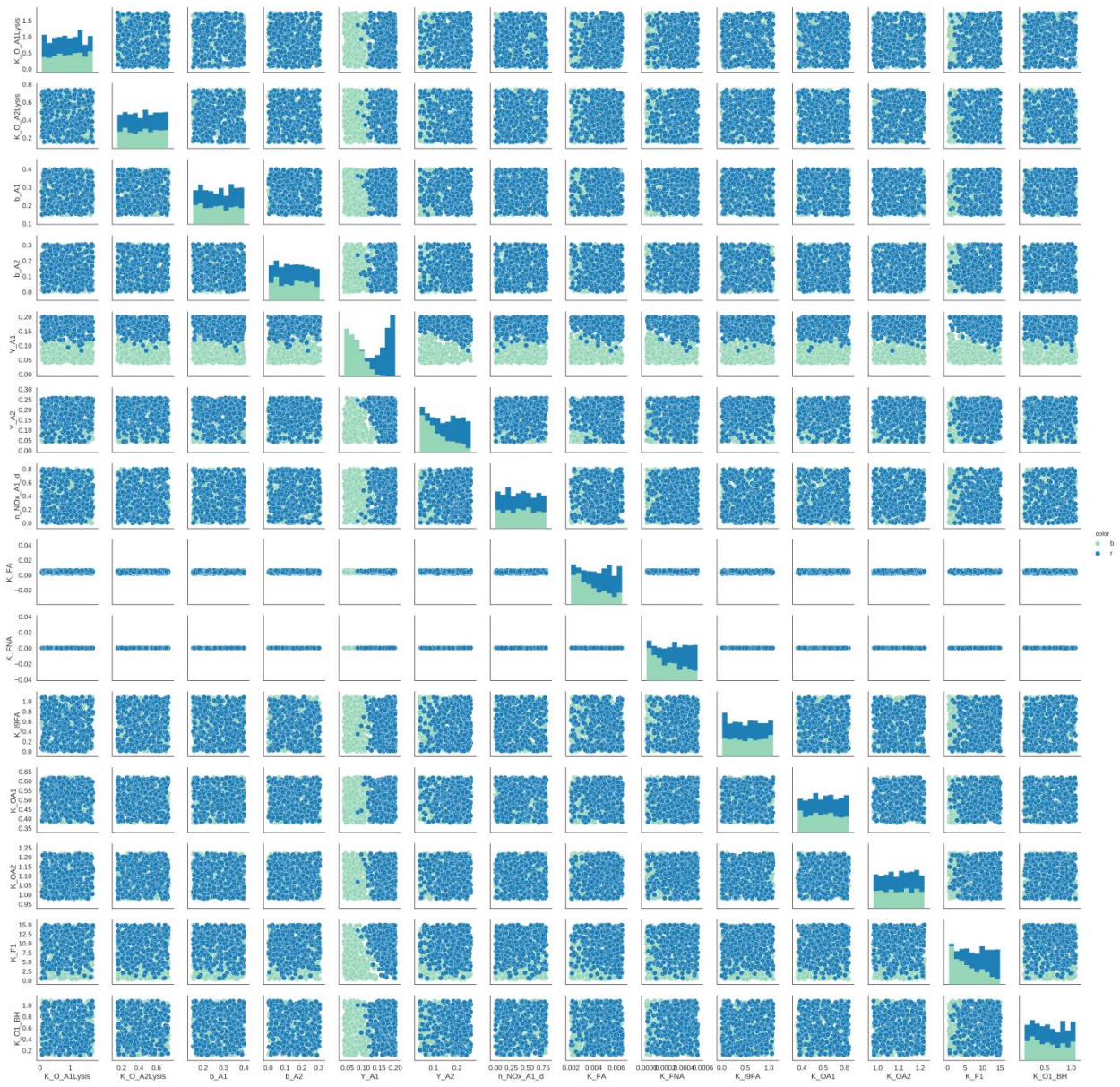

Annex I. 21 - Scatterplot of the parameters reporting both the best (light) and the worst performing scenarios (dark) for the case of DO with the CM layout.

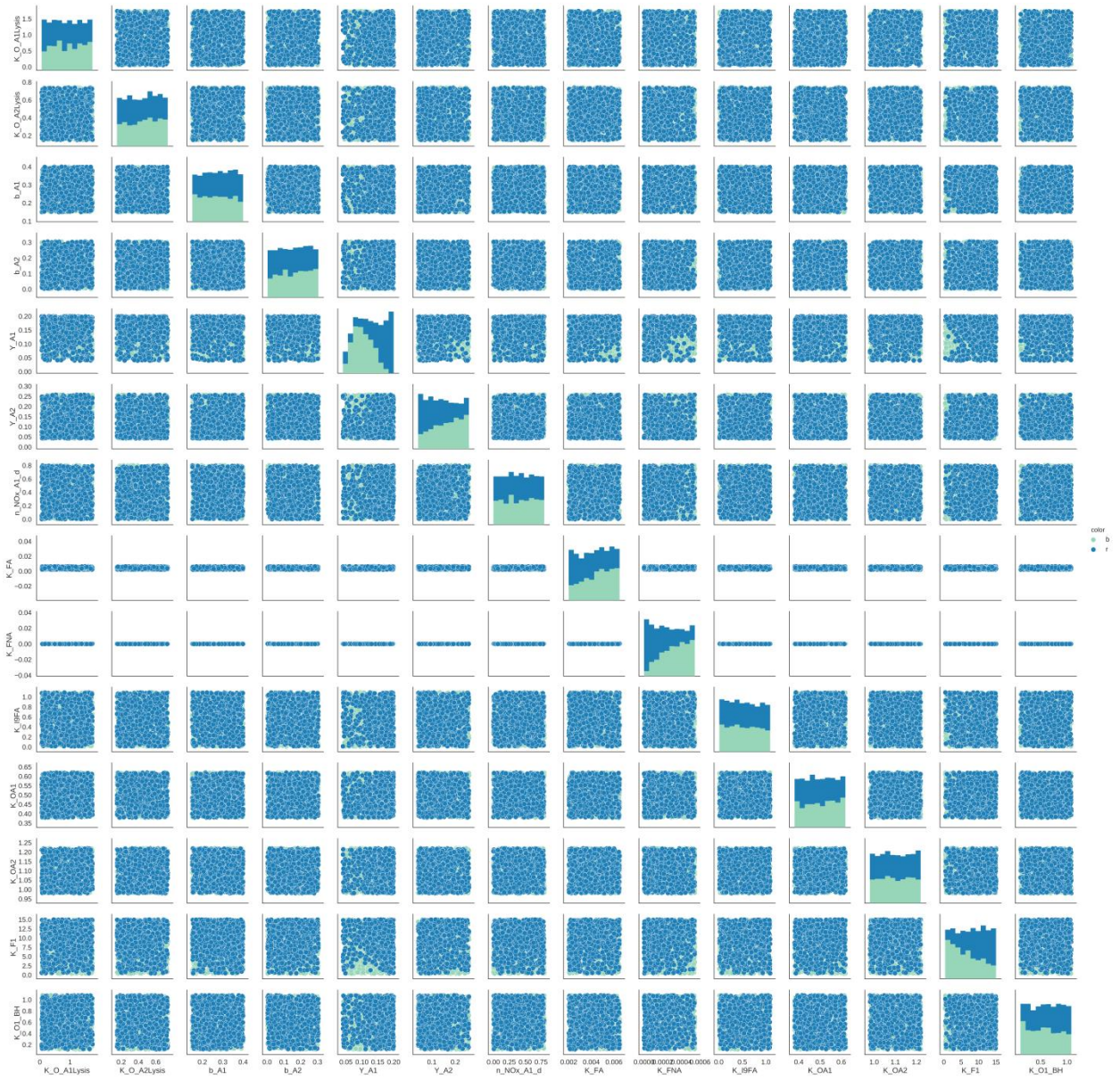

Annex I. 22 - Scatterplot of the parameters reporting both the best (light) and the worst performing scenarios (dark) for the case of N_2O with the CM layout.

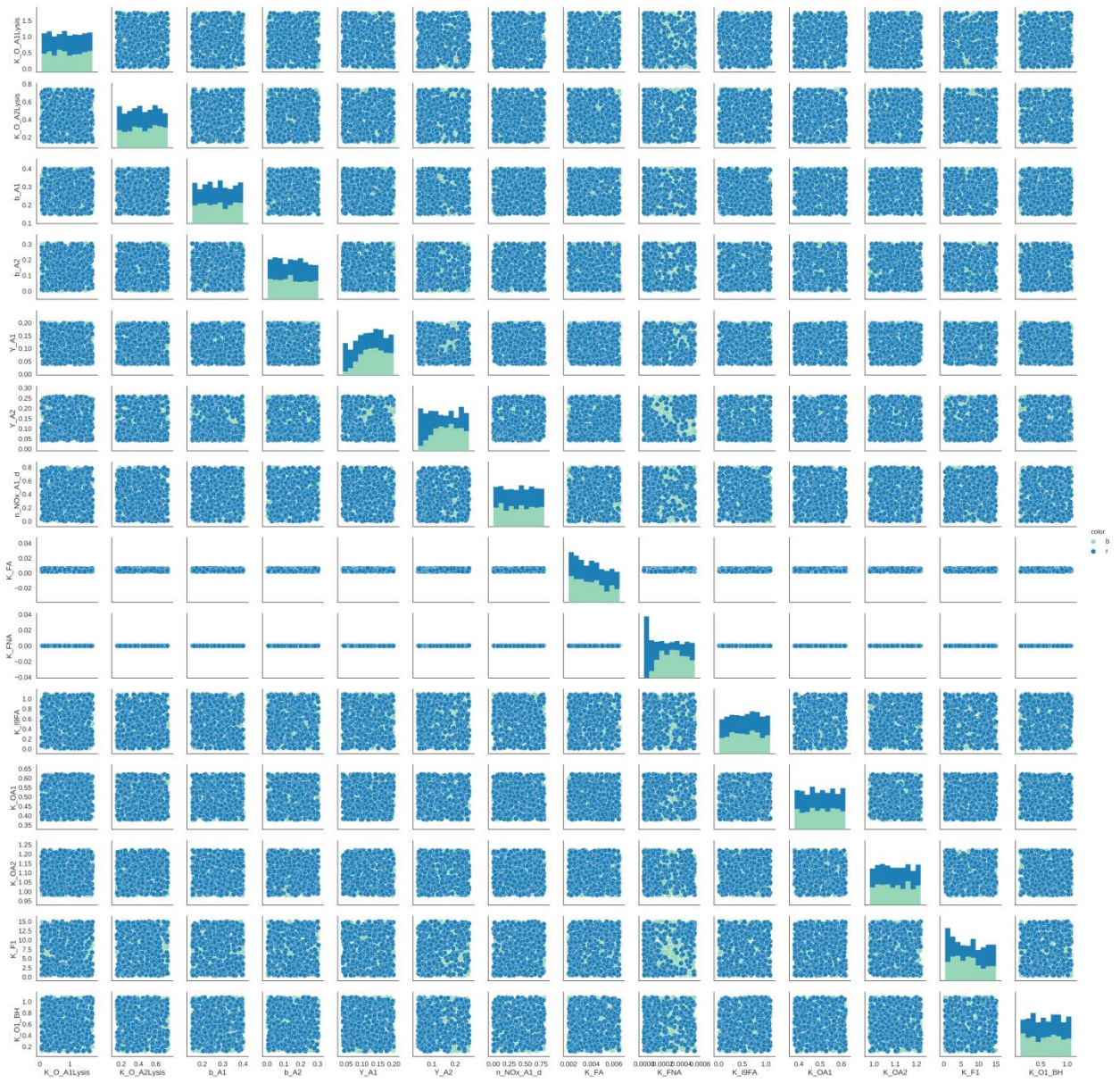

Annex I. 23 - Scatterplot of the parameters reporting both the best (light) and the worst performing scenarios (dark) for the case of NO_3 with the CM layout.

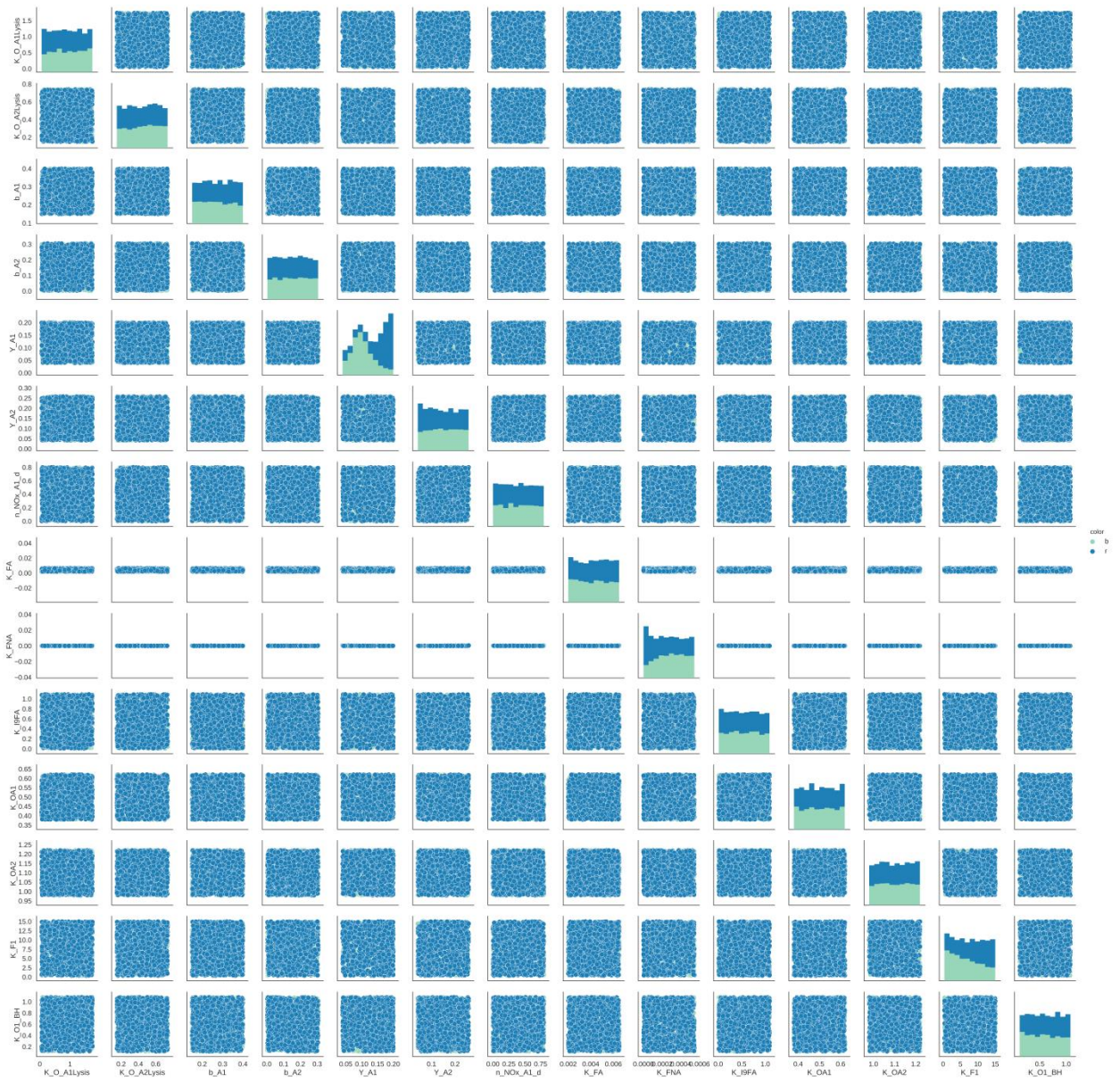

Annex I. 24 - Scatterplot of the parameters reporting both the best (light) and the worst performing scenarios (dark) for the overall case with the CM layout

List of figures

List of tables

Curriculum Vitae

Giacomo Bellandi

Personal information

Date and place of birth	10th May 1983, Pescia (PT), Italy
Address	via dei fornaciai 3, 40128 Bologna (Italy)
E-mail	bellandi.giacomo@gmail.com
Telephone	+39 339 716 3858

Work experience

Jan 2018 – to date **Co-founder, Water Engineer –** Strategic Water

Data-based process monitoring and optimization, strategic planning, logistics and operational management in the water, sanitation and environmental sector.

Sept 2017 – Jan 2018 **Consultant –** technical consultancy for Strategic Water bvba on water treatment technologies, data mining and modelling of pilot and full-scale plants.

Provide technical and scientific expertise to improve process monitoring, operation and automation on conventional plants, membrane and electrochemical applications.

Sept 2014 – to date **Research assistant** - energy and CFP optimization of water treatment
Department of Civil and Environmental Engineering at University of Florence in collaboration with Ghent University.

Design and optimization of WWTPs. Greenhouse gas emissions, aeration efficiency measurements, and modelling for wastewater treatment. Development of standard procedures for full scale treatment plant monitoring and operation.

Ongoing projects:

- LESSWATT – LIFE-EU energetic optimization of water treatment plants (Italy, Belgium, The Netherlands).
- PRIN – Research project of national interest (Italy) "Energy consumption and GHG emissions in wastewater treatment plants: decision support system for planning and management".
- Integrated mathematical / knowledge-based risk assessment of N_2O production (The Netherlands).

Feb. 2011- July 2014 **Technical and scientific assistant** - at BIOMATH, department of Mathematical modelling Statistics and Bioinformatics, Ghent University, Belgium.

Aeration systems testing and characterization. Automation, modelling, data mining, data acquisition, lab/full-scale experimental work.

Projects:

- Kallisto – National project (The Netherlands) for modelling and optimization of the aeration compartment of a urban sewage treatment plant.
- Optimization of an industrial MBR with heterogeneous influent
- Design, realization and control of a resource recovery pilot plant for manure treatment
- Automation of laboratory respirometer for DAQ and data analysis

Education

Sept. 2014 – Oct. 2017 Ph.D. in Civil and Environmental Engineering, joint doctorate program University of Florence and Ghent University.

Aeration efficiency optimization, greenhouse gas emissions minimization, and modelling for wastewater treatment. Development of optimization strategies for WWTP operation.

Sept. 2011 – June 2014 MSc in Environmental Sanitation at BIOMATH, Ghent University, Belgium.
Title of the thesis: "Model-based analysis of aeration in lab and full-scale activated sludge systems".
Supervisor: Prof. Ingmar Nopens.

Sept. 2002 – Sept. 2010 BSc in Environmental Engineering at University of Florence, Italy.
Title of the thesis: "Analysis of the operation of a MBR reactor through principal component analysis".
Supervisors: Prof. Stefano Marsili Libelli and Prof. Ingmar Nopens.

1997-2002 Diploma of agronomist, Istituto Tecnico Agrario Statale D. Anzilotti, Pescia (PT), Italy.

Tutored students

Thesis Title	Subject	AY	Student
Optimization of an off-gas analyzer for aeration efficiency testing. Laboratory and field validation test.	Env. Eng.	2016-2017	Elisa Senesi
Operation and optimization of an aerobic granular reactor for urban wastewater treatment.	Env. Eng.	2016-2017	Serena Falcioni

Design, realization and set-up of an instrument for estimating GHGs emission from biological wastewater treatment	Env. Eng.	2015-2016	Michele Abruzzese
The impact of fluctuating energy prices on WWTP cost optimization	Biosc. Eng	2015-2016	Vincent Van De Maele

Technical courses and internships

Oct. 2017 — Safety specialist course (16 hours) for operating on water treatment plants with biological risk.

Sept. 2012 — Department of Process Engineering, University of Applied Sciences of Osnabrück, Germany, under the supervision of Prof. Sandra Rosenberger

Title: "The effect of shear forces on the viscosity and particle size distribution of activated sludge from MBR".

Publications

- Bellandi G., Porro J., Senesi E., Caretti C., Caffaz S., Weijers S., Nopens I. and Gori R. "Multi-point monitoring of nitrous oxide emissions in three full-scale conventional activated sludge tanks in Europe" (2017) *Water Science & Technology, 77(4): 880-890*.
- Neves do Amaral A., Bellandi G., Rehman U., Neves R., Amerlinck Y. and Nopens I. "Towards improved accuracy in modeling aeration efficiency through understanding bubble size distribution dynamics" (2017) *Water Research, 131: 346-355*.
- Neves do Amaral A., Schraa O., Rieger L. Gillot S., Fayolle Y., Bellandi G., Amerlinck Y., Mortier S.T.F.C. Gori R., Neves R. and Nopens I. "Towards advanced aeration modelling: from blower to bubbles to bulk" (2016) *Water Science and Technology, 75 (3): 507 - 517.*
- Caivano M., Bellandi G., Mancini I. M., Masi S., Brienza R., Panariello S., Gori R. and Caniani D. "Monitoring the aeration efficiency and carbon footprint of a medium-sized WWTP: experimental results on oxidation tank and aerobic digester" (2016) *Environmental Technology, Jul 11: 1-10.*
- Amerlinck Y., Bellandi G., Neves do Amaral A., Weijers S. and Nopens I. "Detailed off-gas measurements for improved modelling of the aeration performance at the WWTP of Eindhoven" (2016) *Water Science and Technology; 74 (1): 3-11.*
- Kumar A., Vercruysse J., Bellandi G., Gernaey K. V., Vervaet C., Remon J. P., De Beer T., Nopens I. "Granule size and shape dynamics in twin-screw granulation" (2014), *International Journal of Pharmaceutics; 475 (s 1–2): 485–495*.
- Guo L., Lamaire-Chad C., Bellandi G., Daelman M., Amerlinck Y., Maere T., Nous J., Flameling T., Weijers S., van Loosdrecht M. C. M., Volcke E. I. P., Nopens I., Vanrolleghem P. A. "Full-scale Field Measurement of Nitrous oxide (N2O) Gas Emissions and its Relationship with Other Nitrogen Species under Dry and Wet Weather Conditions" (2014) *Environmental Science & Technology, Submitted.*

- Torfs E., Bellandi G., Nopens I. "Towards mechanistic models for activated sludge flocculation under different conditions based on inverse problems" (2012) *Water Science and Technology, 65 (11): 1946-1953*.

Conference proceedings

- Bellandi G., De Mulder C., Van Hoey S., Amerlinck Y., Guo L., Vanrolleghem, P., Weijers S., Gori R. and Nopens, I. "Tanks in series VS compartmental model configuration: considering hydrodynamics helps in parameter estimation for a N2O model" (2018) *WRRmod2018, Québec, Canada. Proceedings.*
- Porro, J., Bellandi G., Rodriguez-Roda, I., Deeke, A., Weijers, S., Vanrolleghem, P., Comas, J. and Nopens, I. "Developing an artificial intelligence-based WRRF nitrous oxide mitigation road map: The Eindhoven N2O mitigation case study" (2017) *WEFTEC 2017, Chicago, Illinois. Papers*
- Bellandi G., Weijers S., Nopens I. and Gori R. "Towards a mitigation strategy for N2O emissions through Principal Components Analysis" (2017) *IWA BeNeLux Young Water Professionals Conference, Ghent, Belgium. Papers*.
- Gori R., Bellandi G., Caretti C., Dugheri S., Cosenza A., Laudicina V. A., Esposito G., Pontoni L., Caniani D., Caivano M., Rosso D. and Mannina G. "Novel comprehensive procedure for estimating greenhouse gas emissions from water resource recovery facilities" (2017) *FICWTM2017, Palermo, Italy. Papers.*
- Bellandi G., Caretti C., Caffaz S., Nopens I., and Gori R. "Multi-point monitoring of nitrous oxide emissions and aeration efficiency in a full-scale conventional activated sludge tank" (2017) *Frontiers International Conference on Wastewater Treatment (FICWTM2017), Palermo, Italy. Papers.*
- Bellandi G., Amerlinck Y., Van Hoey S., Neves do Amaral A. and Nopens I. "Image analysis procedure to derive bubble size distributions for better understanding of the oxygen transfer mechanism" (2016) *7th International Conference and Exhibition on Water, Wastewater & Environmental Monitoring (IT&Water), Telford, UK. Papers.*
- Porro, J., Bellandi, G., Rodriguez-Roda, I., Deeke, A., Weijers, S., Vanrolleghem, P., Comas, J. and Nopens, I. "Measurements and modelling for developing an AI-based DO control for mitigating N2O emissions from WWTPs (2016) *7th International Conference and Exhibition on Water, Wastewater & Environmental Monitoring (IT&Water), Telford, UK. Papers.*
- Caretti C., Bellandi G., Balducci A. and Gori R. "Oxygen transfer efficiency monitoring and aeration control optimization in a large urban WWTP" (2016) *3rd IWA Specialized International Conference on Ecotechnologies for Wastewater Treatment (ecoSTP16), Cambridge, UK. Papers.*
- Gori, R., Bellandi G., Caretti C. "Experiences, progresses and perspectives of off-gas testing in wastewater treatment: from aeration efficiency towards CFP assessment" (2016) *SIDISA 016 Rome, Italy. Papers.*
- Bellandi G., Porro J., Caretti C., Rodriguez-Roda I., Comas J., Nopens I. and Gori R. "Use of artificial intelligence for WRRF knowledge based N2O model selection" (2016) 5th *IWA/WEF Wastewater Treatment Modelling Seminar (WWTmod2016) Annecy, France. Papers.*
- Neves do Amaral A., Schraa O., Rieger L. Gillot S., Fayolle Y., Bellandi G., Amerlinck Y., Mortier S.T.F.C. Gori R., Neves R and Nopens I. "Towards advanced aeration modelling: from blower to bubbles to bulk" (2016) 5th *IWA/WEF Wastewater Treatment Modelling Seminar (WWTmod2016) Annecy, France. Papers.*
- Neves do Amaral A., Bellandi G., Amerlinck Y., Mortier S., Neves R. And Nopens I. "Towards improved accuracy in modelling aeration efficiency by accounting for bubble size distribution dynamics" (2015) *Systems Analysis and Integrated Assessment, 9th IWA Symposium (WATERMATEX 2015) Gold Coast, QLD, Australia. Papers*.

- Amerlinck Y., Bellandi G., Amaral A., Weijers S. and Nopens I. "Detailed off-gas measurements for improved modelling of the aeration performance at the WWTP of Eindhoven" (2015) *New Developments in IT & Water, 2nd Conference. Papers*.
- Torfs E., Mahdavi Mazdeh F., Bellandi G. and Nopens I. "A novel methodology for the calibration of discrete settling behavior of activated sludge" (2014) *Particle Separation, IWA Specialist conference. Papers*.
- Maere T., Bellandi G., Lousada-Ferreira M., De Temmerman L., Willem Mulder J. and Nopens I. "Influent composition effects on sludge particle size distributions in an MBR" (2014) *Particle Separation, IWA Specialist conference. Papers.*
- Bellandi G., Horn W., Naessens W., Maere T., Helmus F., Rosenberger S. and Nopens I. "Effects of shear forces on the particle size distribution and viscosity of activated sludge from an MBR pilot plant" (2013) *IWA BeNeLux Regional Young Water Professionals Conference, 3rd. Papers*.
- Maere T., Bellandi G., Lousada-Ferreira M., De Temmerman L., Mulder J.W. and Nopens I. "Investigating the effect of influent composition on full-scale MBR filtration performance through lab-scale research" (2013) *IWA BeNeLux Regional Young Water Professionals Conference, 3rd. Papers*.
- Guo L., Lamaire-Chad C., Bellandi G., Daelman M., Amerlinck Y., Maere T., Nous J., Flameling T., Weijers S., van Loosdrecht M., Volcke E.I.P., Nopens I., Vanrolleghem P. A. "High-frequency field measurement of nitrous oxide (N2O) gas emissions and influencing factors under dry and wet weather conditions" (2013) *WEF/IWA Nutrient Removal and Recovery. Conference proceedings*.
- Torfs E., Bellandi G., Nopens I. "Construction of mechanistic models for activated sludge flocculation under different conditions based on inverse problems" (2011) *Watermatex 2011: conference proceedings. p.357-366.*
- Bellandi G., Plano S., Rosso D., Maere T., De Keyser W., Weijers S., Flameling T. and Nopens I. "Measuring oxygen transfer efficiency (OTE) at the Eindhoven WWTP using real-time off-gas analysis in circular aeration tank" (2011) *IWA BeNeLux Regional Young Water Professionals Conference, 2nd. Papers*.